UNIVERSIDADE ESTADUAL DE CAMPINAS
Faculdade de Engenharia Mecânica

RYAN DAVID EARL

A Contribution to the Study of Heavy Haul Railway Wagon Pneumatic Braking Systems

Uma Contribuição para o Estudo de Sistemas de Freio Pneumático para Vagões de Alta Carga

CAMPINAS
2022

RYAN DAVID EARL

A Contribution to the Study of Heavy Haul Railway Wagon Pneumatic Braking Systems

Uma Contribuição para o Estudo de Sistemas de Freio Pneumático para Vagões de Alta Carga

Thesis presented to the School of Mechanical Engineering of the University of Campinas in partial fulfillment of the requirements for the degree of Master of Science in Mechanical Engineering, in the area of Solid Mechanics and Mechanical Design.

Dissertação apresentada à Faculdade de Engenharia Mecânica da Universidade Estadual de Campinas como parte dos requisitos exigidos para a obtenção do título de Mestre em Engenharia Mecânica, na Área de Mecânica dos Sólidos e Projeto Mecânico.

Orientador: Prof. Dr. Auteliano Antunes dos Santos Junior

ESTE TRABALHO CORRESPONDE À VERSÃO FINAL DA DISSERTAÇÃO DEFENDIDA PELO ALUNO RYAN DAVID EARL, E ORIENTADA PELO PROF. DR. AUTELIANO DOS SANTOS JUNIOR.

....

ASSINATURA DO ORIENTADOR

CAMPINAS
2022

Ficha catalográfica
Universidade Estadual de Campinas
Biblioteca da Área de Engenharia e Arquitetura
Rose Meire da Silva - CRB 8/5974

Earl, Ryan David, 1988-
Ea73c A contribution to the study of heavy haul railway wagon pneumatic braking systems / Ryan David Earl. – Campinas, SP : [s.n.], 2022.

Orientador: Auteliano Antunes dos Santos Junior.
Dissertação (mestrado) – Universidade Estadual de Campinas, Faculdade de Engenharia Mecânica.

1. Pneumáticos. 2. Ferrovias - Freios. 3. Engenharia ferroviária. 4. Engenharia mecânica - Projetos. I. Santos Junior, Auteliano Antunes dos, 1963-. II. Universidade Estadual de Campinas. Faculdade de Engenharia Mecânica. III. Título.

Informações para Biblioteca Digital

Título em outro idioma: Uma contribuição para o estudo de sistemas de freio pneumático para vagões de alta carga
Palavras-chave em inglês:
Pneumatics
Railway brakes
Railway engineering
Mechanical design engineering
Área de concentração: Mecânica dos Sólidos e Projeto Mecânico
Titulação: Mestre em Engenharia Mecânica
Banca examinadora:
Auteliano Antunes dos Santos Junior [Orientador]
Angel Pontin Garcia
Éric Fujiwara
Data de defesa: 25-02-2022
Programa de Pós-Graduação: Engenharia Mecânica

Identificação e informações acadêmicas do(a) aluno(a)
- ORCID do autor: https://orcid.org/0000-0002-6056-2326
- Currículo Lattes do autor: http://lattes.cnpq.br/8492323265210544

UNIVERSIDADE ESTADUAL DE CAMPINAS
FACULDADE DE ENGENHARIA MECÂNICA

DISSERTAÇÃO DE MESTRADO ACADÊMICO

A Contribution to the Study of Heavy Haul Railway Train Wagon Pneumatic Braking Systems

Uma Contribuição para o Estudo de Sistemas de Freio Pneumático para Vagões de Alta Carga

Autor: Ryan David Earl

Orientador: Prof. Dr. Auteliano Antunes dos Santos Junior
Coorientador: N/A

A Banca Examinadora composta pelos membros abaixo aprovou esta Dissertação/Tese:

Prof. Dr. Auteliano Antunes dos Santos Junior
Departamento de Sistemas Integrados/Faculdade de Engenharia Mecânica/UNICAMP

Prof. Dr. Angel Pontin Garcia
Departamento de Máquinas Agrícolas/Faculdade de Engenharia Agrícola/UNICAMP

Prof. Dr. Paulo Roberto Gardel Kurka
Departamento de Sistemas Integrados/Faculdade de Engenharia Mecânica/UNICAMP

Prof. Dr. Eric Fujiwara
Departamento de Sistemas Integrados/Faculdade de Engenharia Mecânica/UNICAMP

Prof. Dr. Guilherme Fabiano Mendonça dos Santos
Departamento de Engenharia Mecânica/Centro Tecnológico/UFES

A Ata de Defesa com as respectivas assinaturas dos membros encontra-se no SIGA/Sistema de Fluxo de Dissertação/Tese e na Secretaria do Programa da Unidade.

Campinas, 25 de fevereiro de 2022.

Dedication

This work is dedicated to my family and friends, all of whom have supported, loved, and trusted me in my path through life.

Acknowledgements

I would like to thank Prof. Dr. Auteliano dos Santos Junior not only for the opportunity to further my education, but also for giving a chance to a stranger in need. Without the graciousness of Auteliano, my career in Brazil would have abruptly ended before it even started.

I would also like to thank each of my labmates for their support and friendship, and especially PhD candidates Ícaro Pavano Teodoro and Luis Henrique da Silva Teixeira for their help on this work.

Resumo

O sistema de freios pneumáticos para vagões de alta carga é crucial para a segurança e a confiabilidade do transporte ferroviário. Frequentemente, a análise do sistema de freios para vagões foca no desempenho do sistema pneumático que consiste no encanamento geral, nas válvulas de controle e nos reservatórios dos vagões. Porém, mesmo sendo uma tecnologia que já existe há séculos, poucas mudanças estruturais ou novos projetos têm sido lançados para aprimorar o sistema de freios pneumáticos. As duas maiores desvantagens do sistema são a propagação lenta do sinal de pressão e a passagem em série entre os vagões na composição. Essas desvantagens resultam em longas distâncias para parar e, uma vez que os vagões à frente na composição freiam mais cedo que os vagões à trás, choques longitudinais ocorrem entre eles. Mesmo que sistemas de freios eletropneumáticos já existam, a implementação ainda não chegou para vagões de alta carga pois o custo de implementação é muito alto. Portanto, soluções mecânicas e com custos baixos são apresentados neste trabalho. O projeto escolhido é simulado usando modelos matemáticos derivados das equações de Navier-Stokes e implementado na linguagem de programação C++ para verificar o desempenho do sistema. É proposto o uso de um projeto que utiliza o efeito de venturi para gerar uma pressão de vácuo na saída da válvula de controle para e seja possível propagar o sinal de pressão dentro do encanamento geral de maneira mais rápida. Uma dessas soluções de design utiliza um efeito venturi para criar um vácuo perto da saída da válvula de controle pneumático, que permite uma propagação mais rápida do sinal no encanamento geral. A propagação do sinal mais rápido no encanamento foi implementada em um modelo de dinâmica longitudinal, em Matlab e Simulink, para determinar o seu efeito nos acoplamentos. Os resultados indicam que a introdução do efeito venturi pode reduzir o acúmulo de danos nos acoplamentos, em detrimento do ar do reservatório de emergência. No entanto, os resultados da dinâmica longitudinal requerem estudos adicionais antes da implementação do venturi em campo.

Palavras Chave: Sistemas Pneumáticos, Freios de Ar de Vagões, Engenharia Ferroviária, Projetos Mecânicos

Abstract

The pneumatic air brake system in railway trains is critical to the safe and reliable operation of heavy-haul railway transportation. Analysis of the braking performance of the railway wagons often focuses on the behavior and response time of the pneumatic system, consisting of the brake pipe, wagon control valves, wagon brake cylinders, and the wagon air reservoirs. However, for a technology that has been used for centuries and researched for decades in academia, very few architecture or design changes have been introduced to improve the pneumatic air brake system. Two significant design drawbacks of the pneumatic air brake system are slow signal propagation and in series signal passing from wagon to wagon. These drawbacks lead to long stopping distances and, because front wagons begin to brake long before rear wagons, damaging longitudinal shocks between the wagons. While electro-pneumatic brake systems in heavy-haul railway trains are emerging as reliable solutions to the problems faced by purely pneumatic air brake systems, the high cost of implementation and other risk factors have delayed their use in the field. Therefore, purely mechanical, low-cost design solutions are studied in this work. A single design solution has been simulated using mathematical models derived from the Navier-Stokes equations and computationally solved in the C++ programming language to verify system performance. This design solution utilizes a venturi effect to create a vacuum near the outlet of the pneumatic control valve, that enables faster signal propagation through the brake pipe. The faster brake pipe signal was then implemented in a Matlab Simulink longitudinal dynamics model to determine its effect on draft gear couplings. The results indicate that introducing a venturi effect can reduce damage accumulation in the draft gears, at the expense of emergency reservoir air. However, the longitudinal dynamics results require additional study before venturi implementation into the field, as the behavior is not fully controlled and still suffers from similar design flaws as the current system.

Key Words: Pneumatic Systems, Wagon Air Brakes, Railway Engineering, Mechanical Design Engineering

List of Illustrations

List of Tables

List of Abbreviations and Symbols

Latin Letters

A	Cross-sectional area of fatigue specimen	$[m^2]$
A_1	Modified Davis equation coefficient	
A_2	Modified Davis equation coefficient	$[s^2/m]$
A_o	Orifice area	$[m^2]$
A_{bp}	Brake pipe area	$[m^2]$
A_p	Piston area	$[m^2]$
b	y-axis intercept of modified Goodman diagram	
B_1	Modified Davis equation coefficient	[s/m]
c	Speed of sound in air	[m/s]
C	Damping coefficient	[N·s/m]
C_1	Modified Davis equation coefficient	$[s^2/m^2]$
C_f	Pressure loss coefficient	
C_m	Mach correction factor for mass flow through orifice	
C_q	Empirical correction factor for mass flow through orifice	
D	Brake pipe diameter	[m]
$D_{i,j}$	Fatigue damage	
f	Friction coefficient	
f_x	Sum of superficial forces	[N]
F_b	Wagon brake force	[N]
F_d	Locomotive dynamic brake force	[N]
F_{dg}	Draft gear force	[N]
F_j	Draft gear force in all cases except clearance and transition	[N]
F_{ms}	Draft gear main spring force	[N]
F_p	Peak force of force reversal	[N]
F_r	Resistive force	[N]
F_{rs}	Draft gear return spring force	[N]
F_t	Locomotive traction force	[N]
F_v	Valley force of force reversal	[N]
g	Acceleration due to gravity	$[m/s^2]$

h	Criteria to count force reversal	
H	Brake pipe air mass flow in all non-longitudinal directions	[kg/m^3·s]
k	Isentropic bulk modulus of air	
k_{ms}	Draft gear main spring stiffness	[N/m]
k_{rs}	Draft gear return spring stiffness	[N/m]
K	Brake cylinder spring constant	[N/m]
L	Brake pipe length	[m]
L_f	Brake pipe equivalent length	[m]
m	Slope of modified Goodman diagram	
m_L	Locomotive mass	[kg]
m_W	Wagon mass	[kg]
$\dot{m}_{bp,i}$	Brake pipe mass flow rate in all non-longitudinal directions	[kg/s]
$\dot{m}_o$	Orifice air mass flow rate	[kg/s]
$\dot{m}_{tot,i}$	Sum total of air mass flow rate (reservoirs and brake cylinders)	[kg/s]
n	Number of iterations	
n_c	Index of air for chambers (reservoirs and brake cylinders)	
N_a	Number of axles per car body	
N_e	Cycle to failure number at knee point of idealized S-N diagram	
N_f	Fatigue notch factor	
$N_{i,j}$	Cycle to fatigue failure number of the force reversal	
$O_{i,j}$	Reversal occurrences	
P	Non-dimensionalized brake pipe pressure	
p	Force peak to be evaluated	[N]
p_0	Brake pipe initial pressure	[Pa]
p_{atm}	Atmospheric pressure	[Pa]
p_{bc}	Brake cylinder pressure	[Pa]
p_{bp}	Brake pipe pressure	[Pa]
p_{hi}	Orifice pressure, high pressure side	[Pa]
p_{in}	Orifice inlet pressure	[Pa]
p_{lo}	Orifice pressure, low pressure side	[Pa]
p_{res}	Reservoir pressure	[Pa]
r	Slope of idealized S-N diagram	
R	Specific gas constant of air	[J/kg·K]

R_i	Track curvature	[m]
Re	Reynolds number	
t	Time	[s]
T	Non-dimensionalized time	
T_{bc}	Brake cylinder air isothermal temperature	[K]
T_{bp}	Brake pipe air isothermal temperature	[K]
T_{in}	Orifice inlet air temperature	[K]
T_{res}	Reservoir air isothermal temperature	[K]
u	Brake pipe air velocity	[m/s]
U	Non-dimensionalized brake pipe air velocity	
V_{bc}	Brake cylinder volume	[m^3]
V_{res}	Reservoir volume	[m^3]
x	Brake pipe longitudinal position	[m]
x_{fd}	Draft gear displacement	[m]
x_{ms0}	Draft gear main spring pre-deflection	[m]
x_{rs0}	Draft gear return spring pre-deflection	[m]
X	Piston position	[m]
$\dot{X}$	Piston velocity	[m/s]
$\ddot{X}$	Piston acceleration	[m/s^2]
$\ddot{X}_L$	Locomotive acceleration	[m/s^2]
$\ddot{X}_W$	Wagon acceleration	[m/s^2]
Z	Non-dimensionalized length	

Greek Letters and Mathematical Operators

$d\_$	Derivative	
$\Delta\_$	Step interval	
$\partial\_$	Partial derivative	
α	Contact angle between wedge shoe and central wedge	[rad]
α_i	Track ramp angle	[rad]
β	Contact angle between wedge shoe and spring seat	[rad]
μ	Viscosity of air	[Pa·s]
μ_i	Friction coefficient per draft gear component interaction	
μ_k	Kinetic friction coefficient	

μ_s	Static friction coefficient	
ξ	Contact angle between wedge shoe and inner stationary plate	[rad]
ν_i	Relative velocity between draft gear components	[m/s]
ψ	Draft gear force coefficient	
ρ	Density of air	[kg/m^3]
η	Venturi factor	
Σ	Summation	

Table of Contents

1 INTRODUCTION

Aiming to introduce the problem, this section discusses the railway transportation sector in Brazil and its importance to the Brazilian economy. It also introduces the air brake system employed in wagons of heavy haul trains and its basic functionality. Lastly, the objective of this work, under which the work shall be evaluated, is stated.

1.1. Heavy Haul Railway Transportation Background

Like most countries throughout the world, Brazil utilizes railway transportation for both goods and passengers. While passenger railway transportation has often been delayed due to political, infrastructure, or funding problems, goods transportation is a critical pillar to the economic success of Brazil and is in high demand. All of Brazil's top three exports are natural resources, with soybeans, crude petroleum, and iron ore, listed in order of value, respectively (OEC, 2018). Each of these three resources is more than double the monetary value of the fourth top export, and each accounts for more than \$20 billion USD. In 2019, Brazil exported 340 million tonnes of iron ore and expects to export over 300 million tonnes of iron ore in 2020 (MINING.COM, 2020), even amongst the economic uncertainties brought about by the COVID-19 pandemic.

Goods transportation in Brazil is accomplished via heavy haul railway transport, which enables cost efficient distribution of products throughout the country, along with road, air, and water transport. The leading benefit to railway transport compared to other modes of goods transport is ultimately the ratio of carrying capacity to fuel costs and carrying capacity to carbon emissions. Each mode of transport has inherent advantages over others based on its application, but road and railway transport service similar applications. As shown in Figure 1, railway transport and road transport are often direct competitors.

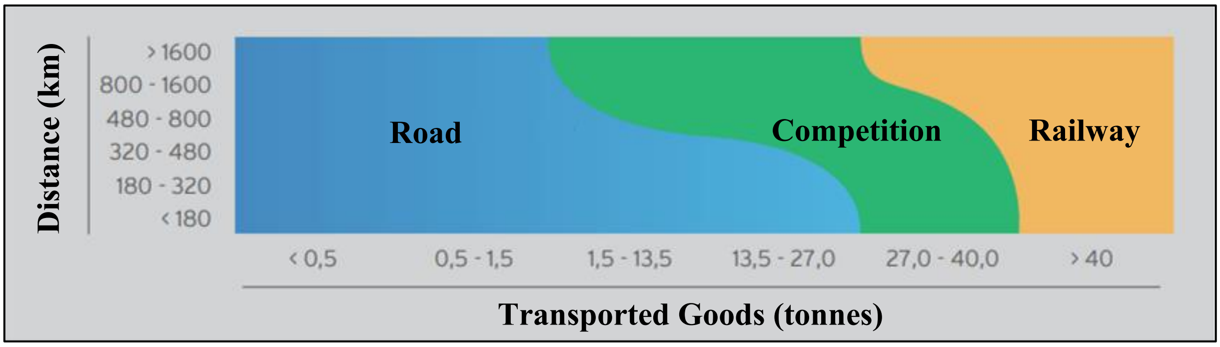

Figure 1 - Market competition between road and railway transport in Brazil. For long distances and high capacity, railway transport is highly competitive. Advancements in railway engineering could lead to a larger market capture. Adapted from: CNT, 2015.

This competition, along with the carry capacity advantages of railway transport, motivates the need to study and improve railway engineering. However, it should be noted that the effectiveness of rail transport does greatly depend on the rail network infrastructure within a country.

Brazil is well situated to utilize railway transport because of its enormous size and widespread population, as well as possessing the 10th longest railway network in the world. As an indicator for potential growth, the density (total length of rail network per area) of Brazil's railway network is only ranked 78th in the world (CNT, 2015). To better understand the potential in Brazil, Figure 2 is provided to demonstrate the necessity and potential of an expanded railway network. The vast majority of the Brazilian population is located in large metropolitan cities, which depend on the efficient transport of goods from desolate or distant sources to the cities scattered throughout the country.

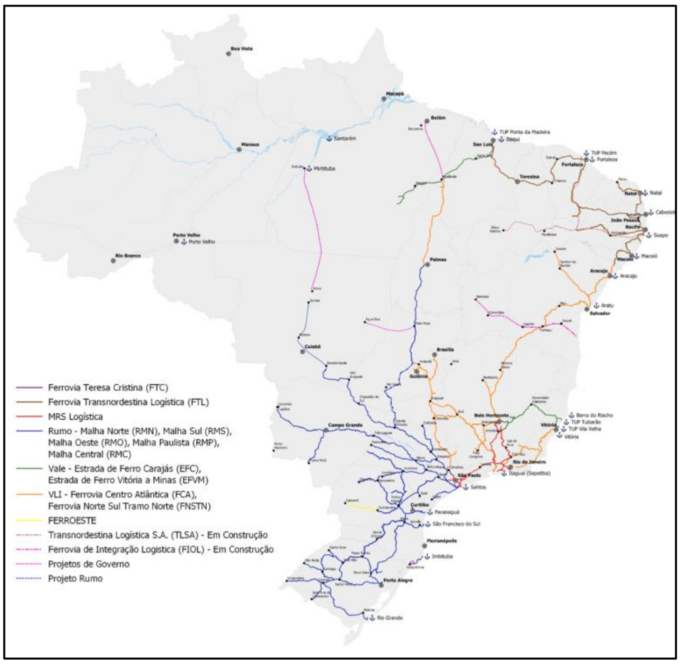

Figure 2 - Railway network of Brazil. Much of the northwestern portion of the country is underserved and provides a growth opportunity for railway service. Source: ANTF, 2019.

Of course, the capacity to grow does not inherently necessitate growth. Economic drivers and market trends ultimately decide where and what market will undergo growth. Recent trends, in terms of goods transported per year, indicate that more goods will be required to be transported in the future, as shown in Figure 3. A means to facilitate the increase in goods transport will be to increase the length of trains or increase wagon carrying capacity, which will stress the current state of technology.

Figure 3 - In 16 years, the increase in TKU (tonnes useful x kilometer) was 133%. This trend indicates higher wagon carrying capacities are to be expected in the future. Adapted from: CNT, 2015.

In addition to the increasing demands of railway transport, the lifetime and longevity of the train components also factors into the prosperity of the railway industry. As of 2015, the expected component lifetime of wagons is only 10 years (CNT, 2015), as shown in Figure 4. This represents nearly half of the life of locomotives and only a quarter of the life of the rails. The discovery of ways to extend the lifetime of wagons would seem to be not only beneficial, but a feasible development objective given the low expected lifetime. By design, wagons make up the bulk of the train composition and therefore present additional potential cost savings by the large quantity.

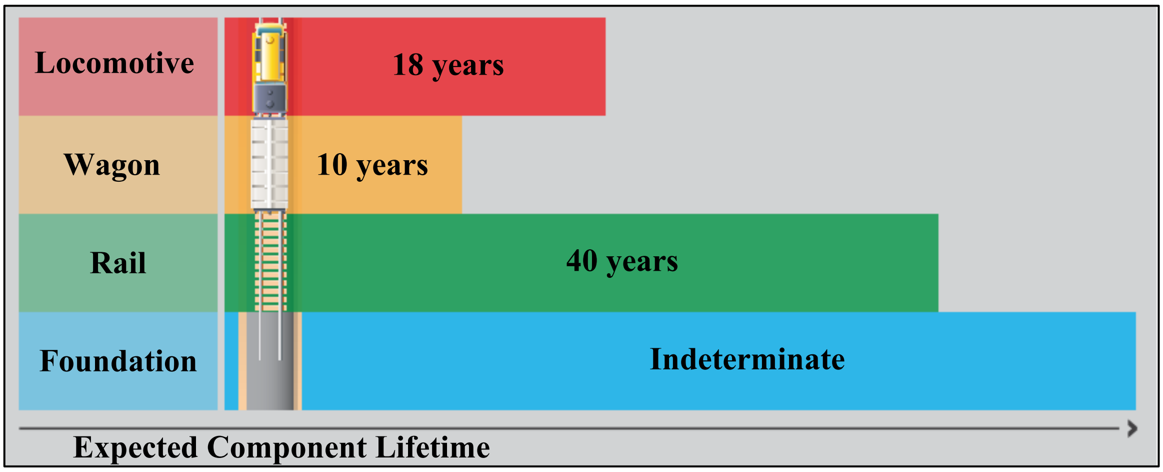

Figure 4 - The overall life of key railway transport components. Wagons, having the lowest lifetime of any key component, could see significant increases in lifetime if performance improvements are discovered. Adapted from: CNT, 2015.

Given these trends, it is the author's opinion that heavy haul railway transport will be even more important in the years to come as higher efficiency is demanded. It is likely that the current infrastructure and railway systems will require improvements and innovation. Thus, railway engineering must receive attention from the research community to enable development and push the railway industry forward. One such area that will require performance improvement is the pneumatic braking system. The pneumatic braking system will require design improvements if industry wishes to increase carrying capacity, increase train composition lengths, improve safety and reliability, or prolong the lifetime and cost efficiency of the train components.

1.2. Pneumatic Air Brake System

The pneumatic air brake system is critical to the safe operation of railway trains. This is even more evident in Brazil, where the majority of heavy haul trains do not implement a combination of pneumatic and electronic braking. For any braking action, either in normal service or in an emergency, the pneumatic air brake system is utilized. Railway trains are composed of at least one locomotive and at least one wagon. However, depending on the use application, trains can be composed of multiple locomotives and are almost always composed of multiple wagons. The locomotives contain the engines and control systems, including the pneumatic air brake system controller, to power the train and pull the trailing wagons. The simple pneumatic air brake layout is shown in Figure 5.

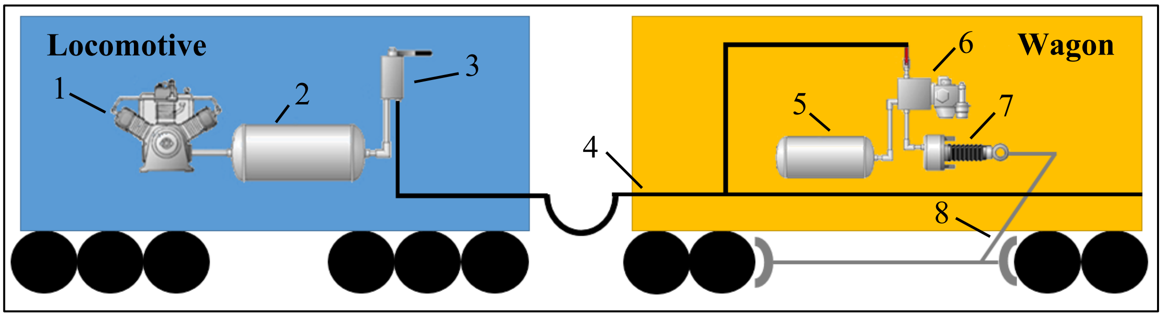

Figure 5 - Simple pneumatic air brake layout of heavy haul railway trains in Brazil. 1 - air compressor; 2 - main reservoir; 3 - driver brake valve; 4 - brake pipe; 5 - air reservoir; 6 - control valve; 7 - brake cylinder; 8 - brake rigging and brake shoes. Adapted from: RIBEIRO, 2017.

The locomotive houses the air compressor, which draws in surrounding air to supply the pneumatic air brake system with a constant source of air. During compression, the air heats up, which requires the air to ultimately be cooled and dried before use in the system. The compressed air is then stored in reservoirs and distributed throughout the train composition via the brake pipe. The locomotive contains the main reservoir and driver brake valve, which are used together to increase or decrease the pressure in the brake pipe and to charge the wagon air reservoirs. The driver brake valve is a complex pneumatic system composed of multiple valves and an equalizing reservoir that enables the train conductor to control the pressure in the brake pipe, and ultimately apply the train brakes. This change in air pressure in the brake pipe is often referred to as the pressure signal. The inner-workings and detailed function of the driver brake valve will not be a focal point of this work, as the wagon pneumatic air brake system is of primary interest. Additionally, the braking system of the locomotives will also not be discussed in this work.

The pressure signal is passed from wagon to wagon in series, from front to back, via the brake pipe and the interconnecting wagon components, known as the angled cock and hose coupling. The wagon pneumatic air brake system is typically composed of a control valve, an air reservoir, a brake cylinder, brake rigging, and brake shoes. Brake pipe and reservoir pressures are typically kept at 90 psi gauge (1 psi = 6894.76 Pa). The control valve senses the pressure signal from the brake pipe and decides whether to apply or to release the brakes. A brake application occurs with a decrease in pressure in the brake pipe, while a brake release occurs with an increase in pressure. A more detailed view of the wagon braking system is shown in Figure 6. To guarantee the wagons remain stationary while not in service, the wagons utilize a manual brake that can be applied by an operator. The manual brake is decoupled from the pneumatic air brake system via chained connections that cannot transmit compressive loads.

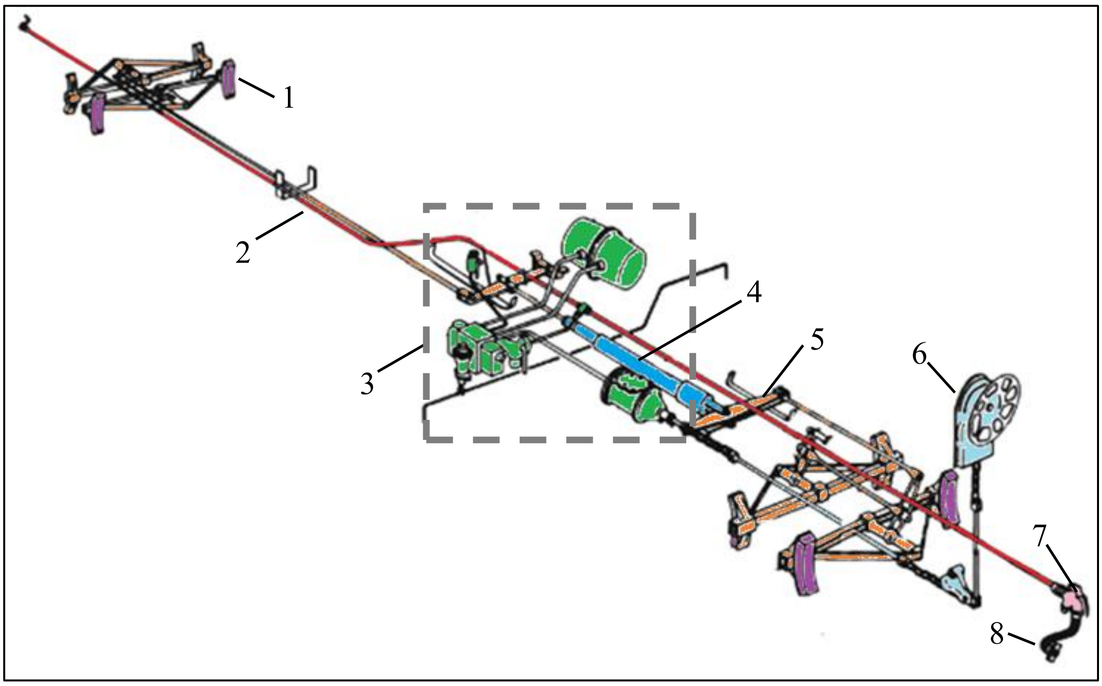

Figure 6 - Common Brazilian heavy-haul wagon brake system layout. 1 - brake shoes (8x, purple); 2 - brake pipe (red); 3 - wagon pneumatic air brake system (green); 4 - slack adjuster (azure); 5 - brake rigging (orange); 6 - manual brake (cyan); 7 - angled cock (pink); 8 - hose coupling (black). Adapted from: LIU, 2017.

In the event of a brake application, the wagon pneumatic air brake system pressurizes the brake cylinder, causing the brake cylinder to extend and push the brake rigging, which then presses the brake shoes onto the wagon wheels. The brake forces applied to the wheels are evenly distributed throughout the wagon via the slack adjuster, an important component within the brake rigging. The magnitude of the brake forces is proportional to the pressure in the brake cylinder. In the event of a brake release, the brake cylinders are evacuated to atmosphere, thereby decreasing the brake forces on the wagon wheels until the brakes are fully disengaged. The relevant pneumatic components and their functions are discussed in more detail below.

The wagon pneumatic air brake system, shown in green in Figure 6, is better illustrated in Figure 7. As previously mentioned, the pressure signal is passed from wagon to wagon via the brake pipe. Each wagon contains a control valve to process the pressure signal, although some wagon configurations share one control valve between two consecutive wagons. There are multiple types of commonly used wagon control valves in Brazil, which will be discussed later in this section.

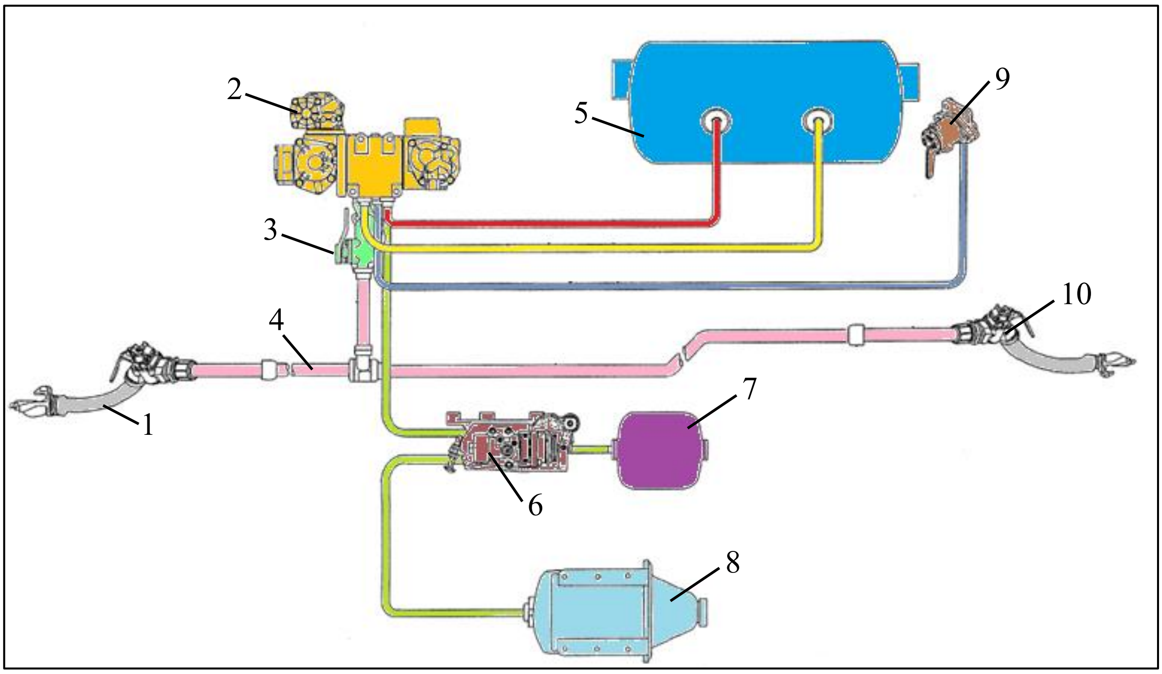

Figure 7 - Common Brazilian wagon pneumatic brake layout. 1 - hose coupling (2x, gray); 2 - wagon control valve (orange); 3 - air filter (green); 4 - brake pipe (pink); 5 - combined wagon air reservoir (blue), emergency reservoir supplied by red pipe, auxiliary reservoir supplied by yellow pipe; 6 - loaded/unloaded valve (maroon); 7 - equalizing volume (purple); 8 - brake cylinder (cyan); 9 - retaining valve (brown); 10 - angled cock (2x, white). Adapted from: LIU, 2017.

The wagon control valve does not just sense the increase or decrease of air pressure in the brake pipe, but also the magnitude of the pressure delta. While the sign of the pressure delta indicates whether to apply or release the brakes, the magnitude of the pressure delta, particularly during a brake application, indicates whether to apply the brakes for a service action or for an emergency action. A large, negative pressure delta results in an emergency brake action, whereas a small, negative pressure delta results in a service brake action. In either brake application situation, service or emergency, the wagon control valve connects the combined tank wagon air reservoir to the brake cylinder. The combined tank wagon air reservoir is so named because it contains two separated, pressurized volumes of air. One of these volumes, often referred to as the auxiliary reservoir, is used during service brake applications, and the other, known as the emergency reservoir, is used during emergency brake applications. In reality, these two reservoirs are not restricted to binary logic, and are often used together regardless of the required action. One example of this is during an emergency brake application, during which both reservoirs supply air to the brake cylinder. It is very important to note that the aforementioned pressure delta is determined by comparing the brake pipe pressure to the auxiliary reservoir pressure.

Once the wagon control valve has connected the combined tank air reservoir to the brake cylinder, the air must first pass through the loaded/unloaded valve. The loaded/unloaded valve detects the weight of the wagon, thereby determining if the wagon has been loaded with goods or is empty. When the wagon is heavily loaded, the maximum brake forces will be required, and the air will pass directly into the brake cylinder. However, if the wagon is empty, maximum braking forces could introduce dynamic instabilities. In the case of an empty or lightly loaded wagon, the loaded/unloaded valve will open to the equalizing volume, thereby reducing the air pressure in the brake cylinder. As expected and intended, this reduced air pressure generates a lower braking force at the wagon wheels.

After a brake application, or even before driving a train on the tracks, the wagon air reservoirs and brake pipe must be recharged. In this condition, the wagon control valve will sense the positive pressure delta in the brake pipe and connect the brake cylinder to the retaining valve. This relieves the brake cylinder to atmosphere. Additionally, the wagon control valve will connect the brake pipe to the wagon air reservoirs to begin recharging the reservoirs. In the event of a service brake application, the emergency reservoir is often used to assist the recharge of the brake pipe and auxiliary reservoir.

The commonly used wagon control valves in Brazil on heavy-haul trains, and those that will be used in this work, are the AB, ABD, and ABDX® control valves. Originally designed and produced by the Westinghouse Air Brake Company, these control valves are now legacy or commercial products of the Wabtec® Corporation. The first of these valves to be introduced into wagons was the AB control valve, shown in Figure 8. The AB control valve enabled more braking actions than the previously existing triple valves. The control valve is separated into two parts, the emergency portion and the service portion. The system consists of numerous valves, orifices, volumes, pistons, and springs to react to the pressure signal from the brake pipe in the desired manner. However, the full design details of each relevant component remain company secrets. Most modeling, as explained later in Section 2, simplifies the valve characteristics to elicit the desired response to the brake pipe signal. The AB control valve enabled improved service and emergency brake applications, improved brake recharging, and simpler system maintenance.

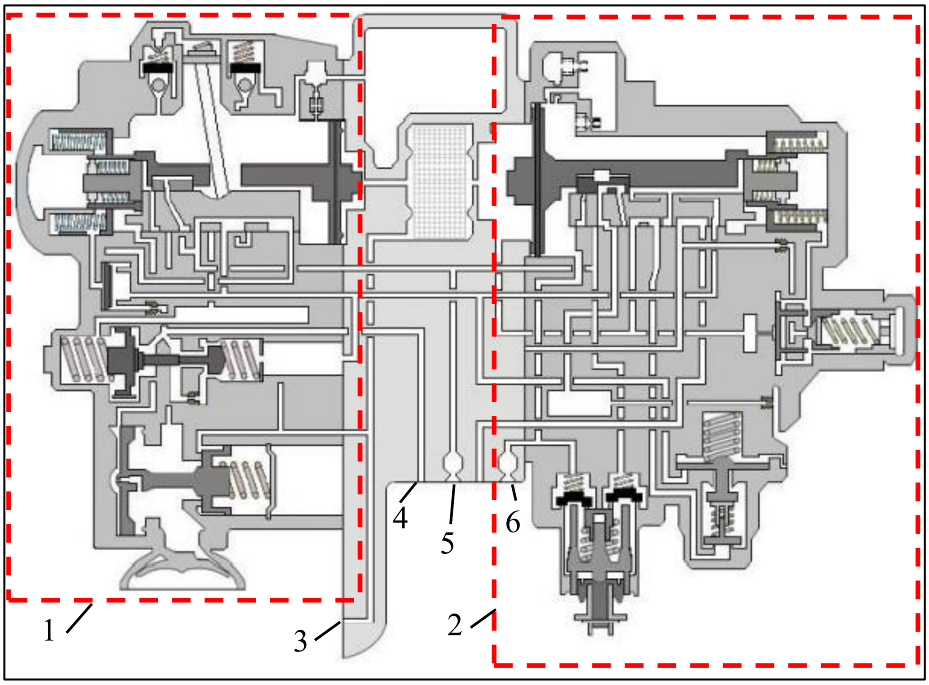

Figure 8 - AB control valve diagram. The AB control valve. 1 - emergency portion; 2 - service portion; 3 - brake pipe port; 4 - brake cylinder port; 5 - auxiliary reservoir port; 6 - emergency reservoir port. Adapted from: RIBEIRO, 2017.

The introduction of the ABD control valve followed that of the AB control valve. The ABD control valve enabled new functionality, as well as improved reliability to reduce the frequency of maintenance. Much of the improvement in reliability and maintenance is attributed to the redesign of the pistons, from a horizontal design to a vertical design. This design change reduced the influence of wheel vibrations and other disturbances caused by the operation of the train. The piston O-rings designed to separate volumes in the AB control valve were replaced by rubber diaphragms in the ABD control valve, thereby reducing the influence of friction on the valve performance. The new functional development introduced with the ABD control valve was the quick relief functionality. The quick relief functionality enabled the control valve to connect the emergency reservoir to the brake pipe to help recharge the brake pipe more quickly during a brake relief action.

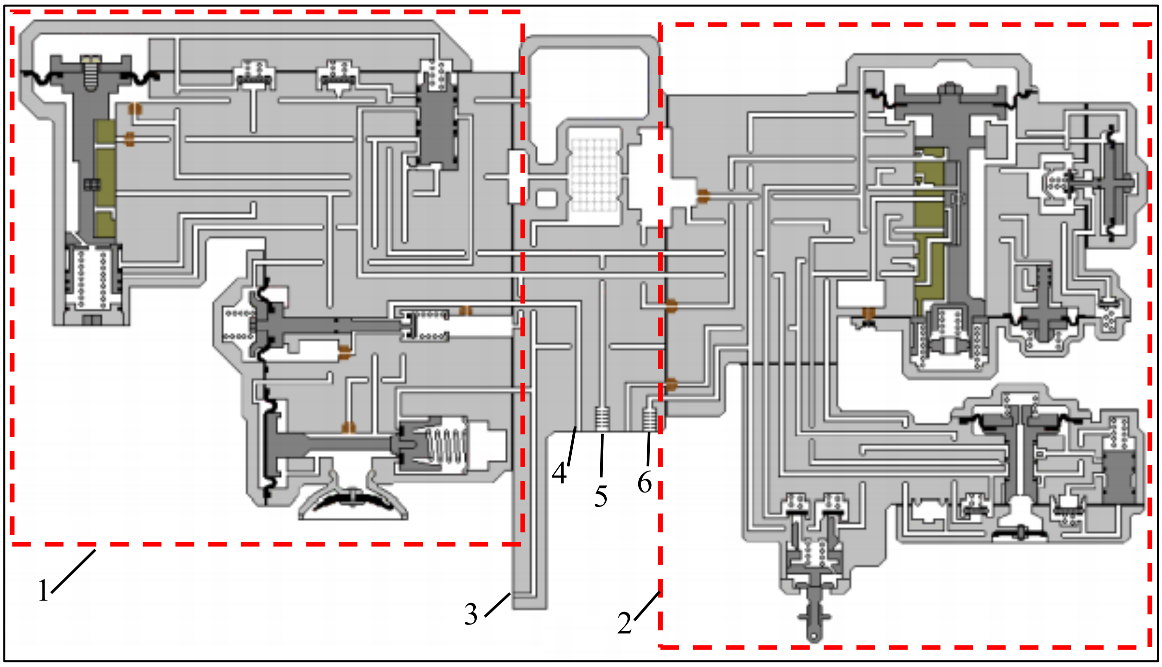

Figure 9 - ABD control valve diagram. The ABD control valve introduced a quick relief functionality. 1 - emergency portion; 2 - service portion; 3 - brake pipe port; 4 - brake cylinder port; 5 - emergency reservoir port; 6 - auxiliary reservoir port. Adapted from: RIBEIRO, 2017.

Before the introduction of the ABDX control valve, an intermediary valve, known as the ABDW control valve, was developed. The ABDW control valve helped speed up the transmission of the pressure signal through the brake pipe by enabling the release of brake pipe air to atmosphere during a service brake application. This functionality in the ABDW control valve was made possible via an externally added component to the ABD control valve. The ABDX control valve was the result of internally integrating this accelerated service application functionality into the emergency portion of the control valve body. The ABDX valve was released in 1989 (RIBEIRO, 2017) and is the preferred wagon control valve for fully pneumatic heavy haul trains today.

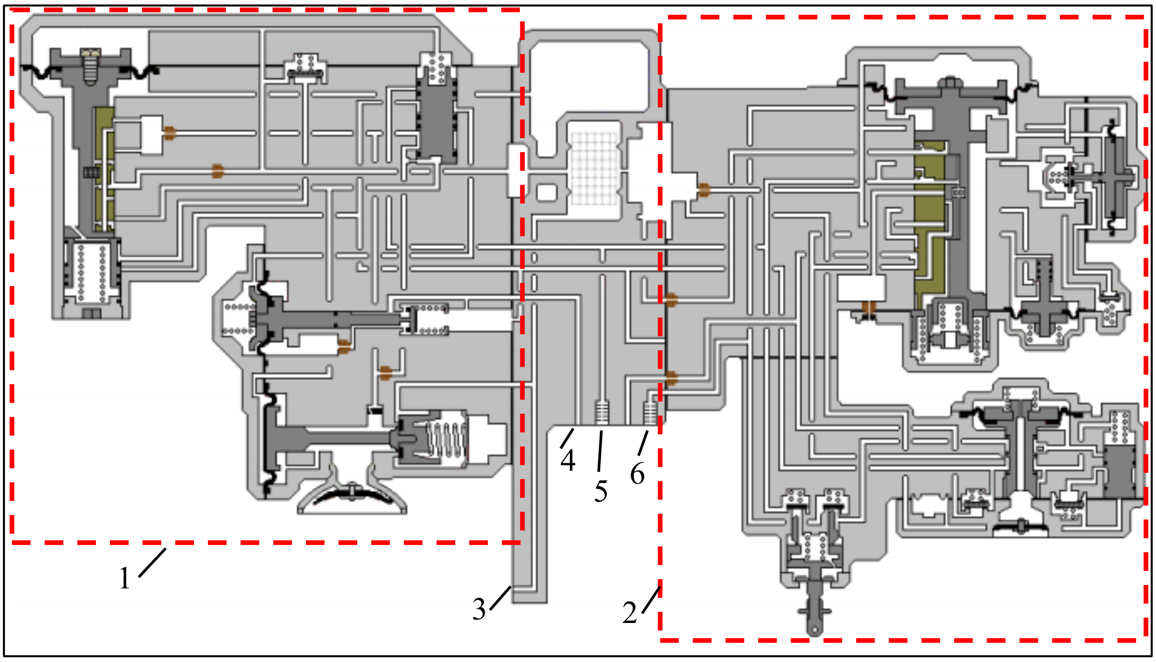

Figure 10 - ABDX control valve diagram. The ABDX control valve introduced an integrated accelerated service application functionality. 1 - emergency portion; 2 - service portion; 3 - brake pipe port; 4 - brake cylinder port; 5 - emergency reservoir port; 6 - auxiliary reservoir port. Adapted from: RIBEIRO, 2017.

1.3. Wagon Connection Device Details

As briefly discussed in the previous section, trains are composed of some combination of locomotives and wagons. The connection devices between the wagons are an integral part of the mechanical architecture and train system functionality. There are two main types of wagon connection devices: couplers and drawbars. Couplers enable two separate wagons to be connected or disconnected via an interlock, as shown in Figure 11, whereas drawbars rigidly connect two separate wagons via a bar. The advantage to drawbars is the reduced amount of slack between the wagons, however, this reduced slack can cause driving issues through tight curves.

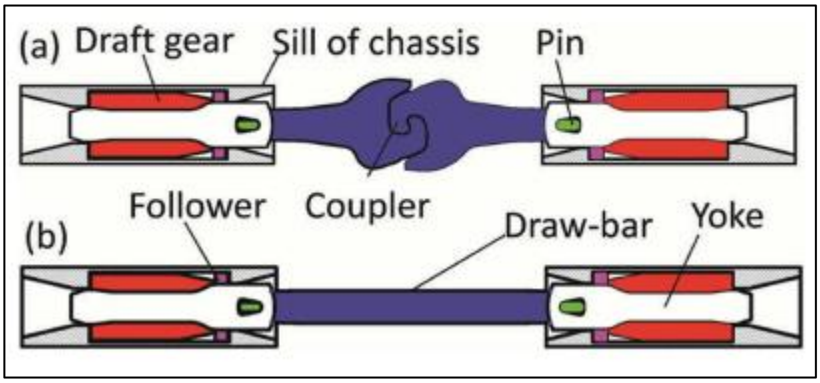

Figure 11 - Wagon connection devices. a - coupler device; b - drawbar device. Source: WU et al., 2020.

Regardless of connection device type, the critical component in relation to in-train forces is the draft gear. The draft gear transmits or dissipates the energy of the wagon connection device when a difference in force is experienced between two adjacent wagons. The differences in forces between adjacent wagons can be caused by any driving or braking action of the train, as well as differences in driving conditions. As described in the previous section, one of the disadvantages of the braking system is the slow transmission of the air pressure signal through the brake pipe. This slow pressure signal contributes to the in-train forces as the front wagons begin to brake sooner than the rear wagons.

The primary types of draft gear in use today are friction draft gears, polymer draft gears, and hydraulic draft gears, as per Wu (2016). While the draft gear can be composed of different materials, the principal energy dissipation mechanism designates the draft gear type. The coupler or drawbar is connected to the yoke via a pin. The draft gear and follower are seated inside the yoke and the sill of the chassis. In the compressive load case, the coupler or drawbar contacts the follower, which compresses the draft gear, and finally transmits the load into the sill of the chassis. In the tensile load case, the coupler or draw bar pulls the pin inside of the yoke, which then pulls the yoke itself. The draft gear seated inside the yoke is then compressed as the follower is pressed up against the sill of the chassis, transmitting the load into the sill. In both the tensile and compressive load cases, the connection devices are designed to always compress the draft gear. An example friction draft gear assembly, consisting of the springs and friction wedge, is shown in Figure 12 below, from Wu (2016). The central wedge generates friction to dissipate the energy generated between the wagons, while the springs reduce the longitudinal forces to help reduce the work done by friction, as well as provide a restoring force.

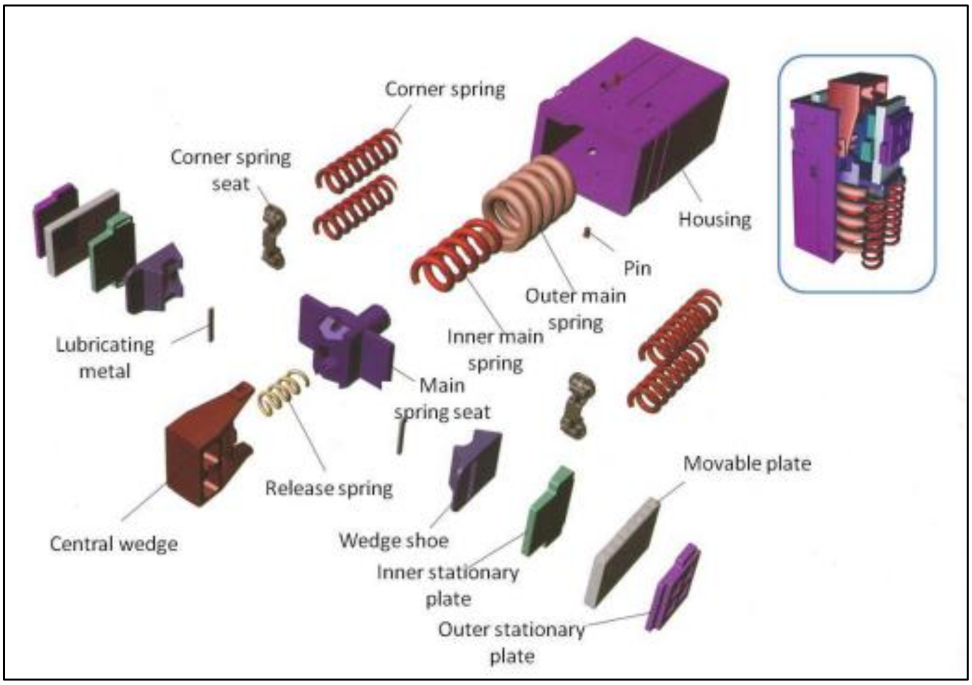

Figure 12 - Example friction draft gear assembly. Source: WU, 2016.

The draft gear is critical in reducing longitudinal shocks that often lead to component failures in the connection devices. Per Wu (2016), most failed components are weakened by fatigue damage over time before eventually succumbing to a large longitudinal shock. Fatigue damage is particularly dangerous as there can be few signs of component degradation, which increases the need to perform frequent maintenance actions or risk field failures. Unsurprisingly, both outcomes increase the operating costs and safety of the railway.

1.4. Pneumatic Air Brake System Design Problems

While previously mentioned, it is important to reiterate the disadvantages of these purely pneumatic braking systems. One of the principal problems to this day of the wagon pneumatic brake system is the slow response times to a brake application or brake release. The limiting factor in each of these situations is the physical limitation of the pressure signal system itself, particularly in long trains. Another problem is that the wagon control valves can only communicate in series, from front to back, thereby exacerbating the pressure signal limitations. Because the system uses pressure deltas and requires the air reservoirs to be recharged, the system is susceptible to conductor errors. Essentially, if a service brake action is demanded before recharging the air reservoirs, the control valve could see additional brake pipe pressure drops and interpret them as brake release signals because the reference pressure in the air reservoir is lower than the brake pipe pressure. Another conductor error that could occur is when a higher brake force is demanded but a lower brake force is applied. This occurs when the air reservoirs have not fully recharged and the control valve sees a reduction in pressure. However, because this reduction in pressure is made without the reference air reservoir fully charged, the pressure delta will be lower and therefore the brake cylinder pressure received from the air reservoir will also be lower. These potential conductor errors can occur in other situations as well, largely because there is no active feedback for the conductor applying or recharging the brakes.

1.5. Thesis Objective

In view of the drawbacks presented, the objective of this work is to investigate design improvements to the wagon pneumatic air brake system in heavy haul freight trains using computational models. The goal of the current study is to evaluate the possibility of reducing detrimental longitudinal shocks between wagons during braking by increasing the brake pipe signal speed, without the addition of electrical wiring between the wagons. This work also aims to enable further study or development, by evaluating the design solution space, of a product that can enable the increase of the brake pipe signal speed.

1.6. Structure of Work

This work is divided into six chapters. The first chapter introduces the pertinent background information of this subject and states the problems to be resolved in this work. The second chapter reviews the state of the scientific literature in this subject and outlines the theoretical modelling approach employed in this work. The third chapter proposes a design solution and describes the methodology used to computationally model the solution. The fourth chapter shows the design development and selection process through computational fluid dynamics and pneumatic modelling. The fifth chapter outlines the test simulations and provides the discussion of the results of the simulations. The sixth chapter summarizes the important conclusions and proposes future work.

2 LITERATURE REVIEW

This section reviews the state of literature regarding railway pneumatic braking systems and potentially relevant system design considerations to improve the overall system performance. The modeling of the wagon pneumatic air brake system common in Brazilian heavy haul transport, adapted from the literature, is also presented.

2.1. State of Literature

The pneumatic braking system on trains had begun to receive attention from the academic research community as early as 1920, with the thesis publication of Wells at the Massachusetts Institute of Technology (MIT) which focused on the history and state of the art of the Type K triple valve. Since that time, the pneumatic braking system has seen drastic improvements in both physical design and theoretical modeling, yet remains open to discovery and improvement.

While this work focuses on the pneumatic air brake system in heavy haul trains, new technologies have been introduced that have improved braking performance for various train types. Both Günay et al. (2020) and Sharma et al (2015) explored the landscape of braking technologies and discussed an approach to determine stopping distance. Each of these technologies introduce the need for an electrical energy source and include electrodynamic braking, electro-pneumatic braking, electromagnetic braking, and aerodynamic braking. In general, these new technologies also depend on an emergency pneumatic air brake system or are used in combination with a pneumatic air brake system. Multiple researchers have studied these braking technologies and the literature available in these technologies is vast. However, the main motivation to focus on the pneumatic air brake system in this work is that the cost to implement these solutions into Brazilian heavy haul trains is currently considered too high.

A potential source of design improvements could be found in the literature of the pneumatic brake system of commercial vehicles, like in the work done by Subramanian (2004). The brake systems of commercial vehicles are like those of heavy haul trains, as they also use compressed air, stored in reservoirs, to control and actuate brake cylinders. However, because commercial vehicles are much shorter and lighter than heavy haul trains, most of their design advantages are unfortunately not applicable to heavy haul trains. Some of the advantages include the use of a relay valve to accelerate the application of the rear brakes and a dual circuit system to guarantee partial braking in the event of a failure in one part of the pneumatic circuit.

While the application of design solutions in commercial vehicles are not easily transferrable, the underlying physics, modeling, and experimental techniques are useful to furthering development of pneumatic air brake systems in heavy haul trains.

The primary focus of the literature review will be on the pneumatic brake system modeling, pneumatic brake system experimental set-ups, and potential design applications or improvements.

2.1.1. Pneumatic Brake Systems

With respect to the development of modeling the braking systems of trains, a good starting point is the work of Wu et al. (2016). The authors discuss the historical approach to modeling train longitudinal dynamics, air brake system models, vehicle connection models, locomotive models, in-train instability models, computing schemes, and more. According to them, the evolution of the air brake models started with analytical and electric analog models between the 1930s and 1960s that determined the largest in-train braking forces. They also mentioned the models of Wikander and Grebenyuk, developed separately, used the ascending time of the brake cylinder and the maximum forces applied by the brake cylinder to develop mass-spring like equations. The authors discussed Lazaryan, who developed electric analog models utilizing voltages, resistances, and elastances.

The authors then wrote of the empirical modeling introduced by Kuzmina in the 1960s, who used an empirical parameter along with the brake delay time and maximum brake force to determine the braking forces in the locomotive. Later they discussed Martin and Hay, who used look up tables of empirical data to specify the brake cylinder pressure in the individual wagons. The later work of Grebenyuk was discussed, who also used look up tables of empirical data and piece-wise equations based on time to determine the wagon brake cylinder pressures. The empirical models had been combined with other vehicle dynamics models, likely to minimize the computational cost whiling maintaining acceptable braking system accuracy.

In Funk and Robe (1970), the authors developed a model based on the Navier-Stokes (NS) equations to describe the pressure transient response of air in a transmission tube connected to a chamber. The models compared the transient response of air using an isothermal assumption and an adiabatic, reversible assumption. Along with the model assumptions, the authors compared large pressure changes (Δ 60 psi) to small pressure changes (Δ 1 psi) to determine the effectiveness of their models and assumptions. Their work largely founded the basis of all subsequent pneumatic air brake models to follow in the research community.

Bharath et al. (1990) extended the work of Funk and Robe, by first adding more chambers in series in an attempt to simulate the brake pipe and brake cylinders throughout the length of a train. The transient models were solved using the same techniques and compared against experimental data, finding that an isothermal flow assumption was more appropriate for the brake pipe analysis. The pressure wave amplitude was found to slow throughout the length of the brake pipe, with turbulent wall shear stresses considered the likely culprit. In a follow up paper (1990a), the authors improved their modeling to include an auxiliary reservoir and brake cylinders with spring preload to better characterize the true pneumatic brake system. The models agreed with the experimental results, but did have some errors and inaccuracies such as the exclusion of branch pipe equations in the model. Another error in the models that the authors noticed was that the pressure rise was slower in the brake cylinders at the rear of the train. Leakage was considered to be the largest contributor to that effect.

In a similar fashion to Bharath et al., Murtaza and Garg (1989) were developing models to represent the pneumatic air brake system of Indian heavy haul trains based on the works of Funk and Robe. The models included some improvements, like including models for the wagon control valves and accounting for bends and cocks in the pipes. Unlike Bharath et al.'s brake cylinder modeling, which used spring-mass-damper equations, Murtaza and Garg used empirical brake cylinder models dependent on only pressure and time along with a pressure change over time equation. The modeling results agreed with the experimental results, and showed that a polytropic process best describes small pressure changes. For larger pressure changes, an isothermal process was more accurate. The model results also showed a faster pressure rise throughout the system compared to the experimental results, which was thought to be the result of frictional losses and spring stiffness variations in the control valve of the experimental set-up.

A new approach to modeling the pneumatic air brake system in European trains was undertaken by Pugi et al. (2004), with the objective to provide a |modeling library for Matlab-Simulink. The models simplified the pneumatic system into a series of pneumatic components consisting of orifices, chambers, and cylinders. The wagon control valve used in the models was the Westinghouse U Distributor and included the first phase device that accelerated the brake pipe signal in downline wagons. The brake pipe pressure was determined using the Navier-Stokes equations, as had become commonplace in pneumatic brake system models. The pressures in the brake cylinders were converted into braking forces to determine the effects on the longitudinal dynamic behavior of the train during braking. The modeling results agreed with the experimental resumeasuremetns and provided one more step to accurately simulating the pneumatic air brake system with rapid braking. The model assumed isothermal processes, which simplified much of the analysis. This simplification soon became the standard in the air brake modeling community.

Cantone et al. (2009) developed a pneumatic braking model for European passenger trains. The brake pipe was modeled using the conservation equations, while the other components in the pneumatic system were modeled using lump parameter equations. The model included a driver brake valve which was represented as a nozzle. The nozzle equivalent diameter was adapted to predict either emergency, service, or release actions. The authors compared the model results to experimental results obtained from the Faivelay Transport Italia test facility. The paper studied the effects of changing the driver brake valve location, as well as the amount of driver brake valves throughout the train. Additionally, the authors analyzed various braking maneuvers, including steady state and transient brake application and release, to determine the robustness of the model. The results from the pneumatic air brake models were then input to a dynamic model to determine the longitudinal forces in the train couplings.

Afshari et al. (2012) and Specchia, et al. (2012) presented an intricate model that combined the driver brake valve, brake pipe, wagon pneumatics, and brake forces to predict the longitudinal train behavior. The driver brake valve was simplified into three active components: the regulating valve, the relay valve, and the brake pipe cutoff valve. Each of these valves was modelled to minimize computational time and were described for brake application and release. Only the brake pipe model utilized the conservation equations (continuity and momentum) to model the changes in pressure mandated by the driver brake valve position. The wagon pneumatics were simplified to include only the supply reservoir, emergency reservoir, wagon control valve and brake cylinder. The control valve was a triple valve capable of apply, release, and lap positions. Finally, the brake force was determined using the brake cylinder displacements and the brake rigging efficiency and leverage. The complicated train dynamics were modelled using trajectory coordinates and the equations of motion. The equations were converted to first order ordinary differential equations, integrated together, and solved simultaneously using a finite element method. The models were compared to existing experimental data in literature and accurately predicted select train behavior.

Around the same time as the previously discussed Italian researchers were advancing the heavy haul freight train modeling community, Wei and his colleagues (2008, 2014, 2015, 2017) began to develop models of Chinese trains. In 2008, they developed a model of the pneumatic air brake system using the 120 control valve and unique modeling techniques to account for frictional losses and branch pipe conditions. The locomotive was modeled as a wagon but utilized a force amplifying term to account for the higher loads required to stop the locomotive. The models were simulated for train lengths of 40 and 120 wagons under various braking conditions. The results of the simulations and experiments showed some inconsistencies in the rear wagons during small service brake applications. The rear wagon brake cylinders increased at a slower rate than the front wagons and also equalized at lower pressures, causing the rear wagon to enter the lapping mode earlier. The pneumatic air brake model was refined, with new findings published in 2017. Modeling improvements were made to the locomotive driver brake valve and a more detailed wagon control valve was developed. The influence of the accelerated release portion in the wagon control valve was much more noticeable, with the pressure drop speed in the rear wagons closer in performance to the front wagons, although still slower.

In the decade after their first publication, Wei et al. began to integrate longitudinal dynamics models of the train with the pneumatic air brake model (2014, 2015). The longitudinal dynamics model was based on the sum of forces experienced by the train mass, including inertial forces, coupler forces, air brake forces, grade resistance forces, curve resistance forces, running resistance forces, and dynamic brake forces. The model simulation results showed a significant influence of air friction in the brake pipe on the coupler forces, when compared to a frictionless brake pipe. Another interesting conclusion from the simulations was made about the coupler force profile along the train over time. For the first 100 seconds, the forces experienced by the couplers for the front and wear wagons were low, whereas the couplers for the intermediate wagons experienced high oscillating forces. After the first 100 seconds, the forces in the front wagon couplers rapidly increased, overtaking the amplitude of the oscillating intermediate coupler forces. Interestingly, the rear wagons did not experience nearly any longitudinal shocks during the entire duration of the braking action.

Perhaps the most detailed pneumatic air brake model in heavy haul trains was developed by Wu et al. (2017). While the brake pipe modeling was similar to previous models, brake pipe connections between wagons were taken into consideration with the use of a pressure loss coefficient and pressure losses were accounted for in the brake pipe tee. The wagon control valve modeling was finely detailed, and included a model of the service piston, sliding valve, and graduating valve. An interesting observation from the simulation and experimental results was that the quick service feature does not activate in the event of an emergency brake application, as the pressure changes are too quick for it to activate. The authors attributed four factors to discrepancies in the model and the experimental results, those being pressure loss modeling in the boundary conditions, pipe wall friction modeling, temperature modeling, and brake pipe leakage. A prevalent issue with pneumatic air brake models is their high computational cost, particularly when combined with longitudinal dynamics models. Wu and Cole tackled the computation problem by implementing three different computing schemes using different numbers of central processing unit (CPU) cores. The three computing schemes, the conventional sequential scheme, a parallel scheme, and a hybrid scheme, were compared by CPU efficiency and execution time. The parallel scheme worsened the computational cost when compared to the conventional sequential scheme, however the hybrid scheme showed a 30% improvement.

Teodoro et al. (2018) developed models, adapted to Brazilian trains, that compared the computational cost of using the NS equations against a lumped parameter simplification on the brake pipe. The lumped parameter simplification of the brake pipe breaks down the individual wagon brake pipes into a series of chambers interconnected via orifices that can be sized to account for the appropriate flow resistance. In addition to these two methodologies, the brake pipe NS equations were solved, and the results compared, using a Runge-Kutta method and an Euler method. The braking system performance and errors were compared to show that the lumped parameter modeling produced results similar to the NS modeling methodology, but in significantly less time. The next step taken by Teodoro et al. (2019) was to implement a parallel computing scheme in order to determine in-train forces for a concurrently running dynamic model. A brake schedule along an existing train route was used for the simulation parameters. In the parallel computing scheme, the CPUs were able to access the same information at the same time via open Multi-Processing (openMP). This methodology resolves the issue with Wu and Cole's parallel computing scheme, and resulted in an 80% reduction in the CPU processing time.

2.1.2. Pneumatic Brake System Experimental Set-ups

Abdol-Hamid´s (1986) doctoral dissertation was one of the first works dedicated to experimentally validating locomotive, brake pipe, and control valve (ABD and ABDW) models. The brake pipe set up included the main reservoir, the driver brake valve (26C locomotive valve), the equalizing reservoir, four pressure transducers, a linear variable differential transducer (LVDT), and a differential pressure transducer. The four pressure transducers were placed at the head end and read of the brake pipe, the inlet of the driver brake valve, and the equalizing reservoir. A full service application and a recharge application were tested, finding the finite element modeling technique to be the most accurate but most computationally demanding. Two additional experimental set-ups were used to validate the control valve modeling, but unfortunately were not depicted well. These set-ups also used a full service application and a recharge application, and measured the brake cylinder pressure, the auxiliary and emergency reservoir pressures, as well as the brake pipe pressure. One of the interesting conclusions from the experiments was that the brake pipe followed a polytropic process rather than isothermal. Leakage throughout the system was also a major concern.

To validate their own pneumatic air brake models in European trains, Piechowiak (2009) developed a novel experimental test rig. A potentially useful temperature measurement technique utilized pressure sensors to indirectly measure temperature. The pressure was measured between volumes separated by orifices until stabilization was reached, since the temperatures would be equal when the pressures stabilized. Combining the heat exchange coefficient of the reservoirs and cylinders with the measurements, the temperature is found via the conservation of mass and the ideal gas law. The test rig included a source pipe, a brake pipe, a driver brake valve, reservoirs, wagon control valves, brake cylinders, a section of additional brake pipe with a branched pipe tee. Three independent test set ups were also built, to enable better characterization of the brake pipe, the brake cylinders, and the brake rigging, respectively. The experimental results matched well with the simulation results. However, some modifications were required to properly simulate the hysteresis within the control valves that the authors attributed to friction, spring constants, and membrane deformations. Additionally, the sensitivity of the driver brake valve was determined during a service brake application.

Two authors that constructed experimental set ups to determine the response times of pneumatic circuits were Gu et al. (2019) and Yang et al. (2017). Like many of the previously discussed authors, their objectives were to validate pneumatic models via experimentation. Interestingly, both researchers utilized a precision pressure regulator upstream of a buffer tank, followed by an upstream solenoid valve, as a means to simplify the driver brake valve and better control the experiments. Pressure sensors were used at the front and rear of the brake pipe. Both experiments demonstrated a significant pressure response time dependence on brake pipe length, while Yang found little influence on pressure response time from the brake pipe diameter. The location of the different orifice sizes also impacted the pressure response time of the brake pipe, resulting in a faster pressure response time if the upstream orifice is larger than the downstream orifice. To determine the flow characteristics of different pneumatic circuits and orifices, Yang et al. (2015) built separate test stands. The upstream constant pressure test stand did not include a buffer tank and solenoid valve, but rather an FRL unit upstream of a precision pressure regulator. The flowrate characteristics test stand did not utilize the FRL unit, relying only on a precision pressure regulator. Each test stand utilized an inline flow meter and a temperature sensor at the inlet of the pipe. The results of these experiments were used to calculate the sonic conductance and critical back-pressure ratio of the pneumatic components.

An experiment to describe the response time parameters of a solenoid valve was carried out by Venkataraman et al. (2013) to determine the feasibility of solenoid valves in pneumatic applications. The solenoid valve in question was a 3/2 normally closed (NC) valve, with two different orifice diameters. The experimental set up consisted of an air reservoir, a pressure regulator, a connecting tube, and a pressure transducer in line with the solenoid valve of interest. The solenoid valve was turned on and off, and the pressure response time was measured for ramp up and ramp down scenarios. At higher pressures, the ramp up and ramp down time was higher than at lower pressures, and especially for the smaller orifice diameter. However, the study indicates that solenoid valves can be well characterized when releasing to atmosphere, and this information could prove useful for future pneumatic test stands.

2.1.3. Potential Design Applications or Improvements

One of the only studies into design improvements of the pneumatic air brake system on heavy haul trains in Australia was performed by Cole and Ripley (2006). A main difference between the Australian system and the Brazilian/American system is the method to quickly deliver air to the brake cylinder. The Australian system uses a bulb in the wagon control valve to equalize with the pressure in the brake pipe, and also sends some brake pipe air directly to the brake cylinder, thereby speeding up the propagation of the pressure signal in the brake pipe. However, once the bulb has filled, it cannot assist any subsequent brake applications. The Brazilian/American system utilizes the rapid service portion that evacuates the brake pipe to atmosphere, as discussed in the Section 241.2. The authors found that increasing the bulb size of the control valve did not improve signal propagation because of internal restrictions. Along with small optimizations in pipe dimensions, an alternative finding to improve the signal propagation would be to connect the control valve at a different port other than the designed pipe bracket connection.

A study by Azzi et al. (2019) investigated the performance differences between pneumatic seals in pistons, and in particular U-cups, X-rings, O-rings, and Rod-Scrappers. The authors tested the effects on friction of the piston rod velocity, the air pressure, the seal diameter, and the seal design. A few important outcomes of the experimental tests included the fact that the frictional force increases in all seal types with air pressure and stroke velocity. Another important outcome was that the U-cups only provided superior friction results at lower pressures in the range of 1-2 bars. At higher pressures, the O-ring, and even the X-ring, performed much better.

Labyrinth seals are often considered a potential solution to pneumatic systems in order to optimize pressures or flows or even to simplify complex systems. Wang et al. (2016) developed a prototype labyrinth passage to study the effects of a series passage versus a parallel passage and to validate their simulation models. The passages consisted of sharp, right angle turns that expanded into slightly larger volumes to avoid cavitation of the studied fluid. The modeling and experimental results showed the series passage to outperform the parallel passage with respect to the pressure drop through the labyrinth. However, the parallel passage labyrinth was shown to control the flow rate better.

Because most heavy haul freight trains are purely pneumatic, electrical energy sources are not available to enable electro-pneumatic design options. One solution to this problem is to add energy harvesting mechanisms to the unpowered wagons that store energy generated from vibrations or other wagon motions. Gao et al. (2019) summarized many of the previously studied energy harvesting mechanisms, including thermoelectric, piezoelectric, and electromagnetic devices. They also modeled and developed a fan-shaped pendulum-resonance-based electromagnetic energy harvester with a maximum input voltage of 6.6V and a DC-DC output voltage of 4.7V. The energy conversion efficiency of their prototype device was between 40-65%, capable of supporting a sensor with a maximum power consumption of 75mW. Another energy harvesting device designed for the use in heavy haul freight trains was a piezoelectric “Zigzag” structure by Santos et al. (2018). The piezoelectric device was optimized for use in wagons that are loaded or unloaded, encompassing the conditions of an iron ore route. The output power of this energy harvester was 9.27mW in the unloaded wagon configuration and 3.7mW in the loaded wagon configuration.

While energy harvesting applications can open the solution space to new architectures and designs, shape memory alloys (SMAs) could also facilitate new, creative solutions. An exhaustive review of high temperature SMAs currently available or studied was released by Ma et al in 2010. SMAs are capable of returning to a preformed shape upon application of heat and are able to recover high amounts of strain as a result of mechanical stress. These phenomena occur because of a reversible martensitic transformation in the material. A few alloys are presented that exhibit 100% strain recovery rate at temperatures up to 200°C, including U-Nb, Ti-Ni-Hf, Ti-Ni-Pd, Ti-Ni-Au, and Ti-Ni-Pt. The temperature range of these alloys is apt for the temperatures experienced by the brake shoes of heavy haul freight trains during braking actions as measured by Walia et al. (2019).

A potential pneumatic design application is the use of venture effect structures, like those studied by Xu et al. (2016) in powder ejector applications. Instead of traditional single venturi effect particle ejectors, Xu et al. also studied the effects of double venturi effect particle ejectors. The double venturi effect generates two vacuum fields as opposed to the one vacuum field generated by a single venturi effect. This results in both larger pressure drops in the double venturi and higher fluid velocities. The optimal nozzle position inside the venturi chamber was experimentally tested with respect to pressure drop, fluid velocity, and particle deposition. Along with the optimization approach, the authors determined that higher nozzle pressures would increase the venturi nozzle performance.

2.1.4. Longitudinal Train Dynamics (LTD)

A comprehensive overview of longitudinal train dynamics was published by Cole et al. (2017). The initial study of longitudinal train dynamics was believed to be motivated by the need to improve the passenger comfort in passenger trains. Later, the study of longitudinal train dynamics in heavy haul trains began and was motivated by the increasing train lengths implemented in the field at the time. The general approach to modeling longitudinal train dynamics is to separate the locomotives and wagons into masses that are connected by elements and experience longitudinal forces. The modeling of the draft gears depends on the type of draft gear, but is guided by loading and unloading curves that are either experimentally measured or theoretically derived. The in-train forces experienced by the masses include the locomotive traction, locomotive dynamic braking, propulsion resistance, curving resistance, gravitational forces, and the wagon pneumatic brake forces.

Modeling the longitudinal dynamics and draft gears was expertly detailed in Wu's (2016) doctoral thesis. Multiple types of draft gears were modeled, including three types of friction draft gears, two types of polymer draft gears, and one friction-polymer draft gear. The draft gears models are segmented into four distinct working processes dependent upon the draft gear type. These segments are the loading stage, with and without the plate group contributing, and the unloading stage, with and without the plate group contributing. For friction draft gears, the force-displacement (F-D) characteristics, the friction model, and the locked stiffness model are the critical components that must be defined. These draft gear models are incorporated into a full train longitudinal dynamics model to later determine their fatigue damage characteristics and to optimize the draft gear design.

Similar to the work of Wu and Cole, Eckert et al. (2021) developed a longitudinal dynamics model based on the train compositions and track conditions of Brazil. The model utilized a friction draft gear that had four working processes and was based on a MARK50 draft gear. A computationally efficient pneumatic brake model was used in the longitudinal dynamics model to compare the simulation time to the prior work of Wu et al. An ODE1 (Euler) integrator was used in the Simulink model because the time steps were small. The simulation followed a brake schedule and logged the in-train forces of various wagons, noting that the pneumatic brake signal delay contributed to longitudinal shocks.

Bowey et al. (2017) instrumented drawbars on trains in Western Australia to measure the in-train forces of the wagons during mainline operation and dumping operations. The authors utilized a rain-flow algorithm to break the in-train forces into individual loading and unloading cycles. A fatigue index was developed using a power three weighting system based on an Australian standard for steel structures to compare the conditions of individual wagon draft gears. The tensile forces were considered to be more significant with respect to component damage, and were found to contribute three times more to damage during dumping than during mainline operation.

The study of draft gear optimizations to prevent fatigue damage has been led by Wu et al. (2017 & 2020). Like Bowey et al., Wu et al. developed a rain-flow algorithm to assess the loading and unloading cycles of the in-train forces. In each paper, the authors ran whole-train simulations and examined the fatigue life of the draft gears. One optimization technique focused on the configuration of the wagon packs, finding that packs of four wagons connected by drawbars outperformed both packs of two wagons connected by drawbars and packs of one wagon connected by drawbars. The other optimization technique focused on using both a genetic algorithm and a particle swarm optimization to converge on friction draft gear variables that provided improved fatigue life. The optimization results showed a performance trade-off existed between fatigue damage improvements and wagon accelerations.

2.2. Pneumatic Air Brake System Modeling

Of the pneumatic models discussed in the previous section, the most pertinent model is that of Pugi et al., which was adapted to Brazilian heavy haul freight trains by Teodoro et al. The model simplifies the pneumatic brake system into three pneumatic components: orifices, reservoirs, and brake cylinders, and uses the Navier Stokes equations to calculate the brake pipe pressure and velocity. A schematic of the model is shown in Figure 13 below. The objective of the model is to quickly aid and support pneumatic design decisions or alterations.

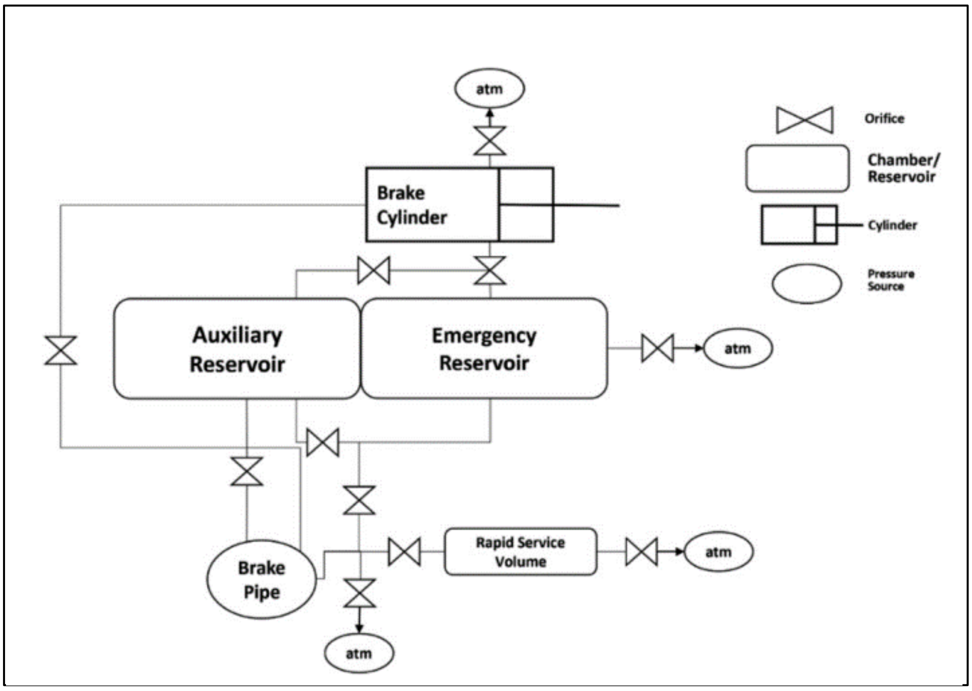

Figure 13 - Pneumatic model schematic diagram. Source: ECKERT et al., 2021.

2.2.1. Orifice Modeling

The orifices are used to connect different components and can be static or switched on and off depending on the system state. The orifices govern the mass flow rate of air, $\dot{m}_o$, into or out of reservoirs, brake cylinders, control valve components, and the brake pipe using Equation (1)

$$\dot{m}_o = A_o C_m C_q \frac{p_{in}}{\sqrt{T_{in}}} \tag{1}$$

where A_o is the orifice area, p_{in} is the orifice inlet pressure, T_{in} is the orifice inlet air temperature, and C_m and C_q are correction factors.

The Mach correction factor for mass flow through an orifice, C_m, is given by Equation (2)

$$C_m = \begin{cases} \sqrt{\frac{2\gamma}{R(\gamma-1)}\left[\left(\frac{p_{lo}}{p_{hi}}\right)^{\frac{2}{\gamma}} - \left(\frac{p_{lo}}{p_{hi}}\right)^{\frac{\gamma+1}{\gamma}}\right]}, & subsonic \\ \sqrt{\frac{\gamma}{R}\left(\frac{2}{\gamma+1}\right)^{\frac{\gamma+1}{\gamma-1}}}, & sonic \\ \sqrt{\frac{2\gamma}{R(\gamma+1)}}\left(\frac{2}{\gamma+1}\right)^{\frac{1}{\gamma-1}}, & supersonic \end{cases} \tag{2}$$

where R is the specific gas constant of air, γ is the heat capacity ratio of air, p_{lo} is the orifice pressure on the low pressure side, and p_{hi} is the orifice pressure on the high pressure side.

Because the real flow is not isentropic, an empirical correction factor for the mass flow through an orifice, C_q, is used as shown by Equation (3).

$$C_q = 0.814 - 0.1002\left(\frac{p_{lo}}{p_{hi}}\right) + 0.8415\left(\frac{p_{lo}}{p_{hi}}\right)^2 - 3.9\left(\frac{p_{lo}}{p_{hi}}\right)^3 + \cdots \\ 4.6001\left(\frac{p_{lo}}{p_{hi}}\right)^4 - 1.6827\left(\frac{p_{lo}}{p_{hi}}\right)^5 \tag{3}$$

2.2.2. Reservoir Modeling

The reservoirs are static chambers that contain a volume of air and a pressure. Equation (4) can be integrated to find the reservoir pressure, p_{res}, for a given static volume, V_{res},

$$\frac{\partial p_{res}}{\partial t} = \frac{n_c R T_{res} \sum_{i=1}^{n} \dot{m}_{tot,i}}{V_{res}} \tag{4}$$

where t is time, n_c is an index of air for chambers (value between 1 and 1.4), T_{res} is the temperature of the air in the reservoir, and $\dot{m}_{tot,i}$ is the sum total of the mass flow rate (total) into and out of the reservoir.

Implementing Euler's method, Equation (5) can be used to determine the reservoir pressure.

$$p_{res,t} = p_{res,t-1} + \frac{\Delta t n_c R T_{res} \sum_{i=1}^{n} \dot{m}_{tot,i}}{V_{res}} \tag{5}$$

2.2.3. Brake Cylinder Modeling

The brake cylinders are dynamic chambers that can expand or retract based on the position of an internal piston. The piston is attached to a restoring spring that opposes the expansion of the cylinder volume.

Using the equations of motion, the brake cylinder system is described by Equation (6)

$$M\ddot{X}_{t+\Delta t} = A_p(p_{bc} - p_{atm}) - C\dot{X}_t - KX_t \tag{6}$$

where M is the piston mass, A_p is the area of the piston, p_{bc} is the brake cylinder pressure, p_{atm} is atmospheric pressure, C is the damping coefficient due to friction, K is the spring constant, t is time, and X, $\dot{X}$, and $\ddot{X}$ are the piston position, velocity, and acceleration, respectively.

The piston position and velocity can be calculated using Euler's method, as shown in Equations (7) and (8).

$$\dot{X}_{t+\Delta t} = \dot{X}_t + \ddot{X}_{t+\Delta t}dt \tag{7}$$

$$X_{t+\Delta t} = X_t + \dot{X}_{t+\Delta t}dt \tag{8}$$

The pressure in the brake cylinders is determined using the same methodology as the reservoirs and shown in Equation (9)

$$\frac{\partial p_{bc}V_{bc}}{\partial t} = n_c RT_{bc} \sum_{i=1}^{n} \dot{m}_{tot,i} \tag{9}$$

where p_{bc} is the pressure in the brake cylinder, V_{bc} is the brake cylinder volume, and T_{bc} is the temperature of the air in the brake cylinder. Because the piston position in the brake cylinder influences the volume, Equation (10) is used

$$\frac{\partial p_{bc}A_pX}{\partial t} = n_c RT_{bc} \sum_{i=1}^{n} \dot{m}_{tot,i} \tag{10}$$

where A_p is the area of the piston.

Assuming that the area of the piston is unchanged, the pressure in the brake cylinder can be determined using Equation (11) below.

$$p_{bc,t} = \frac{1}{X_t}\left(X_{t-1}p_{bc,t-1} + \frac{\Delta t n_c R T_{bc} \sum_{i=1}^{n} \dot{m}_{tot,i}}{A_p}\right) \tag{11}$$

2.2.4. *Brake Pipe Modeling*

The following equations describe the methodology to determine the pressure in the brake pipe, assuming isothermal one dimensional flow in a pipe and the Navier-Stokes equations.

The governing equations, derived from the continuity, momentum and energy equations, are given by Equations (12) and (13)

$$\frac{\partial \rho}{\partial t} + \frac{\partial \rho u}{\partial x} = H \tag{12}$$

$$\frac{\partial \rho u}{\partial t} + \frac{\partial \rho u^2}{\partial x} = -\frac{\partial p_{bp}}{\partial x} + f_x \tag{13}$$

where ρ is the brake pipe air density, u is the brake pipe air velocity, x is the longitudinal position along the brake pipe, H is the brake pipe air mass flow in all non-longitudinal directions, p_{bp} is the brake pipe pressure, and f_x is the sum of superficial forces in the brake pipe.

The brake pipe air mass flow in all non-longitudinal directions, H, was first used by Cantone via Equation (14)

$$H = \frac{\partial}{A_{bp}\partial x}\sum_i \dot{m}_{bp,i} \tag{14}$$

where A_{bp} is the brake pipe area and $\dot{m}_{bp,i}$ is the brake pipe mass flow rate in all non-longitudinal directions.

The sum of the superficial forces is governed by Equation (15)

$$f_x = \frac{\rho f u^2}{2D} C_f \tag{15}$$

where D is the brake pipe diameter, f is the friction coefficient determined from the Reynolds number, Re, using Equation (16) below, and C_f is a pressure loss coefficient.

$$f = \begin{cases} 0, & Re = 0 \\ \frac{64}{Re}, & Re < 2000 \\ \frac{0.0027}{Re^{0.222}}, & 2000 \le Re \le 4000 \\ \frac{0.316}{Re^{0.25}}, & Re > 4000 \end{cases} \tag{16}$$

The Reynolds number and the pressure loss coefficient are determined by Equations (17) and (18)

$$Re = \frac{\rho u D}{\mu} \tag{17}$$

$$C_f = 1 + \frac{L_f}{L} \tag{18}$$

where μ is the viscosity of air, L is the brake pipe length, and L_f is the brake pipe equivalent length.

The relationship between the pressure and density of air is given by Equation (19)

$$p_{bp} = \rho R T_{bp} \tag{19}$$

where T_{bp} is the brake pipe air temperature.

An additional relationship, Equation (20), is used to non-dimensionalize the most important variables via Equation (20)

$$c = \sqrt{kRT_{bp}} \tag{20}$$

where c is the speed of sound in air and k is the isentropic bulk modulus of air.

The variables are non-dimensionalized via the set of equations defined in Equation 21

$$\begin{cases} U = \frac{u}{c} \\ T = \frac{tc}{L} \\ P = \frac{p}{p_0} \\ Z = \frac{x}{L} \end{cases} \tag{21}$$

where p_0 is the initial pressure of the brake pipe, U is the non-dimensionalized brake pipe velocity, T is non-dimensionalized time, P is the non-dimensionalized brake pipe pressure, and Z is the non-dimensionalized brake pipe length.

Rewriting the equations with the non-dimensionalized variables results in Equations (21) and (22).

$$\frac{\partial P}{\partial T} + U\frac{\partial P}{\partial Z} + P\frac{\partial U}{\partial Z} = \frac{c}{RA_{bp}T_{bp}p_0}\frac{\partial \sum_i \dot{m}_{bp,i}}{\partial Z} \tag{21}$$

$$\frac{\partial U}{\partial T} + U\frac{\partial U}{\partial Z} = -\frac{1}{RPT_{bp}}\frac{\partial P}{\partial Z} + \frac{fLU^2}{2D}C_f \tag{22}$$

The equations are finally solved using a 4th order Runge-Kutta method using a backward and forward approach in Equations (23) and (24), respectively.

$$\frac{dP}{dT} = P_i^n\left(\frac{U_i^n - U_{i-1}^n}{\Delta Z}\right) + U_i^n\left(\frac{P_i^n - P_{i-1}^n}{\Delta Z}\right) - \frac{c}{nA_{bp}p_0\Delta Z}\sum_i \dot{m}_{bp,i} \tag{23}$$

$$\frac{dU}{dT} = U_i^n\left(\frac{{U_{i+1}^n}^2 - {U_i^n}^2}{\Delta Z}\right) + \frac{1}{kP}\left(\frac{P_{i+1}^n - P_i^n}{\Delta Z}\right) - \frac{fL{U_i^n}^2}{2D}C_f \tag{24}$$

The pressure and velocity of the brake pipe air is then combined with the models of the control valves and reservoirs to determine the performance of the entire system over time.

2.3. Longitudinal Train Dynamics Modeling and Design Criteria

The longitudinal dynamics model chosen to simulate the wagon behavior is that of Eckert et al. (2021), which adapted longitudinal dynamics models from Cole and draft gear models from Wu to represent Brazilian heavy haul freight train conditions. The model determines the longitudinal forces acting on each wagon to determine the forces experienced by the draft gears. However, the model does not include lateral dynamics impacts from the wheel-rail interaction. The objective of the model is to inexpensively simulate real track conditions and determine the impact of the proposed solutions for the brake system on train performance.

2.3.1. *Longitudinal Dynamics Modeling*

To characterize the longitudinal dynamics of heavy haul freight trains, the longitudinal forces experienced by the wagons must first be described. The forces in the model include the traction force of the locomotive(s), the dynamic braking of the locomotive(s), and the resistive forces to movement: the propulsion resistance, curving resistance, wagon brake forces, and gravity. As shown in Figure 14, the locomotive(s) and wagons are connected like masses in series via spring elements that represent the draft gear forces. The longitudinal dynamics modeling used in this work is that of Eckert et al. (2021), which was adapted to Brazilian heay haul trains using the work of Wu (2016).

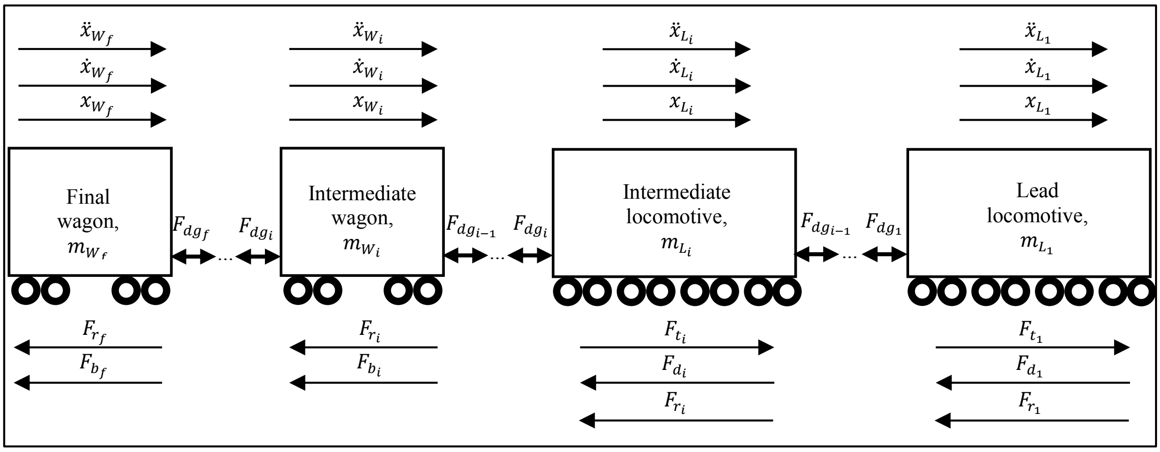

Figure 14 - Force diagram of heavy haul train. Adapted from: ECKERT et al., 2021.

The dynamic equations follow Newton's 2nd law, such that

$$\ddot{x}_{L_1} = \frac{F_{t_1} - F_{d_1} - F_{r_1} - F_{dg_1}}{m_{L_1}} \tag{25}$$

$$\ddot{x}_{L_i} = \frac{F_{t_i} - F_{d_i} - F_{r_i} + F_{dg_{i-1}} - F_{dg_i}}{m_{L_i}} \tag{26}$$

$$\ddot{x}_{W_i} = \frac{-F_{r_i} - F_{b_i} + F_{dg_{i-1}} - F_{dg_i}}{m_{W_i}} \tag{27}$$

$$\ddot{x}_{W_f} = \frac{-F_{r_f} - F_{b_f} + F_{dg_f}}{m_{W_f}} \tag{28}$$

$$F_{r_i} = m_i g \left(A_{1_i} + \frac{A_{2_i} N_{a_i}}{m_i} + B_i \dot{x}_i + C_i \dot{x}_i^2 + \sin(\alpha_i) + \frac{6.116}{g R_i} \right) \tag{29}$$

where $\ddot{x}_{L_1}$ is the longitudinal acceleration of the lead locomotive, $\ddot{x}_{L_i}$ is the longitudinal acceleration of the *i*th locomotive (assumed to not be the last body in the train composition), $\ddot{x}_{W_i}$ is the longitudinal acceleration of the i^{th} wagon, $\ddot{x}_{W_f}$ is the longitudinal acceleration of the final wagon, and $\dot{x}_i$ is the longitudinal velocity of the i^{th} locomotive or wagon. The masses of the bodies are separated into the lead locomotive, m_{L_1}, the i^{th} locomotive, m_{L_i}, the i^{th} wagon, m_{W_i}, and the final wagon, m_{W_f}. The contributing forces are the lead locomotive traction force, F_{t_1}, the lead locomotive dynamic braking force, F_{d_1}, the lead locomotive resistive force, F_{r_1}, the first draft gear force, F_{dg_1}, the i^{th} locomotive traction force, F_{t_i}, the i^{th} locomotive dynamic braking force, F_{d_i}, the i^{th} locomotive or wagon resistive force, F_{r_i}, the draft gear force of the i^{th} draft gear, F_{dg_i}, the draft gear force of the draft gear prior to the i^{th} draft gear, $F_{dg_{i-1}}$, the pneumatic braking force of the i^{th} wagon, F_{b_i}, the resistive force of the final wagon, F_{r_f}, the pneumatic braking force of the final wagon, F_{b_f}, and the draft gear force of the final draft gear, F_{dg_f}. The resistive force of the i^{th} locomotive or wagon is defined by Equation (29), where m_i is the body mass, g is the acceleration due to gravity, A_{1_i}, A_{2_i}, B_i, C_i, are coefficients from the Modified Davis Equation, N_{a_i} is the number of axles per car body, α_i is the track ramp angle, and R_i is the track curvature.

2.3.2. Draft Gear Modeling

As shown in Figure 15 below, the friction draft gear is composed of multiple moving and static parts.

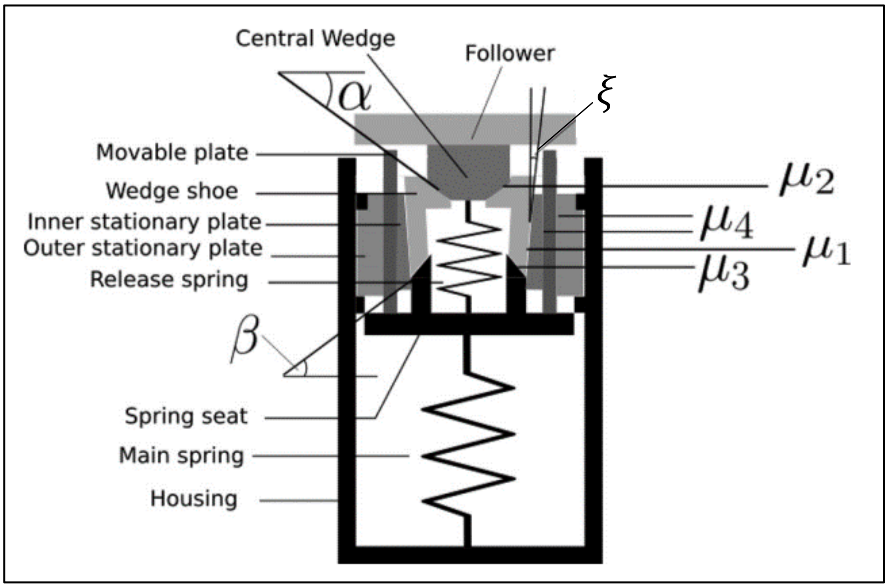

Figure 15 - Schematic of friction draft gear model. Adapted from: ECKERT et al., 2021.

To characterize the draft gear forces in the model, the draft gear is first separated into four operational states as previously discussed in the literature review:

1. The draft gear has begun loading, but the follower has not yet touched the movable plates. Thus, the wedge plate contacting the wedge shoe is the primary energy dissipation mechanism (j =1).
2. The draft gear is undergoing loading and the follower has now touched the movable plates. Both the wedge and plate components are engaged and contribute to energy dissipation (j =2).
3. The draft gear has begun to unload, but the spring seat has not yet touched the movable plates. Thus, the wedge components are the primary energy dissipation mechanism and the plate components do not contribute (j =3).
4. The draft gear is undergoing unloading and the spring seat has now touched the movable plates. Both the wedge and plate components are engaged and contribute to energy dissipation (j =4).

The forces of the main spring, F_{ms}, and the return spring, F_{rs}, are determined by

$$F_{ms} = k_{ms}\left(x_{ms0} + x_{fd}\right) \tag{30}$$

$$F_{rs} = k_{rs}x_{rs0} \tag{31}$$

where k_{ms} is the stiffness of the main spring, x_{ms0} is the pre-deflection of the main spring, x_{fd} is the draft gear displacement, k_{rs} is the return spring stiffness and x_{rs0} is the return spring pre-deflection.

The draft gear force, F_{j_i}, prior to the determination if the draft gear is transitioning between operational states, is given by

$$F_{j_i} = \psi_j F_{ms} - (\psi_j - 1)F_{rs} \tag{32}$$

where ψ_j is the force coefficient based on the operational state of the draft gear.

The force coefficients, ψ_{1-4}, are defined per state by

$$\psi_1 = \frac{1+\tan(\beta+\arctan(\mu_3))\tan(\xi+\arctan(\mu_1))}{1-\tan(\alpha+\arctan(\mu_2))\tan(\xi+\arctan(\mu_1))} \tag{33}$$

$$\psi_2 = \psi_1 + \frac{2\,(1-\mu_1\tan(\xi))\mu_4(\psi_1-1)}{\mu_1+\tan(\xi)} \tag{34}$$

$$\psi_3 = \frac{1+\tan(\beta-\arctan(\mu_3))\tan(\xi-\arctan(\mu_1))}{1-\tan(\alpha+\arctan(\mu_2))\tan(\xi-\arctan(\mu_1))} \tag{35}$$

$$\psi_4 = \frac{\psi_3(\tan(\xi)-\mu_1)}{\tan(\xi)(1-2\mu_1\mu_4+2\mu_1\mu_2\psi_3)+2\mu_4\psi_3-2\mu_4-\mu_1} \tag{36}$$

where α is the contact angle between the wedge shoe and the central wedge, β is the contact angle between the wedge shoe and the spring seat, ξ is the contact angle between the wedge shoe and the inner stationary plate, and μ_{1-4} are the friction coefficients per component interaction.

The friction coefficients per component interaction, μ_i, are defined by

$$\mu_i = \mu_s + (\mu_s - \mu_k)e^{-\sigma|v_i|} \tag{37}$$

where μ_s is the static friction coefficient, μ_k is the kinetic friction coefficient, σ is a friction transition factor, and v_i is the relative velocity between the two components.

The relative velocities between the components are determined by

$$v_1 = \frac{\cos(\alpha)}{\cos(\alpha+\xi)} v_f \tag{38}$$

$$v_2 = \frac{\sin(\xi)}{\cos(\alpha+\xi)} v_f \tag{39}$$

$$v_3 = \frac{\cos(\alpha)\sin(\xi)}{\cos(\alpha+\xi)\cos(\beta)} v_f \tag{40}$$

$$v_4(j) = \begin{cases} \frac{\cos(\alpha)\sin(\xi)}{\cos(\alpha+\xi)\cos(\beta)} v_f, & (j = 4) \\ v_f, & (j = 2) \\ 0, & (j = 1 \text{ or } 3) \end{cases} \tag{41}$$

where v_f is the velocity of the draft gear follower, v_1 is the absolute velocity of the wedge shoe, v_2 is the relative velocity of the wedge shoe with respect to the central wedge, v_3 is the relative velocity of the wedge shoe with respect to the spring seat, and v_4 is the absolute velocity of the movable plate as a function of the operation state, j.

Finally, the draft gear force used in Equations (25-28), F_{dg_i}, is determined by the transition state between the operational states such that

$$F_{dg_i} = \begin{cases} 0, & \text{clearance case} \\ \frac{F_{dg_i}(t-\Delta t)+F_{j_i}(t)}{2}, & \text{transition case} \\ F_{j_i}, & \text{all other cases} \end{cases} \tag{42}$$

where $F_{dg_i}(t-\Delta t)$ is the draft gear force at time $(t-\Delta t)$.

2.3.3. Rain-flow Fatigue Analysis Model

To compare the effectiveness of the design solutions with the current valve design, a rain-flow fatigue criteria developed by Wu et al. (2017) is used. The rain-flow fatigue model is shown below as

$$N_{i,j} = N_e \left(\frac{bA}{(F_p - mF_v)N_f}\right)^{\frac{1}{r}} \tag{43}$$

where $N_{i,j}$ is the cycle to fatigue failure number of the force reversal, N_e is the cycle to failure number at the knee point of the idealized S-N diagram, b is the y-axis intercept of the modified Goodman diagram, A is the cross-sectional area of the specimen, F_p is the peak force of the reversal which has the j^{th} level of magnitude, m is the slope of the modified Goodman diagram, F_v is the valley force of the reversal which has the i^{th} level of magnitude, N_f is the fatigue notch factor, and r is the slope of the idealized S-N diagram.

The fatigue damage caused by the specific level of force reversals, $D_{i,j}$, is then calculated by

$$D_{i,j} = \frac{O_{i,j}}{N_{i,j} \sum O_{i,j}} \tag{44}$$

where $O_{i,j}$ is the reversal occurrences at the same level of force reversals and $N_{i,j}$ is calculated from Equation (43) above.

The rain-flow extraction process, per Wu (2016), follows the format shown in Figure 16 below.

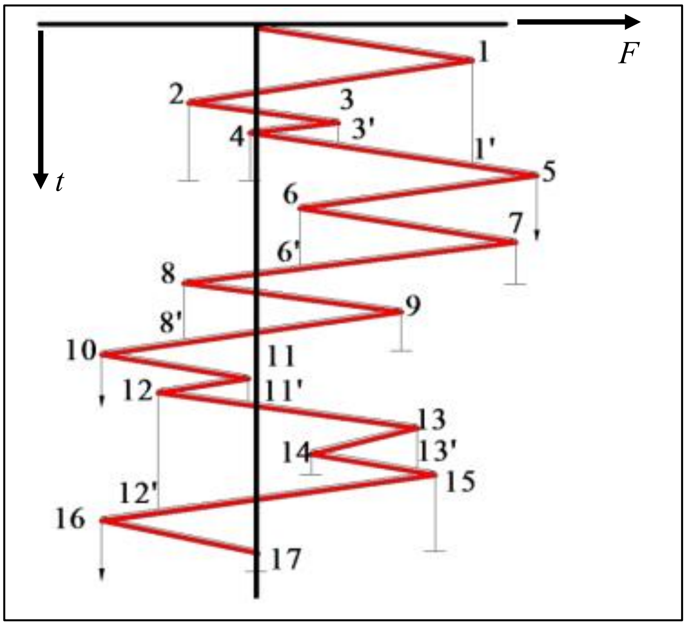

Figure 16 - Rain-flow algorithm extraction process. Adapted from: WU, 2016.

The assigned name of "rain-flow" was given because the end limits of a fatigue cycle are defined similar to how rain drops would fall from a higher roof to a lower roof during a rainstorm. In Figure 16, the force peaks are labeled from 1 to 17 with the downward direction indicating forward progression in time. A force cycle is counted by the algorithm when the magnitude of the force is repeated later in time. The first example of a force cycle is between Point 1 and Point 1'. The force magnitude of Point 1 is equal to the force magnitude of Point 1'. However, there are limits to the amount of cycles to be counted between the end limits of a rain-flow cycle. For four consecutive data points, the following conditions must be met for a force cycle to be counted:

$$h_1 = |p_{i+1} - p_i| \tag{45}$$

$$h_2 = |p_{i-1} - p_i| \tag{46}$$

$$h_3 = |p_{i-1} - p_{i-2}| \tag{47}$$

$$h_1 \geq h_2 \; and \; h_2 < h_3 \tag{48}$$

where p_{i+1}, p_i, p_{i-1}, p_{i-2} are four consecutive peak force magnitudes after the last force reversal, and h_1, h_2, h_3 are the criteria to determine if a force cycle shall be counted. If Equation 48 is met, then p_{i-1} and p_i are counted as a cycle.

3 METHODOLOGY

This section discusses the design methodology and the simulation methodology.

3.1. Design Methodology

The approach to improve the pneumatic air brake performance, as demonstrated by the focus of the literature review, is to first research and understand the pneumatic system through the available models and find potential design solutions. Once a design solution has been selected, its performance is to be simulated and added to the pneumatic brake system model of choice. The design will be refined and then added to a longitudinal dynamics system. Finally, simulations will be run to determine the effect of the design change on the system performance. The methodology is shown graphically by Figure 17 below.

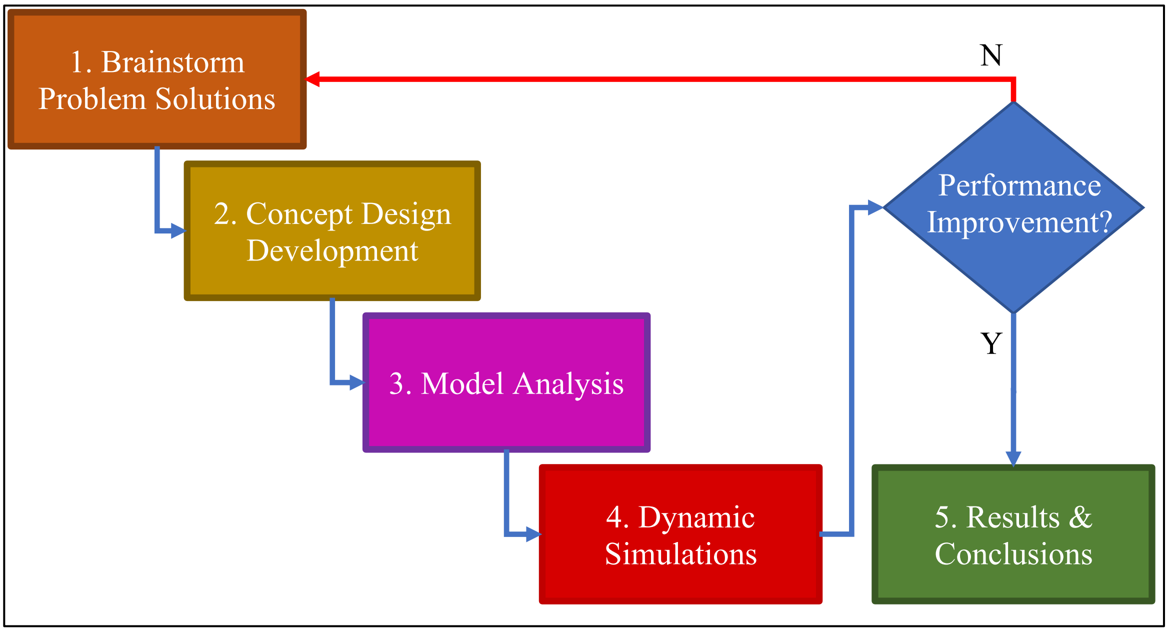

Figure 17 - Design methodology flow chart.

3.1.1. Design Concept

Based on the literature review and creativity, several design ideas were studied during the beginning of this thesis. However, most of the ideas showed to not be useful, mostly because they required an external source of energy to actuate or did not utilize the current brake system.

Some of them required the installation of energy harvesting systems, which is not a possibility because of the rugid environmental conditions and the actraction to burglars. Thus, the focus was to use the pressurized air in the brake system to introduce a potential design improvement.

The design proposed in this work is to utilize a double venturi vacuum effect at the outlet of the rapid service portion in the wagon control valve to accelerate the propagation of the brake pipe signal via a local vacuum. The faster brake pipe signal would cause downline wagons to activate their brake cylinders more quickly, thereby reducing the longitudinal shocks throughout the train. A schematic of the design is shown in Figure 18 below.

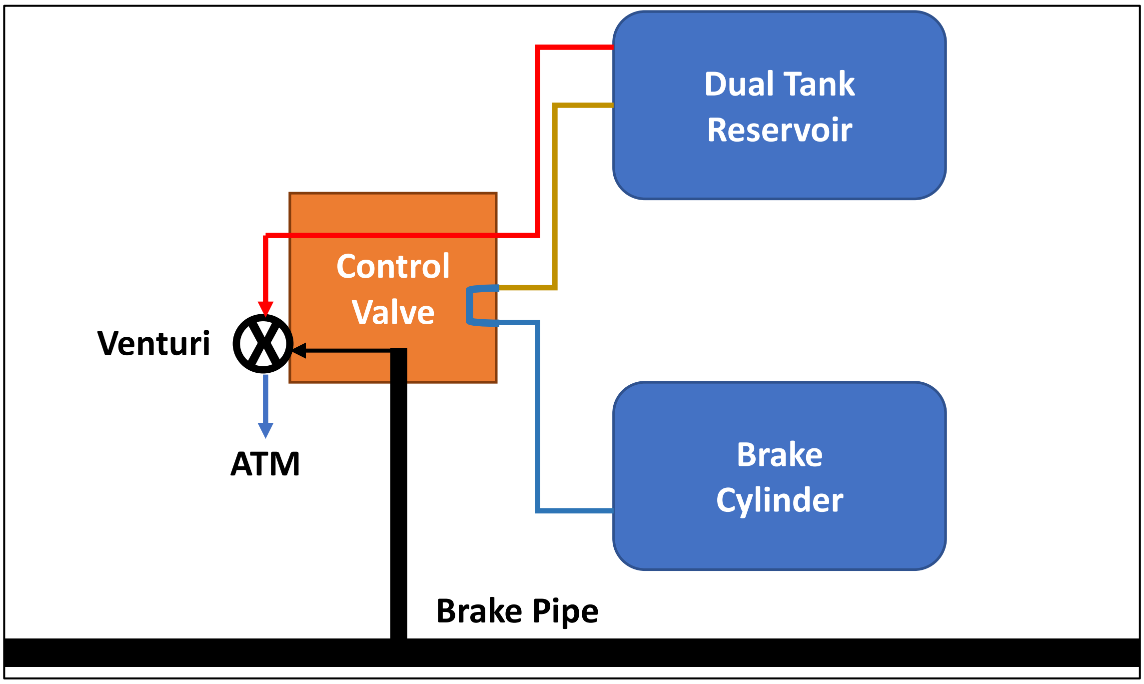

Figure 18 - Schematic of venturi design proposal installed on wagon.

While the concept introduces potential risks and drawbacks, the advantages might outweigh them. One drawback would be the diminished pressure in the emergency reservoir as it is used during a service application, leading to longer recharge times during a brake release action. A potential, albeit costly, addition to the system is a secondary pipe that would refill the reservoirs faster. This approach could mitigate the likely longer reservoir recharge times after a brake application and is already present in some Indian and Italian trains. The risk of triggering a false emergency is considered an unacceptable consequence of the vacuum, and therefore must be analysed to guarantee its impossibility. Another drawback would be that a slightly depleted emergency reservoir would result in significantly worse emergency brake applications. As a human safety issue, the potentially diminished emergency braking forces must be thoroughly analysed and inspected before integrating the Venturi into a real train system. As mentioned before, an additional pipe to refill the reservoirs could prove to be a mitigation of this issue.

Two rejected concepts consisted of adding a labyrinth seal into the pneumatic air brake system or adding an SMA wire to the brake shoes. The labyrinth seal addition was intended to perform one of two performance objectives. The first objective was to restrict the flow of air to the brake cylinders in the leading wagons, thereby reducing the braking forces in the lead wagons so that the middle and rear wagons could contribute more braking force to a brake application. This would reduce the longitudinal shocks between the wagons, while potentially sacrificing overall braking force and stopping time. The second objective would be to calibrate the labyrinth to leak the brake cylinders in the leading wagons so as to provide equal braking throughout the length of the train during a brake application. While these additions to the system could in theory reduce the longitudinal shocks between the wagons, the overall braking performance would likely suffer as a consequence. Besides, in current heavy haul railways, is is unlikely that a wagon is always placed in the same position along the train (front, middle, rear).

The other rejected idea, the addition of an SMA wire to the brake shoes, was considered as a solution to the lack of feedback in the pneumatic air brake system. A coil pack of SMA wires placed on the brake shoes would respond to the heat generated from the shoe and wheel to adjust the air pressure in the brake cylinder or the force delivered through the brake rigging. The heat response would be calibrated to help reduce or even eliminate the longitudinal shocks between the wagons. However, similar to the labyrinth concept, the SMA wire approach would depend on a reduction of the braking forces to balance the force distribution throughout the train and was therefore rejected.

3.2. Simulation Methodology

The simulation methodology is to use MATLAB and Simulink to solve the system using ordinary differential equations (ODEs). The general model layout and information flow is shown in Figure 19 below. For each test case, the Simulink model uses ode1 (Euler) to solve the ODEs. The results of the simulations will be compared using the rain-flow fatigue analysis model described in Section 2.3.3.

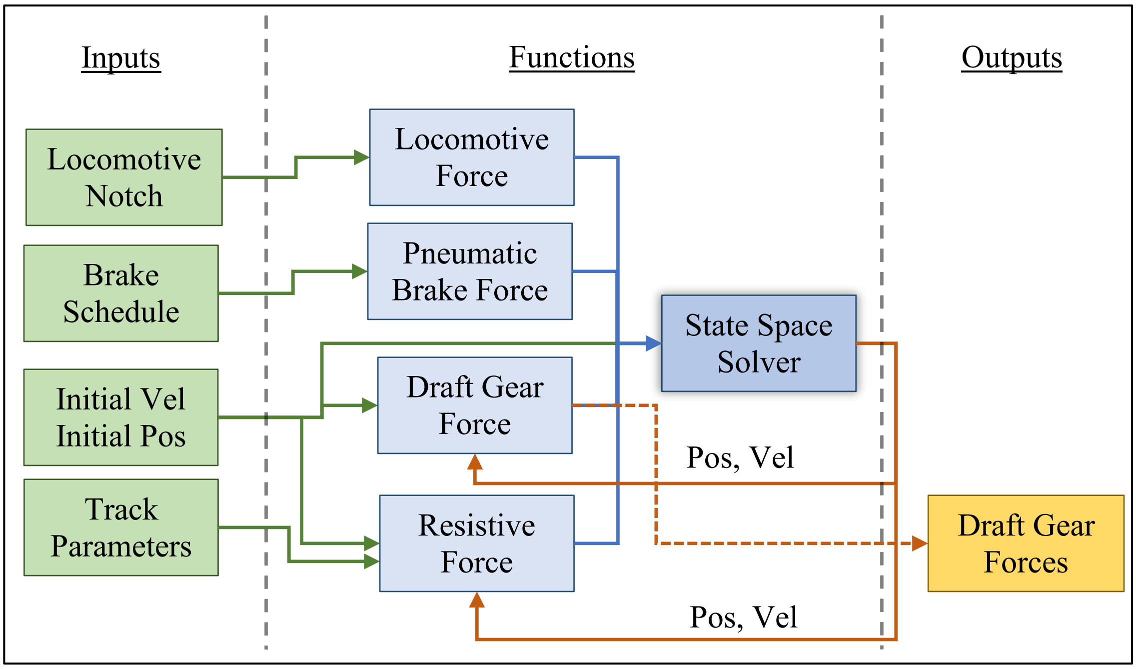

Figure 19 – Simplified longitudinal dynamics flow chart.

3.3. Simulation Test Cases & Parameters

The double venturi design is to be simulated and compared against two baseline test cases. The baseline test cases are the standard, non-venturi control valve and a theoretical maximum venturi capable of sonic flow. This theoretical maximum is, so far, not practically possible and is intended to determine if design optimization towards the theoretical maximum is a worthwhile task. The control valve designs will be tested using two initial velocities and two train compositions selected to resemble real-world conditions. The test will brake the composition using only the pneumatic braking system and record the in-train forces. A real track and train composition, driven under a real brake schedule, is also tested. The real application utilizes two test conditions; one that prioritizes the dynamic braking and one that prioritizes the pneumatic braking. The test cases are detailed below in Table 1 (1 psi = 6894.76 Pa).

Table 1 - Simulated Test Cases

Test Case #	Train Composition	BP Pressure Actuation (psi)	Initial Velocity (km/h)	Track Condition	Control Valve
1	1L84W	84.1	20	Straight	Baseline
2	1L84W	64.3	20	Straight	Baseline

3	1L84W	84.1	80	Straight	Baseline
4	1L84W	64.3	80	Straight	Baseline
5	1L84W	84.1	20	Straight	Venturi
6	1L84W	64.3	20	Straight	Venturi
7	1L84W	84.1	80	Straight	Venturi
8	1L84W	64.3	80	Straight	Venturi
9	1L84W	84.1	20	Straight	Sonic
10	1L84W	64.3	20	Straight	Sonic
11	1L84W	84.1	80	Straight	Sonic
12	1L84W	64.3	80	Straight	Sonic
13	2L168W	84.1	20	Straight	Baseline
14	2L168W	64.3	20	Straight	Baseline
15	2L168W	84.1	80	Straight	Baseline
16	2L168W	64.3	80	Straight	Baseline
17	2L168W	84.1	20	Straight	Venturi
18	2L168W	64.3	20	Straight	Venturi
19	2L168W	84.1	80	Straight	Venturi
20	2L168W	64.3	80	Straight	Venturi
21	2L168W	84.1	20	Straight	Sonic
22	2L168W	64.3	20	Straight	Sonic
23	2L168W	84.1	80	Straight	Sonic
24	2L168W	64.3	80	Straight	Sonic
25	2L168W*	N/A	20	Real-Dyn	Baseline
26	2L168W*	N/A	20	Real-Dyn	Venturi
27	2L168W*	N/A	20	Real-Dyn	Sonic
28	2L168W*	N/A	20	Real-Pneu	Baseline
29	2L168W*	N/A	20	Real-Pneu	Venturi
30	2L168W*	N/A	20	Real-Pneu	Sonic

The compositions are listed as xLyW to indicate there are x front locomotives and y trailing wagons. However, in the real-world application case, the 2L168W* indicates a single front locomotive, pulling 86 wagons, followed by a second in-line locomotive, helping to pull the remaining 82 trailing wagons. The real-world application cases include two different brake schedules, Real-Dyn and Real-Pneu. The 1L84W and 2L168W configurations are based on realistic single or double locomotive configurations, but are not considered applicable to the real-world case. The initial velocities were chosen to represent the average low-speed velocity and desirable high-speed velocity of a heavy haul freight train. A loaded wagon of $88 \cdot 10^3$ kg was used because the provided real-world brake schedule utilized this wagon mass. The brake pipe pressure actuation pressures are based on the minimum and maximum sensed pressures by the wagon control valve during a service brake application.

To compare the influences of the venturi designs on the train longitudinal dynamics, two braking test cases were tested on a theoretically perfect track, as shown in Figure 20 and Figure 21, respectively. The dynamic brake notch is set to zero to indicate that the dynamic brakes do not influence the braking action, nor does the locomotive accelerate during the braking action. The pneumatic brakes, however, are applied immediately in the simulation and are held at constant pressure until the train comes to a full stop.

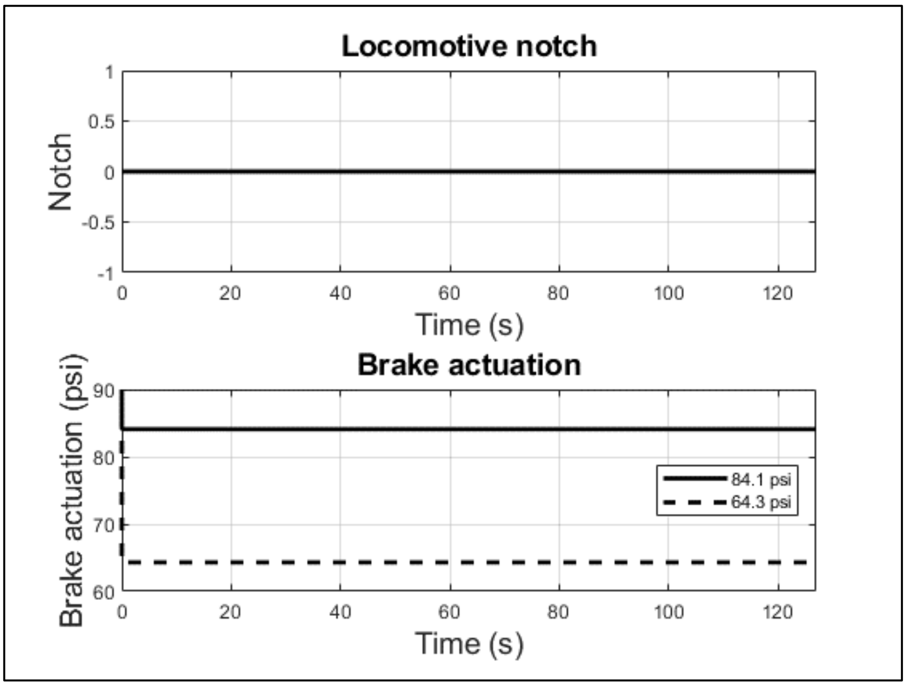

Figure 20 - Brake schedules for theoretical track conditions. Minimum pneumatic brake application of 84.1 psi and maximum pneumatic brake application of 64.3 psi were tested.

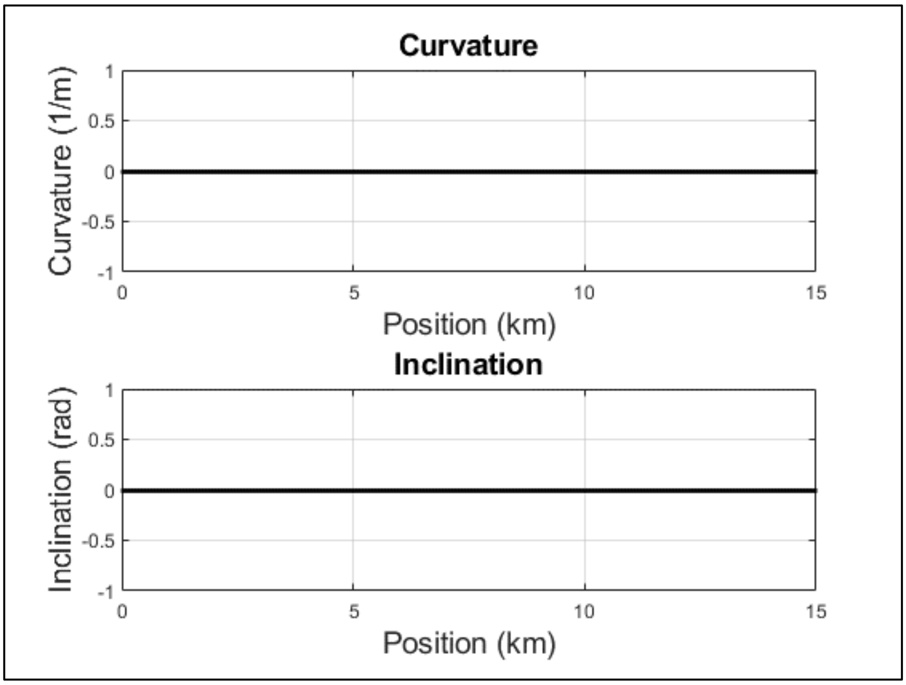

Figure 21- Theoretical track conditions.

The real-world track data was provided by VALE, S.A. and consists of a 15km section of the Estrada de Ferro - Vitória a Minas (EFVM). The curvature and inclination profile of this section is show in Figure 22 below. It should be noted that all of the curve profiles are positive, indicating that the train is only turning in one direction. This is acceptable to the simulation because the lateral dynamics of the system are neglected, where the direction of a turn becomes relevant.

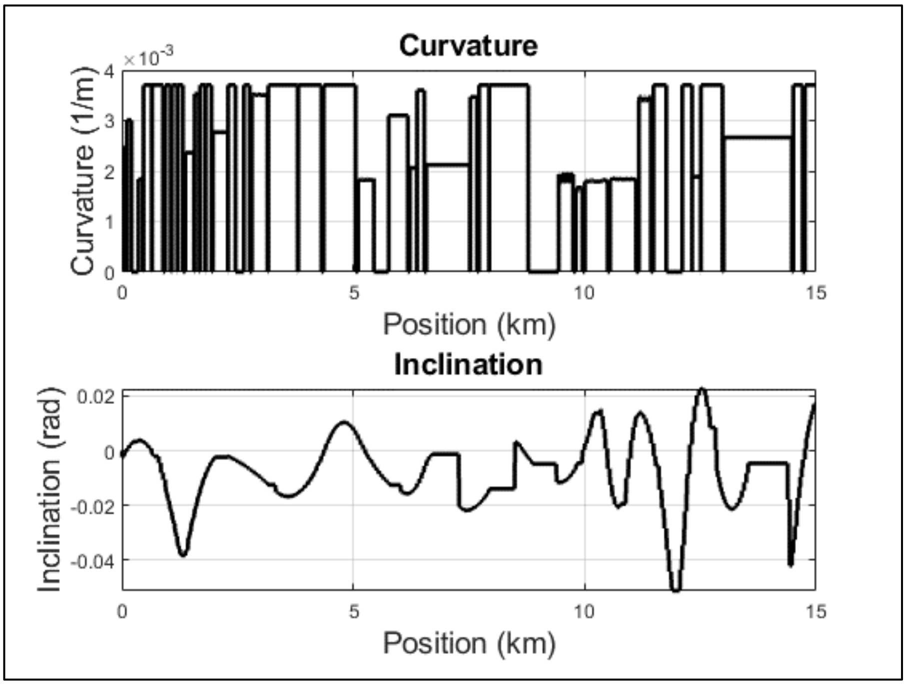

Figure 22 - Real-world track conditions.

The train enters and exists multiple curves and also descends and ascends multiple changes in elevation. Because the track conditions are fixed, the locomotive conductors follow a brake schedule to control a safe train velocity. The brake schedules indicate what notch, or locomotive control setting, the dynamic braking should use and indicate if pneumatic brakes should be applied or not. The notch profiles and dynamic brake capacity are shown in Figure 23 below.

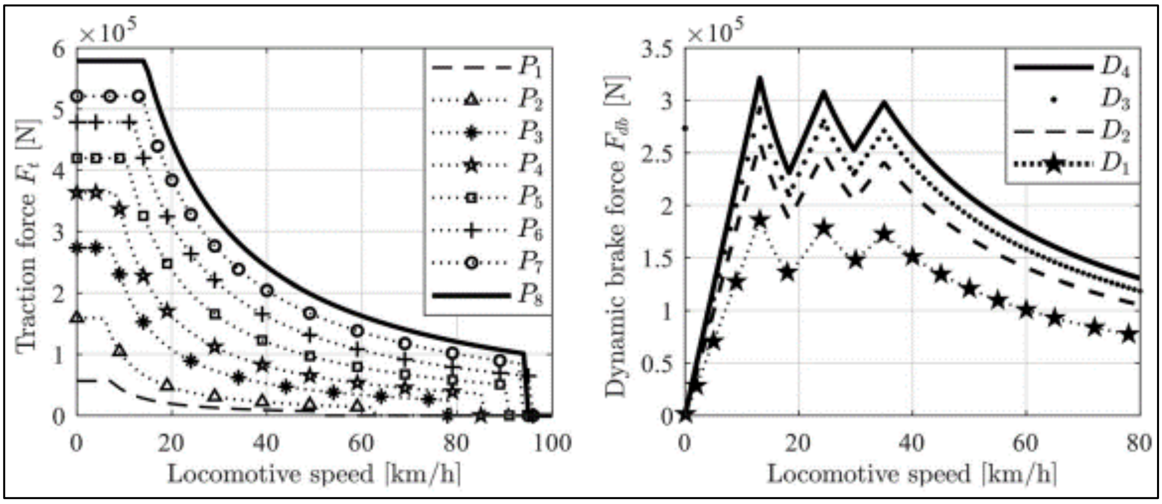

Figure 23 - Locomotive notch settings. Source: ECKERT et al., 2021.

Because the amount of pressure to be released from the brake pipe is not mandated, pneumatic braking is a matter of conductor feel and experience. The brake schedules were designed to the existing control valve technologies, and therefore may not be optimal for the venturi application. However, all control valve test cases in this work utilize the same real-world brake schedule. For the real-world applications, two brake schedules were used to maintain the desired velocity profile. The first brake schedule utilizes the dynamic brakes as the dominant stopping mechanism, and applies only the minimum required pneumatic brake application. The second brake schedule utilizes the pneumatic brakes as the dominant stopping mechanism, and applies only the minimum required dynamic brake application. These two cases are shown below in Figure 24.

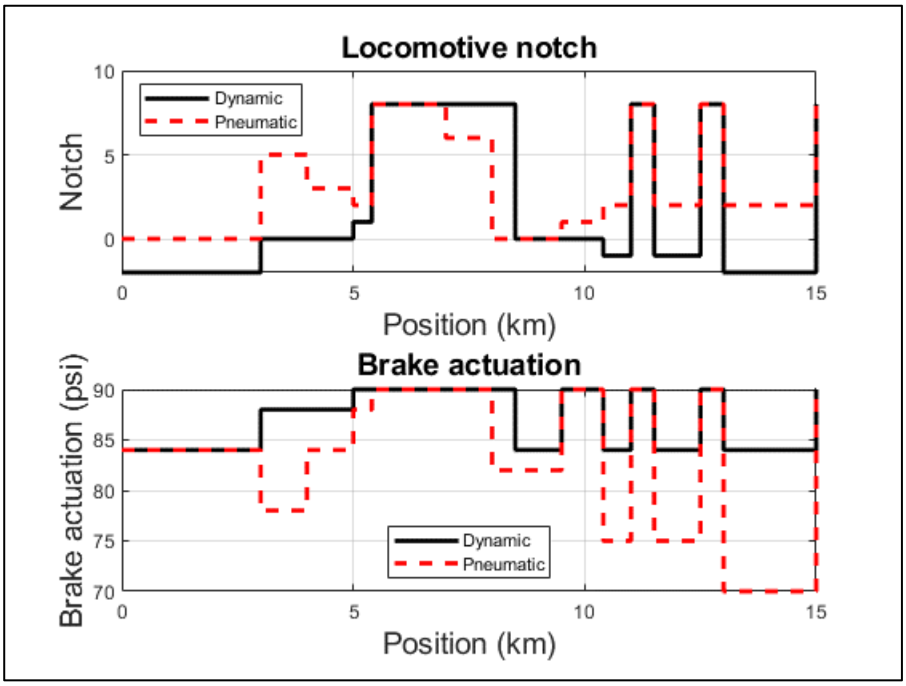

Figure 24 - Real-world brake schedule with dominant dynamic braking and dominant pneumatic braking overlaid.

The relevant longitudinal dynamics parameters are listed in Table 2 below, which describes the parameters of the resistance to movement equation (Davis) and vehicle characteristics.

Table 2 - Relevant longitudinal dynamics simulation parameters.

Parameter	Value		Units
	$\dot{x} \leq 0.1$	$\dot{x} > 0.1$	m/s
Locomotive modified Davis equation coefficient, A_1	5	0.1	-
Locomotive modified Davis equation coefficient, A_2	425	8.5	-
Locomotive modified Davis equation coefficient, B	0	0.00938	-
Locomotive modified Davis equation coefficient, C	0	0.0046	-
Wagon modified Davis equation coefficient, A_1	15	0.15	-
Wagon modified Davis equation coefficient, A_2	425	4.25	-
Wagon modified Davis equation coefficient, B	0	0.007	-
Wagon modified Davis equation coefficient, C	0	0.000325	-
Number of axles per locomotive, N_a	8		-
Number of axles per wagon, N_a	4		-
Locomotive mass, m	$162{\times}10^3$		kg
Loaded wagon mass, m	$88{\times}10^3$		kg
Simulation time step	$1{\times}10^{-3}$		s

4 MODELING AND VENTURI DESIGN SELECTION

This section discusses the results of the CFD modeling and Venturi application to the mathematical model. The experimental set-up and test plan are also explained.

4.1. CFD & Pneumatic Modeling Analysis

An initial attempt to determine the viability of a vacuum effect in the model resulted in an unusual outcome. The pressure drop in the brake pipe upon receiving a pressure signal from the locomotive was severely worse than normal. After a small investigation, it was discovered that the orifice modeling breaks down when the low pressure, p_{lo}, is below atmosphere. In particular, the Mach correction factor, C_m, sharply decreases as the low pressure approaches zero. Because of this modeling error, it was decided to perform computational fluid dynamics (CFD) analysis to adequately determine the flow rate in the rapid service portion orifice with a venturi vacuum effect.

The double venturi model was created in PTC CREO®, as shown below in Figure 25, and represents the air volume and pathing. The double venturi consists of an inlet nozzle supplied by 90 psi (1 psi = 6894.76 Pa) from the emergency reservoir, the brake pipe air outlet with a starting pressure of 90 psi, the venturi volume, the venturi baffle, and the outlet of the venturi nozzle held at 1 atm (1 atm = 101325 Pa).

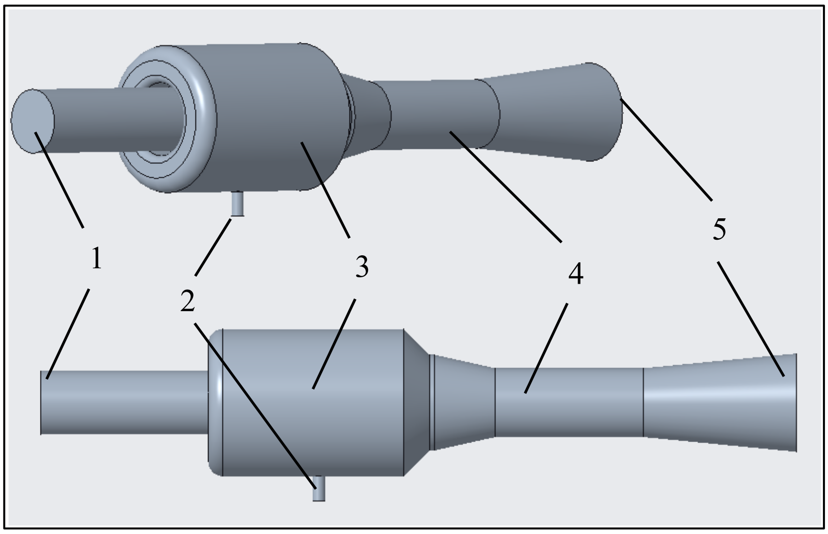

Figure 25 - Double venturi fluid domain. 1 - emergency air inlet; 2 - brake pipe air outlet; 3 - venturi air volume; 4 - venturi air baffle; 5 - venturi air outlet.

The computer aided design (CAD) model was exported to ANSYS CFX, a 3D CFD simulation software. The model was run at steady state with k-ε turbulence convergence error parameters set to 10^{-4} root mean square (RMS). The simulation results were post-processed to determine the fluid velocity and pressure drops in the double venturi, as shown in Figure 26.

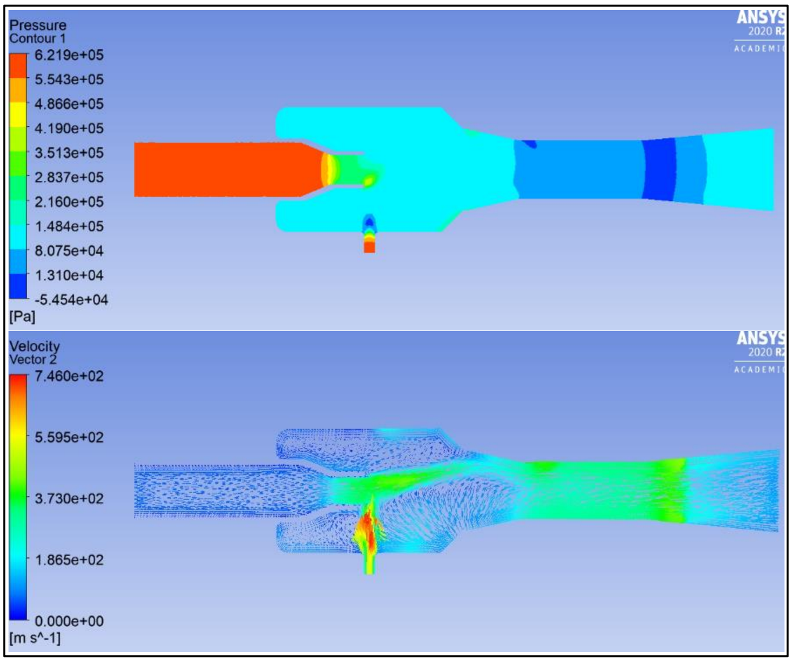

Figure 26 - Pressure and velocity plots of double venturi. Air entrainment and pressure drops increase fluid air velocity.

Interpreting the double venturi CFD results was not entirely clear, so a model of an orifice was generated to be able to compare the CFD results more accurately to the orifice mathematical modeling. This comparison would assist in clarifying the double venturi CFD results. To perform this comparison, an orifice was also modeled in CAD and exported to CFD and simulated using the same initial conditions and geometries as the double venturi. The model and simulation results are shown in Figure 27.

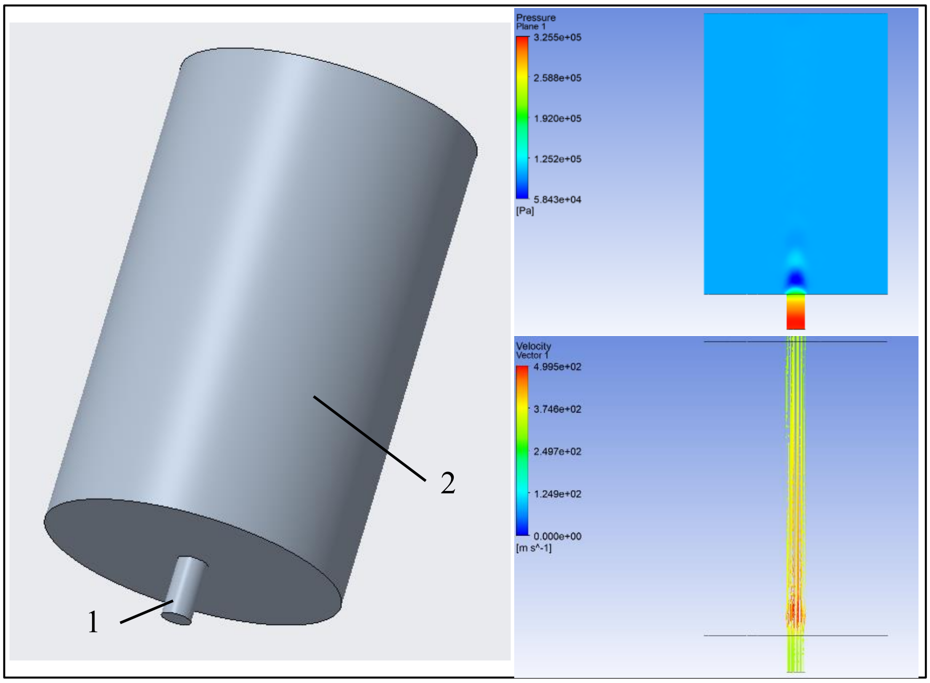

Figure 27 - Pressure and velocity plots of brake pipe orifice vent through control valve. 1 - brake pipe air outlet; 2 - atmospheric air volume.

When comparing the CFD results, the first observation is that the vacuum field developed by the double venturi effect is lower than the local pressure drop in the standard orifice. This observation, however, does not help the pneumatic system modeling as it was already discovered that the models cannot handle pressures below atmosphere. The more useful observation is that the fluid velocity is nearly 1.5 times higher in the double venturi than it is in the standard orifice. This velocity difference is almost identical to the difference between subsonic flow and sonic flow through a standard orifice, as show in Figure 28. From these results, a venturi factor, η, of 1.4 was used to describe sonic flow in the longitudinal dynamics modeling.

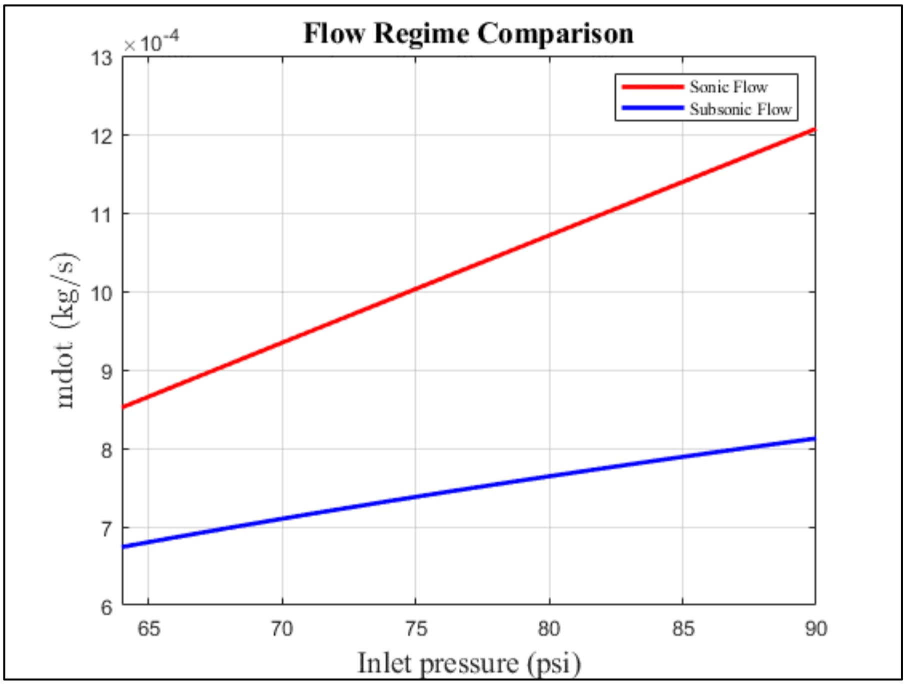

Figure 28 - Flow comparison through the brake pipe orifice showing that above 70 psi, the sonic flow is, on average, 1.4 times higher than the subsonic flow.

Under the assumption of sonic flow, the pneumatic brake system model was run using the parameters in Table 3. The sonic flow was only applied during the rapid service portion of the service brake applications. A small and large pressure drop were applied as a service brake application. Lastly, a brake release and full recharge application was applied. However, the results of the brake release and recharge were not accounted for in the double venturi because the venturi emergency air use has not yet been simulated. Two service brake applications were applied, one small and one large pressure drop After running the models, the results of the sonic flow modeling were compared to the results of the subsonic flow modeling.

Table 3 - Heavy haul train pneumatic model parameters.

Parameter	Value	Units
Wagon brake pipe diameter	0.03	m
Wagon brake pipe length	12.1	m
Auxiliary reservoir volume	0.041	m^3
Emergency reservoir volume	0.057	m^3
Rapid service volume	0.015	m^3

Auxiliary reservoir to brake pipe orifice size	2.5×10^{-6}	m^2
Auxiliary reservoir to emergency reservoir orifice size	1×10^{-6}	m^2
Auxiliary reservoir to brake cylinder orifice size	3.5×10^{-6}	m^2
Emergency reservoir to brake pipe orifice size	4.5×10^{-6}	m^2
Emergency reservoir to brake cylinder orifice size	7.8×10^{-6}	m^2
Brake pipe to atmosphere (emergency application) orifice size	8×10^{-4}	m^2
Brake pipe to atmosphere (rapid service application) orifice size	1×10^{-6}	m^2
Brake pipe to rapid service volume orifice size	1×10^{-6}	m^2
Brake cylinder to atmosphere orifice size	3×10^{-6}	m^2
Brake cylinder piston mass	0.25	kg
Brake cylinder piston area	0.0648	m^2
Brake cylinder spring constant	100	N/m
Brake cylinder piston minimum position	0.0628	m
Brake cylinder piston maximum position	0.1869	m
Simulation time step	5×10^{-5}	s

The overall pneumatic air brake system performance is detailed in Figure 29. The 99th wagon is shown because the pressure changes throughout the system are more noticeable. The two commanded pressure drops from the locomotive are 5.9 psi at four seconds and 19.8 psi at 44 seconds, representing a typical braking schedule during a descent. The wagon pneumatic air brake system performance details the pressure changes in the brake pipe, auxiliary reservoir, emergency reservoir, and brake cylinder over time. It is important to note that the brake release is not representative of reality in the venturi modeling because the air consumption in the emergency reservoir is still unknown.

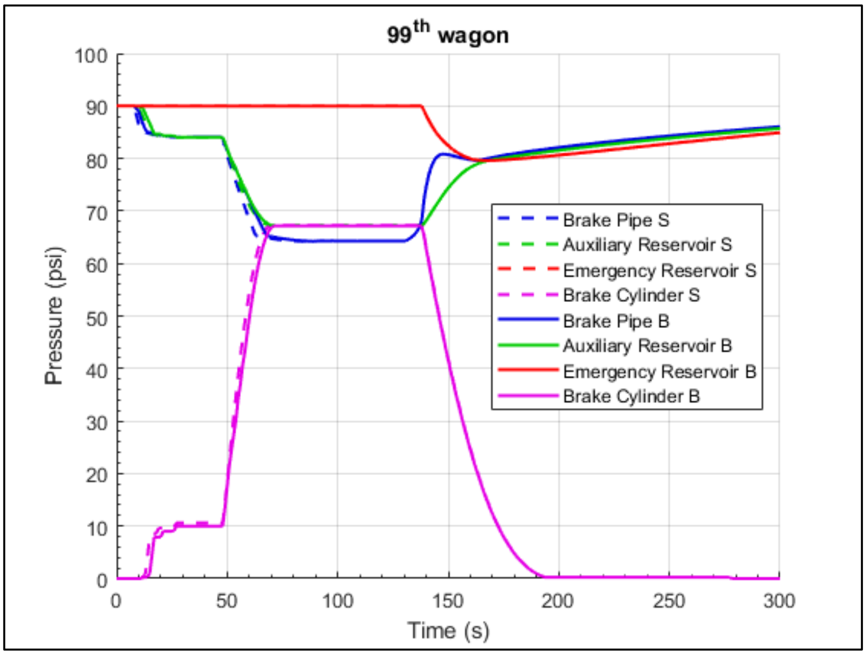

Figure 29 - Wagon pneumatic air brake performance in 99th wagon. B - baseline; S - sonic.

A zoomed in view of the first pressure command is shown in Figure 30. The most noticeable difference is that the brake pipe pressure drops significantly faster when configured with the double venturi. The brake pipe pressure also reaches the transition pressure, the pressure at which the pressure drop slowly and predictably decays to the stabilization pressure, about 3s faster when equipped with the double venturi. Interestingly, the double venturi also initiates the brake pipe pressure drop sooner, but the difference is almost negligible.

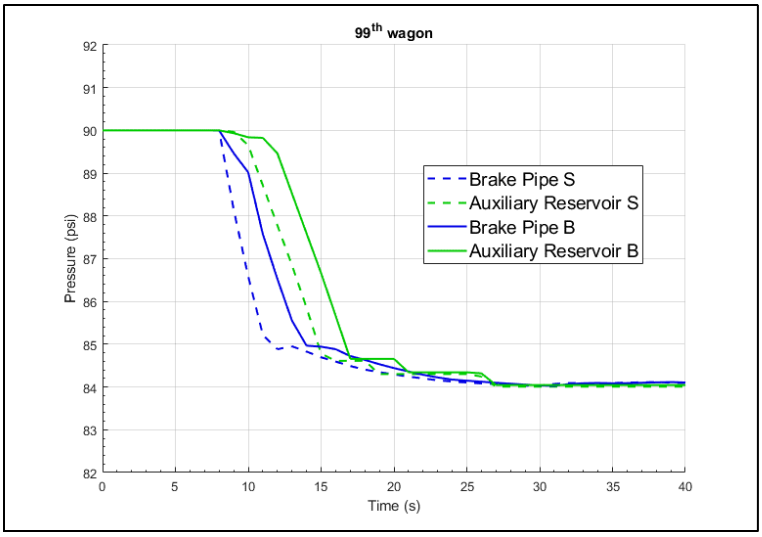

Figure 30 - Brake pipe and auxiliary reservoir pressure changes under a 5.9 psi pressure command. B - baseline; S - sonic.

Likewise, a zoomed in view of the second pressure command is shown in Figure 31. Again, the brake pipe pressure drops significantly faster when configured with the double venturi. Also, the brake pipe pressure also reaches the transition pressure about 5s faster. Here, the double venturi initiates the brake pipe pressure drop about 1s sooner.

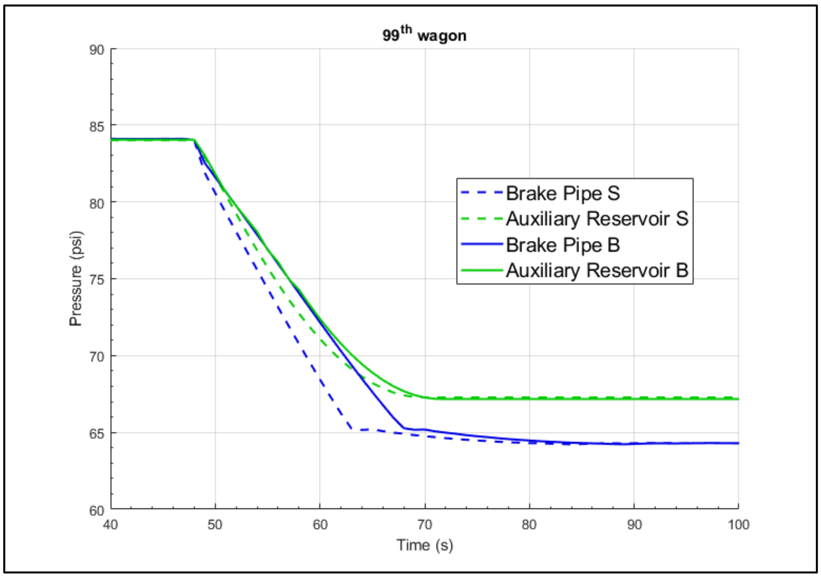

Figure 31 - Brake pipe and auxiliary reservoir pressure changes under a 19.8 psi pressure command. B - baseline; S - sonic.

Lastly, a zoomed in view of the brake cylinder performance is shown in Figure 32. The influence of the double venturi is not noticeable upon the first brake cylinder action because of the limiting valve in the control valve. The limiting valve is necessary to prevent unstable dynamics during initial braking actions. However, during the second braking action, the brake cylinder reaches stabilization pressure about 2s faster in the double venturi equipped wagon.

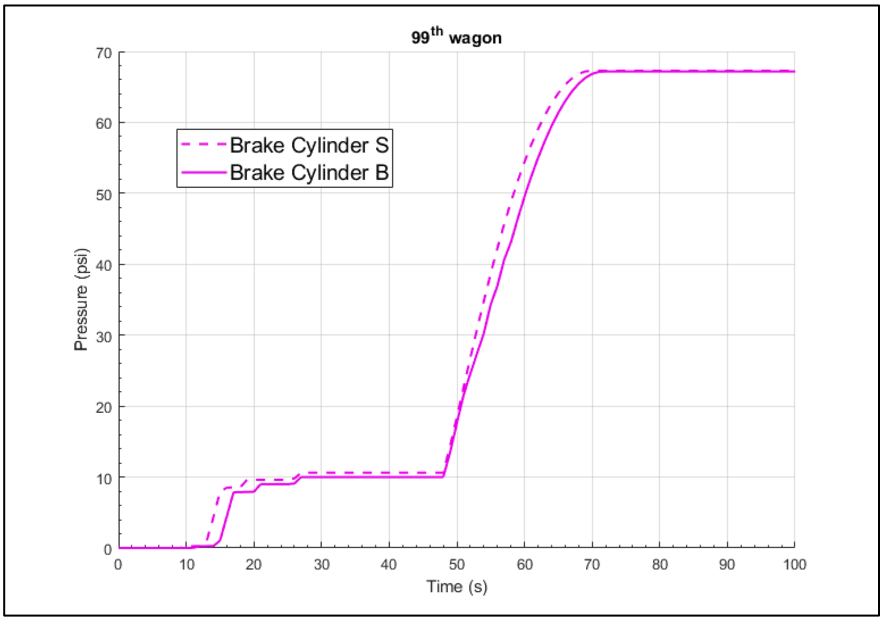

Figure 32 - Brake cylinder pressure changes under a 5.9 and 19.8 psi pressure command. B - baseline; S - sonic.

After the initial sonic venturi modeling, a few mistakes were noticed. First, the pressure inputs for the orifice in the atmosphere modeling and the venturi modeling were not consistent. Additionally, after adding the orifice used in the CFD model to the pneumatic model of the brake system, it was clear that the orifice size used in the venturi design is not viable. When evaluating the emergency reservoir air depletion using this orifice size, the emergency reservoir was immediately evacuated during the first service brake application. For this reason, further modeling of a sonic venturi effect in this work is for gauging the pneumatic limits of a sonic airflow during the rapid service portion.

To avoid the rapid depletion of the emergency reservoir, smaller orifice sizes to direct the emergency air into the venturi were analyzed. As shown in Figure 33 below, an orifice size of 2.5 mm^2 was used to determine the venturi factor. The geometry alterations reduced the overall venturi flow by 20% compared to the previous modeling geometry, as a result of a smaller emergency air inlet diameter.

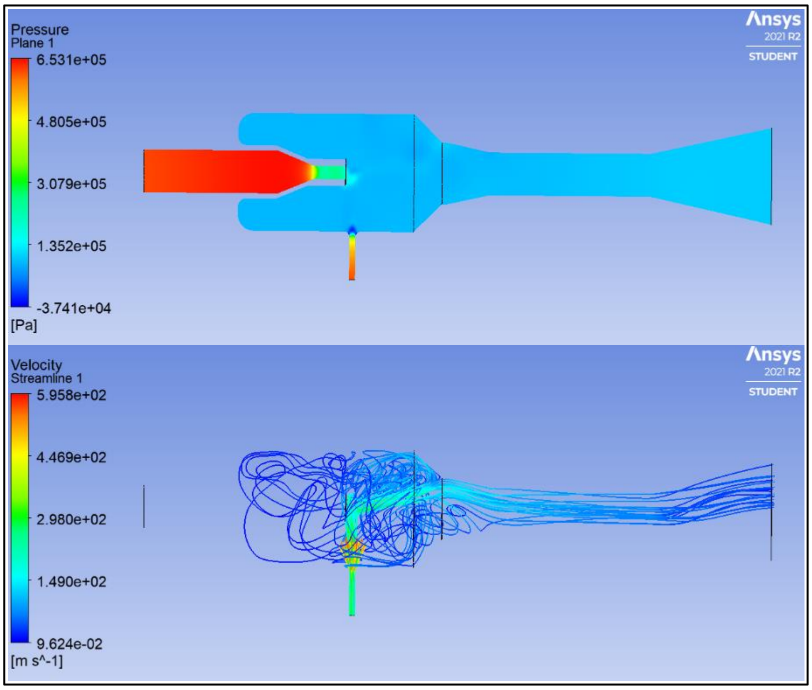

Figure 33 - Pressure and velocity results of the refined venturi design, utilizing an emergency air orifice size of 2.5 mm^2.

A method to calculate airflow through an orifice adapted from Barton et al. was utilized to refine the orifice CFD modeling, as shown in Figure 34. This methodology was chosen because it was supported by the literature, rather than the previous methodology which was a first pass attempt by the author not supported by the literature.

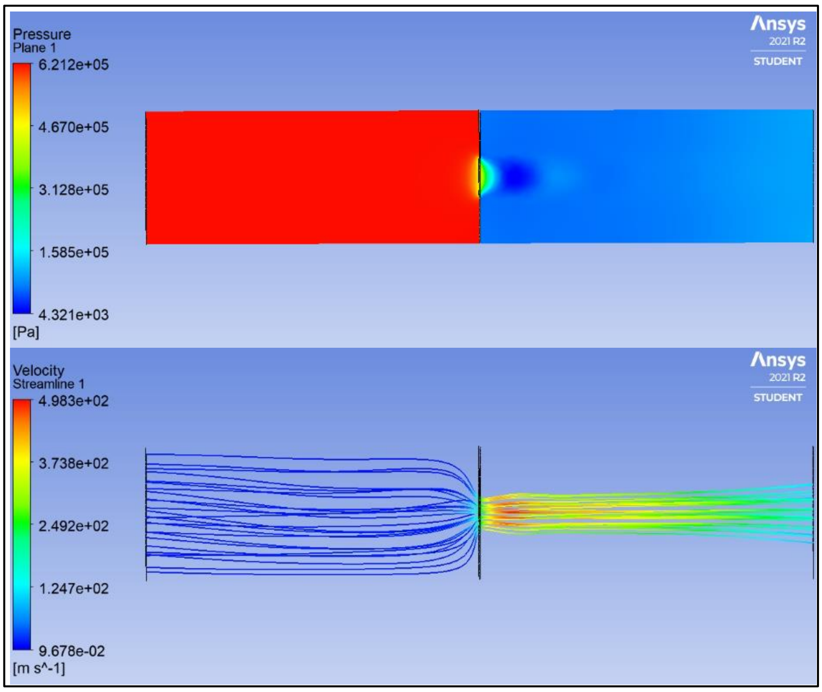

Figure 34 - Alternative orifice modeling technique.

With the new orifice modeling technique and the modified venturi geometry, the current venturi design does not achieve sonic flow. Because sonic flow is not achieved, the addition of sonic flow to the longitudinal dynamics simulator is purely theoretical. However, a conservative venturi effect was analyzed in the simulator. Additionally, pneumatic model results will only be further analyzed in the longitudinal dynamics simulation results because the longitudinal dynamics simulator utilizes a pneumatic model during simulations. The emergency reservoir orifice sizes and venturi factors used in the longitudinal dynamics simulator are shown in Table 4 below. Rejected alternative venturi designs are shown in Appendix C.

Table 4 - Venturi geometries used in longitudinal dynamics simulator

Case	Emg. Res. Orifice Size (mm^2)	Venturi Factor (η)
Baseline	-	-
Venturi	2	1.05
Sonic	7.8	1.4

5 LTD SIMULATION RESULTS AND DISCUSSION

This section shows the results of the dynamic simulation and discusses the important aspects of the data. It is broken into sections by train composition.

5.1. One Locomotive, Eighty-Four Wagons Configuration

The principal evaluation criteria from the simulations are compiled in Table 5 below, which compiles the criteria during a brake application until the locomotive comes to a stop. The evaluated criteria were the total energy dissipated by the draft gears, the total damage accumulated per the fatigue criteria, the stopping time, and the stopping distance. The position of max coupler damage was also included, but not as a criterion. In the 80 km/h, small pressure reduction of 84.1 psi (1 psi = 6894.76 Pa) cases (2,6,10), the train does not come to a full stop, therefore the stopping time is not evaluated.

Table 5 - Longitudinal dynamics performance comparisons for 1 locomotive – 84 wagon configuration.

Case	Total Dissipated Energy (kJ)	Total Accumulated Damage (10^{-3})	Position of Max Damage (Coupler #)	Stopping Time (s)	Distance Traveled (m)
Baseline (1)	16.0	1.9	64	92.6	266.8
Venturi (5)	-18%	-37%	75	-0.1%	-0.1%
Sonic (9)	-71%	-100%	84	-1.2%	-1.8%
Baseline (2)	37.1	37.1	18	39.0	133.6
Venturi (6)	-37%	-70%	26	-1.0%	-1.0%
Sonic (10)	-72%	-97%	84	-1.6%	-1.6%
Baseline (3)	80.0	18.7	2	197.7	2855.1
Venturi (7)	-0.5%	+7.0%	23	-	-0.0%
Sonic (11)	-13.5%	+3.2%	23	-	-0.4%
Baseline (4)	141.4	$2.7x10^6$	81	114.5	1352.5
Venturi (8)	-2.5%	-11.5%	83	-0.1%	-0.2%
Sonic (12)	-6.7%	-88%	77	-0.3%	-0.6%

The following figures are listed by the case number indicated in Table 1. The figures contain the fatigue index summation for each connection device along the train composition. Because the current average velocity of a heavy haul trip is 20 km/h, these results are shown below. The pneumatic and brake cylinder force results are independent of velocity and are therefore listed by the pressure drop magnitude. Additional results are available in Appendix D.

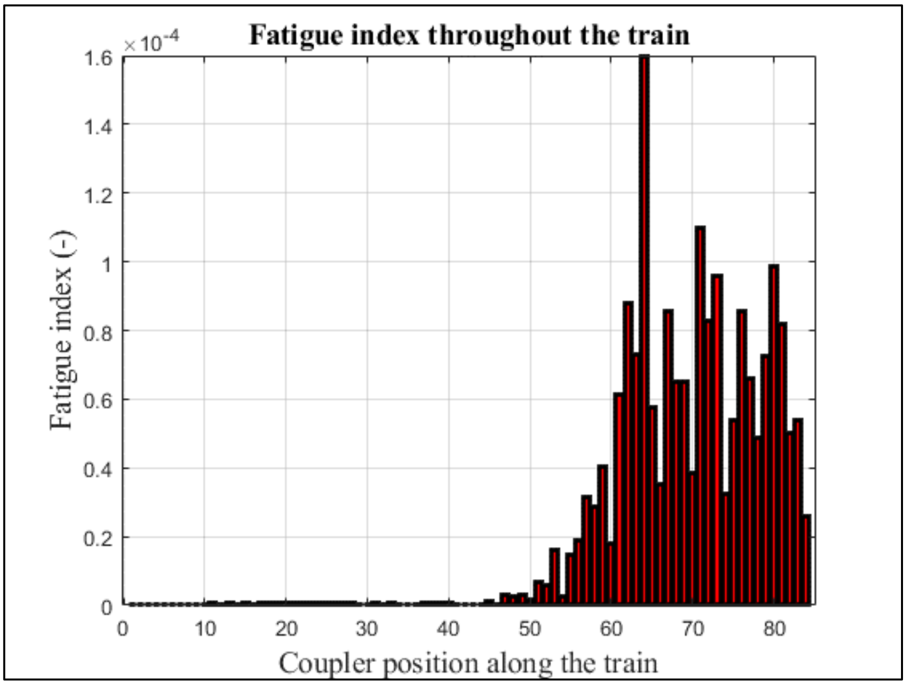

Figure 35 - Case 1: Accumulated fatigue damage of the connection devices in the train.

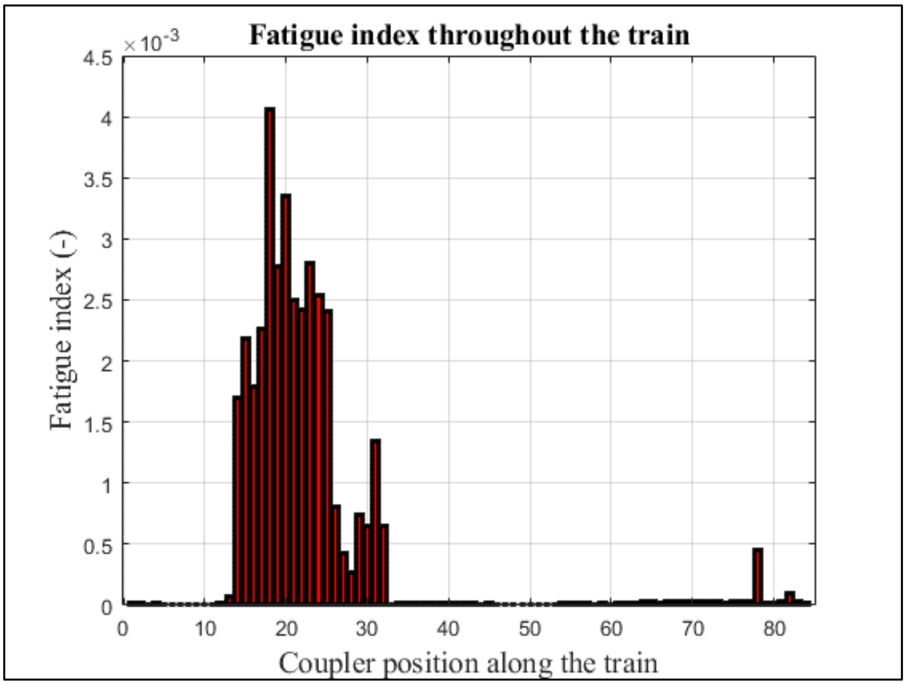

Figure 36 - Case 2: Accumulated fatigue damage of the connection devices in the train.

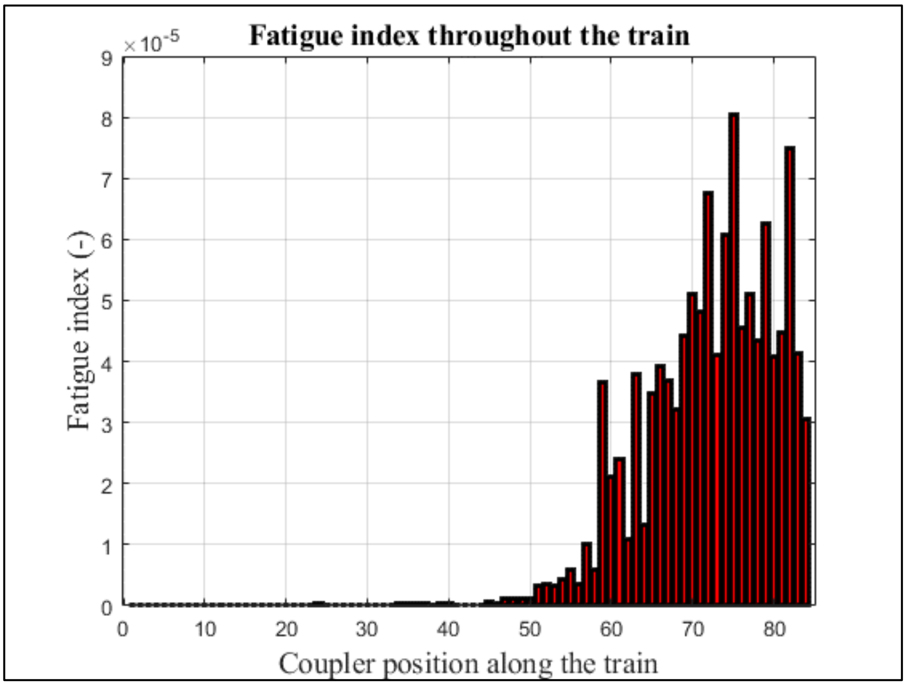

Figure 37 - Case 5: Accumulated fatigue damage of the connection devices in the train.

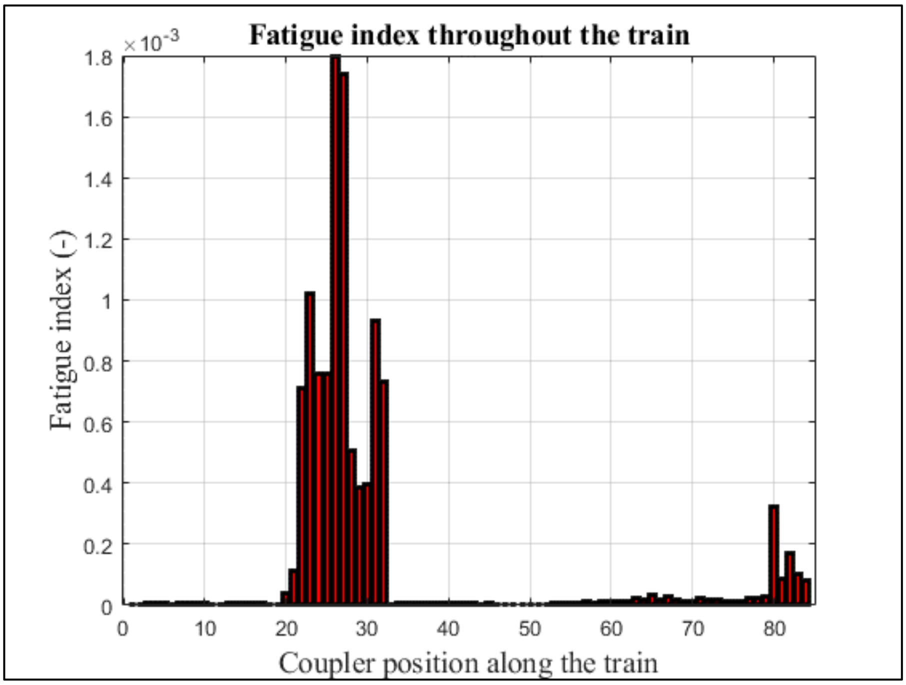

Figure 38 - Case 6: Accumulated fatigue damage of the connection devices in the train.

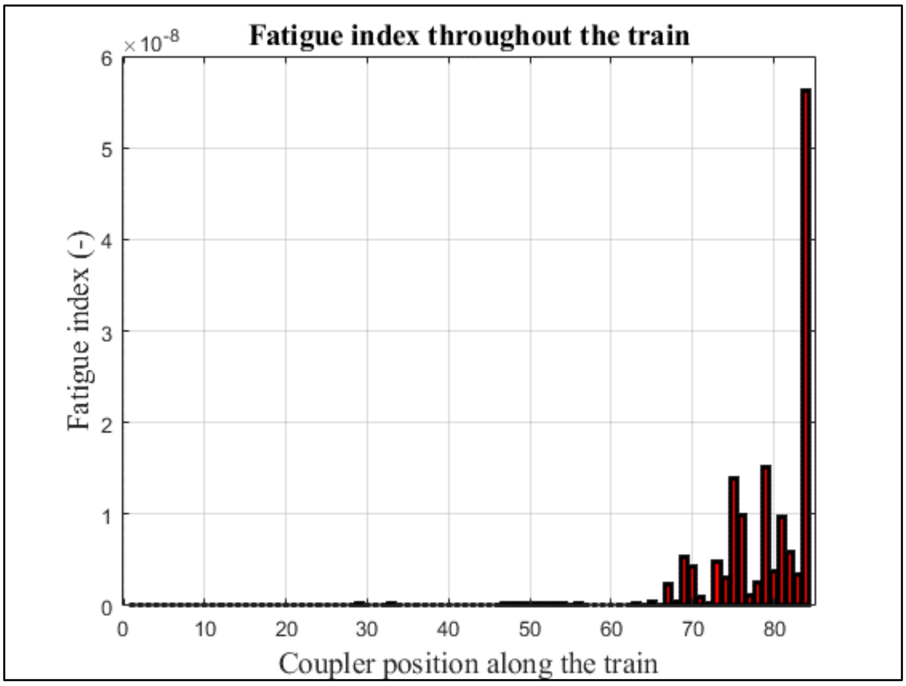

Figure 39 - Case 9: Accumulated fatigue damage of the connection devices in the train.

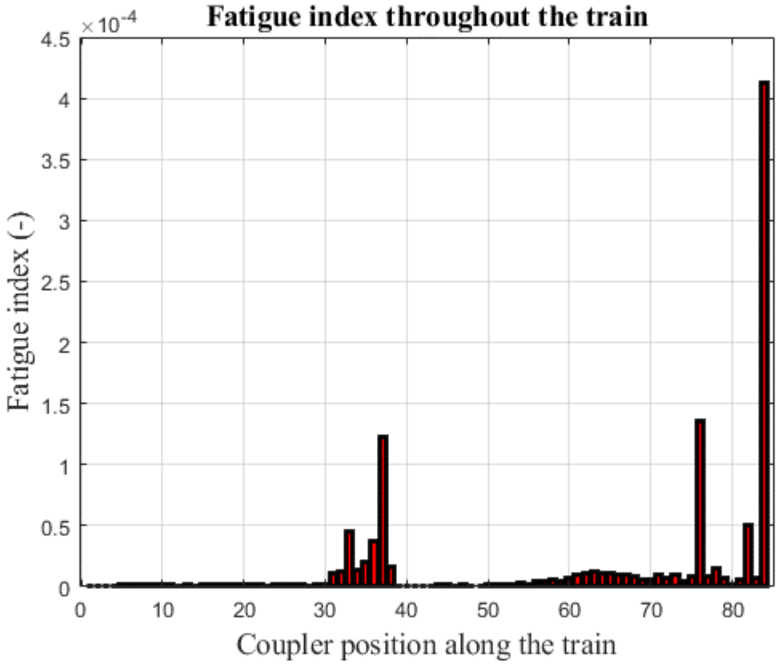

Figure 40 - Case 10: Accumulated fatigue damage of the connection devices in the train.

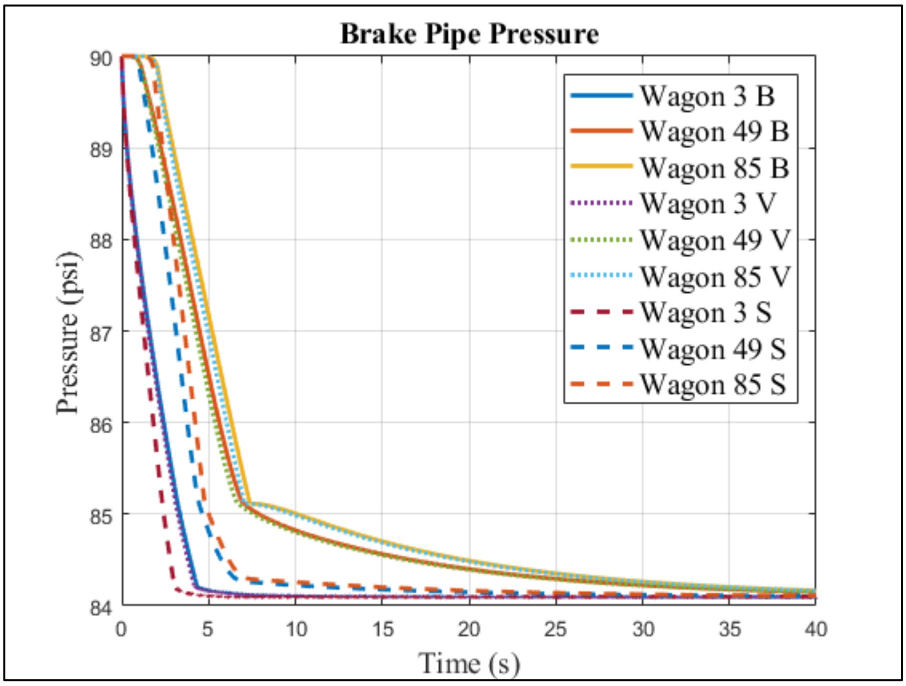

Figure 41 - Brake pipe pressure comparison of 1L84W with a small pressure drop.

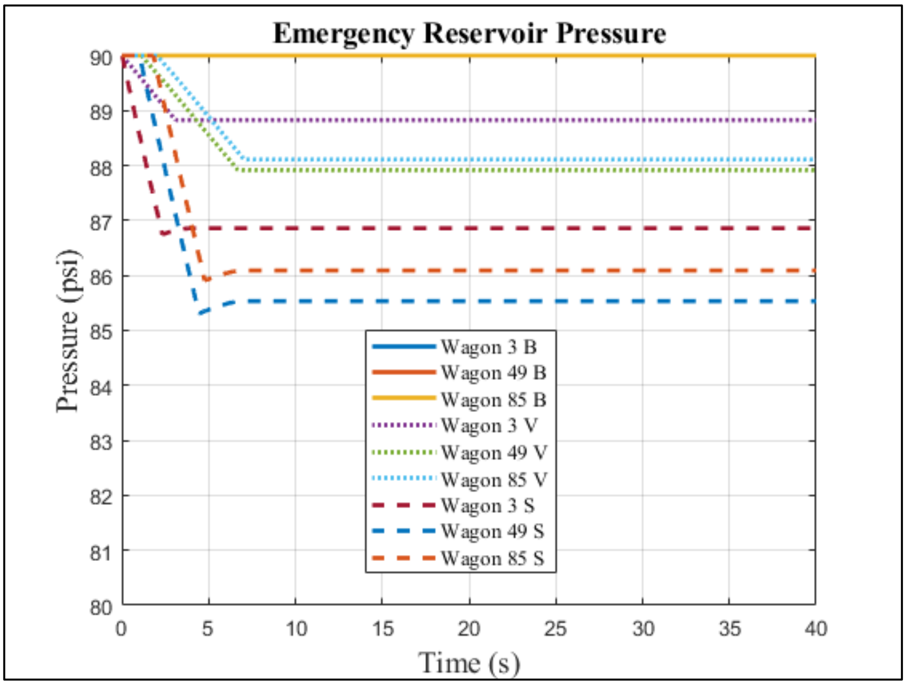

Figure 42 - Emergency reservoir air pressure comparison of 1L84W with a small pressure drop.

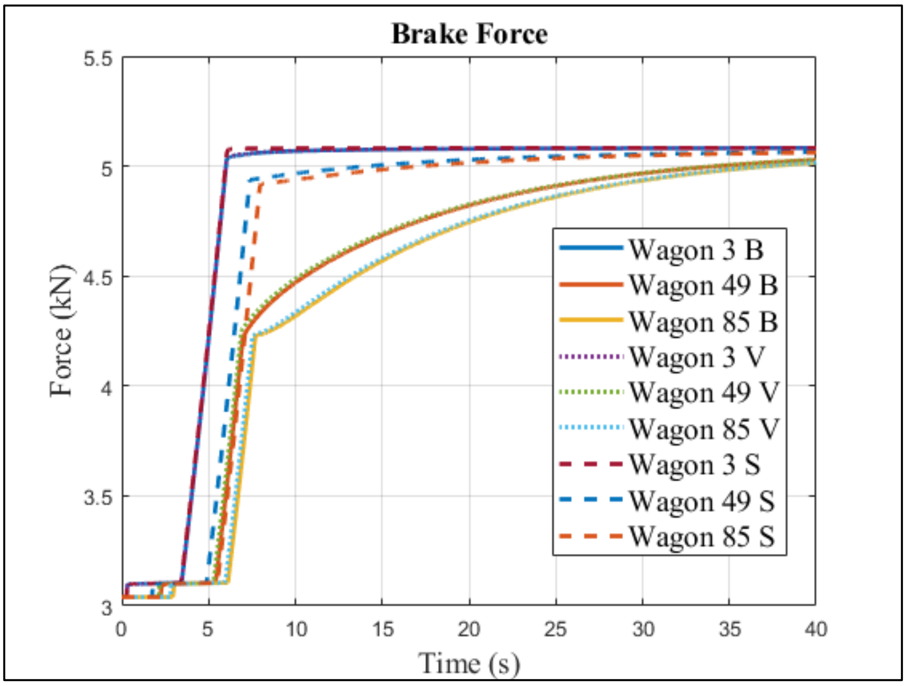

Figure 43 - Brake force comparison of 1L84W with a small pressure drop.

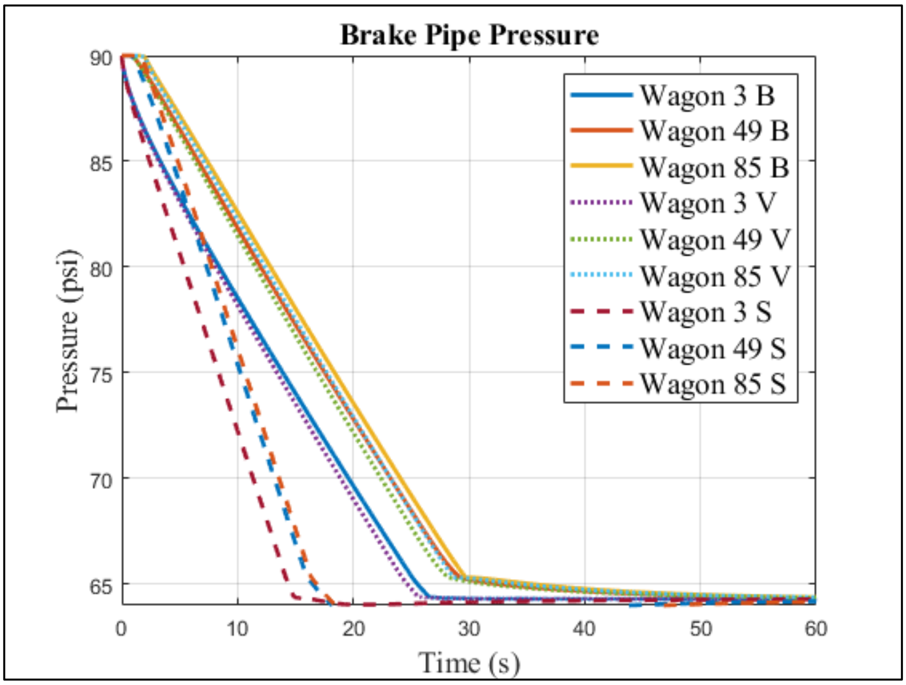

Figure 44 - Brake pipe pressure comparison of 1L84W with a large pressure drop.

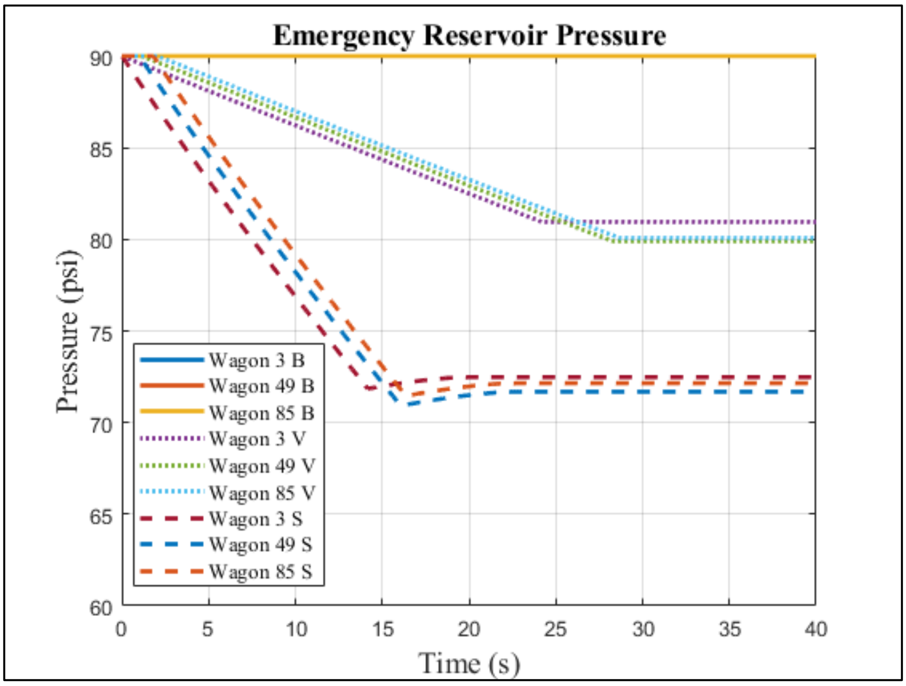

Figure 45 - Emergency reservoir air pressure comparison of 1L84W with a large pressure drop.

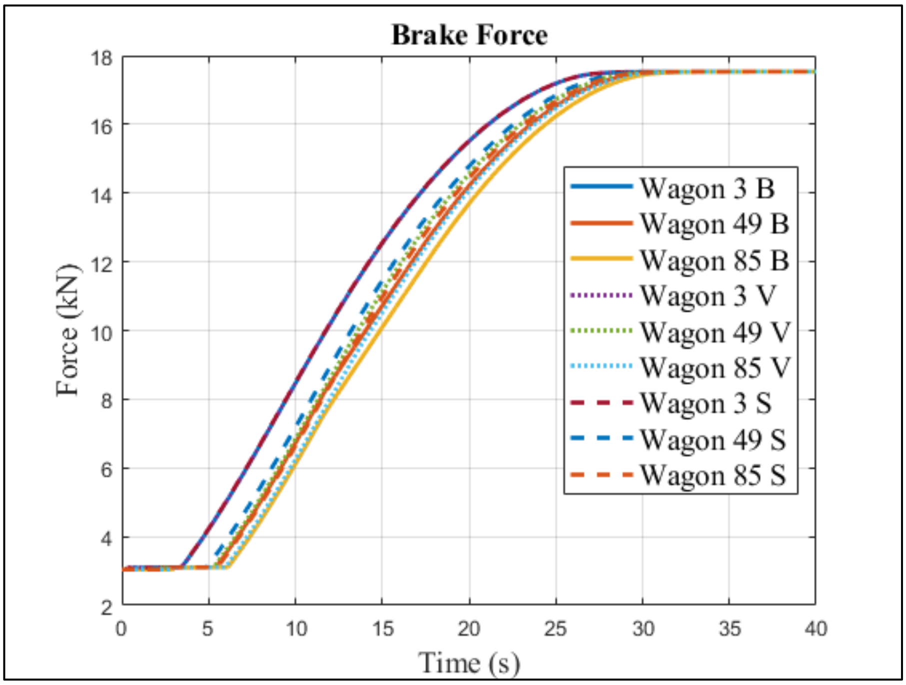

Figure 46 - Brake force comparison of 1L84W with a large pressure drop.

5.2. Two Locomotives, One Hundred Sixty-Eight Wagon Configuration

The principal evaluation criteria from the simulations are compiled in Table 6 below, which compiles the criteria during a brake application until the locomotive comes to a stop. The evaluated criteria were the total energy dissipated by the draft gears, the total damage accumulated per the fatigue criteria, the stopping time, and the stopping distance. The position of max coupler damage was also included, but not as a criterion. In the 80 km/h, small pressure reduction of 84.1 psi cases (14,18,22), the train does not come to a full stop, therefore the stopping time is not evaluated.

Table 6 - Longitudinal dynamics performance comparisons for 2 locomotive – 168 wagon configuration.

Case	Total Dissipated Energy (kJ)	Total Accumulated Damage (10^{-3})	Position of Max Damage (Coupler #)	Stopping Time (s)	Distance Traveled (m)
Baseline (13)	47.0	11.0	41	96.9	278.2
Venturi (17)	-2.0%	+9.0%	38	-0.2%	-0.3%
Sonic (21)	-47%	-99%	30	-5.0%	-5.0%
Baseline (14)	475.3	$1.8x10^8$	16	41.4	140.6

Venturi (18)	-25%	-35%	150	-0.4%	-1.4%
Sonic (22)	-87%	-100%	106	-3.8%	-4.8%
Baseline (15)	324.9	1.2×10^7	162	197.7	2891
Venturi (19)	-1.1%	-21%	166	-	-0.0%
Sonic (23)	-21%	-93%	164	-	-1.4%
Baseline (16)	1082	1.1×10^9	162	115	1371
Venturi (20)	-6.4%	-31%	158	-0.3%	-0.4%
Sonic (24)	-35%	-73%	164	-1.0%	-1.4%

The following figures are listed by the case number indicated in Table 1. The figures contain the fatigue index summation for each connection device along the train composition. Because the current average velocity of a heavy haul trip is 20 km/h, these results are shown below. The pneumatic and brake cylinder force results are independent of velocity and are therefore listed by the pressure drop magnitude. Additional results are available in Appendix D.

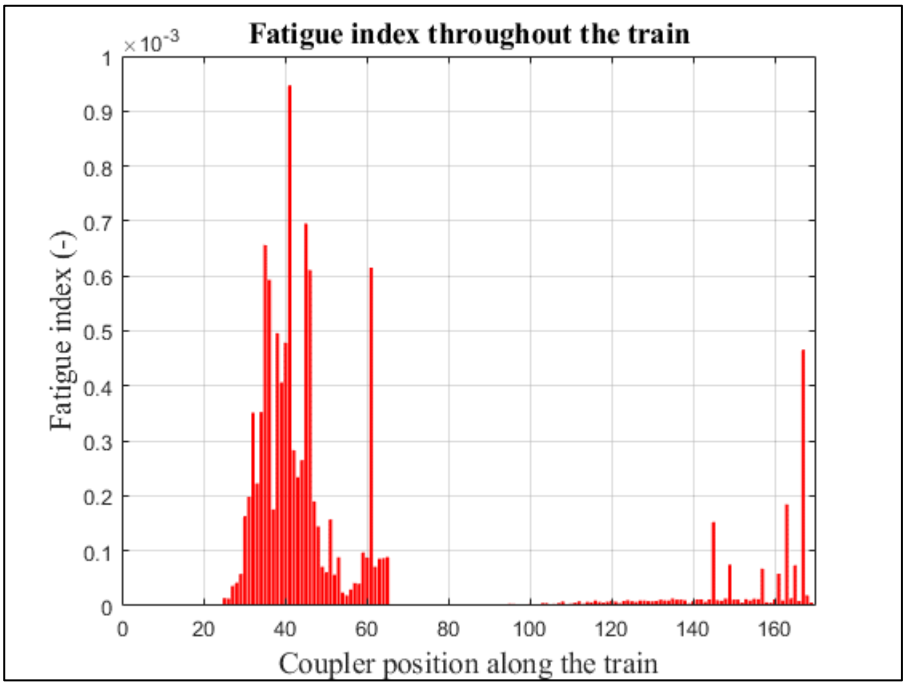

Figure 47 - Case 13: Accumulated fatigue damage of the connection devices in the train.

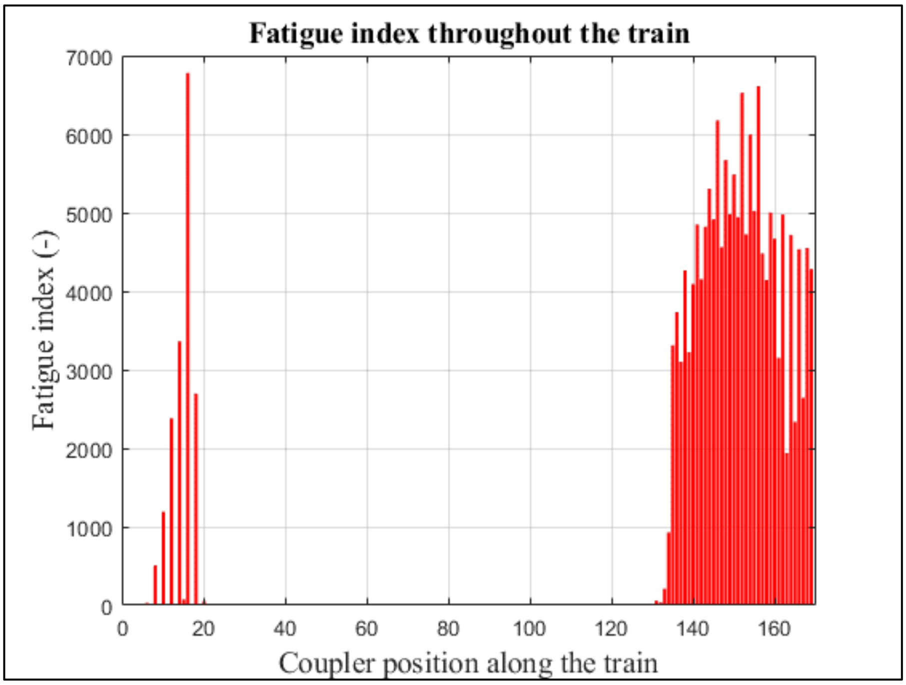

Figure 48 - Case 14: Accumulated fatigue damage of the connection devices in the train.

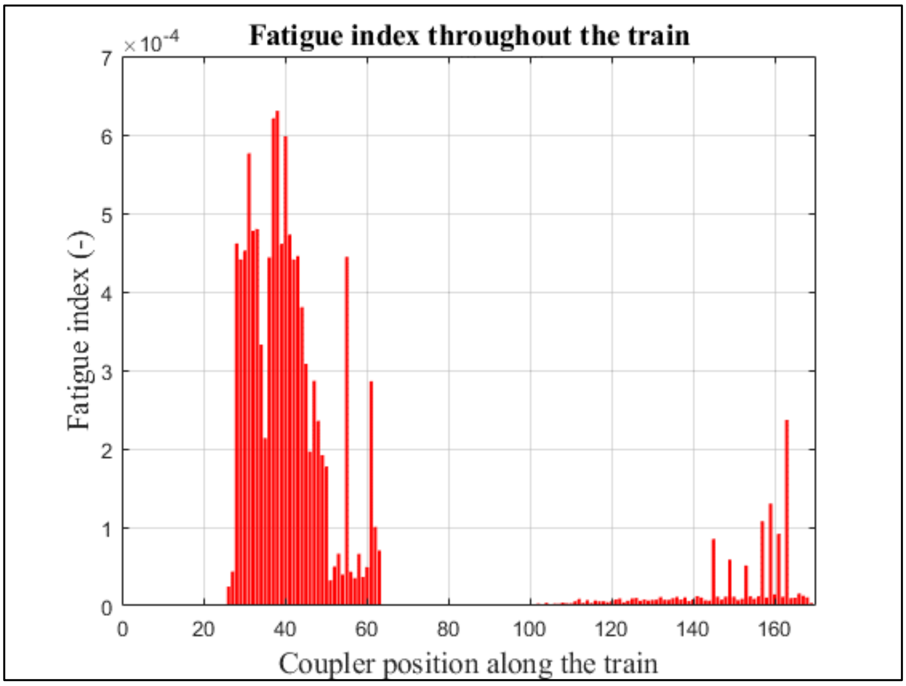

Figure 49 - Case 17: Accumulated fatigue damage of the connection devices in the train.

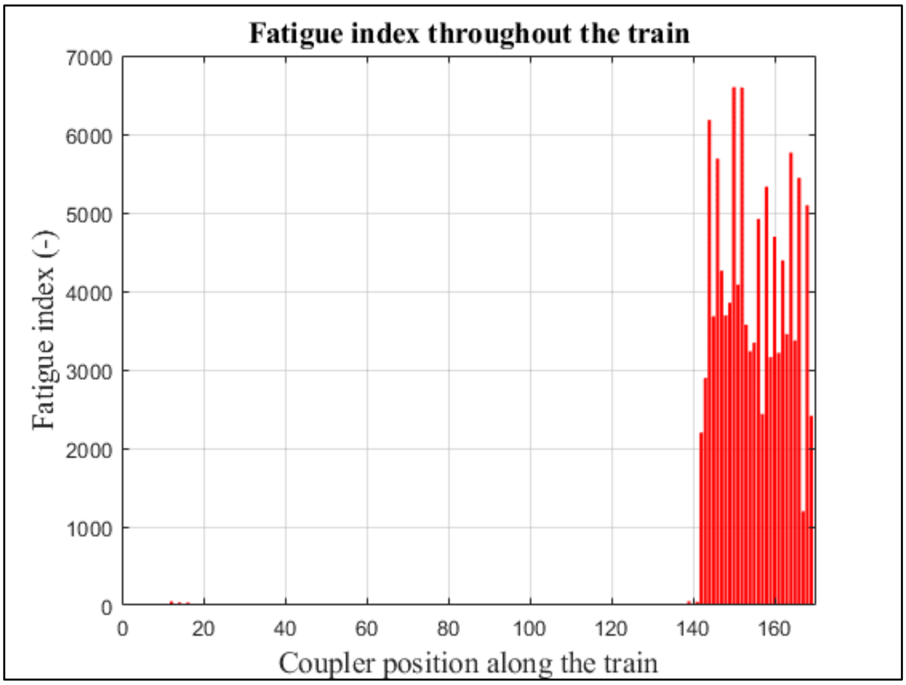

Figure 50 - Case 18: Accumulated fatigue damage of the connection devices in the train.

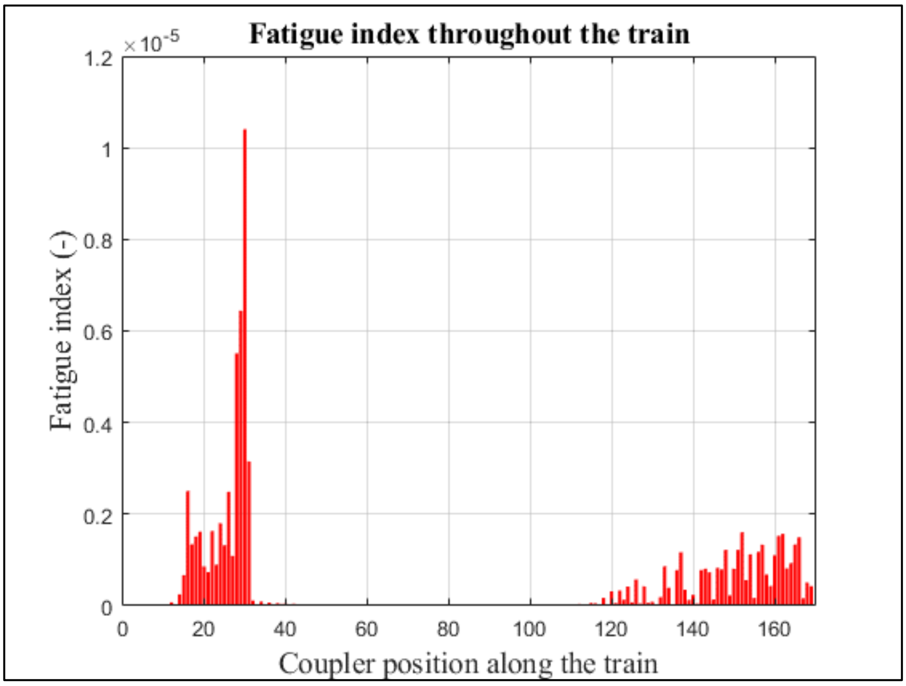

Figure 51 - Case 21: Accumulated fatigue damage of the connection devices in the train.

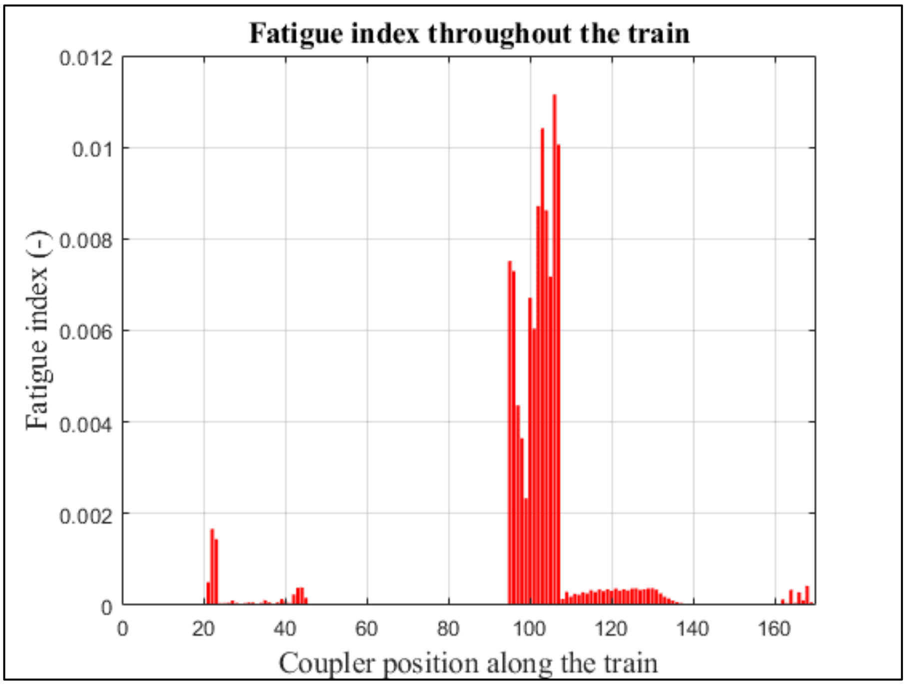

Figure 52 - Case 22: Accumulated fatigue damage of the connection devices in the train.

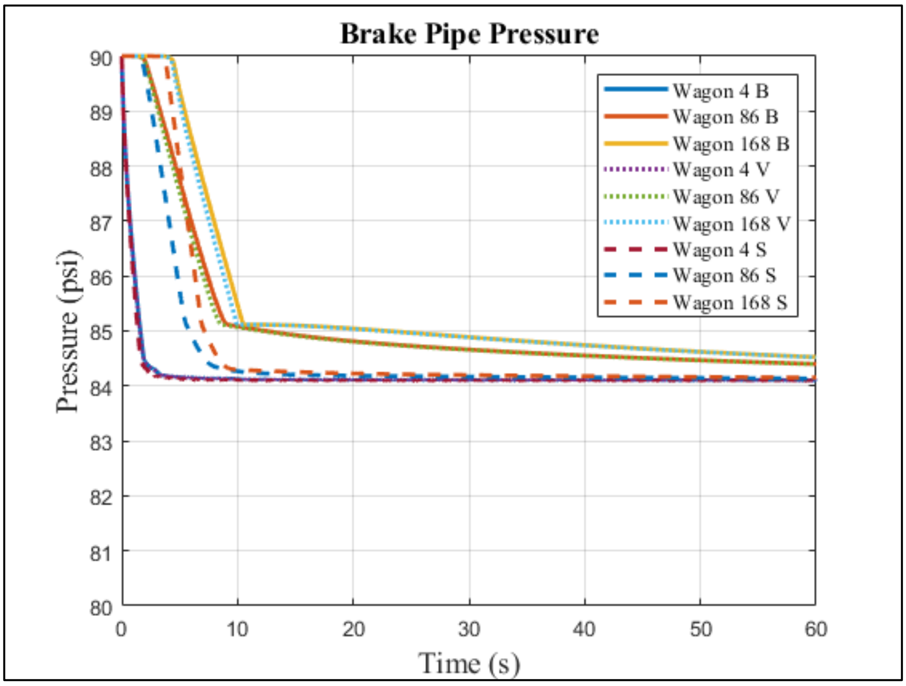

Figure 53 - Brake pipe pressure comparison of 2L168W with a small pressure drop.

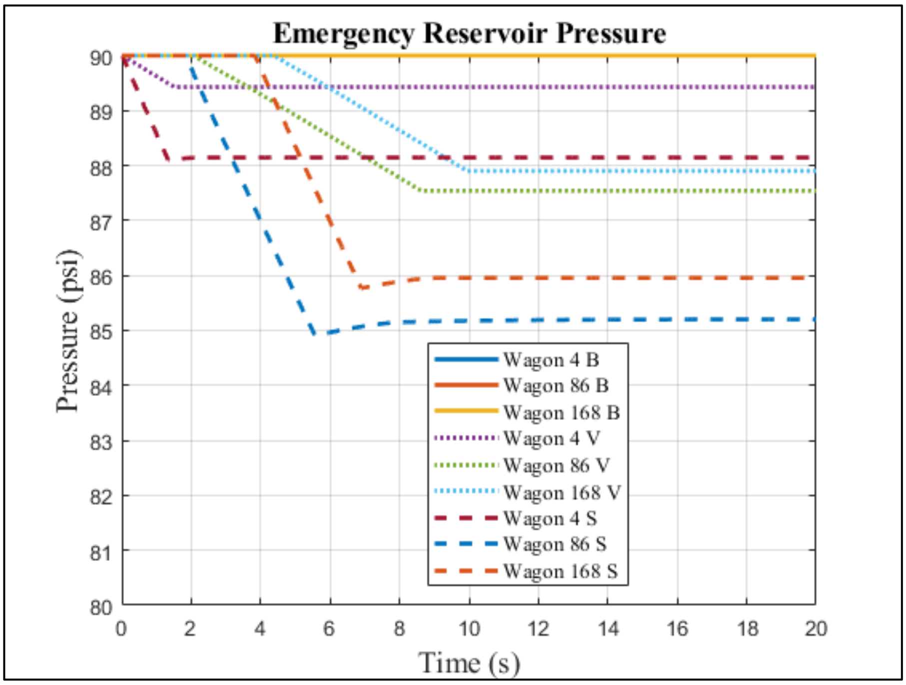

Figure 54 - Emergency reservoir air pressure comparison of 2L168W with a small pressure drop.

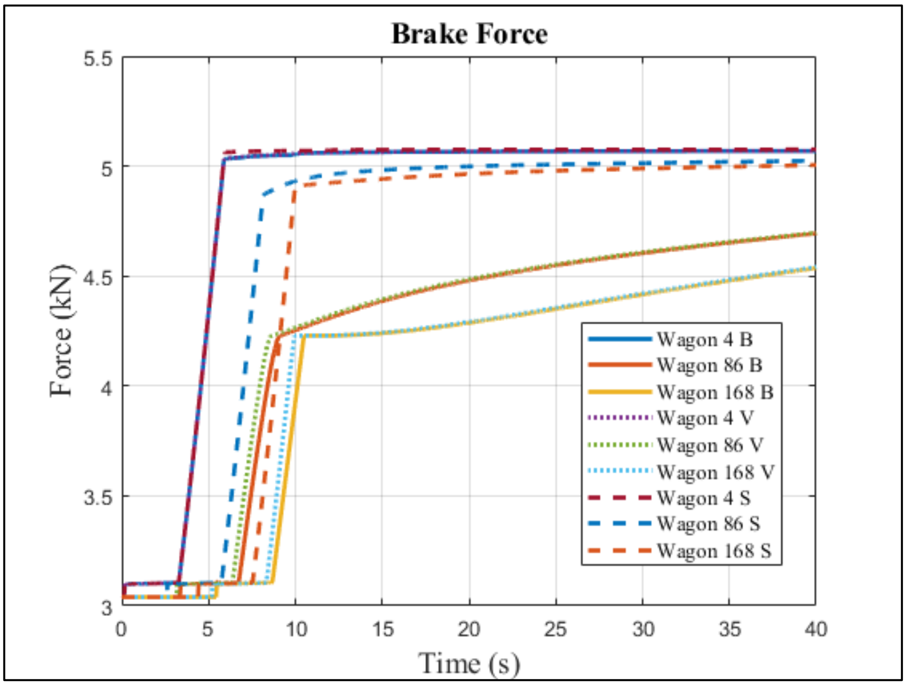

Figure 55 - Brake force comparison of 2L168W with a small pressure drop.

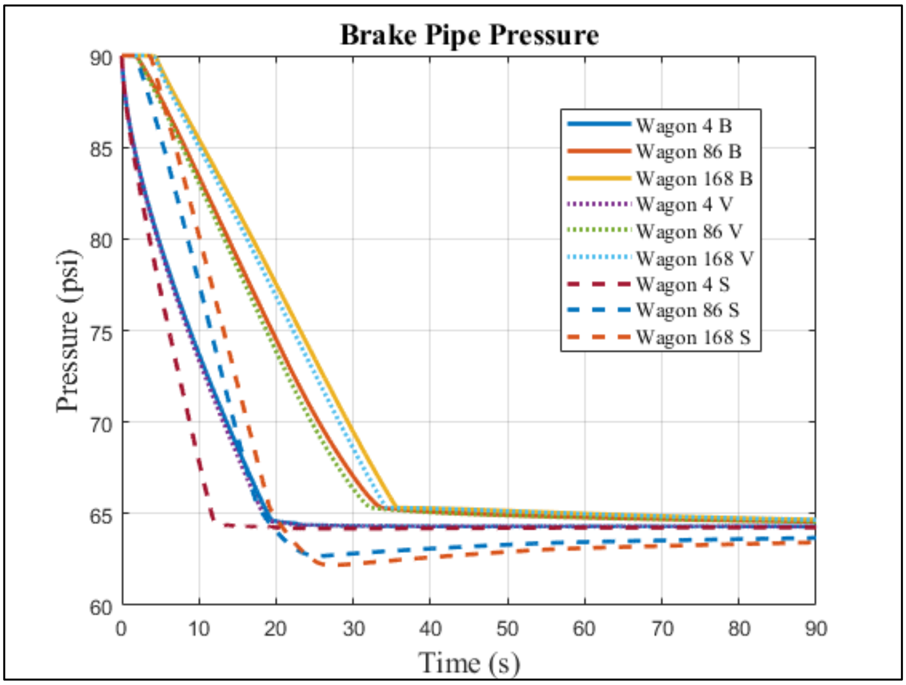

Figure 56 - Brake pipe pressure comparison of 2L168W with a large pressure drop.

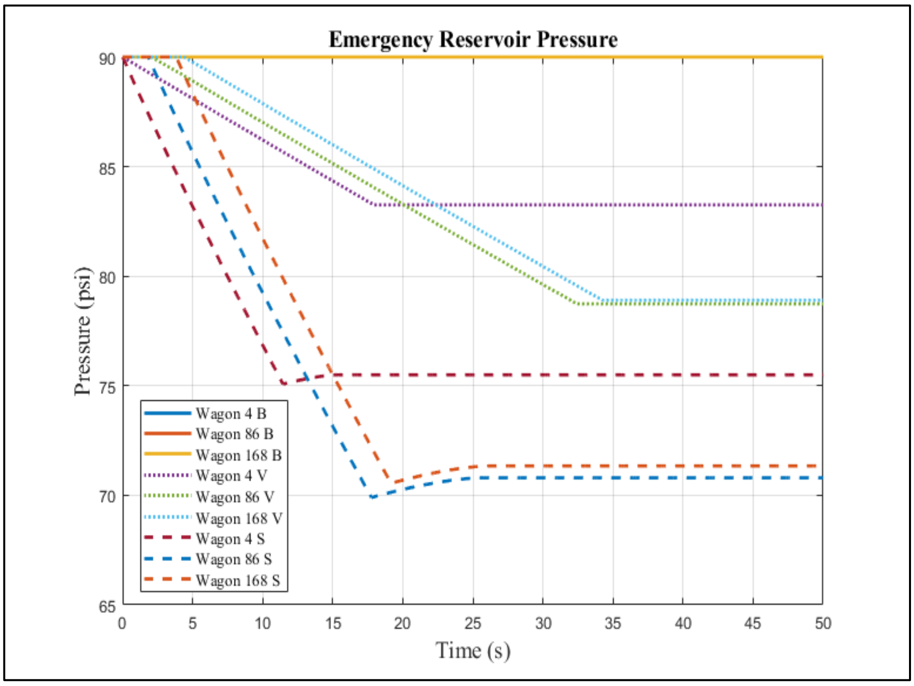

Figure 57 - Emergency reservoir air pressure comparison of 2L168W with a large pressure drop.

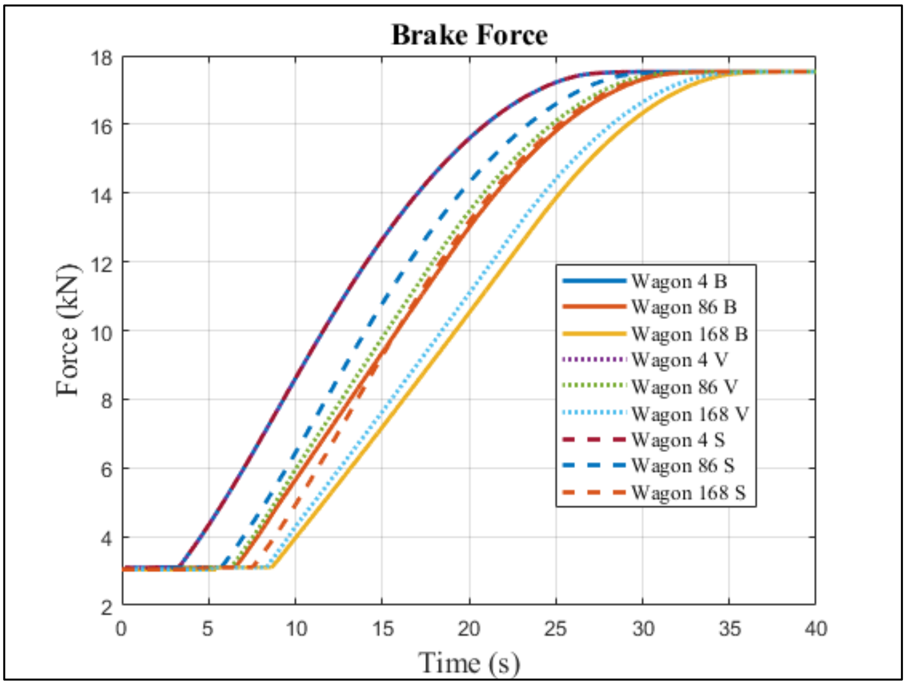

Figure 58 - Brake force comparison of 2L168W with a large pressure drop.

5.3. Real-World Configurations

The principal evaluation criteria from the simulations are compiled in Table 7 below, which compiles the criteria during a real-world trip over 15 km of the EFVM train route. The evaluated criteria were the total energy dissipated by the draft gears, the total damage accumulated per the fatigue criteria, and the distance traveled. The position of max coupler damage was also included, but not as a criterion. Because the simulations were run for 1000 seconds, the train does not complete the entirety of the 15 km track. Additionally, there is no stopping time criteria as the objective of these simulations are to compare a real trip along the route which does not include stopping the locomotive.

Table 7 - Longitudinal dynamics performance comparisons for real-world configuration.

Case	Total Dissipated Energy (MJ)	Total Accumulated Damage (10^8)	Position of Max Damage (Coupler #)	Stopping Time (s)	Distance Traveled (km)
Baseline (25)	6.2	5.2	87	-	10.6
Venturi (26)	+17%	+20%	97	-	+1.2%
Sonic (27)	+23%	+24%	83	-	+5.3%

Baseline (28)	5.4	4.2	88	-	9.7
Venturi (29)	-11%	-40%	95	-	+0.7%
Sonic (30)	-13%	-51%	94	-	+1.6%

In all test cases, but especially in the real-world application cases, a filter was used to reduce noise in the data and also decrease the results file sizes. The data was filtered and downsampled using Matlab's built in lowpass 8^{th} order Chebyshev Type I filter, "decimate," with a sampling rate of 10 kHz. The difference in the raw data and the filtered data is shown below.

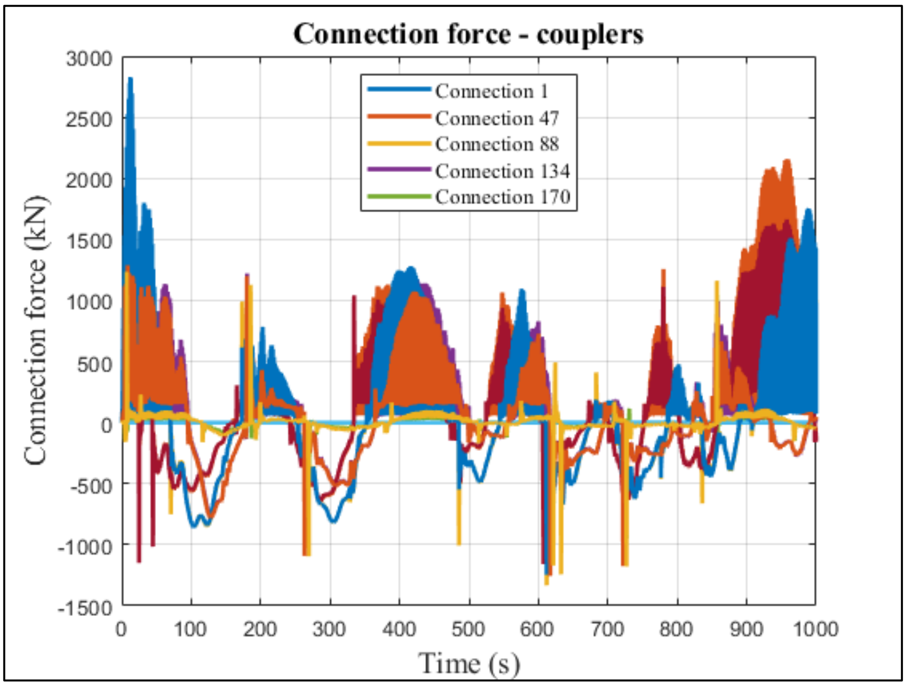

Figure 59 - Raw draft gear force data before filter application.

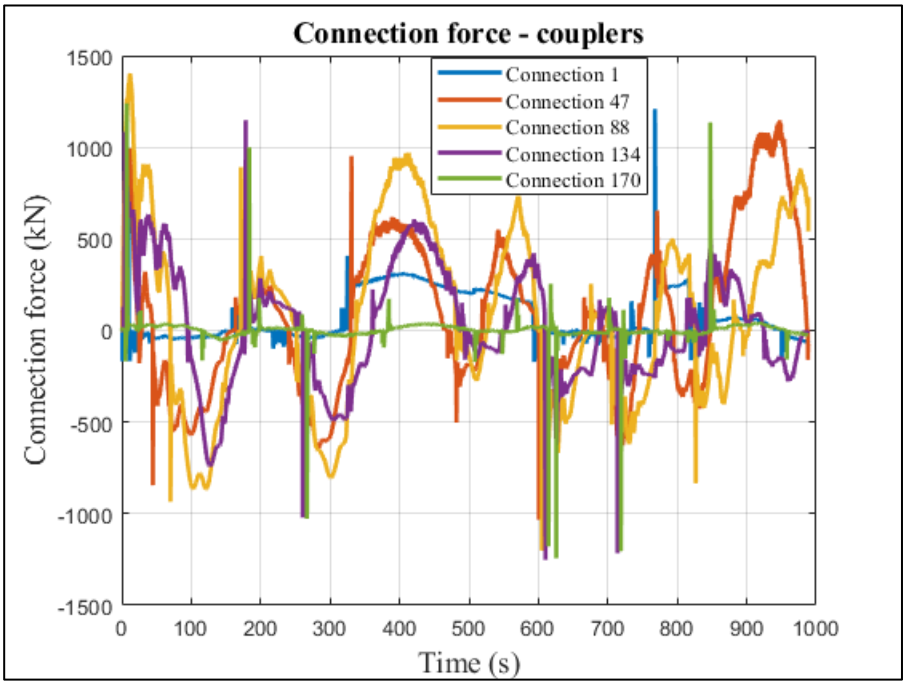

Figure 60 - Filtered draft gear force data.

The following figures are listed by the case number indicated in Table 1. The figures contain the fatigue index summation for each connection device along the train composition. Additional plots are available in Appendix D.

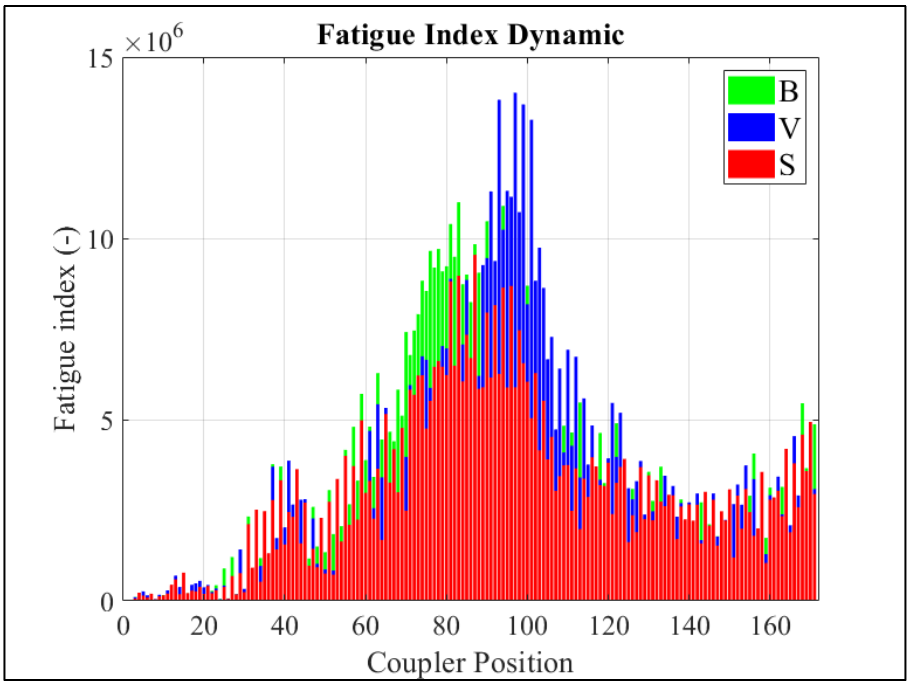

Figure 61 - Accumulated fatigue damage of the connection devices in the train using dynamic brake dominant brake schedule. B – baseline; V – venturi; S – sonic.

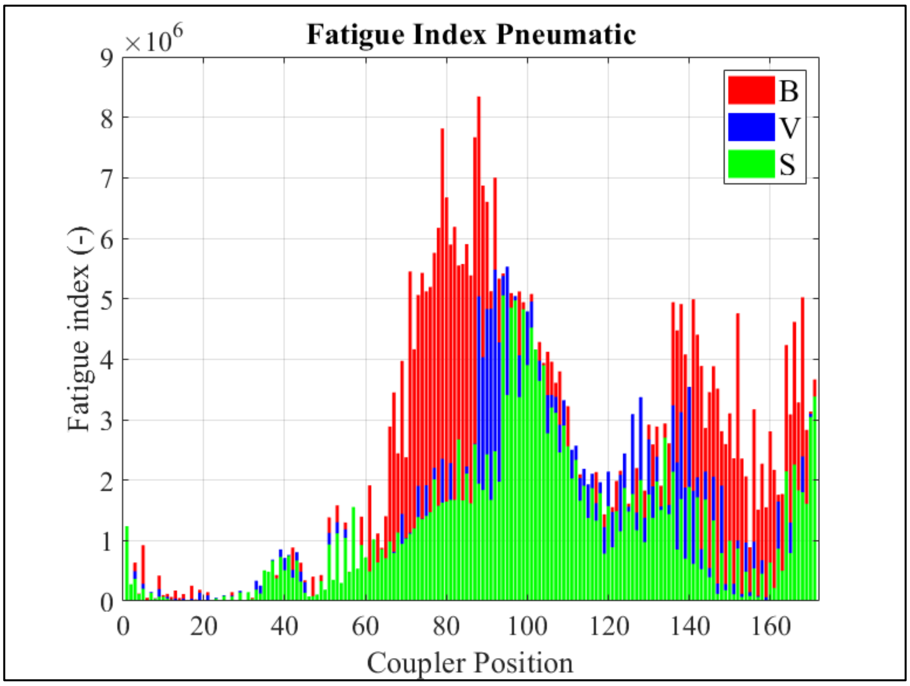

Figure 62 - Accumulated fatigue damage of the connection devices in the train using pneumatic brake dominant brake schedule. B – baseline; V – venturi; S – sonic.

The pneumatic results are listed in the figures below. Each case was divided into two different graphs to more clearly show the front wagons and the rear wagons.

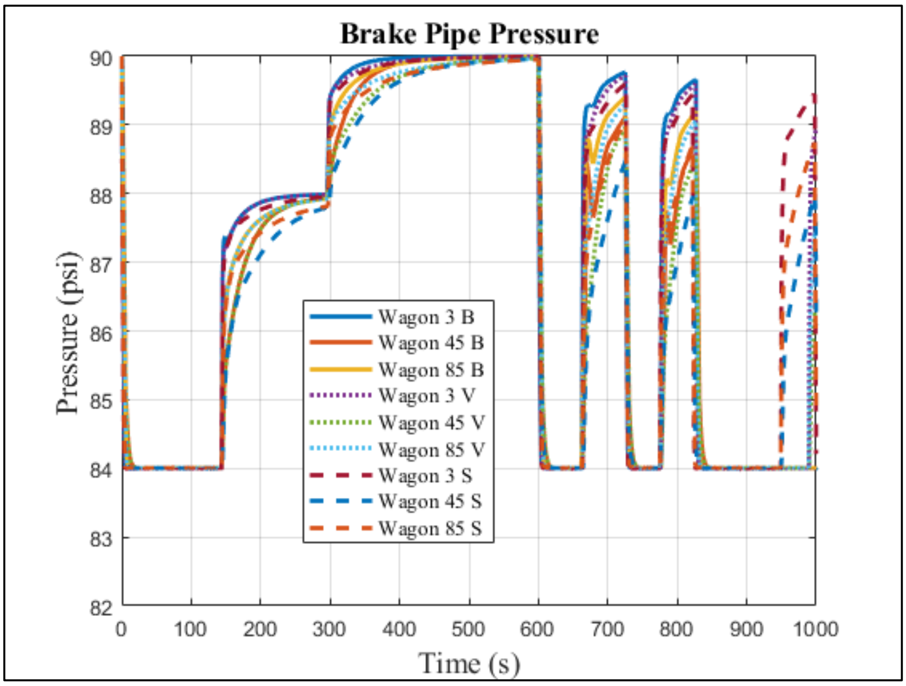

Figure 63 - Case 25-27: Brake pipe pressure in the front wagons. B – baseline; V – venturi; S – sonic.

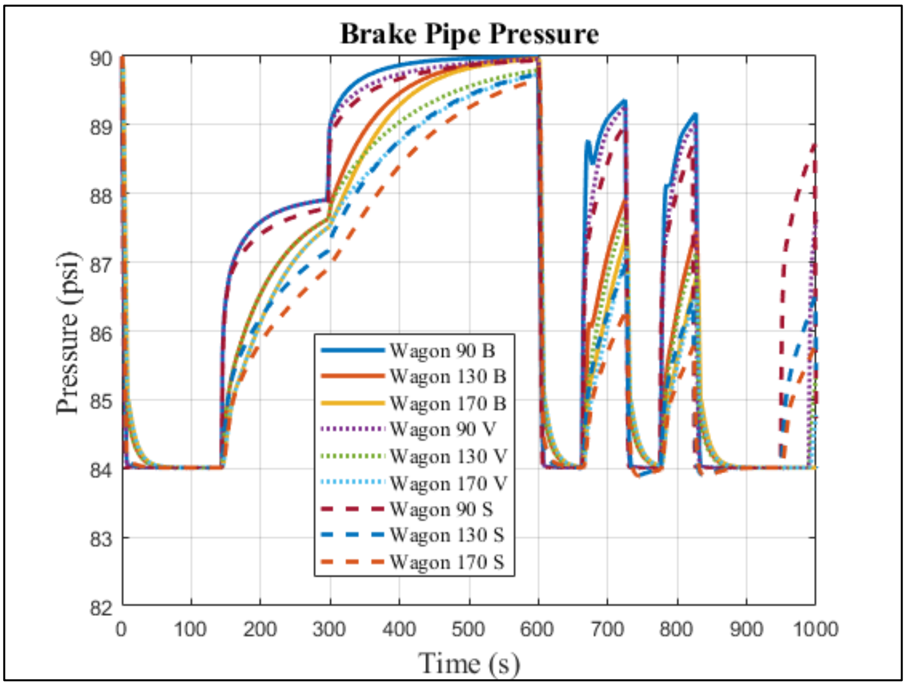

Figure 64 - Case 25-27: Brake pipe pressure in the rear wagons. B – baseline; V – venturi; S – sonic.

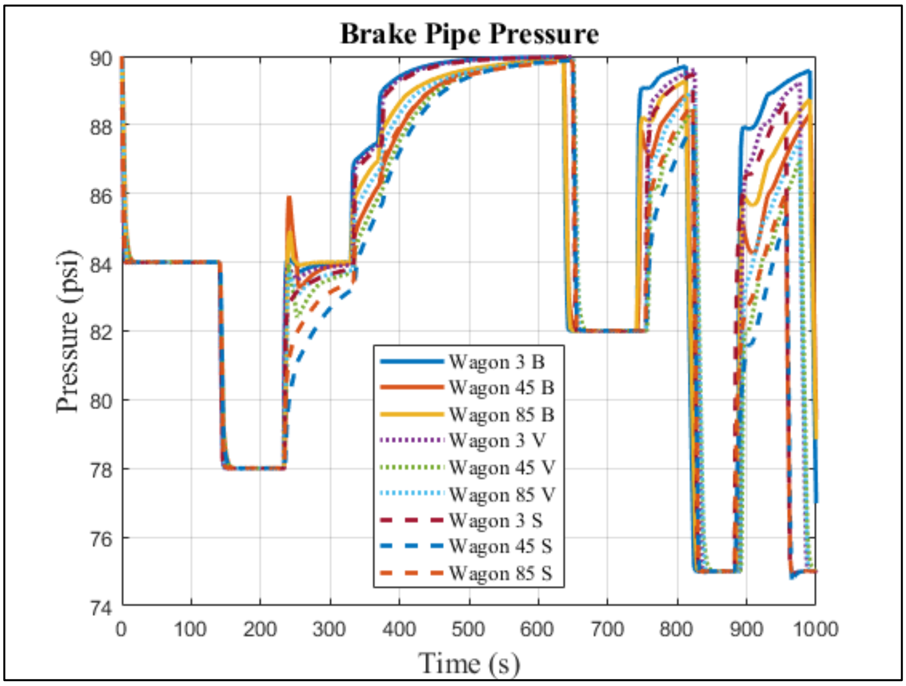

Figure 65 - Case 28-30: Brake pipe pressure in the front wagons. B – baseline; V – venturi; S – sonic.

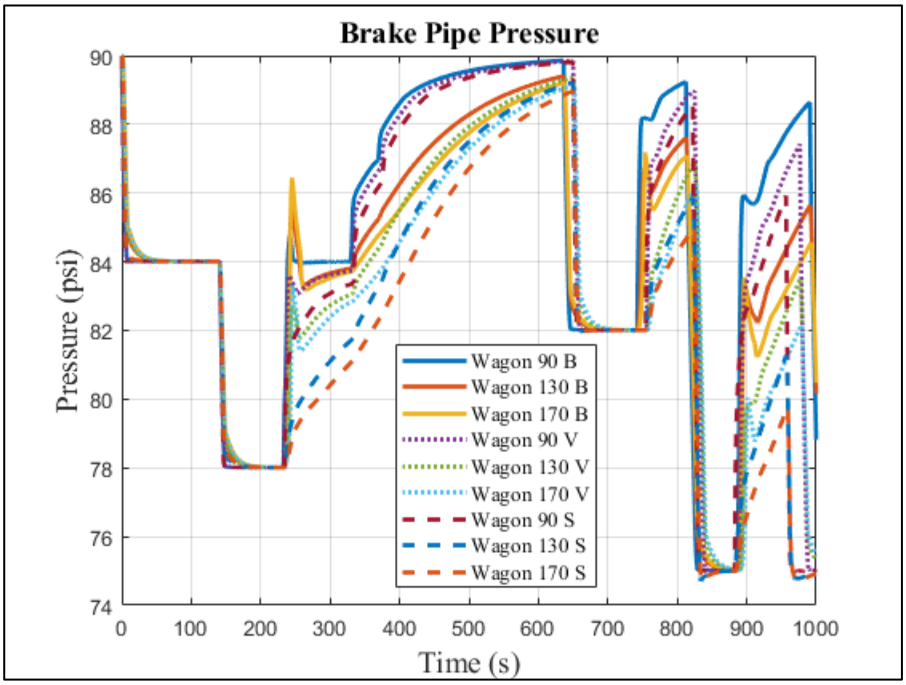

Figure 66 - Case 28-30: Brake pipe pressure in the rear wagons. B – baseline; V – venturi; S – sonic.

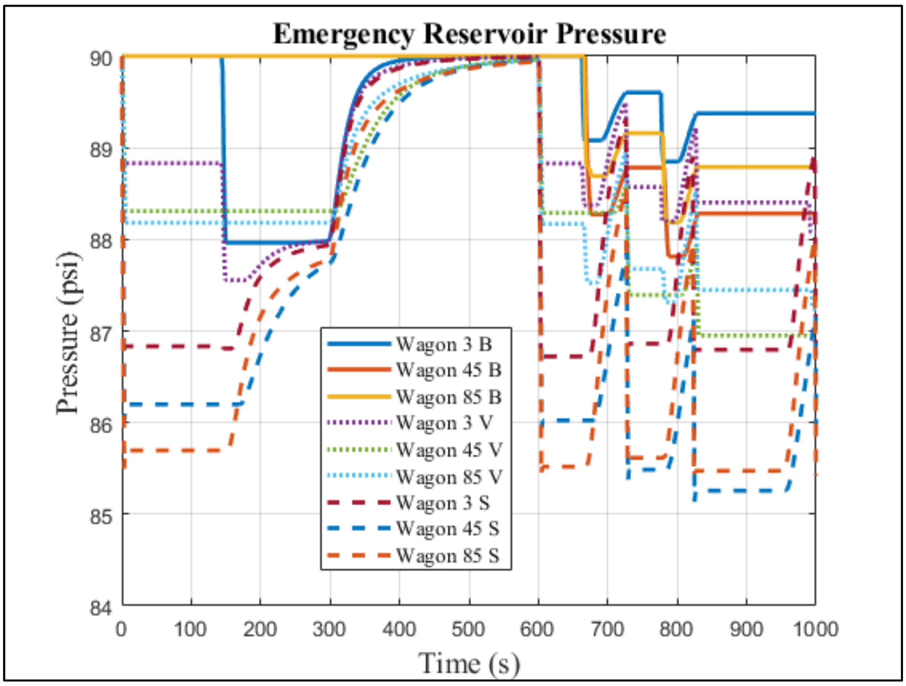

Figure 67 - Case 25-27: Emergency reservoir pressure in the front wagons. B – baseline; V – venturi; S – sonic.

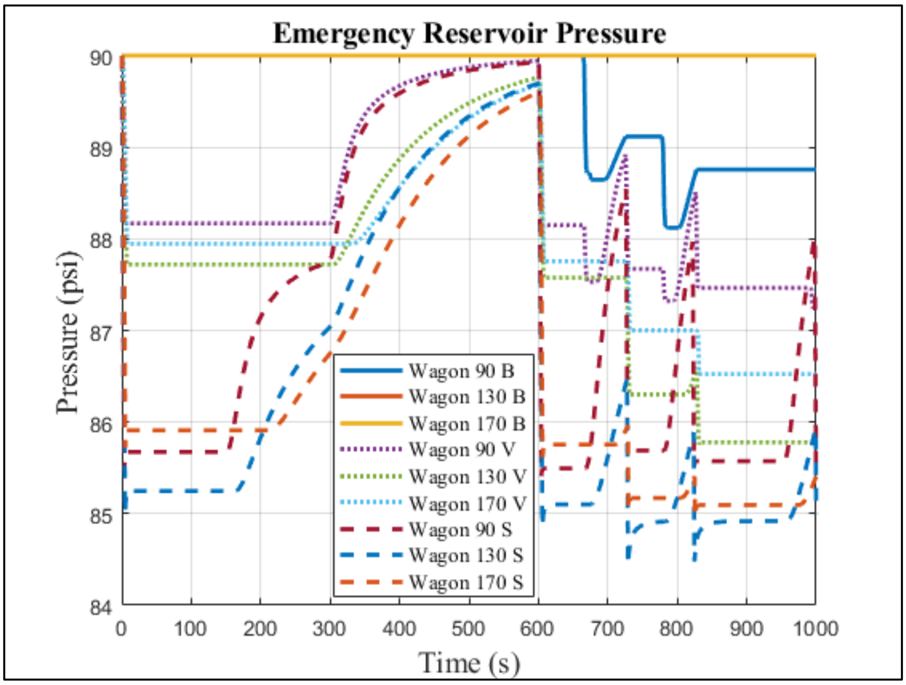

Figure 68 - Case 25-27: Emergency reservoir pressure in the rear wagons. B – baseline; V – venturi; S – sonic.

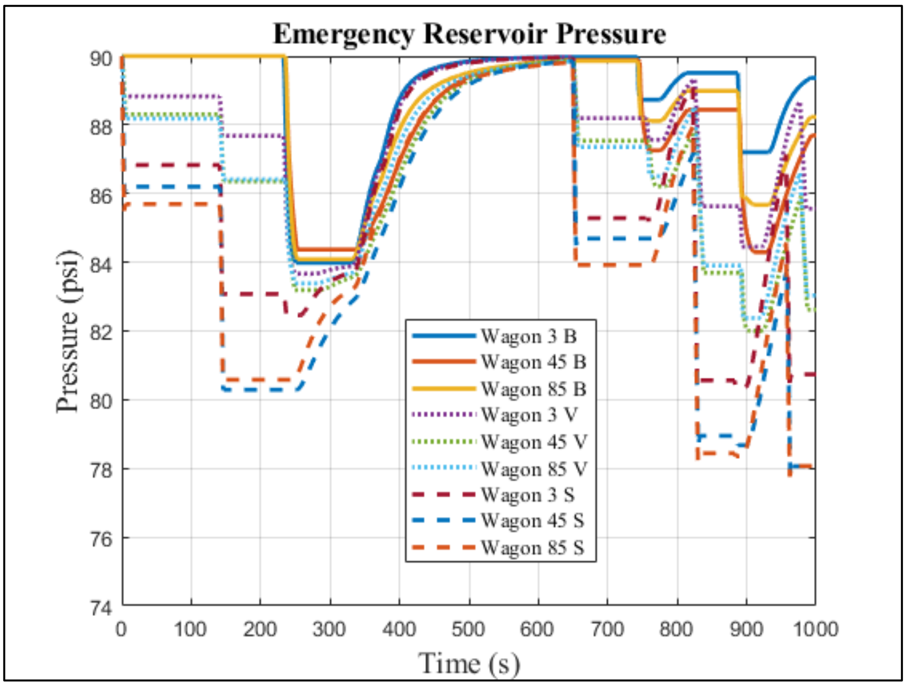

Figure 69 - Case 28-30: Emergency reservoir pressure in the front wagons. B – baseline; V – venturi; S – sonic.

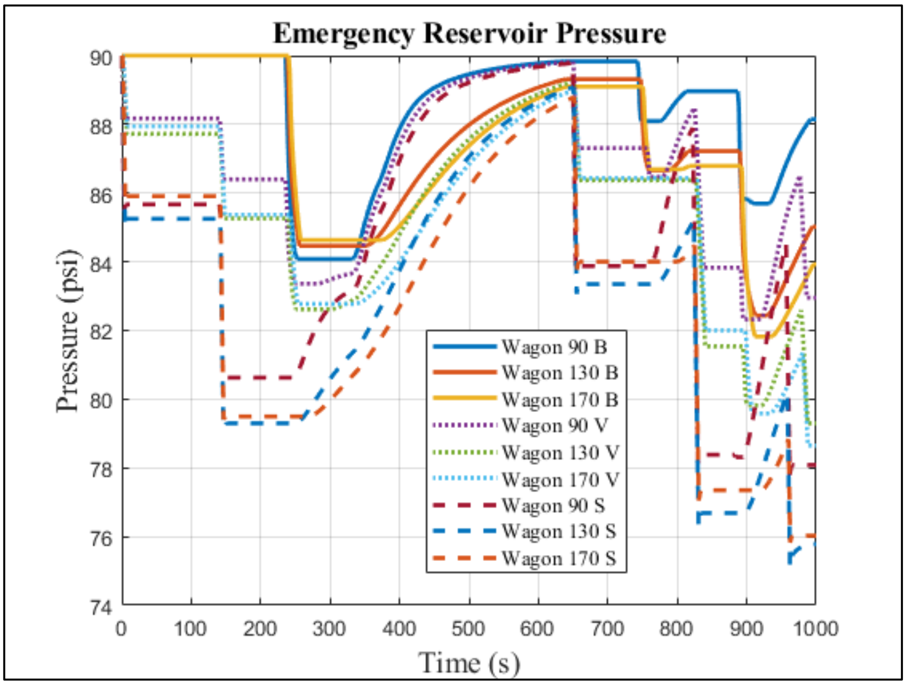

Figure 70 - Case 28-30: Emergency reservoir pressure in the rear wagons. B – baseline; V – venturi; S – sonic.

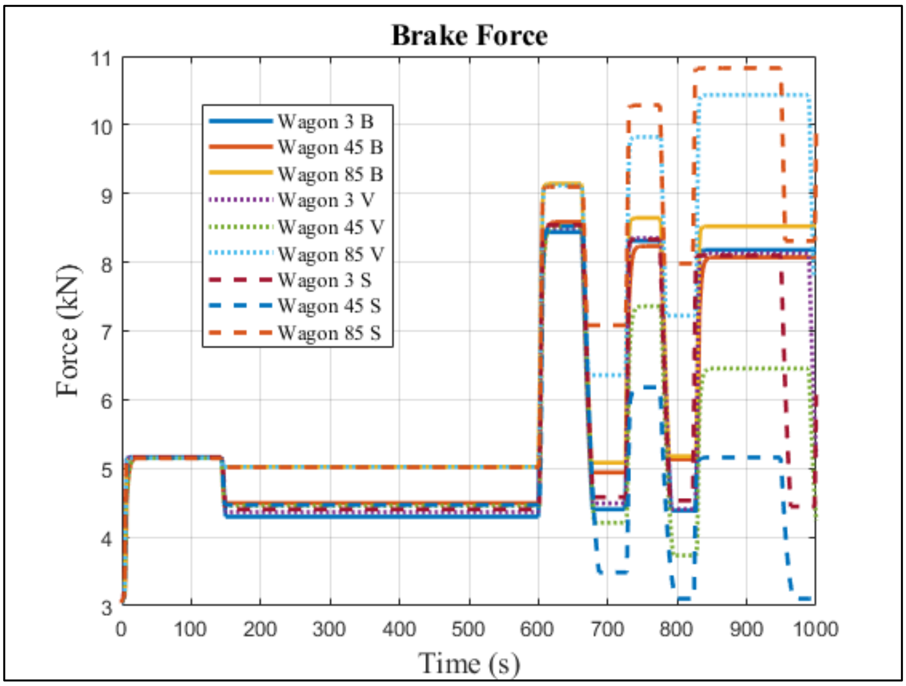

Figure 71 - Case 25-27: Brake forces in the front wagons. B – baseline; V – venturi; S – sonic.

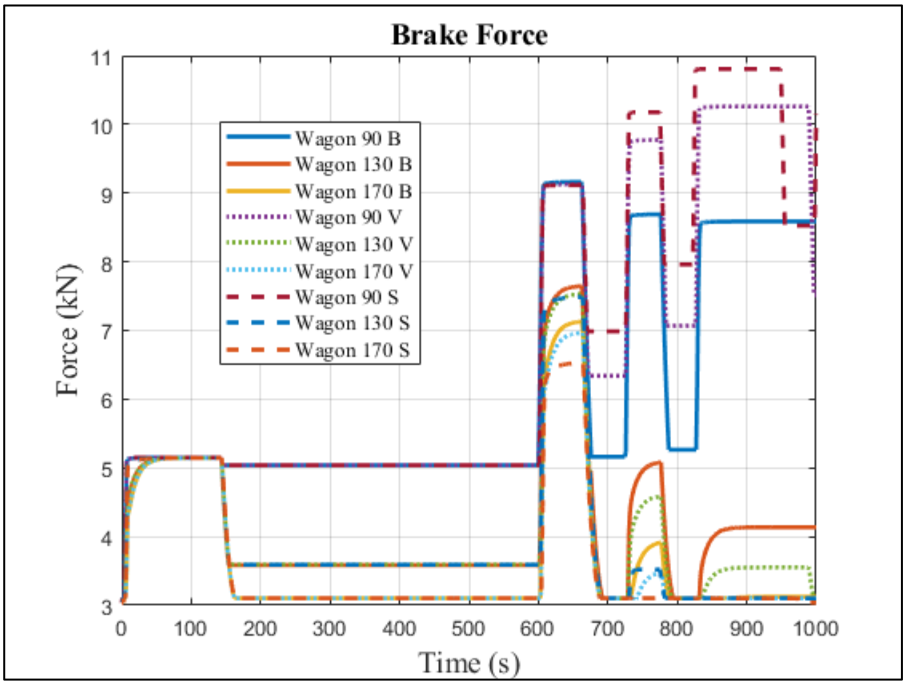

Figure 72 - Case 25-27: Brake forces in the rear wagons. B – baseline; V – venturi; S – sonic.

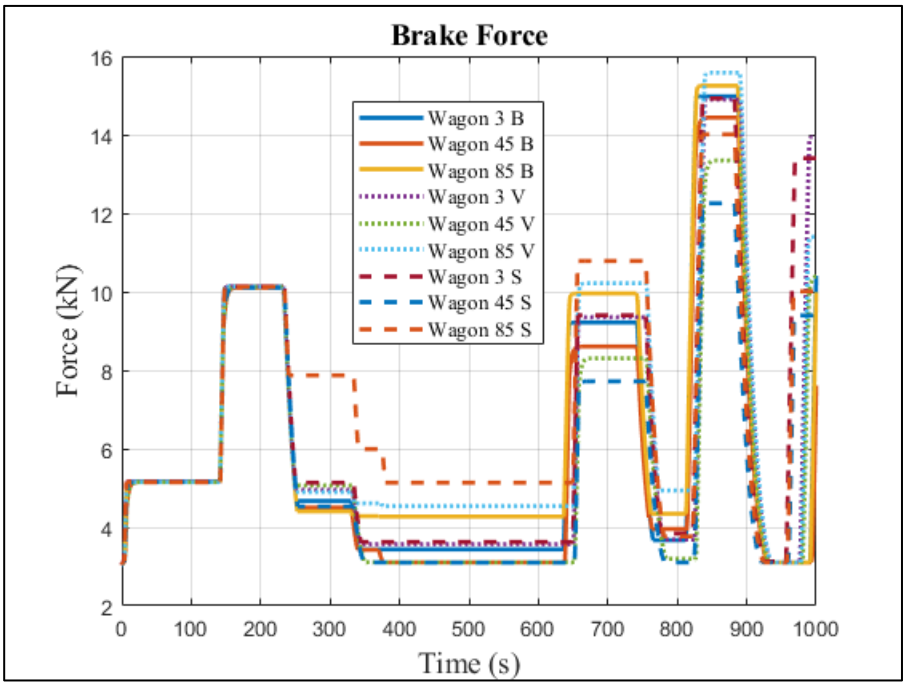

Figure 73 - Case 28-30: Brake forces in the front wagons. B – baseline; V – venturi; S – sonic.

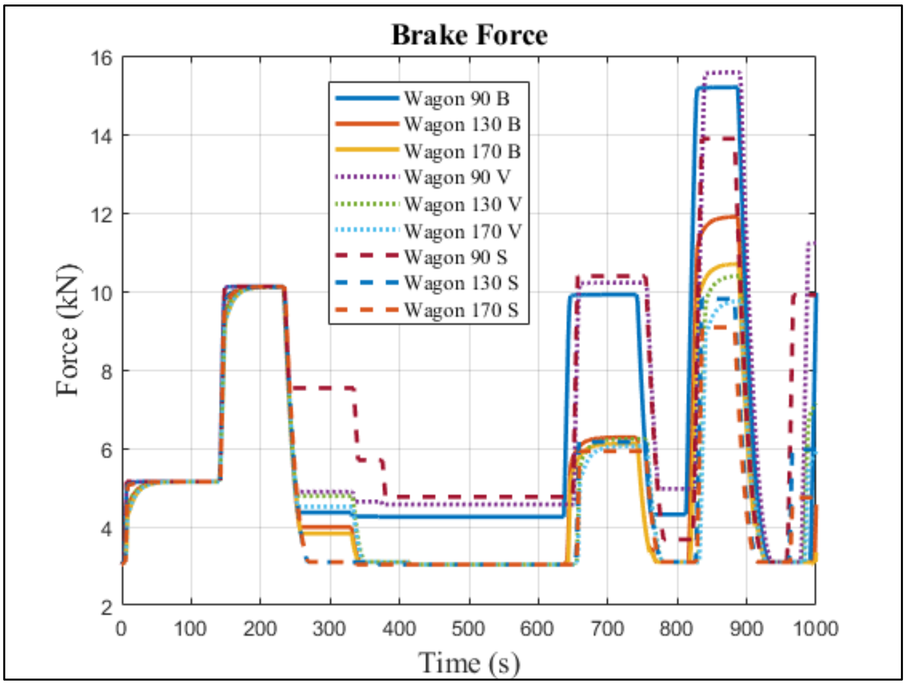

Figure 74 - Case 28-30: Brake forces in the rear wagons. B – baseline; V – venturi; S – sonic.

5.4. Discussion

From the theoretical straight and flat track test results, the current venturi design and the theoretical sonic venturi reduce draft gear energy dissipation and damage accumulation in all but two test cases. One case in which the damage accumulation worsened was in the case of one locomotive pulling 84 wagons at an initial velocity of 80 km/h with a large pressure drop. The other case was two locomotives pulling 186 wagons at an initial velocity of 80 km/h with a small pressure drop. There was no case in which the draft gear energy dissipation increased. In these cases, the worst damage accumulation is a result of the transition in the model and is likely not a real phenomenon. The reason for this is that as the velocity of the locomotive(s) or wagons drops below 0.1 m/s, the modified Davis equation constants switch to the higher values shown in Table 2. This transition causes the resistive forces to increase, thereby causing oscillations in the force magnitudes that the filter does not eliminate. To improve the model transition, a new condition could be applied to indicate when the wagon or locomotive is decelerating, rather than accelerating, because the higher resistive forces at velocities below 0.1 m/s are meant to simulate overcoming static bodies with high inertia. As expected, the only forces that contribute to the draft gear energy dissipation in these cases are the brake forces and the resistive forces.

The transition in the model also influences the position of the draft gear that experiences the highest damage accumulation. However, in the single locomotive with 84 wagons cases, the draft gear position with the highest damage accumulation is seemingly random. The only test cases that produce similar max damage positions are the large pressure drop cases, in which the draft gears near the rear of the composition are the most damaged. Additionally, as shown in Figures 35-40, the damage tends to occur in a small batch or area of the composition. For example, in Figure 36, the maximum damage occurs between wagons 14 and 35, with the maximum coupler damage occurring at draft gear 18. A potential area of further study is to determine if the damage accumulation could be fit to a predictive model, as the damage accumulation graphs appear to show a normal distribution about the coupler experiencing the highest damage. In the two locomotives pulling 168 wagons case, the trend of a small batch of adjacent draft gears experiencing high damage accumulation occurs as well. However, there appears to be a secondary grouping of draft gears that experience a lower, yet perceptible, damage accumulation in this case. This phenomenon can be seen in Figure 48, where the first grouping of high damage accumulation occurs between wagons 14 and 20, and the second grouping of high damage accumulation occurs between wagons 130 and 168. Another observation regarding the damage accumulation, is that the draft gears that are connected via drawbars experience higher loads, and therefore higher damage, than the draft gears connected via couplers. This is likely a result of the coupler transition modeling of Equation 42, where clearance cases of zero loading are present. Additionally, as the draft gear couplers are transitioning, the loading will be lower than a constantly loaded case.

In all cases of the straight and level track tests, the venturi and theoretical sonic venturi decreased the time to stop the train and the distance required to stop compared to the baseline. In both train compositions, the venturi stopping distance performance was best in the 20 km/h intial velocity with a large pressure drop case. For the single locomotive configuration, this resulted in a 0.9 m stopping distance improvement and in the double locomotive configuration, a 1.9 m stopping distance improvement. Similarly, the theoretical sonic venturi was best in the same case, being the 20km/h intial velocity with a small pressure drop case. For the single locomotive configuration, this resulted in a 4.7 m stopping distance improvement, and a 13.8 m stopping distance improvement in the double locomotive configuration. Again, in both train compositions, the venturi stopping time was best in the 20 km/h initial velocity with a large pressure drop case. The reduction in stopping time is negligible, less than one second in both cases. Interestingly, the theoretical sonic venturi does not share a single dominant pressure drop case between configurations, but does share a dominant initial velocity of 20 km/h. The single locomotive configuration performs best, relatively in the large pressure drop situation with an improvement of less than a second. However, the double locomotive configuration improves the stopping time by 5 s. With respect to stopping time and stopping distance, there is little to no practical improvement in the single locomotive configuration, whereas there is a slight improvement in the double locomotive configuration.

In the straight, level track cases, the pneumatic air brake system behavior was independent of intial velocity and dependent on train configuration. For this reason, the data presented in Figures 41 to 46 and Figures 53 to 58 are only shown based on pressure drop and configuration. For the single locomotive configuration, the small pressure drop resulted in the brake pipe reaching the transition pressure in 3.05 s, 4.20 s, and 4.35s for the sonic, venturi, and baseline pneumatic systems, respectively, in the front wagon. In the rear wagon, the transition pressure occurs at 4.78 s, 7.05 s, and 7.34 s for the sonic, venturi, and baseline systems, respectively. After the transition pressure, the equalization pressure is similar amongst all pneumatic systems, as the venturi systems do not contribute to the equalization time. As shown in Figure 42, the depletion of the emergency air reservoir is minimal for a small pressure drop. In the theoretical sonic venturi case, the emergency reservoir loses a maximum of 4.5 psi of air pressure, while the chosen venturi design loses a maximum of only 2.1 psi of emergency air pressure. As can be seen in the sonic venturi case, the model overshoots the expected pressure value in the emergency reservoir. This behavior does not appear in the selected venturi case. In the large pressure drop case of the single locomotive configuration, the brake pipe reaches the transition pressure in 15.0 s, 25.6 s, and 26.6 s for the sonic, venturi, and baseline systems, respectively, in the front wagon. In the rear wagon, the transition pressure is reached in 16.5 s, 28.7 s, and 29.7 s for the sonic venturi, and baseline systems, respectively. In these cases, the maximum emergency air pressure loss was 28.3 psi for the sonic venturi and 10.1 psi for the chosen venturi design.

As expected, the double locomotive pulling 168 wagons configuration has larger delays between the wagons in the composition compared to the single locomotive pulling 84 wagons configuration. For the small pressure drop, the brake pipe pressure in the front wagon reaches the transition pressure in 1.7 s, 1.9 s, and 1.9 s for the sonic, venturi, and baseline systems, respectively, and the brake pipe pressure in the rear wagon reaches the transition pressure in 6.9 s, 10.0 s, 10.5 s for the sonic, venturi, and baseline systems, respectively. The maximum pressure loss from the emergency reservoir is 4.8 psi in the sonic venturi case and 2.5 psi in the chosen venturi case. For the large pressure drop, the brake pipe pressure in the front wagon reaches the transition pressure in 12.1 s, 18.9 s, and 19.4 s for the sonic, venturi, and baseline systems, respectively, and the brake pipe pressure in the rear wagon reaches the transition pressure in 20.2 s, 34.3 s, 35.6 s for the sonic, venturi, and baseline systems, respectively. In the sonic case, the brake pipe pressure overshoots the requested pressure drop. There is a condition in the model that compensates this pressure loss to equalize the brake pipe pressure to the requested level. Therefore, the positive pressure delta resulting from this overshoot does not yield a brake release. It is yet to be determined if this phenomon is real or a modeling effect. The maximum pressure loss from the emergency reservoir is 21.3 psi in the sonic venturi case and 29.2 psi in the chosen venturi case.

Given the previously discussed draft gear damage accumulation and draft gear energy dissipation performance, it is clear that these small time differences in brake pipe transition pressure caused by the different pneumatic systems do greatly influence the longitudinal dynamics performance of the system. However, the cases that have been analyzed could be expanded to try to find more trends or predictive behaviors. Regardless of these results, it is important to see if the pneumatic system design changes benefit the system on a real track with a real train composition.

The simulated real-world application is heavily dependent on the brake schedule. In this study, two different brake schedules were utilized to analyze the system performance. The two schedules were chosen to represent a trip mostly dependent on dynamic braking and a trip dependent on pneumatic braking on the same track. As expected, the total energy dissipated by the draft gears and the total accumulated draft gear damage performance are dependent on the brake schedule. In the dynamic dominant braking case, both the energy dissipation and damage accumulation worsened using the venturi and the theoretical sonic venturi. In fact, the sonic venturi performed even worse than the chosen venturi design. This is contrary to the previous straight, level track analyses. One explanation for this downgrade in behavior can be descrbed by the difference in the distance traveled, as both the venturi and sonic venturi traveled farther on the real track than the baseline design. The venturi case traveled an additional 125 m, while the sonic venturi case traveled an additional 561 m. This additional travel distance allows more opportunity for the system to dissipate energy and accumulate damage. In the pneumatic dominant case, however, the total energy dissipated by the draft gears and the total accumulated draft gear damage improved with the addition of the venturi and sonic venturi designs despite traveling a larger distance than the baseline design. Intuitively, the difference between the pneumatic dominant and the dynamic dominant case makes sense. If the main source of braking comes from only two out of 170 components in the composition, as is the case in the dynamic dominant case, it would seem to be more likely to cause damage than if 168 out of 170 components greatly contributed to the braking effort. Interestingly, the damage accumulation of the draft gears seems to follow a similar trened independently of the brake schedule and the brake system design. The majority of the damage accumulation occurs in the middle of the composition, near the second locomotive. The damage accumulation of the surrounding draft gears tends to follow the same trend of a slow increase and then slow decrease of damage centralized about the worst-case draft gear.

The more compelling results of the real track case are the pneumatic results. In Figures 67 to 70, the most apparent brake pipe pressure differences occur during the recharge of the brake pipe. Because the emergency air reservoir is used to increase the brake pipe pressure signal during a service brake action, there is less air available in the emergency reservoir to assist the brake pipe recharge. The brake pipe in the dynamic dominant case, which utilizes smaller pressure drops than the pneumatic dominant case, does not experience performance deficiencies in the front wagons until the third brake application in the venturi and sonic venturi cases. The slower recharge from the venturi cases, causes the brake cylinders to release less air pressure and therefore apply a higher force than the baseline case. Then, because the control valve works under pressure differences and not absolute pressures, the brake cylinders in the venturi cases increase yet again but start at a higher starting pressure than the baseline case. For this reason, the brake forces in the dynamic dominant case are higher in the middle wagons than in the baseline case and lower in the rear wagons compared to the baseline case. This is not a desired behavior by design and appears to negatively impact performance in the dynamic dominant case. The rear wagons experience performance deficiencies during the second brake application in the venturi and sonic venturi cases and have greatly reduced braking forces at the end of the trip. These braking behaviors are caused even with small emergency reservoir air use, as the worst-case emergency reservoir pressure only falls to 84.9 psi in the rear wagons. Because of these lower braking forces, the average velocity of the composition is higher for the venturi cases, therefore explaining the larger distances traveled.

The pneumatic dominant case shows similar behavior to the dynamic dominant case, in that the slower brake pipe recharge time negatively impacts the service brake application. However, in the pneumatic dominant case, the undesired behavior of the venturis benefits the overall system. Again, the deficiencies begin during the third brake application after the brake pipe could not be fully recharged in time before the brake application. Albeit counterintuitive, the larger pressure drops in the pneumatic dominant case negatively affect all pneumatic system designs and the differences are less prominent than in the dynamic dominant case. There are two possible explantions for the venturi systems in the pneumatic dominant case outperforming the baseline system. One is that the venturi cases result in lower loads from the brake cylinders and therefore cause smaller shocks between the wagons. The other possible explanation is that the real track simply aligns with the deficiencies of the venturi systems. For example, the hills might assist the venturi systems in a way the baseline system does not. This second hypothesis can be tested on the straight, level track. In the pneumatic dominant case, the emergency reservoir air pressure does not drop below 75 psi in the worst sonic venturi case and does not drop below 82 psi in the worst venturi design case.

6 CONCLUSIONS

This section concludes the findings of this work. Potential future works are also discussed.

6.1. Final Conclusions

This work provided a study of a potential pneumatic design improvement to the heavy haul train pneumatic air brake system. A literature review was conducted to understand the current system, to find potential design solutions, and to understand the longitudinal dynamic impacts of the pneumatic brake system. A venturi design was proposed to add to the wagon control valves to increase the signal propagation through the brake pipe during the rapid service portion of a service brake application. The venturi design was tested using computational fluid dynamics to characterize its behavior and was implemented into a pneumatic air brake system model to determine its pneumatic impacts on the system. Finally, the venturi design was implemented into a longitudinal dyanmics simulator to determine energy dissipaction and fatige damage accumulation in the draft gears throughout the train composition. All results were compared to the baseline control valve design and a theoretic venturi design capable of producing sonic flow.

The current work showed that the increase in the signal propagation time caused by the insertion of the venturi in the wagon control valve does reduce the damage accumulation in the draft gears for heavy haul freight trains on a straight, level track. As desired, this is accomplished without the addition of an electrical energy source or wiring. When implemented in two real-world simulations, the venturi performance was dependent upon the brake schedule. A brake schedule that utilizes smaller pressure drops with the venturi and depends more heavily on the locomotive dynamic braking, performed worse than the baseline design. However, the brake schedule that utilized larger pressure drops with the venturi and less dynamic braking performed better than the baseline design. Careful attention must be paid to the potential risk of emergency air depletion during the trip via a wisely designed brake schedule, as the performance of the system is highly dependent upon it. Lastly, this work has provided a solution space for the implementation of a venturi in the control valve that can be used to develop and optimize a product improvement based on desired design constraints.

6.2. Improvements & Future Work

As with any engineering or research project, improvements to the work done are most discernable at the conclusion of the work. One of the more important improvement opportunities would have been to develop a focused, holistic approach to the design. Most of the design ideas, and the general design approach in this work, were based on finding pneumatic improvements to the system. However, this approach neglected the overall effect on the entire train system, like the lateral and longitudinal dynamics effects or energy consumption. This would have required more knowledge of the entire system via a more extensive and diverse literature review. With respect to a more extensive literature review, time should have been given to study the effects of increased signal transmission in other systems. This could have provided alternative design ideas to better utilize the faster signal transmission and also provide performance criteria to better evaluate the design effectiveness. Similarly, more attention could have been focused on the electrical train braking models to determine relevant system effects that hinder the superior braking scheme. Lastly, more time could have been spent on other aspects of the brake system to accompany the small pneumatic improvements.

There are many potential options to further or continue this work, that take four distinct paths. The most desirable future work, from the outlook of the author, is to manufacture the venturi and test it on a pneumatic brake system test bench. This would serve to verify the CFD modelling and the pneumatic modelling of the wagon pneumatic brake system. In particular, it would help characterize the orifice mass flow coefficients from Equation 1. It would also serve to better characterize the control valve, thereby providing more opportunity to find design improvements. In fact, a test rig was part of the original approach for this thesis. It was built and is ready to be instrumented, as can be seen in Appenix A. However, the pandemic delayed and ultimately caused the removal of this portion of the project from this work. An alternative path of study would be to develop optimization techniques that could be used to either optimize the existing architecture of the system or to develop brake schedules that minimize unwanted effects in the system, like longitudinal shocks. A third yet similar path would be to optimize the venturi design in an attempt to either reduce emergency air depletion or increase the mass flow rate of brake pipe air. A fourth path, and perhaps the most critical, would be to study the likelihood and costliness of emergency brake applications in the field compared to the potential cost gains of utilizing an optimized venturi system. It could be the case that, from a risk assessment standpoint, the minimization of fatigue damage accumulation outweighs potential emergency brake application situations, thereby providing a business case to implement venturi designs in the field.

References

ABDOL-HAMID, Khaled Sayed. **Analysis and simulation of the pneumatic braking system of freight trains**. 1986. 383p. Dissertation (Doctorate). University of New Hampshire, Durham, 1986.

AFSHARI, Ali; SPECCHIA, Stefano; SHABANA, Ahmed A.; CALDWELL, Nelson. A train air brake force model: Car control unit and numerical results. **Proceedings of the Institution of Mechanical Engineers, Part F: Journal of Rail and Rapid Transit**, v. 227, n. 1, p. 38-55, 2012.

ANTF. **Associação Nacional dos Transportadores Ferroviários**. Available on <http://www.antf.org.br/wp-content/uploads/2019/12/Mapa-Site-Retrato_V02.pdf>. Accessed on Aug. 4, 2020.

AZZI, Abdelhak; MAOUI, Abdelghani; FATU, Aurelian; FILY, Sebastien; SOUCHET, Dominique. Experimental study of friction in pneumatic seals. **Tribology International**, v. 135, p. 432-433, 2019.

BARTON, Neil; READER-HARRIS, Michael; GIBSON, Jeff. "Overview of CFD modelling of orifice plate flometers." **North Sea Flow Measurement Workshop**. Saint Andrews, Fife, UK. October 26-29, 2004.

BELFORTE, P.; CHELI, F.; DIANA, G.; MELZI, S. Numerical and experimental approach for the evaluation of severe longitudinal dynamics of heavy freight trains. **Vehicle System Dynamics: International Journal of Vehicle Mechanics and Mobility**, v. 46, n. s1, p. 937-955, 2008.

BHARATH, S.; NAKRA, B. C.; GUPTA, K. N. A distributed mathematical model for pressure transient analysis in railway pneumatic brake system. **International Journal of Mechanical Sciences**, v. 32, n. 2, p. 133-145, 1990.

BHARATH, S.; NAKRA, B. C.; GUPTA, K. N. Mathematical model of a railway pneumatic brake system with varying cylinder capacity effects. **Journal of Dynamic Systems, Measurement and Control**, v. 112, n. 3, p. 456-462, 1990a.

BOWEY, R.; SHAMDANI, A.; STEVENS, A. "Monitoring, managing and mitigating in-train forces." **Proceedings of the 11th International Heavy Haul Conference.** Cape Town, South Africa. September 2-6, 2017.

CANTONE, L.; CRESCENTINI, E.; VERZICCO, R.; VULLO, V. A numerical model for the analysis of unsteady train braking and releasing manoeuvres. **Proceedings of the Institution of Mechanical Engineers, Part F: Journal of Rail and Rapid Transit**, v. 223, n. 3, p. 305-317, 2009.

CHANG, Chongyi; GUO, Gang; WANG, Junbiao; MA, Yingming. Study on longitudinal force simulation of heavy-haul train. **Vehicle System Dynamics: International Journal of Vehicle Mechanics and Mobility**, v. 55, n. 4, p. 571-582, 2017.

CHEN, Shuai; ZHAO, Guotang; WANG, Hengyu; TAO, Gongquan; WEN, Zefeng; WU, Lei. Study of wheel wear influenced by tread temperature rising during tread braking. **Wear**, v. 438-439, 2019.

CHILDS, Peter R. N. **Mechanical Design Engineering Handbook**. Butterworth-Heinemann, 2014, ch. 18, p. 735-759.

CNT. **Confederação Nacional do Transporte**. Available on <http://www.cnt.org.br/Sistema-ferroviario-brasileiro>. Accessed on Aug. 4, 2020.

COLE, Colin; Ripley, Ian. “Investigation of application delays in Australian train brake systems.” **Conference on Railway Engineering.** Melbourne, Victoria, Australia. April 30 - May 3, 2006.

COLE, Colin; Spiryagin, Maksym; Wu, Qing; Sun, Yan Quan. “Modelling, simulation and applications of longitudinal train dynamics.” **Vehicle System Dynamics: International Journal of Vehicle Mechanics and Mobility**, v. 55, n. 10, p. 1498-1571, 2017.

ECKERT, Jony J.; TEODORO, Ícaro P.; TEIXEIRA, Luis H.; MARTINS, Thiago S.; KURKA, Paulo R. G.; SANTOS, Auteliano A. A fast simulation approach to assess draft gear loads for heavy haul trains during braking. **Mechanics Based Design of Structures and Machines**, 2021.

FREDERICO, GUILHERME F.; CAVENAGHI, VAGNER. Measuring Performance in Rail Freight Transportation Companies. **International Business Research**, v. 10, n. 11, p. 117-128, 2017.

FUNK, J. E.; ROBE, T. R. Transients in pneumatic transmission lines subjected to large pressure changes. **International Journal of Mechanical Sciences**, v. 12, n. 3, p. 245-257, 1970.

GAO, Mingyuan; CONG, Jianli; XIAO, Jieling; HE, Qing; LI, Shoutai; WANG, Yuan; YAO, Ye; CHEN, Rong; WANG, Ping. Dynamic modeling and experimental investigation of self-powered sensor nodes for freight rail transport. **Applied Energy**, v. 257, n. 1, 2020.

GU, Zhiqiang; HU, Shiyu; YANG, Fan; YANG, Rui; HUA, Jian. A new calculating method of pressure response time of pneumatic brake pipe based on experiments. **Mathematical Problems in Engineering**, v. 2019, 2019.

GÜNAY, Mustafa; KORKMAZ, Mehmet Erdi; ÖZMEN, Ramazan. An investigation on braking systems used in railway vehicles. **Engineering Science and Technology, an International Journal**, v. 23, n. 2, p. 421-431, 2020.

KAMIŃSKI, Zbigniew. A simplified lumped parameter model for pneumatic tubes. **Mathematical and Computer Modelling of Dynamical Systems**, v. 23, n. 5, p. 523-535, 2017.

KERN, Richard. Physical modelling of a long pneumatic transmission line: models of successively decreasing complexity and their experimental validation. **Mathematical and Computer Modelling of Dynamical Systems**, v. 23, n. 5, p. 536-553, 2017.

KRICHEL, Susanne V.; SAWODNY, Oliver. Non-linear friction modelling and simulation of long pneumatic transmission lines. **Mathematical and Computer Modelling of Dynamical Systems**, v. 20, n. 1, p. 23-44, 2014.

LIU, C.; **Wabtec Brasil**. Sistema de freio vagões de carga. Presented on May, 4 2017.

MA, J.; KARAMAN, I.; NOEBE, R. D. High temperature shape memory alloys. **International Materials Reviews**, v. 55, n. 5, p. 257-315, 2013.

MINING.COM. **Glacier Media Group**. Available on <http://www.mining.com/iron-ore-exports-from-brazil-hit-highest-level-since-2015>. Accessed on Oct. 21, 2020.

MURTAZA, M. A.; GARG, S. B. L. Brake modelling in train simulation studies. **Proceedings of the Institution of Mechanical Engineers, Part F: Journal of Rail and Rapid Transit**, v. 203, n. 2, p. 87-95, 1989.

NAM, Seong-Won; KIM, Hyeong-Jin. A study on the improvement of release application characteristics of pneumatic brakes for freight train. **KSME International Journal**, v. 16, n. 6, p. 776-784, 2002.

NASR, A.; MOHAMMADI, S. The effects of train brake delay time on in-train forces. **Proceedings of the Institution of Mechanical Engineers, Part F: Journal of Rail and Rapid Transit**, v. 224, n. 6, p. 523-534, 2010.

OEC. **The Observatory of Economic Complexity**. Available on <http://www.oec.world/en/profile/country/bra>. Accessed on Oct. 21, 2020.

PIECHOWIAK, Tadeusz. Pneumatic train brake simulation method. **Vehicle System Dynamics: International Journal of Vehicle Mechanics and Mobility**, v. 47, n. 12, p. 1473-1492, 2009.

PIECHOWIAK, Tadeusz. Verification of pneumatic railway brake models. **Vehicle System Dynamics: International Journal of Vehicle Mechanics and Mobility**, v. 48, n. 3, p. 283-299, 2010.

PUGI, L.; MALVEZZI, M.; ALLOTTA, B.; BANCHI, L.; PRESCIANI, P. A parametric library for the simulation of a Union Internationale des Chemins de Fer (UIC) pneumatic braking system. **Proceedings of the Institution of Mechanical Engineers, Part F: Journal of Rail and Rapid Transit**, v. 218, p. 117-132, 2004.

PUGI, Luca; MALVEZZI, Monica; PAPINI, Susanna; VETTORI, Gregorio. Design and preliminary validation of a tool for the simulation of train braking performance. **Journal of Modern Transportation**, v. 24, n. 4, p. 247-257, 2013.

RIBEIRO, Daniel Fernandes. **Desenvolvimento de modelos para simulação em tempo real da frenagem de composições ferroviárias de carga**. 2017. 114p. Thesis (Master's). Faculdade de Engenharia Mecânica, Universidade Estadual de Campinas, Campinas, 2017.

SANTOS, Auteliano A.; LOPES, Matheus V.; GONÇALVES, Vanessa; ECKERT, Jony J.; MARTINS, Thiago S. "Vibration energy harvesting to power ultrasonic sensors in heavy haul railway cars." **Proceedings of the ASME 2018 International Mechanical Engineering Congress and Exposition**. Pittsburgh, Pennsylvania, USA. November 9-15, 2018.

SERAJIAN, Reza; MOHAMMADI, Saeed; NASR, Asghar. Influence of train length on in-train longitudinal forces during brake application. **Vehicle System Dynamics: International Journal of Vehicle Mechanics and Mobility**, v. 57, n. 2, p. 192-206, 2018.

SHARMA, Rakesh Chandmal; DHINGRA, Manish, PATHAK, Rajeev Kumar. Braking systems in railway vehicles. **International Journal of Engineering Research & Technology**, v. 4, n. 1, p. 206-211, 2015.

SPECCHIA, Stefano; AFSHARI, Ali; SHABANA, Ahmed A.; CALDWELL, Nelson. A train air brake force model: Locomotive automatic brake valve and brake pipe flow formulations. **Proceedings of the Institution of Mechanical Engineers, Part F: Journal of Rail and Rapid Transit**, v. 227, n. 1, p. 19-37, 2012.

SUBRAMANIAN, Shankar C.; DARBHA, Swaroop; RAJAGOPAL, K. R. Modeling the pneumatic subsystem of an S-cam air brake system. **Journal of Dynamic Systems, Measurement, and Control**, v. 126, p. 36-46, 2004.

TEODORO, Ícaro Pavani. **Estudo do comportamento do sistema de freio pneumático de trens de carga utilizando o método dos volumes finitos**. 2017. 130p. Thesis (Master's). Faculdade de Engenharia Mecânica, Universidade Estadual de Campinas, Campinas, 2017.

TEODORO, Ícaro P.; ECKERT, Jony J.; LOPES, Pedro F.; MARTINS, Thiago S.; SANTOS, Auteliano A. Parallel simulation of railway pneumatic brake using openMP. **International Journal of Rail Transportation**, v. 8, n. 2, p. 180-194, 2019.

TEODORO, Ícaro P.; RIBEIRO, Daniel F.; BOTARI, Tiago; MARTINS, Thiago S.; SANTOS, Auteliano A. Fast simulation of railway pneumatic brake systems. **Proceedings of the Institution of Mechanical Engineers, Part F: Journal of Rail and Rapid Transit**, v. 233, n. 4, p. 420-430, 2018.

VENKATARAMAN, K. A.; KANTHAVEL, K.; KUMAR, B. Nimal. Investigations of response time parameters of a pneumatic 3/2 direct acting solenoid valve under various working pressure conditions. **Engineering, Technology & Applied Science Research**, v. 3, n. 4, p. 502-505, 2013.

WALIA, Mandeep; VERNERSSON, Tore; LUNDÉN, Roger; BLENNOW, Fredrik; MEINEL, Markus. Temperatures and wear at railway tread braking: Field experiments and simulations. **Wear**, v. 440-441, 2019.

WANG, Hai-min; ZHAO, Yue; WANG, Jian-xing; KONG, Xiang-shuai; LIU, Huan; LI, Ke-liang; WANG, Xi-fang. Numerical simulation of flow characteristics for a labyrinth passage in a pressure valve. **Journal of Hydrodynamics**, v. 28, n. 4, p. 629-636, 2016.

WEI, W.; LIN, Y. Simulation of a freight train brake system with 120 valves. **Proceedings of the Institution of Mechanical Engineers, Part F: Journal of Rail and Rapid Transit**, v. 223, n. 1, p. 85-92, 2009.

WEI, Wei; AHMADIAN, Mehdi; ZHANG, Jun. "Heavy haul train simulation of air brake system and longitudinal dynamics." **Proceedings of the 2014 Joint Rail Conference**. Colorado Springs, Colorado, USA. April 2-4, 2014.

WEI, Wei; HU, Yang; WU, Qing; ZHAO, Xubao; ZHANG, Jun; ZHANG, Yuan. An air brake model for longitudinal train dynamic studies. **Vehicle System Dynamics: International Journal of Vehicle Mechanics and Mobility**, v. 55, n. 4, p. 517-533, 2017.

WEI, Wei; ZHANG, Jun; ZHAO, Xubao; ZHANG, Yuan. "Simulation research on effect of air brake system on longitudinal impulse of heavy haul train." **IHHA 2015 Conference**. Perth, Australia. June 21-24, 2015.

WELLS, Franklin H. **The development of the modern air brake**. 1920. 33p. Thesis (Master's) - Mechanical Engineering Department, Massachusetts Institute of Technology, Cambridge, 1920.

WU, Qing. **Optimisations of draft gear designs for heavy haul trains**. 2016. 239p. Thesis (Doctorate). School of Engineering and Technology Centre for Railway Engineering, Central Queensland University, Australia, 2016.

WU, D.; BURTON, R.; SCHOENAU, G.; BITNER, D. Analysis of a pressure-compensated flow control valve. **Journal of Dynamic Systems, Measurement, and Control**, v. 129, n. 2, p. 203-211, 2007.

WU, Qing; COLE, Colin. Computing schemes for longitudinal train dynamics: sequential, parallel and hybrid. **Journal of Computational and Nonlinear Dynamics**, v. 10, n. 6, 2015.

WU, Qing; COLE, Colin; SPIRYAGIN, Maksym. Assessing wagon pack sizes in longitudinal train dynamics simulations. **Australian Journal of Mechanical Engineering**, v. 18, n. 3, p. 277-287, 2020.

WU, Qing; COLE, Colin; SPIRYAGIN, Maksym; MCSWEENEY, Tim. Parallel multiobjective optimisations of draft gear designs. **Proceedings of the Institution of Mechanical Engineers, Part F: Journal of Rail and Rapid Transit**, v. 232, n. 3, 2017.

WU, Qing; COLE, Colin; SPIRYAGIN, Maksym; WANG, Yucang; MA, Weihua; WEI, Chongfeng. Railway air brake model and parallel computing scheme. **Journal of Computational and Nonlinear Dynamics**, v. 12, n. 5, 2017.

WU, Qing; LUO, Shihui; COLE, Colin. Longitudinal dynamics and energy analysis for heavy haul trains. **Journal of Modern Transportation**, v. 22, n. 3, p. 127-136, 2014.

WU, Qing; SPIRYAGIN, Maksym; COLE, Colin. Longitudinal train dynamics: an overview. **Vehicle System Dynamics: International Journal of Vehicle Mechanics and Mobility**, v. 54, n. 12, p. 1688-1714, 2016.

XU, Jing; LIU, Xuedong; PANG, Mingjun. Numerical and experimental studies on transport properties of powder ejector based on double venture effect. **Vacuum**, v. 134, p. 92-98, 2016.

YANG, Fan; LI, Gangyan; HU, Jian; LIU, Wengfeng; QI, Wang. “Method for resultant and calculating the flow-rate characteristics of pneumatic circuit.” **2015 International Conference on Fluid Power and Mechatronics (FPM)**. Harbin, China. August 5-7, 2015.

YANG, Fan; LI, Gangyan; HUA, Jian; LI, Xingli; KAGAWA, Toshiharu. A new method for analysing the pressure response delay in a pneumatic brake system caused by the influence of transmission pipes. **Applied Sciences**, v. 7, n. 9, p. 941-961, 2017.

APPENDIX A – Originally Planned Work

Prior to the Covid-19 pandemic, the objective of this work was to build and test a pneumatic test bench per Figure 75. The experimental set-up was designed to represent a double wagon configuration pneumatic air brake system and is shown in Figure 76.

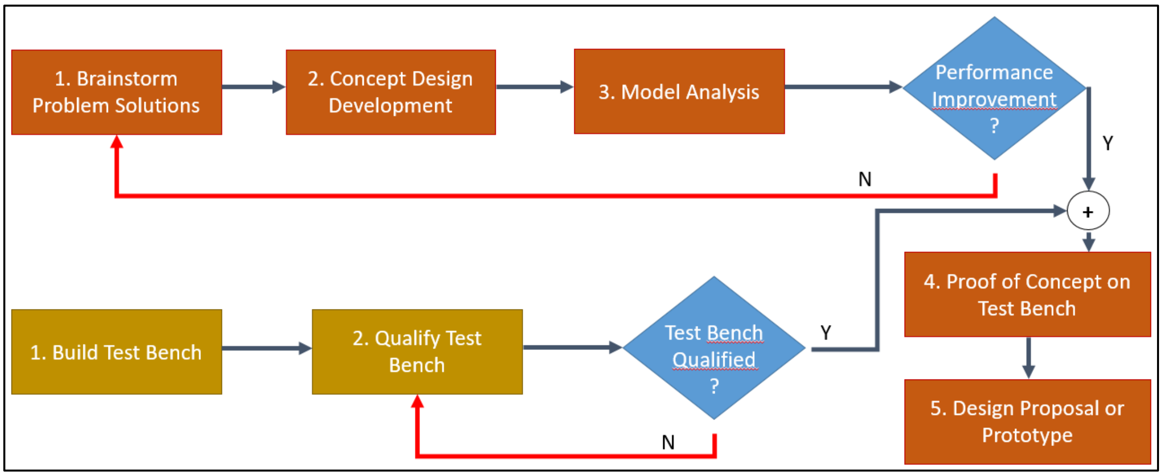

Figure 75 - Original workflow plan.

The test bench is to be equipped with the major components of the wagon pneumatic air brake system, including the auxiliary reservoir, emergency reservoir, relief valve, wagon control valve, control valve inlet air filter, loaded/unloaded valve, equalizing chamber, and two brake cylinders. Four pressure transducers are to be installed in the brake pipe of the first wagon, the brake cylinder of the first wagon, and in the auxiliary and emergency reservoirs. The components that enable the control and simulation of any wagon position along the train are the two inlet and outlet proportional valves. The buffer tank is to be included in order to control the response time of the inlet proportional valve and also eliminate noise and instabilities in the measurement system. The pressure transducers and proportional valves are to be controlled and have their data recorded by a local data acquisition (DAQ) system and personal computer (PC).

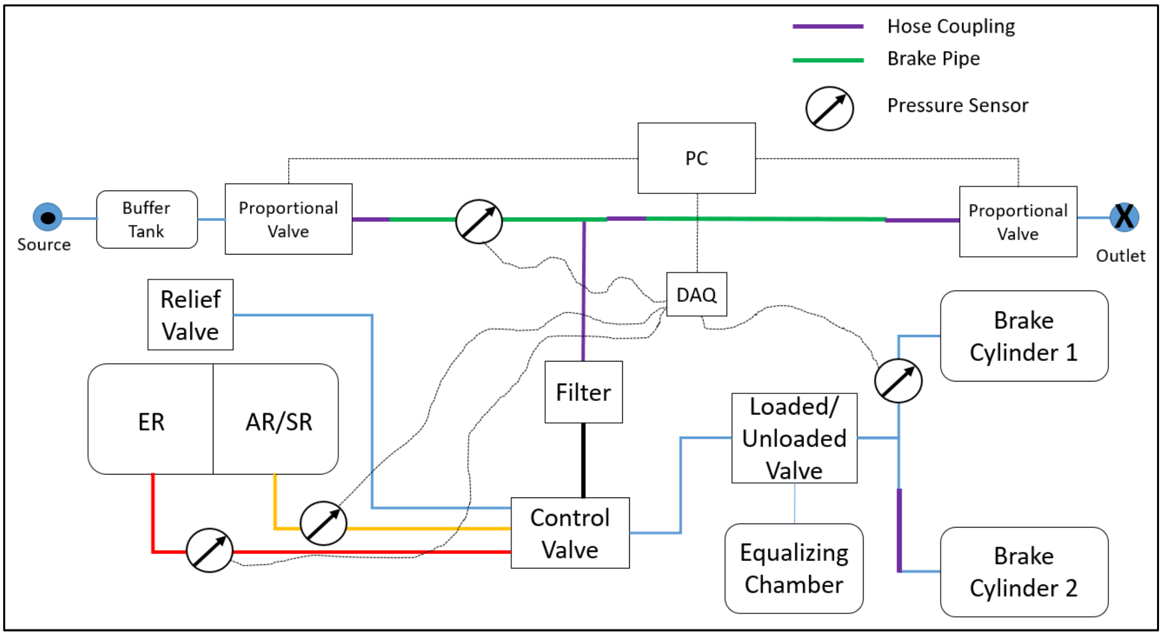

Figure 76 - Experimental set-up schematic.

In order to build the test bench, the entire system was modeled in CAD as shown Figure 77. The main design consideration, aside from representing a double wagon configuration, was to be able to build the test bench in the available laboratory space of 4m by 2m. For this reason, the wagon brake pipes were bent into loops, as well as the brake cylinder pipes. Because of the frame does not have strict dynamic or vibration specifications, the frame was designed for cost by utilizing L-bars.

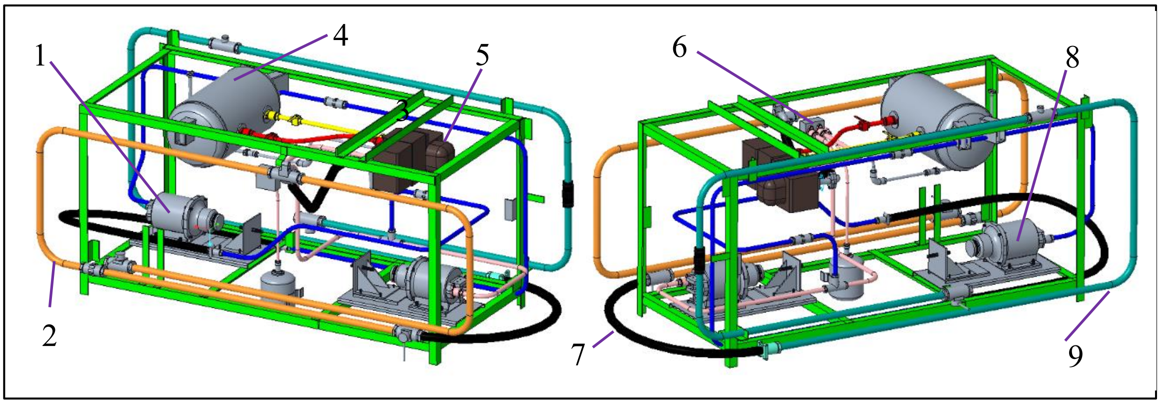

Figure 77 - Experimental set-up CAD model. 1 - wagon 2 brake cylinder (dark blue pipe), 2 - wagon 1 brake pipe (orange pipe, inlet), 3 - equalizing volume, 4 - dual tank air reservoir (auxiliary yellow pipe, emergency red pipe), 5 - wagon control valve, 6 - loaded/unloaded valve, 7 - hose couplings (black pipes), 8 - wagon 1 brake cylinder, 9 - wagon 2 brake pipe (light blue pipe, outlet).

The current status of the experimental test rig is shown in Figure 78 and Figure 79. A single hose is still to be installed, while the entirety of the instrumentation and controlling valves are still required.

Figure 78 - Experimental set-up while under construction.

Figure 79 - Current build status of experimental set-up.

The current test plan is focused on determining the wagon pneumatic air brake performance for any wagon position along the train.

1. Leak check entire assembly
    a. Fill and hold assembly at 90 psi for 5 minutes

   b. Listen for and investigate observable leaks
   c. Shut off 90 psi supply and close inlet and outlet valves
   d. Measure assembly pressure at outlet for 10 minutes
2. Verify sensor and DAQ functionality
   a. Fill and assembly at 90 psi for 5 minutes
   b. Verify each sensor is functioning and read by DAQ
   c. Verify stability of sensors
3. Verify proportional valve and ABDX control valve functionality and sensitivity in service application with loaded/unloaded valve closed
   a. Fill and assembly at 90 psi for 5 minutes
   b. Reduce brake pipe pressure via proportional valve by
      i. 1 psi and measure pressure sensor response over 5 minutes
      ii. Repeat (i) for 2, 5, 10, 20, and 26 psi
   c. Fill and hold brake pipe pressure at 64 psi for 5 minutes
   d. Increase brake pipe pressure via proportional valve by
      i. 1 psi and measure pressure sensor response over 10 minutes
      ii. Repeat (i) for 2, 5, 10, 20, and 26 psi
   e. Repeat (a)-(d) with the loaded/unloaded valve open
4. Verify proportional valve and ABDX control valve functionality and sensitivity in emergency application with loaded/unloaded valve closed
   a. Fill and assembly at 90 psi for 5 minutes
   b. Reduce brake pipe pressure via proportional valve by
      i. 90 psi and measure pressure sensor response over 10 minutes
      ii. Repeat (i) for 70, 80, 85, 88, and 89 psi
   c. Increase brake pipe pressure via proportional valve by
      i. 90 psi and measure pressure sensor response over 10 minutes

ii. Repeat (i) for 70, 80, 85, 88, and 89 psi

d. Repeat (a)-(d) with the loaded/unloaded valve open

5. Repeat 3 & 4 for intermediate wagons positions of choosing in a train composed of 100 wagons

    a. Test, at minimum, Wagon 1, 25, 50, 75, and 100

6. Repeat 3-5 as required with ABD control valve installed

7. Repeat 3-5 as required with AB control valve installed

8. Implement design changes

    a. Repeat 1-7 as required.

APPENDIX B – Simulation Code

Original Pneumatic Model in C++:

```
#define _CRT_SECURE_NO_DEPRECATE

#include <math.h>
#include <stdio.h>
#include <stdlib.h>
#include <windows.h>
#include <omp.h>

#define NMAX 1000

//Parametros de inicializacao (dados de entrada)
double vagao_duplo = 2; //vagao simples ou duplo. vagao simples = 1; vagao duplo = 2
double n_loco = 1; //numero de locomotivas na composicao
double pos_loco[10]; //posicoes das locomotivas (inclusive a cabeca) - entre a 1 e a 6, por exemplo, haveria 4 vagoes (ou dois duplos)
double n_vagoes = 50; //numero de vagoes
double t0 = 0; // [s]  - tempo inicial de simulacao
double t_final = 368; // [s]  - tempo final de simulacao
double Ppi = 90; // [psi] pressao inicial no encanamento
double Pei = 140;
double Prini = 140;
double Psi = 140;
double Pauxi = 90; // [psi] pressao inicial no reservatorio auxiliar
double Pemgi = 90; // [psi] pressao inicial no reservatorio de emergencia
double Pcfi = 0; // [psi] pressao inicial no cilindro de freio
int valvula = 1; //tipo de valvula 1=AB, 2=ABD, 3=ABDX
double w10t[30];
double w10p[30];
double w10a[30];
double w10pc[30];
int manipu;
double Al;
double Asl;
double Z, Z1, Q;
double gi;

//Parametros de ajuste gerais
double dx; // [m] discretizacao no espaco (utilizando o tamanho do vagao)
double dt;  // [s] discretizazacao no tempo
double rEG;                // [m] raio do encanamento geral
double A_ent_loco; //[m2] area de entrada de ar do compressor para a locomotiva
double A_sai_loco; //[m2] area de saida de ar do compressor para a locomotiva
double AorificioEG; // [m2] area do orificio do EG entre locomotivas para o método de volumes e orificios

                                    //Parametros de ajuste por valvula
double at_EMG1, at_EMG2, at_EMG3, at_EMG4 = 544738; //[Pa] Diferenca de pressao para ativar a emergencia
double Vaux1, Vaux2, Vaux3;      // [m3] volume auxiliar
double Vemg1, Vemg2, Vemg3;    // [m3] volume emergencia
double Vsr1, Vsr2, Vsr3;                   // [m3] volume (hipotetico) servico rapido
double Aent1, Aent2, Aent3;        // [m2] area de entrada para o auxiliar e emergencia
double Asp1, Asp2, Asp3;            // [m2] area de saida do encanamento (durante emergencia)
double Asp_1, Asp_2, Asp_3;        // [m2] area de saida do encanamento (plicação acelerada ABDX)
double Aesr1, Aesr2, Aesr3;        // [m2] area de entrada do servico rapido
double Assr1, Assr2, Assr3;        // [m2] area de saida do SR. Compromisso entre aplic. e emerg.
double Assr_1, Assr_2, Assr_3; // [m2] area de saida do SR (plicação acelerada ABDX)
double Assr_emg1, Assr_emg2, Assr_emg3; // [m2] area de saida do SR na emergencia
double Aeemg1, Aeemg2, Aeemg3;             // [m2] area de entrada da emergencia
double Asemg1, Asemg2, Asemg3;             // [m2] area de saida da emergencia para a conexao com aux e cf
double Aecf1, Aecf2, Aecf3;        // [m2] area de entrada do cilindro de freio
double Ascf1, Ascf2, Ascf3;        // [m2] area de saida do silindro de freio pra atmosfera (alivio)
double Alim1, Alim2, Alim3;  // [m2] area de passagem da valvula limitadora
double Aassal1, Aassal2, Aassal3; // [m2] area de passagem da valvula asseguradora de alivio
double Aegatm1, Aegatm2, Aegatm3; // [m2] area de saida de ar do EG para atm no início da aplicação
double Acfeg1, Acfeg2, Acfeg3;  // [m2] area de saida de ar do CF para EG no alívio de emergência
long double Aebc; // [m2] area de entrada da pinça de freio
double Asbc; // [m2] area de saida da pinça de freio para a armosfera
double Aerin; // [m2] area de entrada do reservatorio principal
double Aes; // [m2] area de entrada do reservatório suplementar do reservatorio principal
double Aes2; // [m2] area de entrada do reservatorio suplementar do EG
double Vcf; // [m3] volume do volume falso
double Vrin; // [m3] volume do reservatorio principal
double Vs; // [m3] volume do reservatório suplementar
double Vbc; // [m3] volume da tubulação até a pinça



                        //cilindro de freio
double m1, m2, m3; // [kg] massa do cilindro de freio
double k1, k2, k3; // [N/m] constante elastica da mola
double c1, c2, c3; // [N.s/m] constante de amortecimento do pistao
double F1, F2, F3; // [N] pre-carga na mola
double Acf1, Acf2, Acf3; // [m2] area do cilindro de freio
double Xmin1, Xmin2, Xmin3; // [m] posicao minima do CF
double Xst1, Xst2, Xst3; // [m] posicao maxima do CF

                                    //Parametros de diferenças de pressao

double dpSReg1, dpSReg2, dpSReg3; //[Pa]
double dpSReg_1, dpSReg_2, dpSReg_3; //[Pa]
double dpEGsr1, dpEGsr2, dpEGsr3; //[Pa]
double dpCFeg1, dpCFeg2, dpCFeg3; //[Pa]
double dpEGatm1, dpEGatm2, dpEGatm3; //[Pa]
double dpATMeg1, dpATMeg2, dpATMeg3; //[Pa]
```

```
double dpEMGcf1, dpEMGcf2, dpEMGcf3; //[Pa]
double dpEMGeg1, dpEMGeg2, dpEMGeg3; //[Pa] alívio acelerado nas valvulas ABD e ABDX
double at_ap1, at_ap2, at_ap3; //[Pa]
double at_apr1, at_apr2, at_apr3; //[Pa]
double at_car1, at_car2, at_car3; //[Pa]
double at_rec1, at_rec2, at_rec3; //[Pa]
double at_al1, at_al2, at_al3; //[Pa]
double at_lim1, at_lim2, at_lim3; //[Pa]
double inicio_ap1, inicio_ap2, inicio_ap3; //[Pa]
double ass_al1, ass_al2, ass_al3; //[Pa]

                                                                    //Parametros do ambiente
double visc = 1.86e-5;  // [Pa.s] viscosidade do ar
double R = 287;                         // [J/(kg.K)] constante do ar
double T = 298;                         // [K] temperatura ambiente
double Patm = 1.01325e5;  // [Pa] pressao atmosferica
double y = 1.4;                         //coeficiente isentropico do ar
double B = sqrt(R * T); //velocidade do som
double k4 = 1. / (pow(B, 2.));
double c4 = sqrt(1.4 / k4);
double Pvac = 1.0e3; //[Pa] potential vacuum pressure

//Outras variaveis nao alteraveis
int n_cars; //numero total de veiculos
int ultimo; //apenas para controle
int  i, j; //variaveis para loop
double t; //tempo
double pi = 3.141592; //pi
double conv = 6894.76; //Pa para psi
double Pen, Pen2; // pressao de entrada
double Paux[400]; // pressao auxiliar
double Pemg[400]; // pressao emergencia
double Pcf[400]; // pressao cilindro de freio
double Pbc[400]; // pressao pinça freio
double Psr[400]; // pressao servico rapido
double Pp[400]; // pressao encanamento geral
int AT[400]; // auxiliar para controle de operacoes
double media[400];
int VAG[400]; // auxiliar para controle de vagoes duplos e locomotivas
double X[400]; // posicoes dos pistoes do CF
double X1[400]; // velocidades dos pistoes do CF
double fluxo_massico_encanamento[400], fluxo_massico_encanamento2[400]; // fluxo massico entre EG e valvulas (em cada vagao)
double M[400]; // fluxo massico no EG
double P[400], U[4][400], Dens[4][400], Pep[400], Pe[400];
double Ps[400];
double Prin[400];
double T1[2][400], E[2][400];

double fluxo_massico_entrada; // fluxo massico que entra nas locomotivas
double D, A, Cp; // diametro, area e "capacidade" do EG

                                        //funcao de pressao de entrada
int aplication_number = 0;
double entrada(double tt)
{
        if ((tt > w10t[aplication_number]) && (tt < w10t[aplication_number + 1]))
        {
                Pen2 = w10pc[aplication_number] * conv + Patm;
                manipu = w10a[aplication_number];
                return w10p[aplication_number] * conv + Patm;
        }
        else {
                aplication_number = aplication_number + 1;
                Pen2 = w10pc[aplication_number] * conv + Patm;
                manipu = w10a[aplication_number];
                return w10p[aplication_number] * conv + Patm;
        }
}

//funcao de sinal (para verificar o sentido do fluxo)
int sig(double dP)
{
        if (dP > 0.0)
        {
                return 1.0;
        }
        else if (dP == 0.0)
        {
                return 0.0;
        }
        else
        {
                return -1.0;
        }
}

//Calculo do coeficiente Cm na funcao de orificio
double funcao_Cm(double Pe, double Ps)
{
        double Cm;
        double f_Ps_Pe;
        f_Ps_Pe = Ps / Pe;
        Cm = sqrt((2.0 * y) / (R * (y - 1))) * sqrt(pow(f_Ps_Pe, (2.0 / y)) - pow(f_Ps_Pe, (1.0 + 1.0 / y))); //always assumes subsonic flow

        return Cm;
}

//Calculo do coeficiente Cq na funcao de orificio
double funcao_Cq(double Pe, double Ps)
{
        double Cq;
```

```
	double f_Ps_Pe;
	f_Ps_Pe = Ps / Pe;
	Cq = 0.8414 - 0.1002 * (f_Ps_Pe)+0.8415 * pow(f_Ps_Pe, 2.0) - 3.9 * pow(f_Ps_Pe, 3.0) + 4.6001 * pow(f_Ps_Pe, 4.0) - 1.6827 * pow(f_Ps_Pe, 5.0);
	return Cq;

}

//calculo do fluxo massico (orificio)
double funcao_dm_dt(double A0, double Pe, double Ps, double Te)
{
	double dm_dt;
	double Cm;
	double Cq;

	Cm = funcao_Cm(Pe, Ps);
	Cq = funcao_Cq(Pe, Ps);
	dm_dt = A0 * Cq * Cm * (Pe / sqrt(Te));
	return dm_dt;
}

//Funcao de orificio de entrada de ar (nas locomotivas)
double Orificio_ent(double P1, double P2, double Ao)
{
	double fluxo_massico_entrada;
	double Pe;
	double Ps;
	double Preg;
	Preg = 7.21853156e5;			////pressÃ£o no reservatÃ³rio equilibrante (90psi)
	if (P1 >= P2)
	{
		Pe = P1;			////PressÃ£o de Entrada = PressÃ£o no manipulador
		Ps = P2;			////PressÃ£o de Saida = PressÃ£o no EG
		if (P2 >= Preg && P1 >= Preg)
		{
			fluxo_massico_entrada = 0;
		}
		else
		{
			fluxo_massico_entrada = funcao_dm_dt(Ao, Pe, Ps, T);
		}
	}
	else
	{
		Pe = P2;				////PressÃ£o de Entrada = PressÃ£o no EG
		Ps = Patm;				////PressÃ£o de SaÃ-da = PressÃ£o no manipulador
		Ao = A_sai_loco;					////m2
		fluxo_massico_entrada = -1 * funcao_dm_dt(Ao, Pe, Ps, T);
	}

	return fluxo_massico_entrada;
}

//orificio utilizado para representar a valvula limitadora
double orificiolim(double P1, double P2, double A)
{
	double Pe, Ps;

	if (P1 >= P2)
	{
		Pe = P1; //%PressÃ£o de Entrada = PressÃ£o no EG
		Ps = P2; //%PressÃ£o de SaÃ-da = PressÃ£o no AUX
		return funcao_dm_dt(A, Pe, Ps, T);
	}
	else
	{
		return 0;
	}
}

//funcao de orificio (geral)
double orificio(double P1, double P2, double A, double T3)
{
	double fluxo_massico = 0.0;
	int sentido;
	double Pe, Ps;

	if (P1 >= P2)
	{
		Pe = P1;				////PressÃ£o de Entrada = PressÃ£o no maniPelador
		Ps = P2;			////PressÃ£o de SaÃ-da = PressÃ£o no EG
		sentido = 1;					////sentido da vazÃ£o de entrada
	}
	else
	{
		Pe = P2;					////PressÃ£o de Entrada = PressÃ£o no EG
		Ps = P1;		////PressÃ£o de SaÃ-da = PressÃ£o no maniPelador
		sentido = -1;					////sentido da vazÃ£o de entrada
	}

	fluxo_massico = sentido * funcao_dm_dt(A, Pe, Ps, T3);

	return fluxo_massico;
}

//function that simulates sonic flow
double orificioventuri(double P1, double P2, double A, double T3)
{
	double fluxo_massico = 0.0;
	int sentido;
	double Pe, Ps;
```

```
		if (P1 >= P2)
		{
			Pe = P1;						////PressÃ£o de Entrada = PressÃ£o no maniPelador
			Ps = P2;					////PressÃ£o de SaÃ-da = PressÃ£o no EG
			sentido = 1;							////sentido da vazÃ£o de entrada
		}
		else
		{
			Pe = P2;							////PressÃ£o de Entrada = PressÃ£o no EG
			Ps = P1;			////PressÃ£o de SaÃ-da = PressÃ£o no maniPelador
			sentido = -1;							////sentido da vazÃ£o de entrada
		}

		fluxo_massico = sentido * A * funcao_Cq(Pe, Ps) * sqrt((y / R) * pow((2 / (y + 1)), (y + 1) / (y - 1))) * Pe / sqrt(T3);

		return fluxo_massico;
}

//orificio para representar o cilindro de freio
double orificio_CF(double P1, double P2, double A)
{
		double Pe, Ps;
		if (P1 >= P2)
		{
			Pe = P1; //%Pressão de Entrada = Pressão no Cilindro de Freio
			Ps = P2; //%Pressão de Saída = Pressão no EG
					//	A=Acf_eg;
			return funcao_dm_dt(A, Pe, Ps, T);
		}
		else if (P1 >= Patm)
		{
			Pe = P1; //%Pressão de Entrada = Pressão no Cilindro de Freio
			Ps = Patm; //%PressÃ£o de SaÃ-da = PressÃ£o ATM
			return funcao_dm_dt(A, Pe, Ps, T);
		}
		else
			return 0;
}

double entradaI(double P11, double P22, double C2, double Dia) {	// calculo da função no ponto desejado
		double A, Cm, Cq, v, m_dot, Pent, Patm, k, Rho;
		Pent = 140. * 6894.76 + 1e5;
		Patm = 1.e5;
		if (P11 > Patm + 10000) {
			if (P11 - P22 >= 100.) {
				Rho = (Pent + P22) / 2. / (287. * T);
				A = pi * pow(Dia / Al, 2.) / 4.;//3.2 for recharge
				Cm = sqrt(2. * 1.4 / (287. * (1.4 - 1))) * sqrt(pow((P22 / Pent), (2. / 1.4)) - pow((P22 / Pent), ((1.4 + 1.)) / 1.4));
				Cq = 0.8414 - 0.1002 * (P22 / Pent) + 0.8415 * pow((P22 / Pent), 2.) - 3.9 * pow((P22 / Pent), 3.) + 4.6001 * pow((P22 / Pent), 4.) - 1.6827 * pow((P22 /
Pent), 5.);
				m_dot = A * Cm * Cq * Pent / (sqrt(T));
				v = m_dot / (A * Rho);
				if (v < C2)
					m_dot = m_dot;
				else if (v > C2) {
					Cm = sqrt(2. * 1.4 / (287. * (1.4 + 1.))) * pow((2. / (1.4 + 1.)), (1. / (1.4 - 1.)));
					m_dot = A * Cm * Cq * Pent / sqrt(T);
				}
				else if (v == C2) {
					Cm = sqrt(1.4 / 287. * pow((2. / (1.4 + 1.)), ((1.4 + 1.) / (1.4 - 1.))));
					m_dot = A * Cm * Cq * Pent / sqrt(T);
				}
				return (m_dot);
			}
			else if (P11 - P22 <= -100.) {
				Rho = (Patm + P22) / 2. / (287. * T);
				A = pi * pow(Dia / Asl, 2.) / 4.;//4.6 for application * maybe we can change Asl for 2
				Cm = sqrt(2. * 1.4 / (287. * (1.4 - 1.))) * sqrt(pow((Patm / P22), (2. / 1.4)) - pow((Patm / P22), ((1.4 + 1.)) / 1.4));
				Cq = 0.8414 - 0.1002 * (Patm / P22) + 0.8415 * pow((Patm / P22), 2.) - 3.9 * pow((Patm / P22), 3.) + 4.6001 * pow((Patm / P22), 4.) - 1.6827 * pow((Patm
/ P22), 5.);
				m_dot = A * Cm * Cq * P22 / (sqrt(T));
				v = m_dot / (A * Rho);
				if (v < C2)
					m_dot = m_dot;
				else if (v > C2) {
					Cm = sqrt(2 * 1.4 / (287. * (1.4 + 1.))) * pow((2. / (1.4 + 1.)), (1. / (1.4 - 1.)));
					m_dot = A * Cm * Cq * P22 / sqrt(T);
				}
				else if (v == C2) {
					Cm = sqrt(1.4 / 287. * pow((2. / (1.4 + 1.)), ((1.4 + 1.) / (1.4 - 1.))));
					m_dot = A * Cm * Cq * P22 / sqrt(T);
				}
				return (-m_dot);
			}
			else if (fabs(P11 - P22) <= 100.) {
				return 0;
			}
			gi = 0;
		}
		else {
			Rho = (Patm + P22) / 2. / (287. * T);
			A = pi * pow(Dia / 2., 2.) / 4.; // for emergency application
			Cm = sqrt(2. * 1.4 / (287. * (1.4 - 1.))) * sqrt(pow((Patm / P22), (2. / 1.4)) - pow((Patm / P22), ((1.4 + 1.)) / 1.4));
			Cq = 0.8414 - 0.1002 * (Patm / P22) + 0.8415 * pow((Patm / P22), 2.) - 3.9 * pow((Patm / P22), 3.) + 4.6001 * pow((Patm / P22), 4.) - 1.6827 * pow((Patm / P22),
5.);
			m_dot = A * Cm * Cq * P22 / (sqrt(T));
			v = m_dot / (A * Rho);
			if (v < C2)
				m_dot = m_dot;
			else if (v > C2) {
				Cm = sqrt(2 * 1.4 / (287. * (1.4 + 1.))) * pow((2. / (1.4 + 1.)), (1. / (1.4 - 1.)));
```

```
				m_dot = A * Cm * Cq * P22 / sqrt(T);
			}
			else if (v == C2) {
				Cm = sqrt(1.4 / 287. * pow((2. / (1.4 + 1.)), ((1.4 + 1.) / (1.4 - 1.))));
				m_dot = A * Cm * Cq * P22 / sqrt(T);
			}
			return (-m_dot);
		}
		gi = 1;
}

void valvulaABDX(double Ppj, double Pauxj, double Psrj, double Pemgj, double Pcfj, int ATj, double Xj, double X1j, double Tj, int j)
{
		double Meaux = 0.0;
		double Mesr = 0.0;
		double Mssr = 0.0;
		double Meemg = 0.0;
		double Msemg = 0.0;
		double Msemgp = 0.0;
		double Mecf = 0.0;
		double Mscf = 0;
		double Msp = 0.0;
		double X2 = 0.0;
		double X0 = 0.0;
		double Mvlim = 0;
		double Ment = 0;
		double Mass_ali = 0;
		double Mal_emg = 0;
		double Msemgventuri = 0.0;

		// porcao de serviço rapido
		if ((Ppj - Psrj) > dpEGsr3 || (Ppj - Psrj) > at_al3 && ATj == -2)  //alivio de emergencia
		{
			Mesr = orificio(Ppj, Psrj, Aesr3, Tj);//massa de entrada sr
			if ((Pcfj - Ppj) > dpCFeg3 && (Ppj - Patm) > dpATMeg3 && ATj == -2) //emergency application?
				Mal_emg = orificio_CF(Pcfj, Ppj, Acfeg3); // massa de saida do cilindro de freio
		}
		else if (((Psrj - Ppj) > dpSReg3) && ((Psrj - Ppj) <= at_EMG3) && (ATj != -2)) //aplicação
		{
			Mssr = orificio(Psrj, Patm, Assr3, T); //massa de saida sr
			//Msemgventuri = orificio(Pemgj, Patm, Assr_3, Tj); //testing the effect of using the venturi during the entire brake application
			//Msp = orificio(Ppj, Patm, Asp_3, T); //testing the effect of using the venturi during the entire brake application, do I need this?
			//Msemgventuri = 0; //do I need this?
			if ((Psrj - Ppj) > dpSReg_3 && (Ppj - Pen) > 7000) { //&& (Ppj - Pen)>7000) this is the only difference between the rapid service portion of the ABD
				Msp = 1.0*orificio(Ppj, Patm, Asp_3, T); //this is the only difference between the rapid service portion of the ABD <-comment this out or add multiplicative
factor for venturi (1.05)
				//Msp = orificioventuri(Ppj, Patm, Asp_3, T); //<-current sonic venturi model
				//Msemgventuri = orificio(Pemgj, Patm, Asemg3, Tj); //<-current venturi model Assr_3, sonic model Asemg3
				//Mssr = 1.05 * Mssr; //massa de saida sr while venturi is activated; could be designed in or designed out in theory
				//Mssr = Mssr + orificio(Psrj, Patm, Asp_3, T); <-this was originally commented out //Mssr = orificio(Psrj, Pvac, Assr3, T); //massa de saida sr <-first
venturi attempt
				//	Mssr = Mssr+orificio(Psrj,Patm,Assr_3);<-this was originally commented out //Msp = orificio(Ppj, Pvac, Asp_3, T); this replaced line 620 <-first
venturi attempt
			}
		}
		else if ((Psrj - Ppj > at_EMG3) || ATj == -2) //aplicação de emergencia
		{
			Mssr = orificio(Psrj, Patm, Assr_emg3, T);					//massa de saida sr
			Msemg = orificio(Pemgj, Pcfj, Asemg3, Tj);
			ATj = -2;
			if (((Ppj - Patm) > dpEGatm3) && (fabs(Pemgj - Pcfj)) > dpEMGcf3)
			{
				Msp = orificio(Ppj, Patm, Asp3, T);					//massa de ar que sai do EG para a atmosfera para acelerar a propagação
da emergência
			}
		}

		//porcao de servico
		if (((Pauxj - Ppj) > at_ap3 && ATj == 1) || ATj < 0 || ((Pauxj - Ppj) > at_apr3 && Pcfj > Patm && ATj == 0))  // aplicacao
		{
			if ((Pauxj - Ppj) < inicio_ap3 && ATj == 1)// && ((Pauxj-Ppj)<1300)) in the ABD valve, this is a standalone (and a bit different) if statement
				Msp = Msp + orificio(Ppj, Patm, Aegatm3, T); //para iniciar a aplicação?
			else {
				Mecf = orificio(Pauxj, Pcfj, Aecf3, Tj); //massa de entrada do cilindro de freio
				if (ATj != -2) //Verificar o sinal de emergência
					ATj = -1;
				if ((Ppj - Pauxj) > at_rec3)  // //recobrimento
					ATj = 0;
			}
		}
		else if ((Ppj - Pauxj) > at_car3 || ATj == 1)					// carregamento ou alivio
		{
			Ment = orificio(Ppj, Pauxj, Aent3, Tj);						//massa de entrada na valvula
			Meemg = orificio(Pauxj, Pemgj, Aeemg3, Tj);			//massa de entrada emg
			if ((Pemgj - Ppj) > dpEMGeg3 && (Ppj - Pauxj) > dpEMGeg3)    //ABD e ABDX
				Msemgp = orificio(Pemgj, Ppj, Acfeg3, Tj);
			Mscf = orificio_CF(Pcfj, Patm, Ascf3); //massa de saida do cilindro de freio //
			ATj = 1;
		}
		else if ((Ppj - Pauxj) > ass_al3) { //asseguradora de alivio
			Mass_ali = orificio(Pauxj, Patm, Aassal3, T);
		}

		if ((ATj <= 0) && (Pcfj - Patm) < at_lim3)  //Valvula Limitadora
			Mvlim = orificiolim(Ppj, Pcfj, Alim3);

		// Calculo da posicao do pistao do cilindro de freio
		X2 = (Acf3 * (Pcfj - Patm) - c3 * X1j - k3 * Xj - F3) / m3;
		X1j = X1j + X2 * dt;
		X0 = Xj;
		Xj = Xj + X1j * dt;
```

```
		if (Xj >= Xst3)
		{
			Xj = Xst3;
			X1j = 0.0;
		}
		else if (Xj <= Xmin3)
		{
			Xj = Xmin3;
			X1j = 0.0;
		}

		Meaux = Ment - Mass_ali - Meemg; //calculo da massa que entra no auxiliar (so entra massa na emg se tambem entra no auxiliar)
		Paux[j] = Pauxj + dt * R * T / Vaux3 * (Meaux - Mecf); //pressao no auxiliar
		Psr[j] = Psrj + dt * R * T / Vsr3 * (Mesr - Mssr); // pressao no sr
		Pemg[j] = Pemgj + dt * R * T / Vemg3 * (Meemg - Msemg - Msemgp); // pressao na emergencia Pemg[j] = Pemgj + dt * R * T / Vemg3 * (Meemg - Msemg - Msemgp - Msemgventuri);
		Pcf[j] = 1 / Xj * (Pcfj * X0 + R * T / Acf3 * (Mecf + Mvlim + Msemg - Mal_emg - Mscf) * dt);//pressao no CF
		AT[j] = ATj;
		X[j] = Xj;
		X1[j] = X1j;
		media[j] = media[j] + AT[j]; //not used in pneumatic only

		fluxo_massico_encanamento[j] = Msp + Ment - Mal_emg + Mvlim - Msemgp;
}

// Calcular a pressao no EG
void calculate_pressao_EG()
{
		for (j = 0; j < n_cars - 1; j++)
		{
			Pp[j] = dt * (-fluxo_massico_encanamento[j] + M[j] - M[j + 1]) / Cp + Pp[j];
		}
		if (Pp[0] >= 7.21853156e5)
			Pp[0] = 7.21853156e5;
		else if (Pp[0] <= Patm)
			Pp[0] = Patm;
		Pp[n_cars - 1] = dt * (-fluxo_massico_encanamento[n_cars - 1] + M[n_cars - 1]) / Cp + Pp[n_cars - 1];
}

//inicializacao dos vetores
int inicial()
{

		int number_of_parameters = 6, number_of_parameters_valv = 42, number_of_parameters_ent = 19, number_of_parameters_vet = 5, number_of_parameters_pass = 9;
		char buff[255], buff_ent[255], buff_vet[255], buff_valv[255], buff_train[255];
		double parameters_array[6], parameters_array_valv[42], parameters_array_ent[19], parameters_array_pass[9];
		int i, j;
		FILE* file;

		file = fopen("parametros.txt", "r");
		for (i = 0; i < number_of_parameters; i++)
		{
			fscanf(file, "%s", buff);
			fscanf(file, "%s", buff);
			parameters_array[i] = atof(buff);
		}

		dx = parameters_array[0];
		dt = parameters_array[1];
		rEG = parameters_array[2];
		A_ent_loco = parameters_array[3];
		A_sai_loco = parameters_array[4];
		AorificioEG = parameters_array[5];

		file = fopen("parametrosEP60.txt", "r");
		for (i = 0; i < number_of_parameters_pass; i++)
		{
			fscanf(file, "%s", buff);
			fscanf(file, "%s", buff);
			parameters_array_pass[i] = atof(buff);
		}
		Aebc = parameters_array_pass[0];
		Asbc = parameters_array_pass[1];
		Aerin = parameters_array_pass[2];
		Aes = parameters_array_pass[3];
		Aes2 = parameters_array_pass[4];
		Vcf = parameters_array_pass[5];
		Vrin = parameters_array_pass[6];
		Vs = parameters_array_pass[7];
		Vbc = parameters_array_pass[8];


		file = fopen("parametrosAB.txt", "r");
		for (i = 0; i < number_of_parameters_valv; i++)
		{
			fscanf(file, "%s", buff_valv);
			fscanf(file, "%s", buff_valv);
			parameters_array_valv[i] = atof(buff_valv);
		}

		at_EMG1 = parameters_array_valv[0];
		Vaux1 = parameters_array_valv[1];
		Vemg1 = parameters_array_valv[2];
		Vsr1 = parameters_array_valv[3];
		Aent1 = parameters_array_valv[4];
		Asp1 = parameters_array_valv[5];
		Asp_1 = parameters_array_valv[6];
		Aesr1 = parameters_array_valv[7];
		Assr1 = parameters_array_valv[8];
		Assr_1 = parameters_array_valv[9];
		Assr_emg1 = parameters_array_valv[10];
```

```
Aeemg1 = parameters_array_valv[11];
Asemg1 = parameters_array_valv[12];
Aecf1 = parameters_array_valv[13];
Ascf1 = parameters_array_valv[14];
Alim1 = parameters_array_valv[15];
Aassal1 = parameters_array_valv[16];
Aegatm1 = parameters_array_valv[17];
Acfeg1 = parameters_array_valv[18];
m1 = parameters_array_valv[19];
k1 = parameters_array_valv[20];
c1 = parameters_array_valv[21];
F1 = parameters_array_valv[22];
Acf1 = parameters_array_valv[23];
Xmin1 = parameters_array_valv[24];
Xst1 = parameters_array_valv[25];
dpSReg1 = parameters_array_valv[26];
dpSReg_1 = parameters_array_valv[27];
dpEGsr1 = parameters_array_valv[28];
dpCFeg1 = parameters_array_valv[29];
dpEGatm1 = parameters_array_valv[30];
dpATMeg1 = parameters_array_valv[31];
dpEMGcf1 = parameters_array_valv[32];
dpEMGeg1 = parameters_array_valv[33];
at_ap1 = parameters_array_valv[34];
at_apr1 = parameters_array_valv[35];
at_car1 = parameters_array_valv[36];
at_rec1 = parameters_array_valv[37];
at_al1 = parameters_array_valv[38];
at_lim1 = parameters_array_valv[39];
inicio_ap1 = parameters_array_valv[40];
ass_al1 = parameters_array_valv[41];

file = fopen("parametrosABD.txt", "r");
for (i = 0; i < number_of_parameters_valv; i++)
{
        fscanf(file, "%s", buff_valv);
        fscanf(file, "%s", buff_valv);
        parameters_array_valv[i] = atof(buff_valv);
}

at_EMG2 = parameters_array_valv[0];
Vaux2 = parameters_array_valv[1];
Vemg2 = parameters_array_valv[2];
Vsr2 = parameters_array_valv[3];
Aent2 = parameters_array_valv[4];
Asp2 = parameters_array_valv[5];
Asp_2 = parameters_array_valv[6];
Aesr2 = parameters_array_valv[7];
Assr2 = parameters_array_valv[8];
Assr_2 = parameters_array_valv[9];
Assr_emg2 = parameters_array_valv[10];
Aeemg2 = parameters_array_valv[11];
Asemg2 = parameters_array_valv[12];
Aecf2 = parameters_array_valv[13];
Ascf2 = parameters_array_valv[14];
Alim2 = parameters_array_valv[15];
Aassal2 = parameters_array_valv[16];
Aegatm2 = parameters_array_valv[17];
Acfeg2 = parameters_array_valv[18];
m2 = parameters_array_valv[19];
k2 = parameters_array_valv[20];
c2 = parameters_array_valv[21];
F2 = parameters_array_valv[22];
Acf2 = parameters_array_valv[23];
Xmin2 = parameters_array_valv[24];
Xst2 = parameters_array_valv[25];
dpSReg2 = parameters_array_valv[26];
dpSReg_2 = parameters_array_valv[27];
dpEGsr2 = parameters_array_valv[28];
dpCFeg2 = parameters_array_valv[29];
dpEGatm2 = parameters_array_valv[30];
dpATMeg2 = parameters_array_valv[31];
dpEMGcf2 = parameters_array_valv[32];
dpEMGeg2 = parameters_array_valv[33];
at_ap2 = parameters_array_valv[34];
at_apr2 = parameters_array_valv[35];
at_car2 = parameters_array_valv[36];
at_rec2 = parameters_array_valv[37];
at_al2 = parameters_array_valv[38];
at_lim2 = parameters_array_valv[39];
inicio_ap2 = parameters_array_valv[40];
ass_al2 = parameters_array_valv[41];

file = fopen("parametrosABDX.txt", "r");
for (i = 0; i < number_of_parameters_valv; i++)
{
        fscanf(file, "%s", buff_valv);
        fscanf(file, "%s", buff_valv);
        parameters_array_valv[i] = atof(buff_valv);
}

at_EMG3 = parameters_array_valv[0];
Vaux3 = parameters_array_valv[1];
Vemg3 = parameters_array_valv[2];
Vsr3 = parameters_array_valv[3];
Aent3 = parameters_array_valv[4];
Asp3 = parameters_array_valv[5];
Asp_3 = parameters_array_valv[6];
Aesr3 = parameters_array_valv[7];
Assr3 = parameters_array_valv[8];
Assr_3 = parameters_array_valv[9];
```

```
Assr_emg3 = parameters_array_valv[10];
Aeemg3 = parameters_array_valv[11];
Asemg3 = parameters_array_valv[12];
Aecf3 = parameters_array_valv[13];
Ascf3 = parameters_array_valv[14];
Alim3 = parameters_array_valv[15];
Aassal3 = parameters_array_valv[16];
Aegatm3 = parameters_array_valv[17];
Acfeg3 = parameters_array_valv[18];
m3 = parameters_array_valv[19];
k3 = parameters_array_valv[20];
c3 = parameters_array_valv[21];
F3 = parameters_array_valv[22];
Acf3 = parameters_array_valv[23];
Xmin3 = parameters_array_valv[24];
Xst3 = parameters_array_valv[25];
dpSReg3 = parameters_array_valv[26];
dpSReg_3 = parameters_array_valv[27];
dpEGsr3 = parameters_array_valv[28];
dpCFeg3 = parameters_array_valv[29];
dpEGatm3 = parameters_array_valv[30];
dpATMeg3 = parameters_array_valv[31];
dpEMGcf3 = parameters_array_valv[32];
dpEMGeg3 = parameters_array_valv[33];
at_ap3 = parameters_array_valv[34];
at_apr3 = parameters_array_valv[35];
at_car3 = parameters_array_valv[36];
at_rec3 = parameters_array_valv[37];
at_al3 = parameters_array_valv[38];
at_lim3 = parameters_array_valv[39];
inicio_ap3 = parameters_array_valv[40];
ass_al3 = parameters_array_valv[41];

file = fopen("entrada.txt", "r");
for (i = 0; i < number_of_parameters_ent; i++)
{
		fscanf(file, "%s", buff_ent);
		fscanf(file, "%s", buff_ent);
		parameters_array_ent[i] = atof(buff_ent);
}

vagao_duplo = parameters_array_ent[0];
n_loco = parameters_array_ent[1];
n_vagoes = parameters_array_ent[2];
t0 = parameters_array_ent[3];
t_final = parameters_array_ent[4];
Ppi = parameters_array_ent[5];
Pauxi = parameters_array_ent[6];
Pemgi = parameters_array_ent[7];
Pcfi = parameters_array_ent[8];
valvula = parameters_array_ent[9];
T = parameters_array_ent[10];
Al = parameters_array_ent[11];
Asl = parameters_array_ent[12];
Z = parameters_array_ent[13];
Z1 = parameters_array_ent[14];
Q = parameters_array_ent[15];
Pei = parameters_array_ent[16];
Prini = parameters_array_ent[17];
Psi = parameters_array_ent[18];


file = fopen("vetores.txt", "r");
for (i = 0; i < number_of_parameters_vet; i++) {
		fscanf(file, "%s", buff_vet);
		//	printf("Parametro : %s = ", buff_vet);
		if (i == 0) {
				for (j = 0; j < 6; j++) {
						fscanf(file, "%s", buff_vet);
						//		printf("%s ",buff_vet);
						pos_loco[j] = atof(buff_vet);
				}
		}
		else if (i == 1) {
				for (j = 0; j < 30; j++) {
						fscanf(file, "%s", buff_vet);
						//		printf("%s ",buff_vet);
						w10t[j] = atof(buff_vet);
				}
		}
		else if (i == 2) {
				for (j = 0; j < 30; j++) {
						fscanf(file, "%s", buff_vet);
						//		printf("%s ",buff_vet);
						w10p[j] = atof(buff_vet);
				}
		}
		else if (i == 3) {
				for (j = 0; j < 30; j++) {
						fscanf(file, "%s", buff_vet);
						//		printf("%s ",buff_vet);
						w10a[j] = atof(buff_vet);
				}
		}
		else if (i == 4) {
				for (j = 0; j < 30; j++) {
						fscanf(file, "%s", buff_vet);
						//		printf("%s ",buff_vet);
						w10pc[j] = atof(buff_vet);
				}
		}
```

```
		//	printf("\n");
	}

	Pauxi = Pauxi * conv + Patm;
	Pemgi = Pemgi * conv + Patm;
	Ppi = Ppi * conv + Patm;
	Pei = Pei * conv + Patm;
	Prini = Prini * conv + Patm;
	Psi = Psi * conv + Patm;
	//printf("%lf", Ppi);
	Pcfi = Pcfi * conv + Patm;
	n_cars = n_loco + n_vagoes;
	D = 2 * rEG; //Diameter of brake pipe
	A = pi * pow(rEG, 2); //Cross sectional area of brake pipe
	Cp = A * dx / (R * T); //Common variable to simplify equations but is never used
	k4 = 1 / (R * T); //Common variable to simplify equations
	for (j = 0; j < n_cars; j = j + 1)
	{
		Pp[j] = Ppi;
		Paux[j] = Pauxi;
		Pemg[j] = Pemgi;
		Pe[j] = Pei; //not used in pneumatic only, entrance pressure
		Ps[j] = Psi; //not used in pneumatic only, exit pressure
		Prin[j] = Prini; //not used in pneumatic only
		Psr[j] = Ppi; //rapid service chamber pressure
		Pcf[j] = Pcfi; //brake cylinder pressure
		Pbc[j] = Pcfi; //not used in pneumatic only
		AT[j] = 1;
		media[j] = 0;
		X1[j] = 0.0;
		VAG[j] = 0;
		fluxo_massico_encanamento[j] = 0.0;
		fluxo_massico_encanamento2[j] = 0.0;
		U[0][j] = 0.0;
		U[2][j] = 0.0;
		Dens[0][j] = Ppi * k4;
		Dens[2][j] = Pei * k4;
		T1[0][j] = T;
	}

	i = 0;
	j = 0;

	if (valvula == 0) {
		file = fopen("VAG.dat", "r");
		for (i = 0; i < n_cars; i++) {
			fscanf(file, "%s", buff_train);
			VAG[i] = atoi(buff_train);
			if (VAG[i] == 1) {
				X[i] = Xmin1;
				ultimo = i;
			}
			else if (VAG[i] == 2) {
				X[i] = Xmin2;
				ultimo = i;
			}
			else if (VAG[i] == 3) {
				X[i] = Xmin3;
				ultimo = i;
			}
			else
				X[i] = Xmin3;
		}
	}
	else {
		FILE* pFile_VAG;
		pFile_VAG = fopen("VAG.dat", "w");
		for (i = 0; i < n_cars; i++) {
			if ((i + 1) == pos_loco[j]) {
				VAG[i] = 5;
				if (j < n_loco - 1)
					j = j + 1;
			}
			else if (VAG[i - 1] == 0 || VAG[i - 1] == 5) {
				VAG[i] = valvula;
				ultimo = i;
			}
			else if (vagao_duplo == 1) {
				VAG[i] = valvula;
				ultimo = i;
			}
			if (VAG[i] == 1)
				X[i] = Xmin1;
			else if (VAG[i] == 2)
				X[i] = Xmin2;
			else if (VAG[i] == 3)
				X[i] = Xmin3;
			else
				X[i] = Xmin3;
			fprintf(pFile_VAG, "%d\n", VAG[i]);
		};
	}
	return 0;
}

//Funcao principal
int main()
{
	double Uen = 0., Ree, fe, Nu, Pr = 0.7, Een, Ra, Nu1;
	float* Re = (float*)calloc(NMAX, sizeof(float));
	float* f = (float*)calloc(NMAX, sizeof(float));
```

```
		float* fp = (float*)calloc(NMAX, sizeof(float));
		float* Rep = (float*)calloc(NMAX, sizeof(float));
		double kappa = 1004. * visc / Pr;
		double m_dot, m_dot2, beta = 1 / T;
		double h[400];
		double kaco = 60.5;
		double eaco = 4.85e-3;
		int c = 0;
		int inicio, final, tmili;
		double vr;//reynolds para escoamento cruzado

		inicio = GetTickCount();

		inicial();
		FILE* pFile_Paux;
		FILE* pFile_Pp;
		FILE* pFile_Pemg;
		FILE* pFile_Pcf;
		FILE* pFile_Psr;
		FILE* pFile_AT;
		FILE* pFile_Pe;
		FILE* pFile_Prin;
		FILE* pFile_Ps;
		FILE* pFile_Pbc;
		pFile_Paux = fopen("Paux.dat", "w");
		pFile_Pp = fopen("Pp.dat", "w");
		pFile_Pemg = fopen("Pemg.dat", "w");
		pFile_Pcf = fopen("Pcf.dat", "w");
		pFile_Psr = fopen("Psr.dat", "w");
		pFile_AT = fopen("AT.dat", "w");
		pFile_Pe = fopen("Pe.dat", "w");
		pFile_Prin = fopen("Prin.dat", "w");
		pFile_Pbc = fopen("Pbc.dat", "w");
		pFile_Ps = fopen("Ps.dat", "w");


		t = t0;
		int write_count = 0, contador = 1 / dt;
		while (t < t_final)
		{
			Pen = entrada(t);
			if (valvula == 4) {
				Ree = Pen * k4 * Uen * D / visc;	//Número de Reynolds, considerando o fluxo que chega ao vagão
															//avaliando o fator de atrito
				if (Ree == 0.)
					fe = 0.;
				else if (Ree <= 2000.)
					fe = 64. / Ree;
				else if (Ree > 2000. && Ree < 4000.)
					fe = 0.0027 / pow(Ree, 0.222);
				else
					fe = 0.316 / pow(Ree, 0.25);
				Uen = Uen - dt / dx * (Uen * (U[0][0] - Uen) + 1. / (Pen * k4) * (P[0] - Pen)) - dt * fe * pow(Uen, 2.) / (2. * D) * 1.93 * 2.3;//(1. + (5. * 16. + 2. * 5.)*D / 
dx);


//printf("%lf %lf %lf\n", fe,U[0][0],Uen);
				Een = (717.4 * (T)+pow(Uen, 2) / 2);
#pragma omp parallel for
				for (j = 0; j < n_cars; j++) {
					AT[j] = manipu;
				}

#pragma omp parallel for
				for (j = 0; j < n_cars; j++) {
					Re[j] = Dens[0][j] * fabs(U[0][j]) * D / visc;	//Número de Reynolds, considerando o fluxo que chega ao vagão
																			//avaliando 
o fator de atrito
					if (Re[j] == 0.)
						f[j] = 0.;
					else if (Re[j] <= 2000.)
						f[j] = 64. / Re[j];
					else if (Re[j] > 2000. && Re[j] < 4000.)
						f[j] = 0.0027 / pow(Re[j], 0.222);
					else
						f[j] = 0.316 / pow(Re[j], 0.25);

					//if (Re < 3000)
						//Nu = 4.36;
					//else
						//Nu = (f / 8)*(Re - 1000)*Pr / (1 + 12.7*pow(f / 8., 0.5)*(pow(Pr, 2. / 3.) - 1));

					//if (Q == 1) {
						//Ra = 9.81*beta*fabs(T1[0][j] - T)*pow(D, 3)*Pr / pow(visc, 2);
						//if (Ra > 1e-10 && Ra < 1e-2)
							//Nu1 = 0.675*pow(Ra, 0.058);
						//else if (Ra > 1e-2 && Ra < 1e2)
							//Nu1 = 1.02*pow(Ra, 0.148);
						//else if (Ra > 1e2 && Ra < 1e4)
							//Nu1 = 0.85*pow(Ra, 0.188);
						//else if (Ra > 1e4 && Ra < 1e7)
							//Nu1 = 0.48*pow(Ra, 0.25);
						//else if (Ra > 1e7 && Ra < 1e12)
							//Nu1 = 0.125*pow(Ra, 0.333);
						//else if (Ra == 0)
							//Nu1 = 0;
					//}
					//else {
						//vr = 20. / 3.6*Patm / (R*T)*D / visc;
						//Nu1 = 0.027*pow(vr, 0.805)*pow(Pr, 1. / 3.);
					//}
```

```
//h[j] = 1 / (1 / (Nu*kappa / D) + (1 / (Nu1*kappa / D)) + (eaco / kaco));
if (j == 0) {
	m_dot = entradal(Pen, Pp[j], c4, D);
	Dens[1][0] = Dens[0][j] - dt / dx * (Dens[0][j] * U[0][j] - Dens[0][j] * -U[0][j]) + dt * m_dot / (dx * pi * pow(rEG, 2));
	if (U[0][j] < 0)
		U[1][j] = U[0][j] - dt / (dx) * (U[0][j] * (U[0][j + 1] - U[0][j]) + 1. / Dens[0][j] * (Pp[j + 1] - Pp[j])) - dt * (-f[j] * pow(U[0][j], 2.) / (2. * D) * 2.94 * Z - U[0][j] / Dens[0][j] * m_dot / (dx * pi * pow(rEG, 2)));// (1. + (4. * 16. + 2. * 5.)*D / dx);
	else
		U[1][j] = U[0][j] - dt / (dx) * (U[0][j] * (U[0][j + 1] - U[0][j]) + 1. / Dens[0][j] * (Pp[j + 1] - Pp[j])) - dt * (f[j] * pow(U[0][j], 2.) / (2. * D) * 2.94 * Z - U[0][j] / Dens[0][j] * m_dot / (dx * pi * pow(rEG, 2)));// (1. + (4. * 16. + 2. * 5.)*D / dx);

//E[0][j] = Dens[0][j] * (717.4*T1[0][j] + pow(U[0][j], 2) / 2);

//if (U[0][j]<0)

//E[1][j] = Dens[0][j] * (717.4*T1[0][j] + pow(U[0][j], 2) / 2) - dt / dx*(Dens[0][j] * U[0][j] * (717.4 * T1[0][j] + pow(U[0][j], 2) / 2) - Dens[0][j] * (717.4 * (T1[0][j])+pow(U[0][j], 2) / 2) - kappa*(T1[0][j] - 2.*T1[0][j] + T1[0][j + 1]) / dx + (Pp[j] * U[0][j] - Pp[j]*-U[0][j])) - dt*Dens[0][j] * (h[j] * 4.*dx / D* (T1[0][j] - T) - f*pow(U[0][j], 2.)*2.94 / (2. * D)*(U[0][j])) + dt*(m_dot / (dx*pi*pow(rEG, 2))*(1004.*T1[0][j] + pow(U[0][j], 2) / 2));

//else

//E[1][j] = Dens[0][j] * (717.4*T1[0][j] + pow(U[0][j], 2) / 2) - dt / dx*(Dens[0][j] * U[0][j] * (717.4 * T1[0][j] + pow(U[0][j], 2) / 2) - Dens[0][j] * (717.4 * (T1[0][j]) + pow(U[0][j], 2) / 2) - kappa*(T1[0][j] - 2.*T1[0][j] + T1[0][j + 1]) / dx + (Pp[j] * U[0][j] - Pp[j] * -U[0][j])) - dt*Dens[0][j] * (h[j] * 4.*dx / D* (T1[0][j] - T) + f*pow(U[0][j], 2.)*2.94 / (2. * D)*(U[0][j])) + dt*(m_dot / (dx*pi*pow(rEG, 2))*(1004.*T1[0][j] + pow(U[0][j], 2) / 2));

//T1[1][j] = (E[1][j] / Dens[1][j] - pow(U[1][j], 2) / 2) / 717.4;
	P[j] = Dens[1][j] * R * T1[0][j];
	//printf("%lf %lf\n", Dens[1][j],Dens[0][j]);

}
else if (j != n_cars - 1) {

	if (VAG[j] == 4)
		valvulaeltro(Pp[j], Paux[j], Psr[j], Pemg[j], Pcf[j], AT[j], X[j], X1[j], T1[0][j], j);
	else if (VAG[j] == 5)
		fluxo_massico_encanamento[j] = -entradal(90 * conv + Patm, Pp[j], c4, D);
	else
		fluxo_massico_encanamento[j] = 0;
	Dens[1][j] = Dens[0][j] - dt / (dx) * (Dens[0][j] * (U[0][j] - U[0][j - 1]) + U[0][j] * (Dens[0][j] - Dens[0][j - 1])) - dt * (fluxo_massico_encanamento[j]) / (dx * pi * pow(rEG, 2));//+ orificio(P[j], Patm, 0.e-7)
	if (U[0][j] < 0)
		U[1][j] = U[0][j] - dt / (dx) * (U[0][j] * (U[0][j + 1] - U[0][j]) + 1. / Dens[0][j] * (Pp[j + 1] - Pp[j])) - dt * (-f[j] * pow(U[0][j], 2.) / (2. * D) * 2.94 * Z + U[0][j] / Dens[0][j] * fluxo_massico_encanamento[j] / (dx * pi * pow(rEG, 2)));// (1. + (4. * 16. + 2. * 5.)*D / dx);
	else
		U[1][j] = U[0][j] - dt / (dx) * (U[0][j] * (U[0][j + 1] - U[0][j]) + 1. / Dens[0][j] * (Pp[j + 1] - Pp[j])) - dt * (f[j] * pow(U[0][j], 2.) / (2. * D) * 2.94 * Z + U[0][j] / Dens[0][j] * fluxo_massico_encanamento[j] / (dx * pi * pow(rEG, 2)));// (1. + (4. * 16. + 2. * 5.)*D / dx);

//E[0][j] = Dens[0][j] * (717.4*T1[0][j] + pow(U[0][j], 2) / 2);

//if (U[0][j]<0)

//E[1][j] = Dens[0][j] * (717.4*T1[0][j] + pow(U[0][j], 2) / 2) - dt / dx*(Dens[0][j] * U[0][j] * (717.4 * T1[0][j] + pow(U[0][j], 2) / 2) - Dens[0][j - 1] * U[0][j - 1] * (717.4 * T1[0][j - 1] + pow(U[0][j - 1], 2.) / 2.) - kappa*(T1[0][j - 1] - 2.*T1[0][j] + T1[0][j + 1]) / dx + (Pp[j] * U[0][j] - Pp[j - 1] * U[0][j - 1])) - dt*Dens[0][j] * (h[j] * 4.*dx / D * (T1[0][j] - T) - f*pow(U[0][j], 2.)*2.94 / (2. * D)*(U[0][j])) - dt*(fluxo_massico_encanamento[j]) / (dx*pi*pow(rEG, 2))*(1004.*T1[0][j] + pow(U[0][j], 2) / 2);

//else

//E[1][j] = Dens[0][j] * (717.4*T1[0][j] + pow(U[0][j], 2) / 2) - dt / dx*(Dens[0][j] * U[0][j] * (717.4 * T1[0][j] + pow(U[0][j], 2) / 2) - Dens[0][j - 1] * U[0][j - 1] * (717.4 * T1[0][j - 1] + pow(U[0][j - 1], 2.) / 2.) - kappa*(T1[0][j - 1] - 2.*T1[0][j] + T1[0][j + 1]) / dx + (Pp[j] * U[0][j] - Pp[j - 1] * U[0][j - 1])) - dt*Dens[0][j] * (h[j] * 4.*dx / D * (T1[0][j] - T) + f*pow(U[0][j], 2.)*1.94 / (2. * D)*(U[0][j])) - dt*(fluxo_massico_encanamento[j]) / (dx*pi*pow(rEG, 2))*(1004.*T1[0][j] + pow(U[0][j], 2) / 2);

//T1[1][j] = (E[1][j] / Dens[1][j] - pow(U[1][j], 2.) / 2.) / 717.4;
	P[j] = Dens[1][j] * R * T1[0][j];
	if (P[j] < Patm) {
```

```
                    P[j] = Patm;
                    Dens[1][j] = Patm * k4;
                }
                //printf("%lf %lf\n", Pp[j+1], E[1][j]);


            }
            else {
                if (VAG[j] == 4)
                    valvulaeltro(Pp[j], Paux[j], Psr[j], Pemg[j], Pcf[j], AT[j], X[j], X1[j], T1[0][j], j);
                else if (VAG[j] == 5)
                    fluxo_massico_encanamento[j] = entradal(90 * conv + Patm, Pp[j], c4, D);
                else
                    fluxo_massico_encanamento[j] = 0;
                Dens[1][j] = Dens[0][j] - dt / dx * ((U[0][j] - U[0][j - 1]) * Dens[0][j] + U[0][j - 1] * (Dens[0][j] - Dens[0][j - 1])) - dt * (fluxo_massico_encanamento[j]) / (dx * pi * pow(rEG, 2));
                if (U[0][j] < 0)
                    U[1][j] = U[0][j] - dt / (dx) * (U[0][j] * (-U[0][j] - U[0][j])) - dt * (-f[j] * pow(U[0][j], 2.) / (2. * D) * 2.94 * Z + U[0][j] / Dens[0][j] * fluxo_massico_encanamento[j] / (dx * pi * pow(rEG, 2)));// (1. + (4. * 16. + 2. * 5.)*D / dx);
                else
                    U[1][j] = U[0][j] - dt / (dx) * (U[0][j] * (-U[0][j] - U[0][j])) - dt * (f[j] * pow(U[0][j], 2.) / (2. * D) * 2.94 * Z + U[0][j] / Dens[0][j] * fluxo_massico_encanamento[j] / (dx * pi * pow(rEG, 2)));// (1. + (4. * 16. + 2. * 5.)*D / dx);


                        //E[0][j] = Dens[0][j] * (717.4*T1[0][j] + pow(U[0][j], 2) / 2);


                        //if (U[0][j]<0)


                        //E[1][j] = Dens[0][j] * (717.4*T1[0][j] + pow(U[0][j], 2) / 2) - dt / dx*(Dens[0][j] * U[0][j] * (717.4 * T1[0][j] + pow(U[0][j], 2) / 2) - Dens[0][j - 1] * U[0][j - 1] * (717.4 * T1[0][j - 1] + pow(U[0][j - 1], 2) / 2) - kappa*(T1[0][j - 1] - 2.*T1[0][j] + T1[0][j]) / dx + (Pp[j] * U[0][j] - Pp[j - 1] * U[0][j - 1])) - dt*Dens[0][j] * (h[j] * 4.*dx / D* (T1[0][j] - T) - f*pow(U[0][j], 2.)*2.94 / (2. * D)*(U[0][j])) - dt*(fluxo_massico_encanamento[j]) / (dx*pi*pow(rEG, 2))*(1004.*T1[0][j] + pow(U[0][j], 2) / 2);


                        //else


                        //E[1][j] = Dens[0][j] * (717.4*T1[0][j] + pow(U[0][j], 2) / 2) - dt / dx*(Dens[0][j] * U[0][j] * (717.4 * T1[0][j] + pow(U[0][j], 2) / 2) - Dens[0][j - 1] * U[0][j - 1] * (717.4 * T1[0][j - 1] + pow(U[0][j - 1], 2) / 2) - kappa*(T1[0][j - 1] - 2.*T1[0][j] + T1[0][j]) / dx + (Pp[j] * U[0][j] - Pp[j - 1] * U[0][j - 1])) - dt*Dens[0][j] * (h[j] * 4.*dx / D* (T1[0][j] - T) + f*pow(U[0][j], 2.)*1.94 / (2. * D)*(U[0][j])) - dt*(fluxo_massico_encanamento[j]) / (dx*pi*pow(rEG, 2))*(1004.*T1[0][j] + pow(U[0][j], 2) / 2);


                        //1[1][j] = (E[1][j] / Dens[1][j] - pow(U[1][j], 2) / 2) / 717.4;
                P[j] = Dens[1][j] * R * T1[0][j];
                if (P[j] < Patm) {
                    P[j] = Patm;
                    Dens[1][j] = Patm * k4;
                }


            }
        }
    }
    else if (valvula == 6) {
        Ree = Pen * k4 * Uen * D / visc;    //Número de Reynolds, considerando o fluxo que chega ao vagão
                                                                        //avaliando o fator de atrito
        if (Ree == 0.)
            fe = 0.;
        else if (Ree <= 2000.)
            fe = 64. / Ree;
        else if (Ree > 2000. && Ree < 4000.)
            fe = 0.0027 / pow(Ree, 0.222);
        else
            fe = 0.316 / pow(Ree, 0.25);
        //Uen = Uen - dt / dx*(Uen*(U[0][0] - Uen) + 1. / (Pen*k4)*(P[0] - Pen)) - dt*fe*pow(Uen, 2.) / (2.*D)*1.93*2.3;//(1. + (5. * 16. + 2. * 5.)*D / dx);
        //printf("%lf %lf %lf\n", fe,U[0][0],Uen);
        //Een = (717.4*(T)+pow(Uen, 2) / 2);
#pragma omp parallel for
        for (j = 0; j < n_cars; j++) {
            AT[j] = manipu;
        }
#pragma omp parallel for
        for (j = 0; j < n_cars; j++) {
            Re[j] = Dens[0][j] * fabs(U[0][j]) * D / visc;    //Número de Reynolds, considerando o fluxo que chega ao vagão
                                                                                    //avaliando
o fator de atrito
            Rep[j] = Dens[2][j] * fabs(U[2][j]) * D / visc;
            if (Re[j] == 0.)
                f[j] = 0.;
            else if (Re[j] <= 2000.)
                f[j] = 64. / Re[j];
            else if (Re[j] > 2000. && Re[j] < 4000.)
                f[j] = 0.0027 / pow(Re[j], 0.222);
            else
                f[j] = 0.316 / pow(Re[j], 0.25);
            if (Rep[j] == 0.)
                fp[j] = 0.;
            else if (Rep[j] <= 2000.)
                fp[j] = 64. / Rep[j];
            else if (Rep[j] > 2000. && Rep[j] < 4000.)
                fp[j] = 0.0027 / pow(Rep[j], 0.222);
            else
```

```
                        fp[j] = 0.316 / pow(Rep[j], 0.25);

                //if (Re[j] < 3000)
                        //Nu = 4.36;
                //else
                        //Nu = (f / 8)*(Re - 1000)*Pr / (1 + 12.7*pow(f / 8., 0.5)*(pow(Pr, 2. / 3.) - 1));

                //if (Q == 1) {
                        //Ra = 9.81*beta*fabs(T1[0][j] - T)*pow(D, 3)*Pr / pow(visc, 2);
                        //if (Ra > 1e-10 && Ra < 1e-2)
                                //Nu1 = 0.675*pow(Ra, 0.058);
                        //else if (Ra > 1e-2 && Ra < 1e2)
                                //Nu1 = 1.02*pow(Ra, 0.148);
                        //else if (Ra > 1e2 && Ra < 1e4)
                                //Nu1 = 0.85*pow(Ra, 0.188);
                        //else if (Ra > 1e4 && Ra < 1e7)
                                //Nu1 = 0.48*pow(Ra, 0.25);
                        //else if (Ra > 1e7 && Ra < 1e12)
                                //Nu1 = 0.125*pow(Ra, 0.333);
                        //else if (Ra == 0)
                                //Nu1 = 0;
                //}
                //else {
                        //vr = 20. / 3.6*Patm / (R*T)*D / visc;
                        //Nu1 = 0.027*pow(vr, 0.805)*pow(Pr, 1. / 3.);
                //}


                //h[j] = 1 / (1 / (Nu*kappa / D) + (1 / (Nu1*kappa / D)) + (eaco / kaco));
                if (j == 0) {
                        m_dot = entradal(Pen, Pp[j], c4, D);
                        Dens[1][0] = Dens[0][j] - dt / dx * (Dens[0][j] * U[0][j] - Dens[0][j] * -U[0][j]) + dt * m_dot / (dx * pi * pow(rEG, 2));
                        if (U[0][j] < 0)
                                U[1][j] = U[0][j] - dt / (dx) * (U[0][j] * (U[0][j + 1] - U[0][j]) + 1. / Dens[0][j] * (Pp[j + 1] - Pp[j])) - dt * (-f[j] * pow(U[0][j], 2.) / (2. * D) * 2.94 * Z - U[0][j] / Dens[0][j] * m_dot / (dx * pi * pow(rEG, 2)));// (1. + (4. * 16. + 2. * 5.)*D / dx);
                        else
                                U[1][j] = U[0][j] - dt / (dx) * (U[0][j] * (U[0][j + 1] - U[0][j]) + 1. / Dens[0][j] * (Pp[j + 1] - Pp[j])) - dt * (f[j] * pow(U[0][j], 2.) / (2. * D) * 2.94 * Z - U[0][j] / Dens[0][j] * m_dot / (dx * pi * pow(rEG, 2)));// (1. + (4. * 16. + 2. * 5.)*D / dx);


                                                                        //E[0][j] = Dens[0][j] * (717.4*T1[0][j] + pow(U[0][j], 2) / 2);


                                                                        //if (U[0][j]<0)


                                                                        //E[1][j] = Dens[0][j] * (717.4*T1[0][j] + pow(U[0][j], 2) / 2) - dt / dx*(Dens[0][j] * U[0][j] * (717.4 * T1[0][j] + pow(U[0][j], 2) / 2) - Dens[0][j] * (717.4 * (T1[0][j])+pow(U[0][j], 2) / 2) - kappa*(T1[0][j] - 2.*T1[0][j] + T1[0][j + 1]) / dx + (Pp[j] * U[0][j] - Pp[j]*-U[0][j])) - dt*Dens[0][j] * (h[j] * 4.*dx / D* (T1[0][j] - T) - f*pow(U[0][j], 2.)*2.94 / (2. * D)*(U[0][j])) + dt*(m_dot / (dx*pi*pow(rEG, 2))*(1004.*T1[0][j] + pow(U[0][j], 2) / 2));


                                                                        //else


                                                                        //E[1][j] = Dens[0][j] * (717.4*T1[0][j] + pow(U[0][j], 2) / 2) - dt / dx*(Dens[0][j] * U[0][j] * (717.4 * T1[0][j] + pow(U[0][j], 2) / 2) - Dens[0][j] * (717.4 * (T1[0][j]) + pow(U[0][j], 2) / 2) - kappa*(T1[0][j] - 2.*T1[0][j] + T1[0][j + 1]) / dx + (Pp[j] * U[0][j] - Pp[j] * -U[0][j])) - dt*Dens[0][j] * (h[j] * 4.*dx / D* (T1[0][j] - T) + f*pow(U[0][j], 2.)*2.94 / (2. * D)*(U[0][j])) + dt*(m_dot / (dx*pi*pow(rEG, 2))*(1004.*T1[0][j] + pow(U[0][j], 2) / 2));


                                                                        //T1[1][j] = (E[1][j] / Dens[1][j] - pow(U[1][j], 2) / 2) / 717.4;
                        P[j] = Dens[1][j] * R * T1[0][j];
                        //printf("%lf %lf\n", Dens[1][j],Dens[0][j]);
                        m_dot2 = -orificio(140 * conv + Patm, Pe[j], 1.4e-05, T1[0][j]);
                        Dens[3][0] = Dens[2][j] - dt / dx * (Dens[2][j] * U[2][j] - Dens[2][j] * -U[2][j]) + dt * m_dot2 / (dx * pi * pow(rEG, 2));
                        if (U[2][j] < 0)
                                U[3][j] = U[2][j] - dt / (dx) * (U[2][j] * (U[2][j + 1] - U[2][j]) + 1. / Dens[2][j] * (Pe[j + 1] - Pe[j])) - dt * (-fp[j] * pow(U[2][j], 2.) / (2. * D) * 2.94 * Z - U[2][j] / Dens[2][j] * m_dot2 / (dx * pi * pow(rEG, 2)));// (1. + (4. * 16. + 2. * 5.)*D / dx);
                        else
                                U[3][j] = U[2][j] - dt / (dx) * (U[2][j] * (U[2][j + 1] - U[2][j]) + 1. / Dens[2][j] * (Pe[j + 1] - Pe[j])) - dt * (fp[j] * pow(U[2][j], 2.) / (2. * D) * 2.94 * Z - U[2][j] / Dens[2][j] * m_dot2 / (dx * pi * pow(rEG, 2)));// (1. + (4. * 16. + 2. * 5.)*D / dx);


                                                                        //E[0][j] = Dens[0][j] * (717.4*T1[0][j] + pow(U[0][j], 2) / 2);


                                                                        //if (U[0][j]<0)


                                                                        //E[1][j] = Dens[0][j] * (717.4*T1[0][j] + pow(U[0][j], 2) / 2) - dt / dx*(Dens[0][j] * U[0][j] * (717.4 * T1[0][j] + pow(U[0][j], 2) / 2) - Dens[0][j] * (717.4 * (T1[0][j])+pow(U[0][j], 2) / 2) - kappa*(T1[0][j] - 2.*T1[0][j] + T1[0][j + 1]) / dx + (Pp[j] * U[0][j] - Pp[j]*-U[0][j])) - dt*Dens[0][j] * (h[j] * 4.*dx / D* (T1[0][j] - T) - f*pow(U[0][j], 2.)*2.94 / (2. * D)*(U[0][j])) + dt*(m_dot / (dx*pi*pow(rEG, 2))*(1004.*T1[0][j] + pow(U[0][j], 2) / 2));


                                                                        //else
```

```
//E[1][j] = Dens[0][j] * (717.4*T1[0][j] + pow(U[0][j], 2) / 2) - dt / dx*(Dens[0][j] * U[0][j] * (717.4 * T1[0][j] + pow(U[0][j], 2) / 2) - Dens[0][j] * (717.4 * (T1[0][j]) + pow(U[0][j], 2) / 2) - kappa*(T1[0][j] - 2.*T1[0][j] + T1[0][j + 1]) / dx + (Pp[j] * U[0][j] - Pp[j] * -U[0][j])) - dt*Dens[0][j] * (h[j] * 4.*dx / D* (T1[0][j] - T) + f*pow(U[0][j], 2.)*2.94 / (2. * D)*(U[0][j])) + dt*(m_dot / (dx*pi*pow(rEG, 2))*(1004.*T1[0][j] + pow(U[0][j], 2) / 2));

//T1[1][j] = (E[1][j] / Dens[1][j] - pow(U[1][j], 2) / 2) / 717.4;
		Pep[j] = Dens[3][j] * R * T1[0][j];

	}
	else if (j != n_cars - 1) {

		if (VAG[j] == 6)
			valvulaeltropass(Pp, Pe, Paux, Psr, Pemg, Pcf, AT, Prin, Ps, Pbc, T1[0][j], j);
		else if (VAG[j] == 5) {
			fluxo_massico_encanamento[j] = -entradal(90 * conv + Patm, Pp[j], c4, D);
			fluxo_massico_encanamento2[j] = -orificio(140 * conv + Patm, Pe[j], 1.4e-05, T1[0][j]);
		}
		else {
			fluxo_massico_encanamento[j] = 0;
			fluxo_massico_encanamento2[j] = 0;
		}
		//printf("%f\n", fluxo_massico_encanamento[j]);

		Dens[1][j] = Dens[0][j] - dt / (dx) * (Dens[0][j] * (U[0][j] - U[0][j - 1]) + U[0][j] * (Dens[0][j] - Dens[0][j - 1])) - dt * (fluxo_massico_encanamento[j]) / (dx * pi * pow(rEG, 2));//+ orificio(P[j], Patm, 0.e-7)
		if (U[0][j] < 0)
			U[1][j] = U[0][j] - dt / (dx) * (U[0][j] * (U[0][j + 1] - U[0][j]) + 1. / Dens[0][j] * (Pp[j + 1] - Pp[j])) - dt * (-f[j] * pow(U[0][j], 2.) / (2. * D) * 2.94 * Z + U[0][j] / Dens[0][j] * fluxo_massico_encanamento[j] / (dx * pi * pow(rEG, 2)));// (1. + (4. * 16. + 2. * 5.)*D / dx);
		else
			U[1][j] = U[0][j] - dt / (dx) * (U[0][j] * (U[0][j + 1] - U[0][j]) + 1. / Dens[0][j] * (Pp[j + 1] - Pp[j])) - dt * (f[j] * pow(U[0][j], 2.) / (2. * D) * 2.94 * Z + U[0][j] / Dens[0][j] * fluxo_massico_encanamento[j] / (dx * pi * pow(rEG, 2)));// (1. + (4. * 16. + 2. * 5.)*D / dx);


//E[0][j] = Dens[0][j] * (717.4*T1[0][j] + pow(U[0][j], 2) / 2);


//if (U[0][j]<0)


//E[1][j] = Dens[0][j] * (717.4*T1[0][j] + pow(U[0][j], 2) / 2) - dt / dx*(Dens[0][j] * U[0][j] * (717.4 * T1[0][j] + pow(U[0][j], 2) / 2) - Dens[0][j - 1] * U[0][j - 1] * (717.4 * T1[0][j - 1] + pow(U[0][j - 1], 2.) / 2.) - kappa*(T1[0][j - 1] - 2.*T1[0][j] + T1[0][j + 1]) / dx + (Pp[j] * U[0][j] - Pp[j - 1] * U[0][j - 1])) - dt*Dens[0][j] * (h[j] * 4.*dx / D * (T1[0][j] - T) - f*pow(U[0][j], 2.)*2.94 / (2. * D)*(U[0][j])) - dt*(fluxo_massico_encanamento[j]) / (dx*pi*pow(rEG, 2))*(1004.*T1[0][j] + pow(U[0][j], 2) / 2);


//else


//E[1][j] = Dens[0][j] * (717.4*T1[0][j] + pow(U[0][j], 2) / 2) - dt / dx*(Dens[0][j] * U[0][j] * (717.4 * T1[0][j] + pow(U[0][j], 2) / 2) - Dens[0][j - 1] * U[0][j - 1] * (717.4 * T1[0][j - 1] + pow(U[0][j - 1], 2.) / 2.) - kappa*(T1[0][j - 1] - 2.*T1[0][j] + T1[0][j + 1]) / dx + (Pp[j] * U[0][j] - Pp[j - 1] * U[0][j - 1])) - dt*Dens[0][j] * (h[j] * 4.*dx / D * (T1[0][j] - T) + f*pow(U[0][j], 2.)*1.94 / (2. * D)*(U[0][j])) - dt*(fluxo_massico_encanamento[j]) / (dx*pi*pow(rEG, 2))*(1004.*T1[0][j] + pow(U[0][j], 2) / 2);


//T1[1][j] = (E[1][j] / Dens[1][j] - pow(U[1][j], 2.) / 2.) / 717.4;
		P[j] = Dens[1][j] * R * T1[0][j];
		if (P[j] < Patm) {
			P[j] = Patm;
			Dens[1][j] = Patm * k4;
		}
		//printf("%lf %lf\n", Pp[j+1], E[1][j]);
		Dens[3][j] = Dens[2][j] - dt / (dx) * (Dens[2][j] * (U[2][j] - U[2][j - 1]) + U[2][j] * (Dens[2][j] - Dens[2][j - 1])) - dt * (fluxo_massico_encanamento2[j]) / (dx * pi * pow(rEG, 2));//+ orificio(P[j], Patm, 0.e-7)
		if (U[2][j] < 0)
			U[3][j] = U[2][j] - dt / (dx) * (U[2][j] * (U[2][j + 1] - U[2][j]) + 1. / Dens[2][j] * (Pe[j + 1] - Pe[j])) - dt * (-fp[j] * pow(U[2][j], 2.) / (2. * D) * 2.94 * Z + U[2][j] / Dens[2][j] * fluxo_massico_encanamento2[j] / (dx * pi * pow(rEG, 2)));// (1. + (4. * 16. + 2. * 5.)*D / dx);
		else
			U[3][j] = U[2][j] - dt / (dx) * (U[2][j] * (U[2][j + 1] - U[2][j]) + 1. / Dens[2][j] * (Pe[j + 1] - Pe[j])) - dt * (fp[j] * pow(U[2][j], 2.) / (2. * D) * 2.94 * Z + U[2][j] / Dens[2][j] * fluxo_massico_encanamento2[j] / (dx * pi * pow(rEG, 2)));// (1. + (4. * 16. + 2. * 5.)*D / dx);


//E[0][j] = Dens[0][j] * (717.4*T1[0][j] + pow(U[0][j], 2) / 2);


//if (U[0][j]<0)


//E[1][j] = Dens[0][j] * (717.4*T1[0][j] + pow(U[0][j], 2) / 2) - dt / dx*(Dens[0][j] * U[0][j] * (717.4 * T1[0][j] + pow(U[0][j], 2) / 2) - Dens[0][j - 1] *
```

```
U[0][j - 1] * (717.4 * T1[0][j - 1] + pow(U[0][j - 1], 2.) / 2.) - kappa*(T1[0][j - 1] - 2.*T1[0][j] + T1[0][j + 1]) / dx + (Pp[j] * U[0][j] - Pp[j - 1] * U[0][j - 1])) - dt*Dens[0][j] * (h[j] * 4.*dx / D * (T1[0][j] - T) - f*pow(U[0][j], 2.)*2.94 / (2. * D)*(U[0][j])) - dt*(fluxo_massico_encanamento[j]) / (dx*pi*pow(rEG, 2))*(1004.*T1[0][j] + pow(U[0][j], 2) / 2);

        //else

        //E[1][j] = Dens[0][j] * (717.4*T1[0][j] + pow(U[0][j], 2) / 2) - dt / dx*(Dens[0][j] * U[0][j] * (717.4 * T1[0][j] + pow(U[0][j], 2) / 2) - Dens[0][j - 1] * U[0][j - 1] * (717.4 * T1[0][j - 1] + pow(U[0][j - 1], 2.) / 2.) - kappa*(T1[0][j - 1] - 2.*T1[0][j] + T1[0][j + 1]) / dx + (Pp[j] * U[0][j] - Pp[j - 1] * U[0][j - 1])) - dt*Dens[0][j] * (h[j] * 4.*dx / D * (T1[0][j] - T) + f*pow(U[0][j], 2.)*1.94 / (2. * D)*(U[0][j])) - dt*(fluxo_massico_encanamento[j]) / (dx*pi*pow(rEG, 2))*(1004.*T1[0][j] + pow(U[0][j], 2) / 2);

        //T1[1][j] = (E[1][j] / Dens[1][j] - pow(U[1][j], 2.) / 2.) / 717.4;
                Pep[j] = Dens[3][j] * R * T1[0][j];

            }
            else {
                if (VAG[j] == 6)
                    valvulaeltropass(Pp, Pe, Paux, Psr, Pemg, Pcf, AT, Prin, Ps, Pbc, T1[0][j], j);
                else if (VAG[j] == 5) {
                    fluxo_massico_encanamento[j] = entradal(90 * conv + Patm, Pp[j], c4, D);
                    fluxo_massico_encanamento2[j] = -orificio(140 * conv + Patm, Pe[j], 1.4e-05, T1[0][j]);
                }
                else {
                    fluxo_massico_encanamento[j] = 0;
                    fluxo_massico_encanamento2[j] = 0;
                }

                Dens[1][j] = Dens[0][j] - dt / dx * ((U[0][j] - U[0][j - 1]) * Dens[0][j] + U[0][j - 1] * (Dens[0][j] - Dens[0][j - 1])) - dt * (fluxo_massico_encanamento[j]) / (dx * pi * pow(rEG, 2));
                if (U[0][j] < 0)
                    U[1][j] = U[0][j] - dt / (dx) * (U[0][j] * (-U[0][j] - U[0][j])) - dt * (-f[j] * pow(U[0][j], 2.) / (2. * D) * 2.94 * Z + U[0][j] / Dens[0][j] * fluxo_massico_encanamento[j] / (dx * pi * pow(rEG, 2)));// (1. + (4. * 16. + 2. * 5.)*D / dx);
                else
                    U[1][j] = U[0][j] - dt / (dx) * (U[0][j] * (-U[0][j] - U[0][j])) - dt * (f[j] * pow(U[0][j], 2.) / (2. * D) * 2.94 * Z + U[0][j] / Dens[0][j] * fluxo_massico_encanamento[j] / (dx * pi * pow(rEG, 2)));// (1. + (4. * 16. + 2. * 5.)*D / dx);

                        //E[0][j] = Dens[0][j] * (717.4*T1[0][j] + pow(U[0][j], 2) / 2);

                        //if (U[0][j]<0)

                        //E[1][j] = Dens[0][j] * (717.4*T1[0][j] + pow(U[0][j], 2) / 2) - dt / dx*(Dens[0][j] * U[0][j] * (717.4 * T1[0][j] + pow(U[0][j], 2) / 2) - Dens[0][j - 1] * U[0][j - 1] * (717.4 * T1[0][j - 1] + pow(U[0][j - 1], 2) / 2) - kappa*(T1[0][j - 1] - 2.*T1[0][j] + T1[0][j + 1]) / dx + (Pp[j] * U[0][j] - Pp[j - 1] * U[0][j - 1])) - dt*Dens[0][j] * (h[j] * 4.*dx / D* (T1[0][j] - T) - f*pow(U[0][j], 2.)*2.94 / (2. * D)*(U[0][j])) - dt*(fluxo_massico_encanamento[j]) / (dx*pi*pow(rEG, 2))*(1004.*T1[0][j] + pow(U[0][j], 2) / 2);

                        //else

                        //E[1][j] = Dens[0][j] * (717.4*T1[0][j] + pow(U[0][j], 2) / 2) - dt / dx*(Dens[0][j] * U[0][j] * (717.4 * T1[0][j] + pow(U[0][j], 2) / 2) - Dens[0][j - 1] * U[0][j - 1] * (717.4 * T1[0][j - 1] + pow(U[0][j - 1], 2) / 2) - kappa*(T1[0][j - 1] - 2.*T1[0][j] + T1[0][j]) / dx + (Pp[j] * U[0][j] - Pp[j - 1] * U[0][j - 1])) - dt*Dens[0][j] * (h[j] * 4.*dx / D* (T1[0][j] - T) + f*pow(U[0][j], 2.)*1.94 / (2. * D)*(U[0][j])) - dt*(fluxo_massico_encanamento[j]) / (dx*pi*pow(rEG, 2))*(1004.*T1[0][j] + pow(U[0][j], 2) / 2);

                        //1[1][j] = (E[1][j] / Dens[1][j] - pow(U[1][j], 2) / 2) / 717.4;
                P[j] = Dens[1][j] * R * T1[0][j];
                if (P[j] < Patm) {
                    P[j] = Patm;
                    Dens[1][j] = Patm * k4;
                }
                Dens[3][j] = Dens[2][j] - dt / dx * ((U[2][j] - U[2][j - 1]) * Dens[2][j] + U[2][j - 1] * (Dens[2][j] - Dens[2][j - 1])) - dt * (fluxo_massico_encanamento2[j]) / (dx * pi * pow(rEG, 2));
                if (U[2][j] < 0)
                    U[3][j] = U[2][j] - dt / (dx) * (U[2][j] * (-U[2][j] - U[2][j])) - dt * (-fp[j] * pow(U[2][j], 2.) / (2. * D) * 2.94 * Z + U[2][j] / Dens[2][j] * fluxo_massico_encanamento2[j] / (dx * pi * pow(rEG, 2)));// (1. + (4. * 16. + 2. * 5.)*D / dx);
                else
                    U[3][j] = U[2][j] - dt / (dx) * (U[2][j] * (-U[2][j] - U[2][j])) - dt * (fp[j] * pow(U[2][j], 2.) / (2. * D) * 2.94 * Z + U[2][j] / Dens[2][j] * fluxo_massico_encanamento2[j] / (dx * pi * pow(rEG, 2)));// (1. + (4. * 16. + 2. * 5.)*D / dx);

                            //E[0][j] = Dens[0][j] * (717.4*T1[0][j] + pow(U[0][j], 2) / 2);

                            //if (U[0][j]<0)

                            //E[1][j] = Dens[0][j] * (717.4*T1[0][j] + pow(U[0][j], 2) / 2) - dt / dx*(Dens[0][j] * U[0][j] * (717.4 * T1[0][j] + pow(U[0][j], 2) / 2) - Dens[0][j - 1] * U[0][j - 1] * (717.4 * T1[0][j - 1] + pow(U[0][j - 1], 2) / 2) - kappa*(T1[0][j - 1] - 2.*T1[0][j] + T1[0][j]) / dx + (Pp[j] * U[0][j] - Pp[j - 1] * U[0][j - 1])) - dt*Dens[0][j] * (h[j] * 4.*dx / D* (T1[0][j] - T) - f*pow(U[0][j], 2.)*2.94 / (2. * D)*(U[0][j])) - dt*(fluxo_massico_encanamento[j]) / (dx*pi*pow(rEG, 2))*(1004.*T1[0][j] + pow(U[0][j], 2) / 2);
```

```
//else

//E[1][j] = Dens[0][j] * (717.4*T1[0][j] + pow(U[0][j], 2) / 2) - dt / dx*(Dens[0][j] * U[0][j] *
(717.4 * T1[0][j] + pow(U[0][j], 2) / 2) - Dens[0][j - 1] * U[0][j - 1] * (717.4 * T1[0][j - 1] + pow(U[0][j - 1], 2) / 2) - kappa*(T1[0][j - 1] - 2.*T1[0][j] + T1[0][j]) / dx + (Pp[j] * U[0][j] -
Pp[j - 1] * U[0][j - 1])) - dt*Dens[0][j] * (h[j] * 4.*dx / D* (T1[0][j] - T) + f*pow(U[0][j], 2.)*1.94 / (2. * D)*(U[0][j])) - dt*(fluxo_massico_encanamento[j]) / (dx*pi*pow(rEG,
2))*(1004.*T1[0][j] + pow(U[0][j], 2) / 2);

//1[1][j] = (E[1][j] / Dens[1][j] - pow(U[1][j], 2) / 2) / 717.4;
                        Pep[j] = Dens[3][j] * R * T1[0][j];

                    }
                }
            }
            else {
                if (manipu == 1) {
                    if (c != 1) {
#pragma omp parallel for
                        for (j = 0; j < n_cars; j++)
                            U[0][j] = -U[0][j];
                    }
                    c = 1;
                    Ree = Pen * k4 * Uen * D / visc;
                    if (Ree == 0.)
                        fe = 0.;
                    else if (Ree <= 2000.)
                        fe = 64. / Ree;
                    else if (Ree > 2000. && Ree < 4000.)
                        fe = 0.0027 / pow(Ree, 0.222);
                    else
                        fe = 0.316 / pow(Ree, 0.25);
                    Uen = Uen - dt / dx * (Uen * (U[0][0] - Uen) + 1. / (Pen * k4) * (P[0] - Pen)) - dt * fe * pow(Uen, 2.) / (2. * D) * 1.93 * 2.3;
                    Een = (717.4 * (T)+pow(Uen, 2) / 2);
#pragma omp parallel for
                    for (j = 0; j < n_cars; j++) {
                        Re[j] = Dens[0][j] * fabs(U[0][j]) * D / visc;
                        if (Re[j] <= 0.01)
                            f[j] = 0.;
                        else if (Re[j] <= 2000.)
                            f[j] = 64. / Re[j];
                        else if (Re[j] > 2000. && Re[j] < 4000.)
                            f[j] = 0.0027 / pow(Re[j], 0.222);
                        else
                            f[j] = 0.316 / pow(Re[j], 0.25);

                        if (j == 0) {
                            m_dot = entradal(Pen, Pp[j], c4, D);
                            Dens[1][0] = Dens[0][j] - dt / dx * (Dens[0][j] * U[0][j] - Dens[0][j] * -U[0][j]) + dt * m_dot / (dx * pi * pow(rEG, 2));
                            if (U[0][j] < 0)
                                U[1][j] = U[0][j] - dt / (dx) * (U[0][j] * (U[0][j + 1] - U[0][j]) + 1. / Dens[0][j] * (Pp[j + 1] - Pp[j])) - dt *
(-f[j] * pow(U[0][j], 2.) / (2. * D) * 2.94 * Z);
                            else
                                U[1][j] = U[0][j] - dt / (dx) * (U[0][j] * (U[0][j + 1] - U[0][j]) + 1. / Dens[0][j] * (Pp[j + 1] - Pp[j])) - dt *
(f[j] * pow(U[0][j], 2.) / (2. * D) * 2.94 * Z);

                            P[j] = Dens[1][j] * R * T1[0][j];
                        }
                        else if (j != n_cars - 1) {

                            if (VAG[j] == 1)
                                valvulaAB(Pp[j], Paux[j], Psr[j], Pemg[j], Pcf[j], AT[j], X[j], X1[j], T1[0][j]);
                            else if (VAG[j] == 2)
                                valvulaABD(Pp[j], Paux[j], Psr[j], Pemg[j], Pcf[j], AT[j], X[j], X1[j], T1[0][j]);
                            else if (VAG[j] == 3)
                                valvulaABDX(Pp[j], Paux[j], Psr[j], Pemg[j], Pcf[j], AT[j], X[j], X1[j], T1[0][j], j);
                            else if (VAG[j] == 5)
                                fluxo_massico_encanamento[j] = -entradal(Pen, Pp[j], c4, D);
                            else
                                fluxo_massico_encanamento[j] = 0;

                            Dens[1][j] = Dens[0][j] - dt / (dx) * (Dens[0][j] * (U[0][j] - U[0][j - 1]) + U[0][j] * (Dens[0][j] - Dens[0][j - 1])) - dt *
(fluxo_massico_encanamento[j]) / (dx * pi * pow(rEG, 2));
                            if (U[0][j] < 0)
                                U[1][j] = U[0][j] - dt / (dx) * (U[0][j] * (U[0][j + 1] - U[0][j]) + 1. / Dens[0][j] * (Pp[j + 1] - Pp[j])) - dt *
(-f[j] * pow(U[0][j], 2.) / (2. * D) * 2.94 * Z);
                            else
                                U[1][j] = U[0][j] - dt / (dx) * (U[0][j] * (U[0][j + 1] - U[0][j]) + 1. / Dens[0][j] * (Pp[j + 1] - Pp[j])) - dt *
(f[j] * pow(U[0][j], 2.) / (2. * D) * 2.94 * Z);




                            P[j] = Dens[1][j] * R * T1[0][j];
                            if (P[j] < Patm) {
                                P[j] = Patm;
                                Dens[1][j] = Patm * k4;
                            }
                        }
                        else {

                            if (VAG[j] == 1)
                                valvulaAB(Pp[j], Paux[j], Psr[j], Pemg[j], Pcf[j], AT[j], X[j], X1[j], T1[0][j]);
                            else if (VAG[j] == 2)
                                valvulaABD(Pp[j], Paux[j], Psr[j], Pemg[j], Pcf[j], AT[j], X[j], X1[j], T1[0][j]);
                            else if (VAG[j] == 3)
```

```
valvulaABDX(Pp[j], Paux[j], Psr[j], Pemg[j], Pcf[j], AT[j], X[j], X1[j], T1[0][j], j);
else if (VAG[j] == 5)
    fluxo_massico_encanamento[j] = -entradal(Pen, Pp[j], c4, D);
else
    fluxo_massico_encanamento[j] = 0;

Dens[1][j] = Dens[0][j] - dt / dx * ((U[0][j] - U[0][j - 1]) * Dens[0][j] + U[0][j - 1] * (Dens[0][j] - Dens[0][j - 1])) - dt
* (fluxo_massico_encanamento[j]) / (dx * pi * pow(rEG, 2));
if (U[0][j] < 0)
    U[1][j] = U[0][j] - dt / (dx) * (U[0][j] * (-U[0][j] - U[0][j])) - dt * (-f[j] * pow(U[0][j], 2.) / (2. * D) * 2.94
* Z);
else
    U[1][j] = U[0][j] - dt / (dx) * (U[0][j] * (-U[0][j] - U[0][j])) - dt * (f[j] * pow(U[0][j], 2.) / (2. * D) * 2.94
* Z);
P[j] = Dens[1][j] * R * T1[0][j];
if (P[j] < Patm) {
    P[j] = Patm;
    Dens[1][j] = Patm * k4;
}


        }
    }
}
else {
    if (c == 1) {
#pragma omp parallel for
        for (j = 0; j < n_cars; j++)
            U[0][j] = -U[0][j];
    }
    c = 0;
    Ree = Pen * k4 * Uen * D / visc;
    if (Ree == 0.)
        fe = 0.;
    else if (Ree <= 2000.)
        fe = 64. / Ree;
    else if (Ree > 2000. && Ree < 4000.)
        fe = 0.0027 / pow(Ree, 0.222);
    else
        fe = 0.316 / pow(Ree, 0.25);
    Uen = Uen - dt / dx * (Uen * (U[0][0] - Uen) + 1. / (Pen * k4) * (P[0] - Pen)) - dt * fe * pow(Uen, 2.) / (2. * D) * 1.93 * 2.3;
    Een = (717.4 * (T)+pow(Uen, 2) / 2);
#pragma omp parallel for
    for (j = 0; j < n_cars; j++) {
        Re[j] = Dens[0][j] * fabs(U[0][j]) * D / visc;
        if (Re[j] <= 0.01)
            f[j] = 0.;
        else if (Re[j] <= 2000.)
            f[j] = 64. / Re[j];
        else if (Re[j] > 2000. && Re[j] < 4000.)
            f[j] = 0.0027 / pow(Re[j], 0.222);
        else
            f[j] = 0.316 / pow(Re[j], 0.25);

        if (j == 0) {
            m_dot = entradal(Pen, Pp[j], c4, D);
            Dens[1][0] = Dens[0][j] - dt / dx * (-Dens[0][j + 1] * U[0][j + 1] + Dens[0][j] * U[0][j]) + dt * m_dot / (dx * pi *
pow(rEG, 2));
            if (U[0][j] < 0)
                U[1][j] = U[0][j] - dt / (dx) * (U[0][j] * (-U[0][j] - (U[0][j])) + 1. / Dens[0][j] * (Pp[j] - Pp[j])) - dt * (-f[j]
* pow(U[0][j], 2.) / (2. * D) * 2.94 * Z);
            else
                U[1][j] = U[0][j] - dt / (dx) * (U[0][j] * (-U[0][j] - (U[0][j])) + 1. / Dens[0][j] * (Pp[j] - Pp[j])) - dt * (f[j] *
pow(U[0][j], 2.) / (2. * D) * 2.94 * Z);
            P[j] = Dens[1][j] * R * T1[0][j];
        }
        else if (j != n_cars - 1) {

            if (VAG[j] == 1)
                valvulaAB(Pp[j], Paux[j], Psr[j], Pemg[j], Pcf[j], AT[j], X[j], X1[j], T1[0][j]);
            else if (VAG[j] == 2)
                valvulaABD(Pp[j], Paux[j], Psr[j], Pemg[j], Pcf[j], AT[j], X[j], X1[j], T1[0][j]);
            else if (VAG[j] == 3)
                valvulaABDX(Pp[j], Paux[j], Psr[j], Pemg[j], Pcf[j], AT[j], X[j], X1[j], T1[0][j], j);
            else if (VAG[j] == 5)
                fluxo_massico_encanamento[j] = -entradal(Pen, Pp[j], c4, D);
            else
                fluxo_massico_encanamento[j] = 0;

            Dens[1][j] = Dens[0][j] - dt / (dx) * (Dens[0][j] * (-U[0][j + 1] + U[0][j]) + U[0][j] * (-Dens[0][j + 1] + Dens[0][j])) -
dt * (fluxo_massico_encanamento[j]) / (dx * pi * pow(rEG, 2));
            if (U[0][j] < 0)
                U[1][j] = U[0][j] - dt / (dx) * (U[0][j] * (-U[0][j] + U[0][j - 1]) + 1. / Dens[0][j] * (-Pp[j] + Pp[j - 1])) - dt
* (-f[j] * pow(U[0][j], 2.) / (2. * D) * 2.94 * Z);
            else
                U[1][j] = U[0][j] - dt / (dx) * (U[0][j] * (-U[0][j] + U[0][j - 1]) + 1. / Dens[0][j] * (-Pp[j] + Pp[j - 1])) - dt
* (f[j] * pow(U[0][j], 2.) / (2. * D) * 2.94 * Z);
            P[j] = Dens[1][j] * R * T1[0][j];
            if (P[j] < Patm) {
                P[j] = Patm;
                Dens[1][j] = Patm * k4;
            }
        }
        else {
            if (VAG[j] == 1)
                valvulaAB(Pp[j], Paux[j], Psr[j], Pemg[j], Pcf[j], AT[j], X[j], X1[j], T1[0][j]);
            else if (VAG[j] == 2)
                valvulaABD(Pp[j], Paux[j], Psr[j], Pemg[j], Pcf[j], AT[j], X[j], X1[j], T1[0][j]);
            else if (VAG[j] == 3)
                valvulaABDX(Pp[j], Paux[j], Psr[j], Pemg[j], Pcf[j], AT[j], X[j], X1[j], T1[0][j], j);
            else if (VAG[j] == 5)
```

```
					fluxo_massico_encanamento[j] = -entradal(Pen, Pp[j], c4, D);
				else
					fluxo_massico_encanamento[j] = 0;

				Dens[1][j] = Dens[0][j] - dt / dx * ((-U[0][j + 1] + U[0][j]) * Dens[0][j] + U[0][j] * (-Dens[0][j] + Dens[0][j])) - dt * (fluxo_massico_encanamento[j]) / (dx * pi * pow(rEG, 2));

				if (U[0][j] < 0)
					U[1][j] = U[0][j] - dt / (dx) * (U[0][j] * (-U[0][j] + U[0][j - 1]) + 1. / Dens[0][j] * (-Pp[j] + Pp[j - 1])) - dt * (-f[j] * pow(U[0][j], 2.) / (2. * D) * 2.94 * Z);
				else
					U[1][j] = U[0][j] - dt / (dx) * (U[0][j] * (-U[0][j] + U[0][j - 1]) + 1. / Dens[0][j] * (-Pp[j] + Pp[j - 1])) - dt * (f[j] * pow(U[0][j], 2.) / (2. * D) * 2.94 * Z);

				P[j] = Dens[1][j] * R * T1[0][j];
				if (P[j] < Patm) {
					P[j] = Patm;
					Dens[1][j] = Patm * k4;
				}
						}
					}
				}
			}
#pragma omp parallel for
			for (j = 0; j < n_cars; j++) {
				Pp[j] = P[j];
				U[0][j] = U[1][j];
				U[2][j] = U[3][j];
				Dens[0][j] = Dens[1][j];
				Dens[2][j] = Dens[3][j];
				Pe[j] = Pep[j];
			}

			if ((write_count == 0) || (write_count == contador))
			{
				write_count = 0;
				int int_n;

				fprintf(pFile_Paux, "%6.4f ", t);
				for (int_n = 0; int_n < n_cars; int_n++)
				{
					fprintf(pFile_Paux, "%6.4f ", Paux[int_n]);
				}
				fprintf(pFile_Paux, "\n");

				fprintf(pFile_Pcf, "%6.4f ", t);
				for (int_n = 0; int_n < n_cars; int_n++)
				{
					fprintf(pFile_Pcf, "%6.4f ", Pcf[int_n]);
				}
				fprintf(pFile_Pcf, "\n");

				fprintf(pFile_Pemg, "%6.4f ", t);
				for (int_n = 0; int_n < n_cars; int_n++)
				{
					fprintf(pFile_Pemg, "%6.4f ", Pemg[int_n]);
				}
				fprintf(pFile_Pemg, "\n");

				fprintf(pFile_Psr, "%6.4f ", t);
				for (int_n = 0; int_n < n_cars; int_n++)
				{
					fprintf(pFile_Psr, "%6.4f ", Psr[int_n]);
				}
				fprintf(pFile_Psr, "\n");

				fprintf(pFile_Pp, "%6.4f ", t);
				for (int_n = 0; int_n < n_cars; int_n++)
				{
					fprintf(pFile_Pp, "%6.4f ", Pp[int_n]);
				}
				fprintf(pFile_Pp, "\n");
				fprintf(pFile_AT, "%6.4f ", t);
				for (int_n = 0; int_n < n_cars; int_n++)
				{
					fprintf(pFile_AT, "%d ", AT[int_n]);
				}
				fprintf(pFile_AT, "\n");
			}
			write_count++;
			t = t + dt;
		}
		free(Re);
		free(f);
		free(Rep);
		free(fp);
		final = GetTickCount();
		tmili = final - inicio;
		printf("Tempo decorrido: %d\n", tmili);
		getchar();
		return 0;
}
```

Matlab Simulink Code:

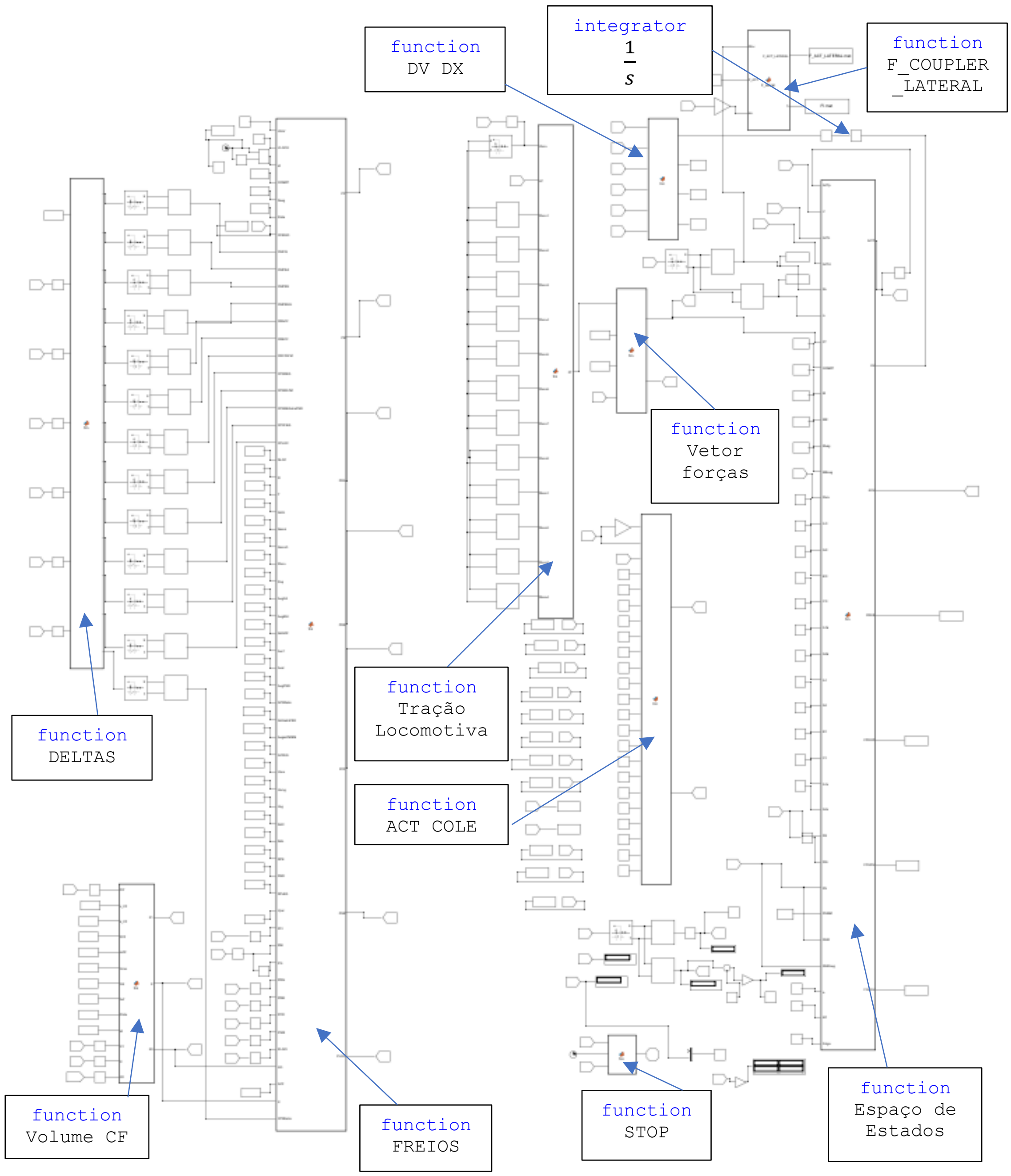

Figure 80 - Simulink model.

```
function
[DeltaEG,DeltaRA,DeltaRE,DeltaREG,DeltaRACF,DeltaRECF,DeltaCFatm,DeltaPSREG,DeltaPSRatm,DeltaEGatmPSR,DeltaCFEG,DeltaLOC,Delt
aREatm] = fcn(Patm,PB,PRA,PRE,PCF,PSR,PLOC)

SPP = size(PB);
SP = SPP(1,1);
DeltaEG = zeros(SPP(1,1),SPP(1,2));
DeltaRA = zeros(SPP(1,1),SPP(1,2));
DeltaRE = zeros(SPP(1,1),SPP(1,2));
DeltaREG = zeros(SPP(1,1),SPP(1,2));
DeltaRACF = zeros(SPP(1,1),SPP(1,2));
DeltaRECF = zeros(SPP(1,1),SPP(1,2));
DeltaCFatm = zeros(SPP(1,1),SPP(1,2));
DeltaPSREG = zeros(SPP(1,1),SPP(1,2));
DeltaPSRatm = zeros(SPP(1,1),SPP(1,2));
DeltaEGatmPSR = zeros(SPP(1,1),SPP(1,2));
```

```
DeltaCFEG = zeros(SPP(1,1),SPP(1,2));
DeltaLOC = zeros(SPP(1,1),SPP(1,2));
DeltaREatm = zeros(SPP(1,1),SPP(1,2));
for k = 1:SP(1,1)-1
    P1 = PB(k,1);
    P2 = PB(k+1,1);
    Pra = PRA(k+1,1);
    Pre = PRE(k+1,1);
    Pcf = PCF(k+1,1);
    Psr = PSR(k+1,1);
    Ploc = PLOC(k,1);

    if P1>P2
        DeltaEG(k,1) = P2/P1;
    else
        DeltaEG(k,1) = P1/P2;
    end

    if P2>Pra
        DeltaRA(k+1,1) = Pra/P2;
    else
        DeltaRA(k+1,1) = P2/Pra;
    end

    if Pra>Pre
        DeltaRE(k+1,1) = Pre/Pra;
    else
        DeltaRE(k+1,1) = Pra/Pre;
    end

    if P2>Pre
        DeltaREG(k+1,1) = Pre/P2;
    else
        DeltaREG(k+1,1) = P2/Pre;
    end

    if Pra>Pcf
        DeltaRACF(k+1,1) = Pcf/Pra;
    else
        DeltaRACF(k+1,1) = Pra/Pcf;
    end

    if Pre>Pcf
        DeltaRECF(k+1,1) = Pcf/Pre;
    else
        DeltaRECF(k+1,1) = Pre/Pcf;
    end

    if Patm>Pcf
        DeltaCFatm(k+1,1) = Pcf/Patm;
    else
        DeltaCFatm(k+1,1) = Patm/Pcf;
    end

    if Patm>Psr
        DeltaPSRatm(k+1,1) = Psr/Patm;
    else
        DeltaPSRatm(k+1,1) = Patm/Psr;
    end

    if P2>Psr
        DeltaPSREG(k+1,1) = Psr/P2;
    else
        DeltaPSREG(k+1,1) = P2/Psr;
    end

    if P2>=Patm
        DeltaEGatmPSR(k+1,1) = Patm/P2;
    else
        DeltaEGatmPSR(k+1,1) = P2/Patm;
    end

    if P2>=Pcf
        DeltaCFEG(k+1,1) = Pcf/P2;
    else
        DeltaCFEG(k+1,1) = P2/Pcf;
    end

    if P1>=Ploc
        DeltaLOC(k,1) = Ploc/P1;
    else
        DeltaLOC(k,1) = P1/Ploc;
    end
    if Pre>=Patm
        DeltaREatm(k+1,1) = Patm/Pre;
    else
        DeltaREatm(k+1,1) = Pre/Patm;
    end
end


function [PF,PB,PRA,PRE,PCF,PSR,PLOC] = fcn(VALV,VLOCO,dt,COMPP,Nvag,...
    Patm,CFREIO,CMCQ,CMPRA,CMPRE,CMPREG,CRACF,CRECF,CRCFATM,CPSREG,...
    CPSRATM,CPSREGatmPSR,CPCFEG,CPLOC,NLOC,R,T,AEG,AlocoI,AlocoO,Ploco,...
    Peq,AegAX,AegEM,AEGCF,Ascf,Aesr,AegPSR,APSRatm,AEGatmPSR,AegaATMEM,...
    ACFEG, Vaux,Vemg,Veg,DAC,DAL,DPE,DSR,DPcEG,Vpsr, PFI,PBI,P3i,...
    PRAI,PREI,PCFI,PSRI,PLOCI,XO,ACF,X,CPREatm)


PB = PBI;
PF = PFI;
PRA = PRAI;
```

```
PRE = PREI;
PCF =PCFI;
PSR = PSRI;
PLOC = PLOCI;
VMPSRin_vec = 0*PCFI;

if VALV == 0 %ABDX baseline (no venturi)
    cont  = 1;
    for k = 1:Nvag+NLOC
        if  cont ==1
            if CFREIO>Peq
                if PB(cont,1)<=Peq
                    PB(cont,1) = Ploco;
                else
                    PB(cont,1) = Peq;
                end
            else
                if VLOCO<=0.01
                    PB(cont,1) = Ploco;
                else
                    if  PB(cont+1,1)>CFREIO
                        PB(cont,1) = Patm;
                    else
                        PB(cont,1) = CFREIO;
                    end
                end
            end
            cont = cont+1;

        elseif COMPP(cont,1)==1 && cont >=2
            P1 = PBI(cont-1,1);
            P2 = PBI(cont,1);
            P3 = PBI(cont+1,1);
            if cont == 2
                if P1>P2
                    A = AlocoI;
                else
                    if CFREIO == Patm
                        A = 2*AlocoO;
                    else
                        A = AlocoO;
                    end
                end
            else
                A = AEG;
            end

            if P1>P2
                VM1 = A*CMCQ(cont-1,1)*P1/sqrt(T);
            else
                VM1 = -A*CMCQ(cont-1,1)*P2/sqrt(T);
            end

            if P2>P3
                VM2 = AEG*CMCQ(cont,1)*P2/sqrt(T);
            else
                VM2 = -AEG*CMCQ(cont,1)*P3/sqrt(T);
            end

            if CFREIO>Peq
                if PB(cont,1)<=Peq
                    PLOC(cont,1) = Ploco;
                else
                    PLOC(cont,1) = Peq;
                end
            else
                if VLOCO<=0.01
                    PLOC(cont,1) = Ploco;
                else
                    if  PB(cont+1,1)>CFREIO
                    PLOC(cont,1) = Patm;
                    else
                    PLOC(cont,1) = CFREIO;
                    end
                end
            end

            if PLOC(cont,1)>P2
                ALOC = AlocoI;
            else
                if CFREIO == Patm
                    ALOC = 2*AlocoO;
                else
                    ALOC = AlocoO;
                end
            end

            if P2>PLOC(cont,1)
                VMlocT = -ALOC*CPLOC(cont,1)*P2/sqrt(T);
            else
                VMlocT = ALOC*CPLOC(cont,1)*PLOC(cont,1)/sqrt(T);
            end
            PB(cont,1) =  P2 +(R*T)/Veg*(VM1-VM2+VMlocT)*dt;
            cont = cont+1;

        else
            P1 = PBI(cont-1,1);
            P2 = PBI(cont,1);
            P3 = PBI(cont+1,1);
            if  k == Nvag+NLOC
                P4 = PBI(cont+1,1);
            else
                P4 = PBI(cont+2,1);
```

```
end
PAX = PRAI(cont+1,1);
PEX = PREI(cont+1,1);
Pcf = PCFI(cont+1,1);
Psr = PSRI(cont+1,1);

if cont == 2
    if COMPP(cont-1,1)== 1
        if P1>P2
            A = AlocoI;
        else
            if CFREIO == Patm
                A = 2*AlocoO;
            else
                A = AlocoO;
            end
        end
    else
        A = AEG;
    end
else
    A = AEG;
end

if P1>P2
    VM1 = A*CMCQ(cont-1,1)*P1/sqrt(T);
else
    VM1 = -A*CMCQ(cont-1,1)*P2/sqrt(T);
end

if P2>P3
    VM2 = AEG*CMCQ(cont,1)*P2/sqrt(T);
else
    VM2 = -AEG*CMCQ(cont,1)*P3/sqrt(T);
end
PB(cont,1) =  P2 +(R*T)/Veg*(VM1-VM2)*dt;

if P3>PAX
    VMPAX = AegAX*CMPRA(cont+1,1)*PAX/sqrt(T);
else
    VMPAX = 0;
end

if PAX>PEX
    VMPEX = AegEM*CMPRE(cont+1,1)*PEX/sqrt(T);
else
    VMPEX = 0;
end

if P3>=Psr
    VMPSRin = AegPSR*CPSREG(cont+1,1)*Psr/sqrt(T);
else
    VMPSRin = 0;
end

if Psr-P3>=DSR && Psr-P3<=DPE
    if Psr<=Patm
        VMPSRATM = -APSRatm*CPSRATM(cont+1,1)*Patm/sqrt(T);
    else
        VMPSRATM = APSRatm*CPSRATM(cont+1,1)*Psr/sqrt(T);
    end
    if Psr-P3>=DSR && (P3-CFREIO) > 7000
        if P3<=Patm
            VMEGATM =  -AegPSR*CPSREGatmPSR(cont+1,1)*Patm/sqrt(T);
        else
            VMEGATM =  AegPSR*CPSREGatmPSR(cont+1,1)*P3/sqrt(T);
        end
    else
        VMEGATM =0;
    end
else
    VMPSRATM = 0;
    VMEGATM =0;
end

if P3>P4
    VM3 = AEG*CMCQ(cont+1,1)*P3/sqrt(T);
else
    VM3 = -AEG*CMCQ(cont+1,1)*P4/sqrt(T);
end
if k == Nvag+NLOC
    VM3 =0;
end

if PAX-P3>DAC
    if PAX>=Pcf
        VMAXCF = AEGCF*CRACF(cont+1,1)*PAX/sqrt(T);
    else
        VMAXCF = -AEGCF*CRACF(cont+1,1)*Pcf/sqrt(T);
    end
else
    VMAXCF = 0;
end

if Psr-P3>DPE
    if VLOCO<=0.01
        VMEGATM =0;
    else
        if P3<=Patm
            VMEGATM =  -AegaATMEM*CPSREGatmPSR(cont+1,1)*Patm/sqrt(T);
        else
            VMEGATM =  AegaATMEM*CPSREGatmPSR(cont+1,1)*P3/sqrt(T);
        end
```

```
                if Psr<=Patm
                    VMPSRATM = -APSRatm*CPSRATM(cont+1,1)*Patm/sqrt(T);
                else
                    VMPSRATM = APSRatm*CPSRATM(cont+1,1)*Psr/sqrt(T);
                end
            end
            if PEX>=Pcf
                VMEXCF = AEGCF*CRECF(cont+1,1)*PEX/sqrt(T);
            else
                VMEXCF = -AEGCF*CRECF(cont+1,1)*Pcf/sqrt(T);
            end
        else
            VMEXCF = 0;
            if P3<=Patm && CFREIO<Peq && VLOCO>0.01
                if P3<=Patm
                    VMEGATM =  -AegaATMEM*CPSREGatmPSR(cont+1,1)*Patm/sqrt(T);
                else
                    VMEGATM =  AegaATMEM*CPSREGatmPSR(cont+1,1)*P3/sqrt(T);
                end
            end
        end

        if P3-DAL>=PAX
            VSATM = Ascf*CRCFATM(cont+1,1)*Pcf/sqrt(T);
            if PEX>=P3
                VRERA = Aesr*CMPREG(cont+1,1)*PEX/sqrt(T);
            else
                VRERA = 0;
            end
            if P3<PAX
                VMPAX = -AegAX*CMPRA(cont+1,1)*PAX/sqrt(T);
            end
        else
            if VLOCO<=0.01  ||P3>=P3i(cont+1,1)
                VSATM = Ascf*CRCFATM(cont+1,1)*Pcf/sqrt(T);
            else
                VSATM =0;
            end
            if P3>=CFREIO-DPcEG && P3<=CFREIO+2*DPcEG || P3<=11E4
                VSATM =0;
            end
            VRERA =0;
        end

        if Pcf> P3 && P3> Psr
            VCFEG = ACFEG*CPCFEG(cont+1,1)*Pcf/sqrt(T);
        else
            VCFEG = 0;
        end
        x0 = XO(cont+1, 1);
        x = X(cont+1, 1);

        PB(cont+1,1) =  P3 +(R*T)/Veg*(VM2-VM3-VMPAX-VMPEX-VMPSRin-VMEGATM+VRERA+VCFEG)*dt;

        PCF(cont+1,1) =  1/x*(Pcf*x0 + (R*T/ACF)*(VMAXCF+VMEXCF-VSATM-VCFEG)*dt);


        PRA(cont+1,1) =  PAX +(R*T)/Vaux*(VMPAX-VMAXCF)*dt;

        PRE(cont+1,1) =  PEX +(R*T)/Vemg*(VMPEX-VMEXCF-VRERA)*dt;

        PSR(cont+1,1) =  Psr +(R*T)/Vpsr*(VMPSRin-VMPSRATM)*dt;

        VMPSRin_vec(cont+1, 1)  = VMPSRin;

        PF(cont,1) =  PCF(cont+1,1);
        PF(cont+1,1) = PCF(cont+1,1);
        cont = cont+2;
    end
end


elseif VALV == 1 %ABDX sonic venturi
      cont  = 1;
    for k = 1:Nvag+NLOC
        if  cont ==1
        if CFREIO>Peq
            if PB(cont,1)<=Peq
                PB(cont,1) = Ploco;
            else
                PB(cont,1) = Peq;
            end
        else
            if VLOCO<=0.01
                PB(cont,1) = Ploco;
            else
                if  PB(cont+1,1)>CFREIO
                    PB(cont,1) = Patm;
                else
                    PB(cont,1) = CFREIO;
                end
            end
        end
        cont = cont+1;

    elseif COMPP(cont,1)==1 && cont >=2
        P1 = PBI(cont-1,1);
        P2 = PBI(cont,1);
        P3 = PBI(cont+1,1);
        if cont == 2
            if P1>P2
                A = AlocoI;
            else
```

```
            if CFREIO == Patm
                A = 2*AlocoO;
            else
                A = AlocoO;
            end
        end
    else
        A = AEG;
    end

    if P1>P2
        VM1 = A*CMCQ(cont-1,1)*P1/sqrt(T);
    else
        VM1 = -A*CMCQ(cont-1,1)*P2/sqrt(T);
    end

    if P2>P3
        VM2 = AEG*CMCQ(cont,1)*P2/sqrt(T);
    else
        VM2 = -AEG*CMCQ(cont,1)*P3/sqrt(T);
    end

    if CFREIO>Peq
        if PB(cont,1)<=Peq
            PLOC(cont,1) = Ploco;
        else
            PLOC(cont,1) = Peq;
        end
    else
        if VLOCO<=0.01
            PLOC(cont,1) = Ploco;
        else
            if  PB(cont+1,1)>CFREIO
                PLOC(cont,1) = Patm;
            else
                PLOC(cont,1) = CFREIO;
            end
        end
    end

    if PLOC(cont,1)>P2
        ALOC = AlocoI;
    else
        if CFREIO == Patm
            ALOC = 2*AlocoO;
        else
            ALOC = AlocoO;
        end
    end

    if P2>PLOC(cont,1)
        VMlocT = -ALOC*CPLOC(cont,1)*P2/sqrt(T);
    else
        VMlocT = ALOC*CPLOC(cont,1)*PLOC(cont,1)/sqrt(T);
    end
    PB(cont,1) =  P2 +(R*T)/Veg*(VM1-VM2+VMlocT)*dt;
    cont = cont+1;

else
    P1 = PBI(cont-1,1);
    P2 = PBI(cont,1);
    P3 = PBI(cont+1,1);
    if  k == Nvag+NLOC
        P4 = PBI(cont+1,1);
    else
        P4 = PBI(cont+2,1);
    end
    PAX = PRAI(cont+1,1);
    PEX = PREI(cont+1,1);
    Pcf = PCFI(cont+1,1);
    Psr = PSRI(cont+1,1);

    if cont == 2
        if COMPP(cont-1,1)== 1
            if P1>P2
                A = AlocoI;
            else
                if CFREIO == Patm
                    A = 2*AlocoO;
                else
                    A = AlocoO;
                end
            end
        else
            A = AEG;
        end
    else
        A = AEG;
    end

    if P1>P2
        VM1 = A*CMCQ(cont-1,1)*P1/sqrt(T);
    else
        VM1 = -A*CMCQ(cont-1,1)*P2/sqrt(T);
    end

    if P2>P3
        VM2 = AEG*CMCQ(cont,1)*P2/sqrt(T);
    else
        VM2 = -AEG*CMCQ(cont,1)*P3/sqrt(T);
    end
    PB(cont,1) =  P2 +(R*T)/Veg*(VM1-VM2)*dt;
```

```
if P3>PAX
    VMPAX = AegAX*CMPRA(cont+1,1)*PAX/sqrt(T);
else
    VMPAX = 0;
end

if PAX>PEX
    VMPEX = AegEM*CMPRE(cont+1,1)*PEX/sqrt(T);
else
    VMPEX = 0;
end

if P3>=Psr
    VMPSRin = AegPSR*CPSREG(cont+1,1)*Psr/sqrt(T);
else
    VMPSRin = 0;
end

if Psr-P3>=DSR && Psr-P3<=DPE
    if Psr<=Patm
        VMPSRATM = -APSRatm*CPSRATM(cont+1,1)*Patm/sqrt(T);
    else
        VMPSRATM = APSRatm*CPSRATM(cont+1,1)*Psr/sqrt(T);
    end
    if Psr-P3>=DSR && (P3-CFREIO) > 7000
        if P3<=Patm
            VMEGATM =  -AegPSR*CPSREGatmPSR(cont+1,1)*Patm/sqrt(T);
            VMREATM = 0; %Venturi
        else
            VMEGATM =  1.4*AegPSR*CPSREGatmPSR(cont+1,1)*P3/sqrt(T);
            VMREATM = 1.0*(7.8E-6)*CPREatm(cont+1,1)*PEX/sqrt(T); %Venturi
        end
    else
        VMEGATM =0;
        VMREATM =0; %Venturi
    end
else
    VMPSRATM = 0;
    VMEGATM =0;
    VMREATM = 0; %Venturi
end

if P3>P4
    VM3 = AEG*CMCQ(cont+1,1)*P3/sqrt(T);
else
    VM3 = -AEG*CMCQ(cont+1,1)*P4/sqrt(T);
end
if k == Nvag+NLOC
    VM3 =0;
end

if PAX-P3>DAC
    if PAX>=Pcf
        VMAXCF = AEGCF*CRACF(cont+1,1)*PAX/sqrt(T);
    else
        VMAXCF = -AEGCF*CRACF(cont+1,1)*Pcf/sqrt(T);
    end
else
    VMAXCF = 0;
end

if Psr-P3>DPE
    if VLOCO<=0.01
        VMEGATM =0;
    else
        if P3<=Patm
            VMEGATM =  -AegaATMEM*CPSREGatmPSR(cont+1,1)*Patm/sqrt(T);
        else
            VMEGATM =  AegaATMEM*CPSREGatmPSR(cont+1,1)*P3/sqrt(T);
        end
        if Psr<=Patm
            VMPSRATM = -APSRatm*CPSRATM(cont+1,1)*Patm/sqrt(T);
        else
            VMPSRATM = APSRatm*CPSRATM(cont+1,1)*Psr/sqrt(T);
        end
    end
    if PEX>=Pcf
        VMEXCF = AEGCF*CRECF(cont+1,1)*PEX/sqrt(T);
    else
        VMEXCF = -AEGCF*CRECF(cont+1,1)*Pcf/sqrt(T);
    end
else
    VMEXCF = 0;
    if P3<=Patm && CFREIO<Peq && VLOCO>0.01
        if P3<=Patm
            VMEGATM =  -AegaATMEM*CPSREGatmPSR(cont+1,1)*Patm/sqrt(T);
        else
            VMEGATM =  AegaATMEM*CPSREGatmPSR(cont+1,1)*P3/sqrt(T);
        end
    end
end

if P3-DAL>=PAX
    VSATM = Ascf*CRCFATM(cont+1,1)*Pcf/sqrt(T);
    if PEX>=P3
        VRERA = Aesr*CMPREG(cont+1,1)*PEX/sqrt(T);
    else
        VRERA = 0;
    end
    if P3<PAX
        VMPAX = -AegAX*CMPRA(cont+1,1)*PAX/sqrt(T);
    end
else
```

```
                if VLOCO<=0.01 ||P3>=P3i(cont+1,1)
                    VSATM = Ascf*CRCFATM(cont+1,1)*Pcf/sqrt(T);
                else
                    VSATM =0;
                end
                if P3>=CFREIO-DPcEG && P3<=CFREIO+2*DPcEG || P3<=11E4
                    VSATM =0;
                end
                VRERA =0;
            end

            if Pcf> P3 && P3> Psr
                VCFEG = ACFEG*CPCFEG(cont+1,1)*Pcf/sqrt(T);
            else
                VCFEG = 0;
            end
            x0 = XO(cont+1, 1);
            x = X(cont+1, 1);

            PB(cont+1,1) =  P3 +(R*T)/Veg*(VM2-VM3-VMPAX-VMPEX-VMPSRin-VMEGATM+VRERA+VCFEG)*dt;

            PCF(cont+1,1) =  1/x*(Pcf*x0 + (R*T/ACF)*(VMAXCF+VMEXCF-VSATM-VCFEG)*dt);


            PRA(cont+1,1) =  PAX +(R*T)/Vaux*(VMPAX-VMAXCF)*dt;

            PRE(cont+1,1) =  PEX +(R*T)/Vemg*(VMPEX-VMEXCF-VRERA-VMREATM)*dt;

            PSR(cont+1,1) =  Psr +(R*T)/Vpsr*(VMPSRin-VMPSRATM)*dt;

            VMPSRin_vec(cont+1, 1)  = VMPSRin;

            PF(cont,1) =  PCF(cont+1,1);
            PF(cont+1,1) = PCF(cont+1,1);
            cont = cont+2;
        end
    end

else %ABDX low venturi
      cont  = 1;
    for k = 1:Nvag+NLOC
        if  cont ==1
            if CFREIO>Peq
                if PB(cont,1)<=Peq
                    PB(cont,1) = Ploco;
                else
                    PB(cont,1) = Peq;
                end
            else
                if VLOCO<=0.01
                    PB(cont,1) = Ploco;
                else
                    if  PB(cont+1,1)>CFREIO
                        PB(cont,1) = Patm;
                    else
                        PB(cont,1) = CFREIO;
                    end
                end
            end
            cont = cont+1;

        elseif COMPP(cont,1)==1 && cont >=2
            P1 = PBI(cont-1,1);
            P2 = PBI(cont,1);
            P3 = PBI(cont+1,1);
            if cont == 2
                if P1>P2
                    A = AlocoI;
                else
                    if CFREIO == Patm
                        A = 2*AlocoO;
                    else
                        A = AlocoO;
                    end
                end
            else
                A = AEG;
            end

            if P1>P2
                VM1 = A*CMCQ(cont-1,1)*P1/sqrt(T);
            else
                VM1 = -A*CMCQ(cont-1,1)*P2/sqrt(T);
            end

            if P2>P3
                VM2 = AEG*CMCQ(cont,1)*P2/sqrt(T);
            else
                VM2 = -AEG*CMCQ(cont,1)*P3/sqrt(T);
            end

            if CFREIO>Peq
                if PB(cont,1)<=Peq
                    PLOC(cont,1) = Ploco;
                else
                    PLOC(cont,1) = Peq;
                end
            else
                if VLOCO<=0.01
                    PLOC(cont,1) = Ploco;
                else
                    if  PB(cont+1,1)>CFREIO
                        PLOC(cont,1) = Patm;
```

```
                else
                    PLOC(cont,1) = CFREIO;
                end
            end
        end

        if PLOC(cont,1)>P2
            ALOC = AlocoI;
        else
            if CFREIO == Patm
                ALOC = 2*AlocoO;
            else
                ALOC = AlocoO;
            end
        end

        if P2>PLOC(cont,1)
            VMlocT = -ALOC*CPLOC(cont,1)*P2/sqrt(T);
        else
            VMlocT = ALOC*CPLOC(cont,1)*PLOC(cont,1)/sqrt(T);
        end
        PB(cont,1) =  P2 +(R*T)/Veg*(VM1-VM2+VMlocT)*dt;
        cont = cont+1;

    else
        P1 = PBI(cont-1,1);
        P2 = PBI(cont,1);
        P3 = PBI(cont+1,1);
        if  k == Nvag+NLOC
            P4 = PBI(cont+1,1);
        else
            P4 = PBI(cont+2,1);
        end
        PAX = PRAI(cont+1,1);
        PEX = PREI(cont+1,1);
        Pcf = PCFI(cont+1,1);
        Psr = PSRI(cont+1,1);

        if cont == 2
            if COMPP(cont-1,1)== 1
                if P1>P2
                    A = AlocoI;
                else
                    if CFREIO == Patm
                        A = 2*AlocoO;
                    else
                        A = AlocoO;
                    end
                end
            else
                A = AEG;
            end
        else
            A = AEG;
        end

        if P1>P2
            VM1 = A*CMCQ(cont-1,1)*P1/sqrt(T);
        else
            VM1 = -A*CMCQ(cont-1,1)*P2/sqrt(T);
        end

        if P2>P3
            VM2 = AEG*CMCQ(cont,1)*P2/sqrt(T);
        else
            VM2 = -AEG*CMCQ(cont,1)*P3/sqrt(T);
        end
        PB(cont,1) =  P2 +(R*T)/Veg*(VM1-VM2)*dt;

        if P3>PAX
            VMPAX = AegAX*CMPRA(cont+1,1)*PAX/sqrt(T);
        else
            VMPAX = 0;
        end

        if PAX>PEX
            VMPEX = AegEM*CMPRE(cont+1,1)*PEX/sqrt(T);
        else
            VMPEX = 0;
        end

        if P3>=Psr
            VMPSRin = AegPSR*CPSREG(cont+1,1)*Psr/sqrt(T);
        else
            VMPSRin = 0;
        end

        if Psr-P3>=DSR && Psr-P3<=DPE
            if Psr<=Patm
                VMPSRATM = -APSRatm*CPSRATM(cont+1,1)*Patm/sqrt(T);
            else
                VMPSRATM = APSRatm*CPSRATM(cont+1,1)*Psr/sqrt(T);
            end
            if Psr-P3>=DSR && (P3-CFREIO) > 7000
                if P3<=Patm
                    VMEGATM =  -AegPSR*CPSREGatmPSR(cont+1,1)*Patm/sqrt(T);
                    VMREATM = 0; %Venturi
                else
                    VMEGATM =  1.05*AegPSR*CPSREGatmPSR(cont+1,1)*P3/sqrt(T);
                    VMREATM = 1.0*AegEM*CPREatm(cont+1,1)*PEX/sqrt(T); %Venturi
                end
            else
                VMEGATM =0;
```

```
        VMREATM = 0; %Venturi
    end
else
    VMPSRATM = 0;
    VMEGATM =0;
    VMREATM = 0; %Venturi
end

if P3>P4
    VM3 = AEG*CMCQ(cont+1,1)*P3/sqrt(T);
else
    VM3 = -AEG*CMCQ(cont+1,1)*P4/sqrt(T);
end
if k == Nvag+NLOC
    VM3 =0;
end

if PAX-P3>DAC
    if PAX>=Pcf
        VMAXCF = AEGCF*CRACF(cont+1,1)*PAX/sqrt(T);
    else
        VMAXCF = -AEGCF*CRACF(cont+1,1)*Pcf/sqrt(T);
    end
else
    VMAXCF = 0;
end


if Psr-P3>DPE
    if VLOCO<=0.01
        VMEGATM =0;
    else
        if P3<=Patm
            VMEGATM =  -AegaATMEM*CPSREGatmPSR(cont+1,1)*Patm/sqrt(T);
        else
            VMEGATM =  AegaATMEM*CPSREGatmPSR(cont+1,1)*P3/sqrt(T);
        end
        if Psr<=Patm
            VMPSRATM = -APSRatm*CPSRATM(cont+1,1)*Patm/sqrt(T);
        else
            VMPSRATM = APSRatm*CPSRATM(cont+1,1)*Psr/sqrt(T);
        end
    end
    if PEX>=Pcf
        VMEXCF = AEGCF*CRECF(cont+1,1)*PEX/sqrt(T);
    else
        VMEXCF = -AEGCF*CRECF(cont+1,1)*Pcf/sqrt(T);
    end
else
    VMEXCF = 0;
    if P3<=Patm && CFREIO<Peq && VLOCO>0.01
        if P3<=Patm
            VMEGATM =  -AegaATMEM*CPSREGatmPSR(cont+1,1)*Patm/sqrt(T);
        else
            VMEGATM =  AegaATMEM*CPSREGatmPSR(cont+1,1)*P3/sqrt(T);
        end
    end
end

if P3-DAL>=PAX
    VSATM = Ascf*CRCFATM(cont+1,1)*Pcf/sqrt(T);
    if PEX>=P3
        VRERA = Aesr*CMPREG(cont+1,1)*PEX/sqrt(T);
    else
        VRERA = 0;
    end
    if P3<PAX
        VMPAX = -AegAX*CMPRA(cont+1,1)*PAX/sqrt(T);
    end
else
    if VLOCO<=0.01 ||P3>=P3i(cont+1,1)
        VSATM = Ascf*CRCFATM(cont+1,1)*Pcf/sqrt(T);
    else
        VSATM =0;
    end
    if P3>=CFREIO-DPcEG && P3<=CFREIO+2*DPcEG || P3<=11E4
        VSATM =0;
    end
    VRERA =0;
end

if Pcf> P3 && P3> Psr
    VCFEG = ACFEG*CPCFEG(cont+1,1)*Pcf/sqrt(T);
else
    VCFEG = 0;
end
x0 = XO(cont+1, 1);
x = X(cont+1, 1);

PB(cont+1,1) =  P3 +(R*T)/Veg*(VM2-VM3-VMPAX-VMPEX-VMPSRin-VMEGATM+VRERA+VCFEG)*dt;

PCF(cont+1,1) =  1/x*(Pcf*x0 + (R*T/ACF)*(VMAXCF+VMEXCF-VSATM-VCFEG)*dt);


PRA(cont+1,1) =  PAX +(R*T)/Vaux*(VMPAX-VMAXCF)*dt;

PRE(cont+1,1) =  PEX +(R*T)/Vemg*(VMPEX-VMEXCF-VRERA-VMREATM)*dt;

PSR(cont+1,1) =  Psr +(R*T)/Vpsr*(VMPSRin-VMPSRATM)*dt;

VMPSRin_vec(cont+1, 1)  = VMPSRin;

PF(cont,1) =  PCF(cont+1,1);
```

```
            PF(cont+1,1) = PCF(cont+1,1);
            cont = cont+2;
        end
    end
end


function [X1,X,X0] = fcn(Pcf, c_CF, k_CF, FCF, mCF, Xmin, Xst, Acf, Patm,...
    dt, X1, X, X0)

for j = 1:1:length(Pcf)
    X2 = (Acf*(Pcf(j) - Patm) - c_CF*X1(j) - k_CF*X(j) - FCF) / mCF;
    X1(j) = X1(j) + X2*dt;
    X0(j) = X(j);
    X(j) = X(j) + X1(j)*dt;
    if (X(j) >= Xst)
        X(j) = Xst;
        X1(j) = 0.0;
    elseif (X(j) <= Xmin)
        X(j) = Xmin;
        X1(j) = 0.0;
    end
end
end


function FT = fcn(Vloco,LP, Ploco1,Ploco2, Ploco3,Ploco4,Ploco5,Ploco6,Ploco7,Ploco8,Dloco1 ,Dloco2 ,Dloco3 ,Dloco4 )

if LP ==1
    FT= Ploco1;
elseif LP ==2
    FT= Ploco2;
elseif LP ==3
    FT= Ploco3;
elseif LP ==4
    FT= Ploco4;
elseif LP ==5
    FT= Ploco5;
elseif LP ==6
    FT= Ploco6;
elseif LP ==7
    FT= Ploco7;
elseif LP ==8
    FT= Ploco8;
elseif  LP ==0
    FT = 0;
elseif LP == -1
    FT = -Dloco1;
elseif LP == -2
    FT = -Dloco2;
elseif LP == -3
    FT = -Dloco3;
elseif LP ==-4
    FT = -Dloco4;
else
    FT = 0;
end

if Vloco<=0 && FT<=0
    FT = 0;
end


function [f_load, f_unload ] = fcn(xfd,DX,v, alfa, beta, gama, xr0, xm01, xm02, xm03, km1, km2, km3, kr, x0, x1, x2, mik,
mis, mikl, misl,h3, Folga)


xfdN =xfd;

SPP = size(DX);
SP = SPP(1,1);
dx = zeros(size(DX));
for k = 1:SP
    if DX(k,1)>1 && DX(k,1)<=Folga(k)*1000
        dx(k,1) = 0.01;
    elseif   DX(k,1)<=1
        X0 = 0.01;
        Y0 = 0;
        X1 = 0.05;
        Y1 = 100;
        Y2 = abs(DX(k,1));
        dx(k,1)= X0*(Y2-Y1)/(Y0-Y1)+X1*(Y2-Y0)/(Y1-Y0);
    else
        X0 = 0.01;
        Y0 = Folga(k)*1000;
        X1 = 0.22;
        Y1 = 220;
        Y2 = abs(DX(k,1));
        dx(k,1)= X0*(Y2-Y1)/(Y0-Y1)+X1*(Y2-Y0)/(Y1-Y0);
    end

    if  xfd(k,1)>0 && xfd(k,1)<=Folga(k)
        xfd(k,1) = 0;
    end

    if  xfd(k,1)>Folga(k)
        xfd(k,1) = xfd(k,1)-Folga(k);
    end
end
% dx = dx/15;
dx = dx/25;
dx1 = dx;
```

```
xfd=abs(xfd);

xfd_p = xfd - x0;
xfd_n = xfd + 0;

% Força nas molas
%Força na mola principal
Fsm1 = km1.*(xm01 + xfd_p) + km2.*(xm02 + xfd_p) + km3.*(xm03 + xfd_p); %if positive
Fsm2 = km1.*(-xm01 + xfd_n) + km2.*(-xm02 + xfd_n) + km3.*(-xm03 + xfd_n); %if negative
%Composição das duas forças
Fsm = Fsm1.*fe(xfd, 0, dx1)+Fsm2.*(1-fe(xfd,0, dx1));
Fsm = Fsm.*(fe(xfd, x0, dx1)+(1-fe(xfd,0, dx1)));

%Força na mola de retorno
Fsr1 = kr.*xr0;     %if positive
Fsr2 = kr.*(-xr0);  %if negative
%Composição das duas forças
Fsr = Fsr1.*fe(xfd, 0, dx1)+Fsr2.*(1-fe(xfd,0, dx1));
Fsr = Fsr.*(fe(xfd, x0, dx1)+(1-fe(xfd,0, dx1)));
% Condições

y1 = ((fe(xfd, -x1+x0, dx).*(1-fe(xfd, 0, dx))) + fe(xfd, 0, dx).*(1- fe(xfd, x1, dx)));
y2 = (fe(xfd, x1, dx)+(1-fe(xfd,-x1+x0,dx)));
y3 = (fe(xfd, x2, dx)+(1-fe(xfd,-x2+x0,dx)));
y4 = ((fe(xfd, -x2+x0, dx).*(1-fe(xfd, 0, dx))) + fe(xfd, 0, dx).*(1- fe(xfd, x2, dx)));

% Cálculo das velocidades relativas dos componentes
v1 = (cos(alfa)./(cos(alfa+gama))).*v;
v2 = (sin(gama)./cos(alfa+gama)).*v;
v3 = ((cos(alfa).*sin(gama))./(cos(alfa+gama).*cos(beta))).*v;

v41 = v.*fe(v, 0, dx).*fe(xfd, 0, dx) + v.*(1-fe(v, 0, dx)).*(1-fe(xfd, 0, dx));

v42 = ((cos(alfa)*cos(gama-beta))./(cos(alfa+gama).*cos(beta))).*v.*(1 - fe(v, 0, dx)).*fe(xfd, 0, dx) +
((cos(alfa)*cos(gama-beta))./(cos(alfa+gama).*cos(beta))).*v.*(fe(v, 0, dx)).*(1-fe(xfd, 0, dx));

v4 = v41+v42;

% Friction (Modelo Exponencial)
h1 = mik;
h2 = mis-mik;
h1_1 = mikl;
h2_1 = misl-mikl;

mi1 = h1_1 + h2_1.*exp(-h3.*abs(v1));
mi2 = h1 + h2.*exp(-h3.*abs(v2));
mi3 = h1 + h2.*exp(-h3.*abs(v3));
mi4 = h1 + h2.*exp(-h3.*abs(v4));

% Força total
psi1 = (1 + ((tan(beta + atan(mi3))).*tan(gama + atan(mi1))))./(1 - (tan(alfa + atan(mi2))).*(tan(gama + atan(mi1))));
psi2 = psi1 + (2.*(1 - mi1.*tan(gama)).*mi4.*(psi1 - 1))./(mi1 + tan(gama));
psi3 = (1 + (tan(beta - atan(mi3))).*tan(gama - atan(mi1)))./(1 - (tan(alfa - atan(mi2))).*tan(gama - atan(mi1)));
psi4 = ((tan(gama) - mi1).*psi3)./(tan(gama).*(1 - 2.*mi1.*mi4 + 2.*mi1.*mi4.*psi3) + 2.*mi4.*psi3 - 2.*mi4 - mi1);

% Carregamento

f1 = (psi1.*Fsm - (psi1 - 1).*Fsr).*y1;
f2 = (psi2.*Fsm - (psi2 - 1).*Fsr).*y2;
f_load = f1+f2;
% f_load = (f1+f2).*fe(v, 0, dx1).*fe(xfd, 0, dx1) + (f1+f2).*(1-fe(v, 0, dx1)).*(1-fe(xfd, 0, dx1));

f3 = (psi3.*Fsm - (psi3 - 1).*Fsr).*y3;
f4 = (psi4.*Fsm - (psi4 - 1).*Fsr).*y4;
f_unload = f3+f4;
% f_unload = (f3+f4).*(1 - fe(v, 0, dx1)).*fe(xfd, 0, dx1) + (f3+f4).*(fe(v, 0, dx1)).*(1-fe(xfd, 0, dx1));


SFF = size(f_unload);
SF = SFF(1,1);
for k = 1:SF
    if xfdN(k,1)>=0 && xfdN(k,1)<=Folga(k)
        f_load(k,1)=0;
        f_unload(k,1)=0;
    end
    if xfdN(k,1)<0
        f_load(k,1)= -f_load(k,1);
        f_unload(k,1)= -f_unload(k,1);
    end
end
f_load(1) = 0;
f_load(end)=0;
f_unload(1) = 0;
f_unload(end)=0;


function [FT, FB] = fcn(FLoco, COMPP,convPF,PF)

FT = COMPP;
PP = size(FT);
FB = zeros(PP(1,1),PP(1,2));
P = PP(1,1);
for k = 1:P
    if FT(k,1) == 1
        FT(k,1) = FLoco;
        FB(k,1) = 0;
        PotB = 0;
    else
        FB(k,1) = PF(k,1)*convPF;
    end
end
```

```
function [V,X,Xloco,Vloco,DXmm,DV] = fcn(VX,COMPP,Lvag,Lloco)


SPP = size(VX);
SP = SPP(1,1);
SK = round(SPP(1,1)/2)+1;

V = VX(1:SK-1,1);
X = VX(SK:end,1);
Xloco = VX(SK,1)/1000;
Vloco = VX(1,1)*3.6;

DXmm = zeros(round(SPP(1,1)/2)+1,1);
DV = zeros(round(SPP(1,1)/2)+1,1);
SDX = round(SPP(1,1)/2);
for k =1:round(SPP(1,1)/2)-1

    DV(k+1,1) = VX(k,1) - VX(k+1,1);

    VAG = COMPP(k,1) + COMPP(k+1,1);
    if VAG ==1
        DXmm(k+1,1) = (VX(SDX+k,1) - (Lloco+Lvag)/2- VX(SDX+k+1,1) )*1000;
    elseif VAG == 2
        DXmm(k+1,1) = (VX(SDX+k,1) - Lloco- VX(SDX+k+1,1) )*1000;
    else
        DXmm(k+1,1) = (VX(SDX+k,1) - Lvag- VX(SDX+k+1,1) )*1000;
    end
end


function [F_ACT_LATERAL, fi] = F_lateral(Rinv, F_ACT, du)
% L = 1.2;
du = du(2:end-1);
B = 5.500;
D = 2*0.400 + 2*du;
Ov = 1.725;
L = 2*Ov + D;
F_ACT = F_ACT(2:end-1);

alfa = (B/2).*Rinv(1:end-1);%interp1(s, Rinv, u(1:end-1));
beta = (B/2).*Rinv(1:end-1);%Rinv(2:end);%interp1(s, Rinv, u(2:end));
gamma = (L.*Rinv(1:end-1))./2;

theta = alfa+beta+(2*gamma);

fi = (L.*(alfa+gamma) - Ov.*theta)./D;
F_ACT_LATERAL = F_ACT.*fi;
end


function [ACTf,AV,AXV, FRES, FPROP, FCURV, FGRAV] =
fcn(ACTp,V,ACTc,ACTd,Rv,Iv,FT,COMPP,M,MR,Mvag,MRvag,Fbra,A1l,A2l,B1l,C1l,A1ls,A2ls,A1,A2,B1,C1,A1s,A2s,DX,DXi,DV,DVMM,SMO,SMO
neg,a,KC,Folga)

SPP = size(FT);
% SP = Nco;
SP = 172;
AV = [zeros(size(V)); V];
FRES = zeros(SP, 1);
AXV = zeros(SP,1);
FPROP = zeros(SP, 1);
FCURV = zeros(SP, 1);
FGRAV = zeros(SP, 1);
% AXV = zeros(SPP(1,1),SPP(1,2));
% ACTf = zeros(SPP(1,1)+1,SPP(1,2));
ACTf = zeros(SP+1,1);
for k = 1:SP

    if COMPP(k,1) ==1
        AA1 = A1l;
        AA2 = A2l;
        BB1 = B1l;
        CC1 = C1l;
        AS1 = A1ls;
        AS2 = A2ls;
    else
        M = Mvag;
        MR = MRvag;
        AA1 = A1;
        AA2 = A2;
        BB1 = B1;
        CC1 = C1;
        AS1 = A1s;
        AS2 = A2s;
    end

    Vkm = V(k,1)*3.6;
    RR = Rv(k,1);
    II = Iv(k,1);
    if Vkm>=0.36
        Fres = M*9.81*(AA1 + AA2/MR + BB1*Vkm + CC1*Vkm^2) + M*1000*9.81*sin(II) + M*(6116*RR);
        Fprop = M*9.81*(AA1 + AA2/MR + BB1*Vkm + CC1*Vkm^2);
        Fgrav = M*1000*9.81*sin(II);
        Fcurv =  M*(6116*RR);
    elseif Vkm ==0
        Fres =0;
        Fprop = 0;
        Fgrav = 0;
        Fcurv = 0;
    elseif Vkm <0
        Fres = -(M*9.81*(AS1 + AS2/MR)+ M*1000*9.81*sin(II) + M*(6116*RR));
        Fprop = -M*9.81*(AA1 + AA2/MR);
        Fgrav =  M*1000*9.81*sin(II);
```

```
    Fcurv =  M*(6116*RR);
else
    Fres = M*9.81*(AS1 + AS2/MR)+ M*1000*9.81*sin(II)+ M*(6116*RR);
    Fprop = M*9.81*(AA1 + AA2/MR);
    Fgrav = M*1000*9.81*sin(II);
    Fcurv = M*(6116*RR);
end


if KC ==1
    if DX(k,1)>=0
        if DV(k,1)>0
            FACTf =  ACTc(k,1);
        elseif DV(k,1)<DVMM
            FACTf =  ACTd(k,1);
        else
            FACTf =  SMO(k,1)*ACTc(k,1)+(1-SMO(k,1))*ACTd(k,1);
        end
    else
        if DV(k,1)<0
            FACTf =  ACTc(k,1);
        elseif DV(k,1)> -DVMM
            FACTf =  ACTd(k,1);
        else
            FACTf =  SMOneg(k,1)*ACTc(k,1)+(1-SMOneg(k,1))*ACTd(k,1);
        end
    end

    if DX(k+1,1)>=0
        if DV(k+1,1)>0
            FACTt =  ACTc(k+1,1);
        elseif DV(k+1,1)<DVMM
            FACTt =  ACTd(k+1,1);
        else
            FACTt =  SMO(k+1,1)*ACTc(k+1,1)+(1-SMO(k+1,1))*ACTd(k+1,1);
        end
    else
        if DV(k+1,1)<0
            FACTt =  ACTc(k+1,1);
        elseif DV(k+1,1)> -DVMM
            FACTt =  ACTd(k+1,1);
        else
            FACTt =  SMOneg(k+1,1)*ACTc(k+1,1)+(1-SMOneg(k+1,1))*ACTd(k+1,1);
        end
    end

else

    if DX(k,1)>=0 && DX(k,1)<=Folga*1000
        dx = 0.000001;
    elseif DX(k,1)<0
        X0 = 0.001;
        Y0 = 0;
        X1 = 0.22;
        Y1 = 100;
        Y2 = abs(DX(k,1));
        dx= X0*(Y2-Y1)/(Y0-Y1)+X1*(Y2-Y0)/(Y1-Y0);
    else
        X0 = 0.001;
        Y0 = Folga*1000;
        X1 = 0.22;
        Y1 = 220;
        Y2 = abs(DX(k,1));
        dx= X0*(Y2-Y1)/(Y0-Y1)+X1*(Y2-Y0)/(Y1-Y0);
    end
    if DX(k,1)>=0
        f_adap_p = (a*ACTp(k,1)+(1-a)*ACTc(k,1));
        f_adap_n = (a*ACTp(k,1)+(1-a)*ACTd(k,1));
    else
        f_adap_p = (a*ACTp(k,1)+(1-a)*ACTd(k,1));
        f_adap_n = (a*ACTp(k,1)+(1-a)*ACTc(k,1));
    end
    fe = 1./(1+exp(-(DX(k,1)-DXi(k,1))/dx));
    f_pos=f_adap_p.*fe;
    f_neg=f_adap_n.*(1-fe);
    FACTf = (f_pos+f_neg);

    if DX(k+1,1)>=0 && DX(k+1,1)<=Folga*1000
         dx = 0.000001;
    elseif DX(k+1,1)<0
        X0 = 0.001;
        Y0 = 0;
        X1 = 0.22;
        Y1 = 100;
        Y2 = abs(DX(k+1,1));
        dx= X0*(Y2-Y1)/(Y0-Y1)+X1*(Y2-Y0)/(Y1-Y0);
    else
        X0 = 0.001;
        Y0 = Folga*1000;
        X1 = 0.22;
        Y1 = 220;
        Y2 = abs(DX(k+1,1));
        dx= X0*(Y2-Y1)/(Y0-Y1)+X1*(Y2-Y0)/(Y1-Y0);
    end

    if DX(k+1,1)>= 0
        f_adap_p = (a*ACTp(k+1,1)+(1-a)*ACTc(k+1,1));
        f_adap_n = (a*ACTp(k+1,1)+(1-a)*ACTd(k+1,1));
    else
        f_adap_p = (a*ACTp(k+1,1)+(1-a)*ACTd(k+1,1));
        f_adap_n = (a*ACTp(k+1,1)+(1-a)*ACTc(k+1,1));
    end
    fe = 1./(1+exp(-(DX(k+1,1)-DXi(k+1,1))/dx));
```

```
        f_pos=f_adap_p.*fe;
        f_neg=f_adap_n.*(1-fe);
        FACTt = (f_pos+f_neg);
    end


    if k ==1
        FACTf=0;
    end

    Ftra = FT(k,1);
    Ffreio = Fbra(k,1);
    AX = (Ftra-Ffreio-Fres+FACTf-FACTt)/(M*1000);

    AV(k,1) =AX;
    AXV(k,1) = AX;
    ACTf(k,1) = FACTf;
    FRES(k) = Fres;
    FPROP(k) = Fprop;
    FGRAV(k) = Fgrav;
    FCURV(k) = Fcurv;
end


function stop = fcn(X,clock,Vloco)

stop =0;

% if X(1,1)>=469
% if X(1,1)>=40
% if X(1,1)>=70
%     stop =1;
% end
if X(1,1)>=15
    stop =1;
end
if Vloco<=0.1 %&& V(size(COMPP,1))<=0.1
   stop =1;
end
```

APPENDIX C – Additional CFD Results

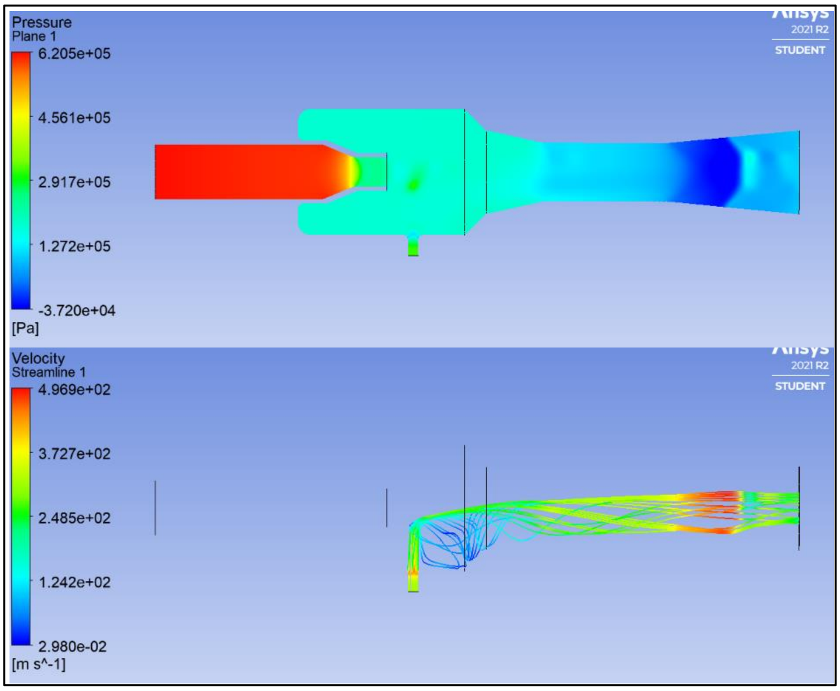

Figure 81 - Venturi design with brake pipe inlet orifice moved 5mm in front of emergency reservoir inlet air.

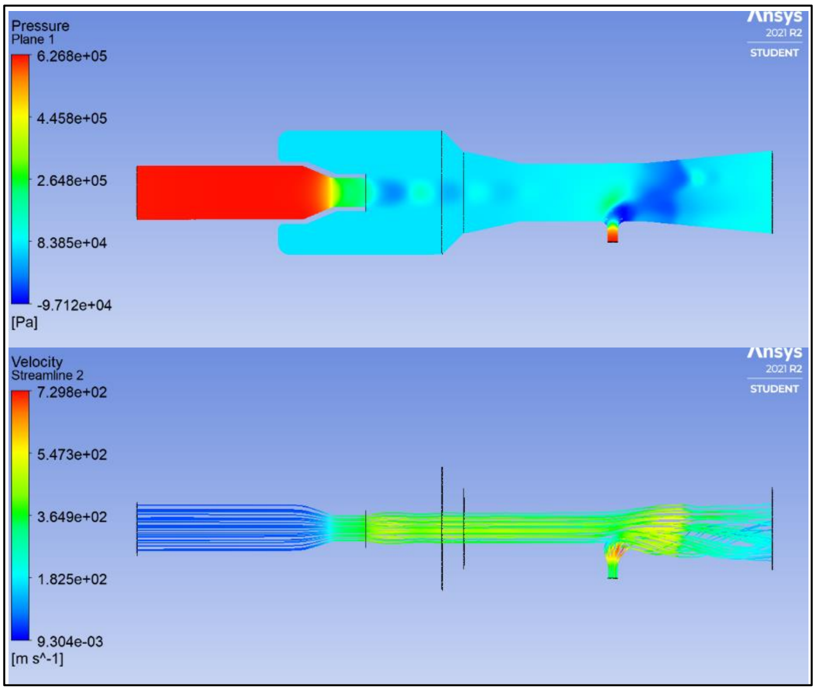

Figure 82 - Venturi design with brake pipe inlet orifice moved to lowest pressure section of venturi.

APPENDIX D – Additional LTD Results

The graphs in this section are from the longitudinal dynamics simulations and are listed sequentially by case number.

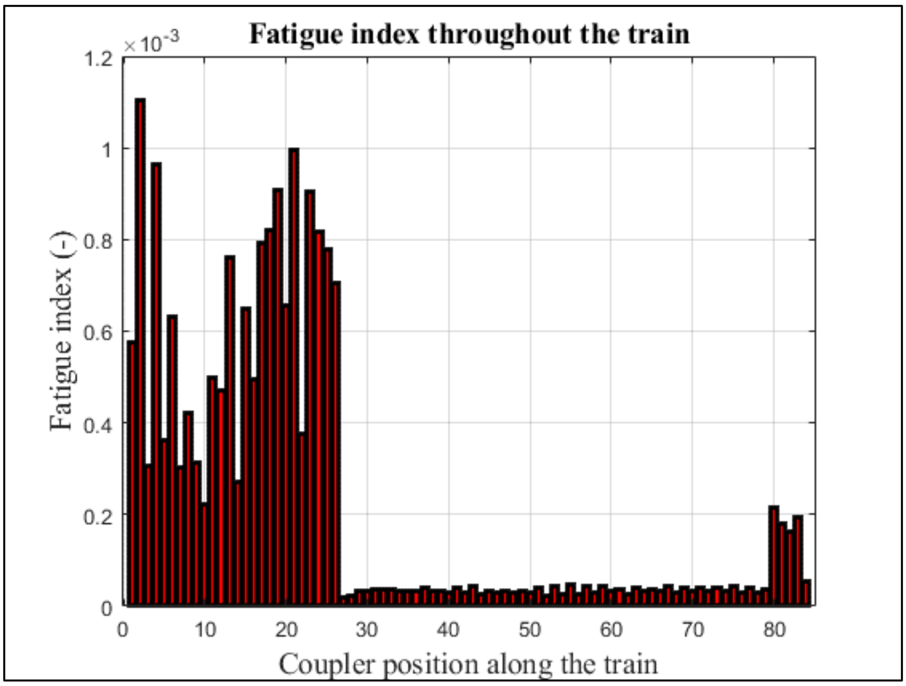

Figure 83 - Case 3: Accumulated fatigue damage of the connection devices in the train.

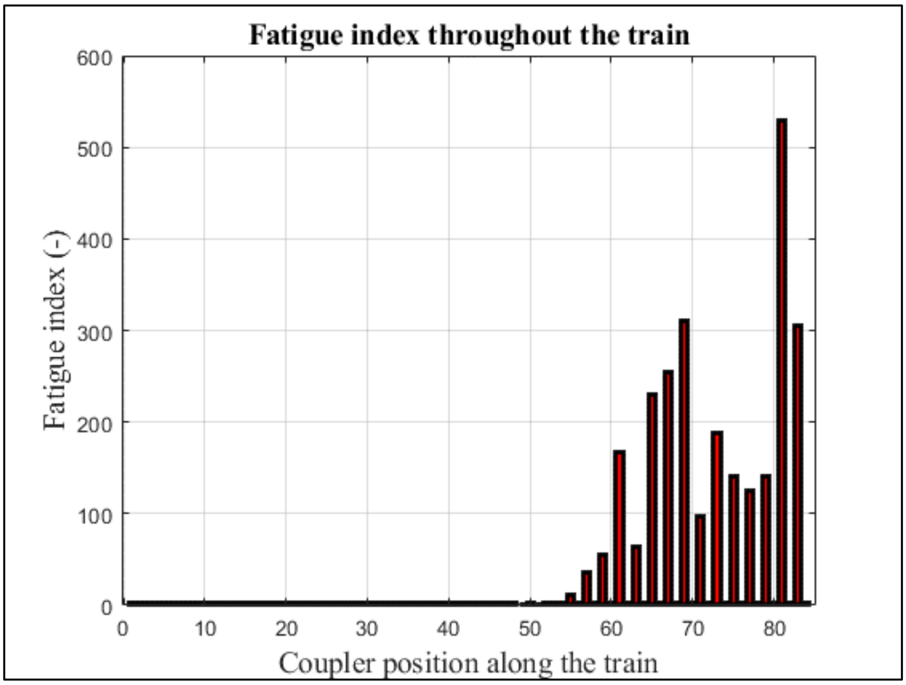

Figure 84 - Case 4: Accumulated fatigue damage of the connection devices in the train.

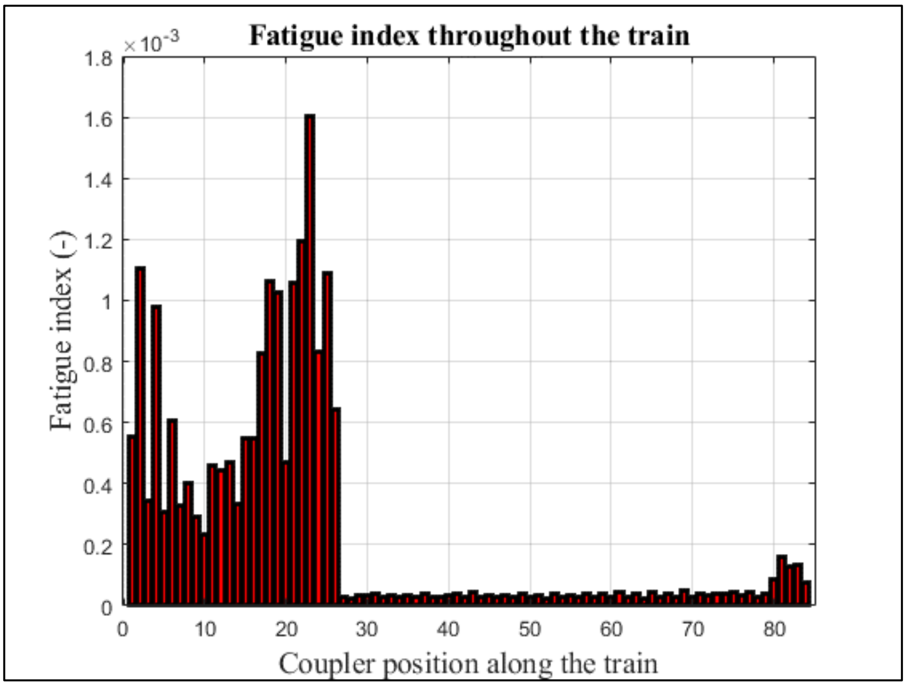

Figure 85 - Case 7: Accumulated fatigue damage of the connection devices in the train.

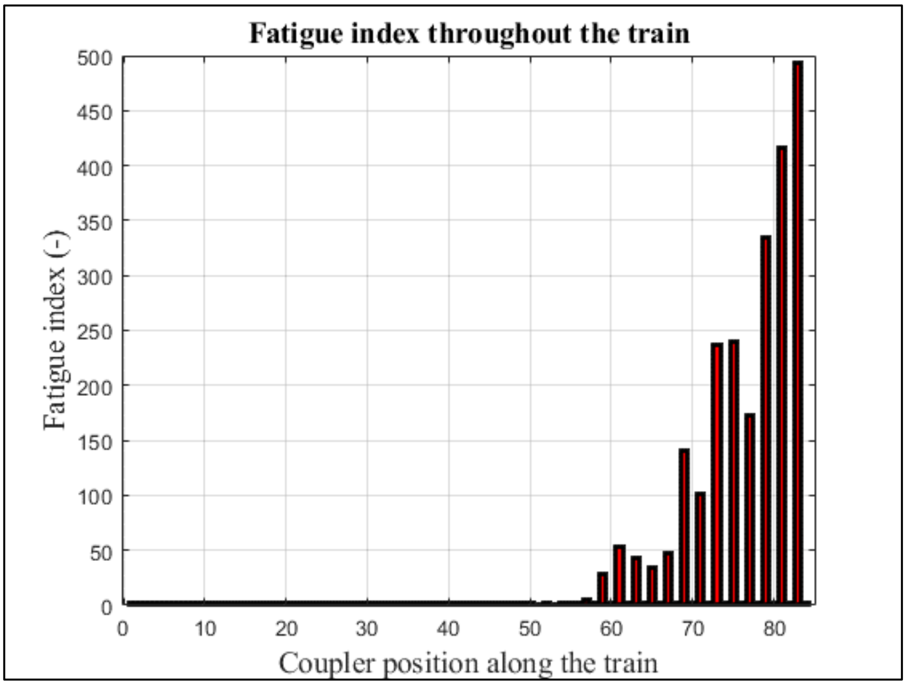

Figure 86 - Case 8: Accumulated fatigue damage of the connection devices in the train.

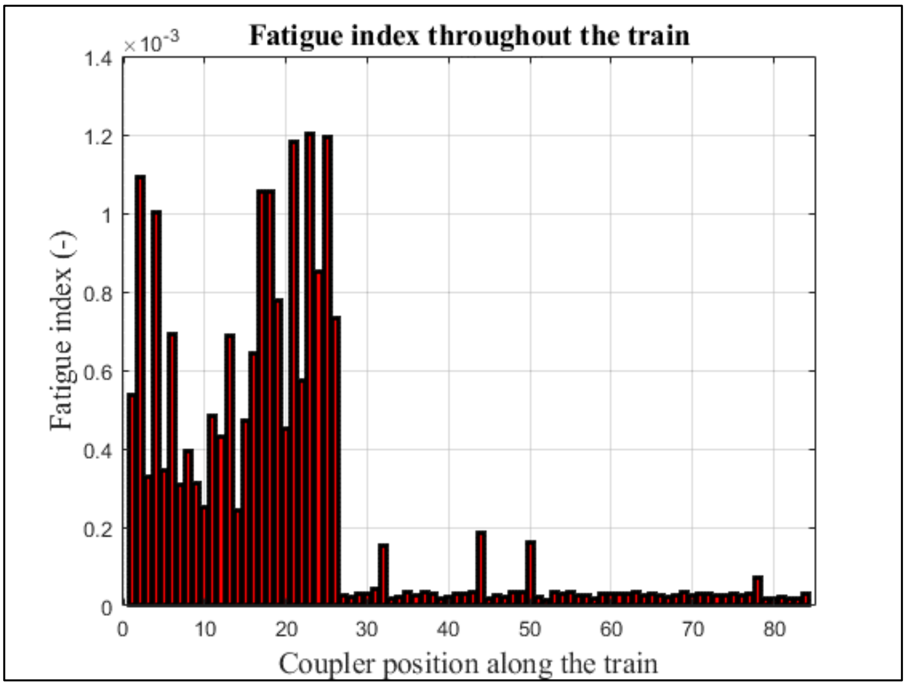

Figure 87 - Case 11: Accumulated fatigue damage of the connection devices in the train.

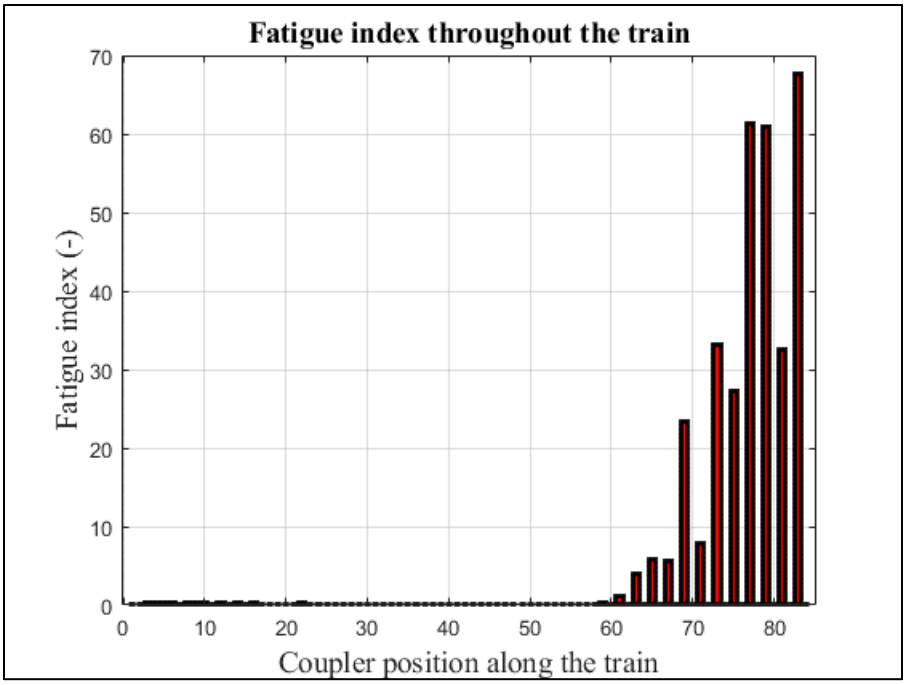

Figure 88 - Case 12: Accumulated fatigue damage of the connection devices in the train.

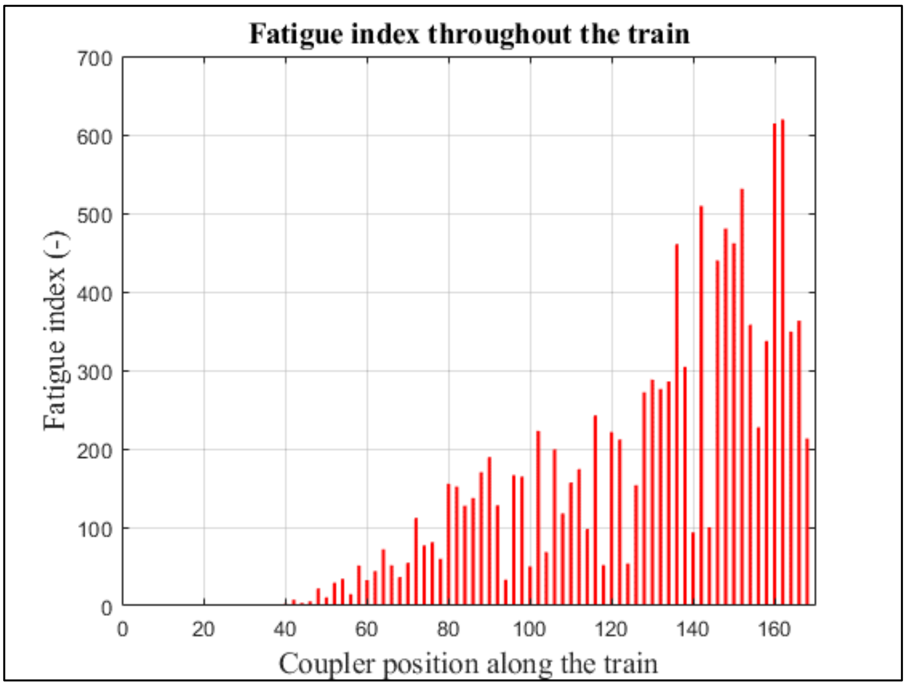

Figure 89 - Case 15: Accumulated fatigue damage of the connection devices in the train.

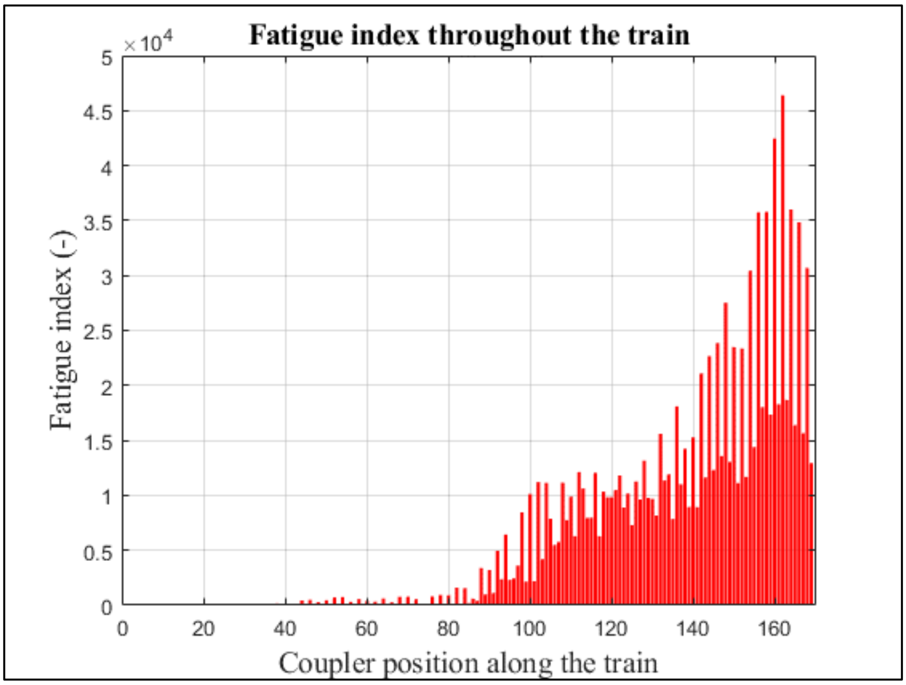

Figure 90 - Case 16: Accumulated fatigue damage of the connection devices in the train.

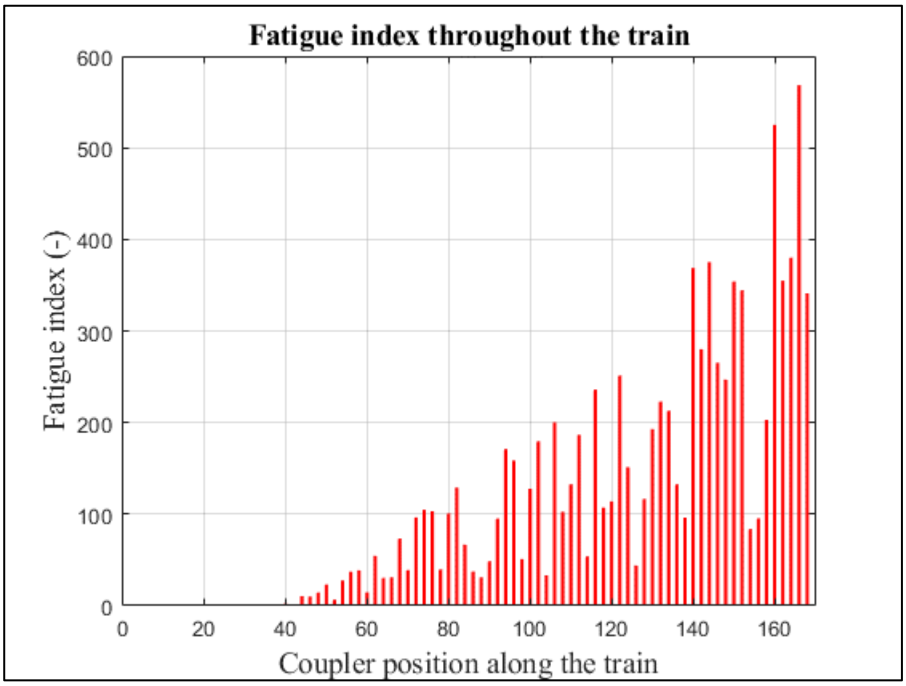

Figure 91 - Case 19: Accumulated fatigue damage of the connection devices in the train.

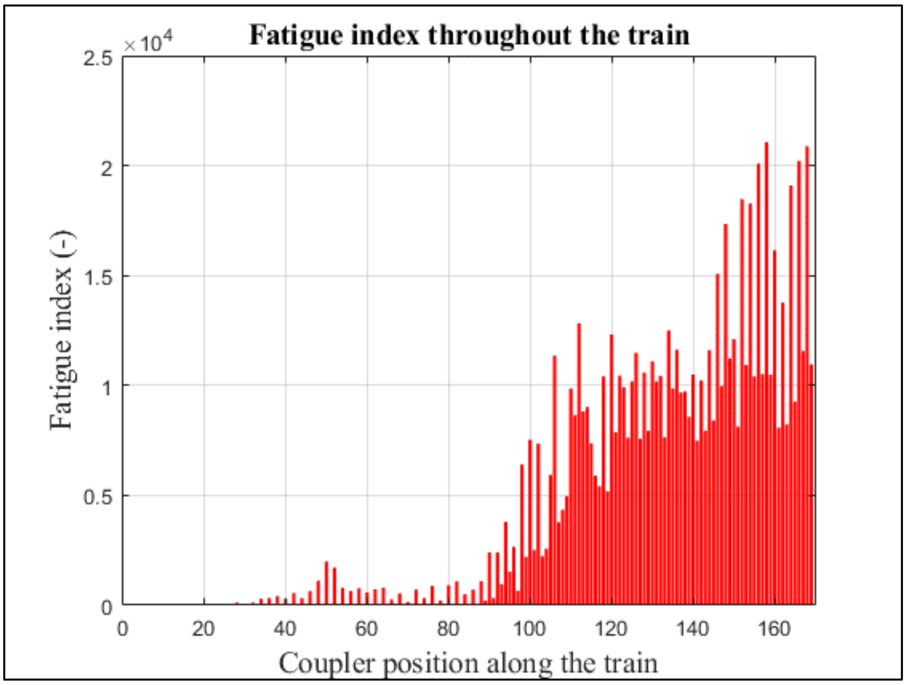

Figure 92 - Case 20: Accumulated fatigue damage of the connection devices in the train.

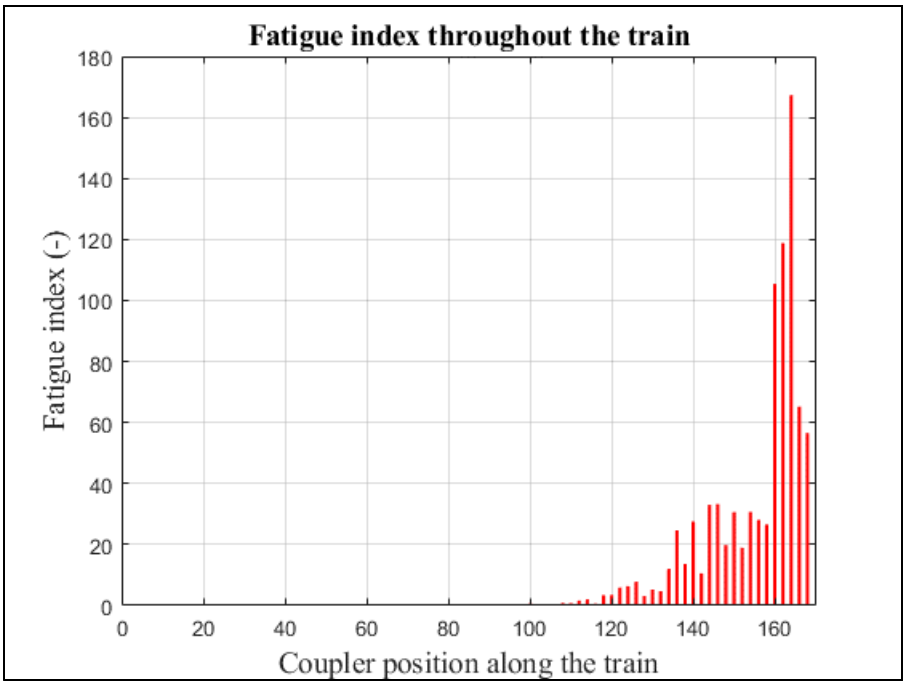

Figure 93 - Case 23: Accumulated fatigue damage of the connection devices in the train.

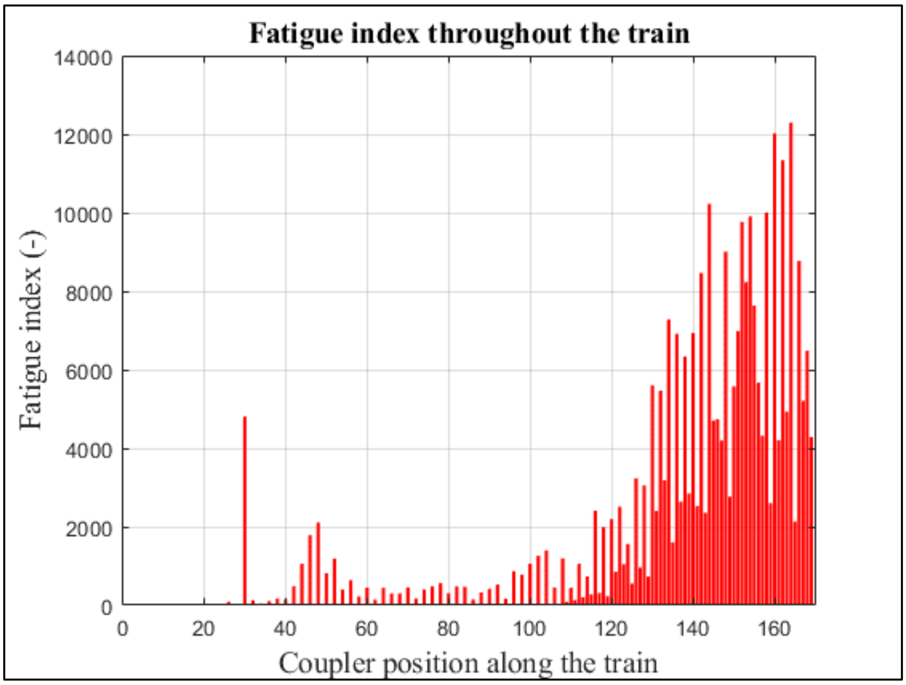

Figure 94 - Case 24: Accumulated fatigue damage of the connection devices in the train.

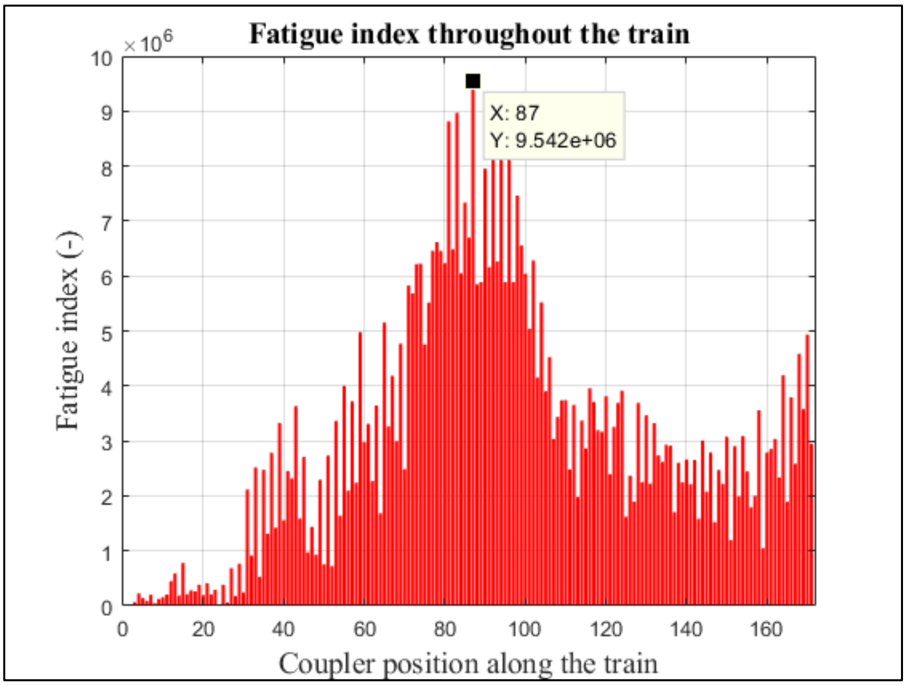

Figure 95 - Case 25: Accumulated fatigue damage of the connection devices in the train.

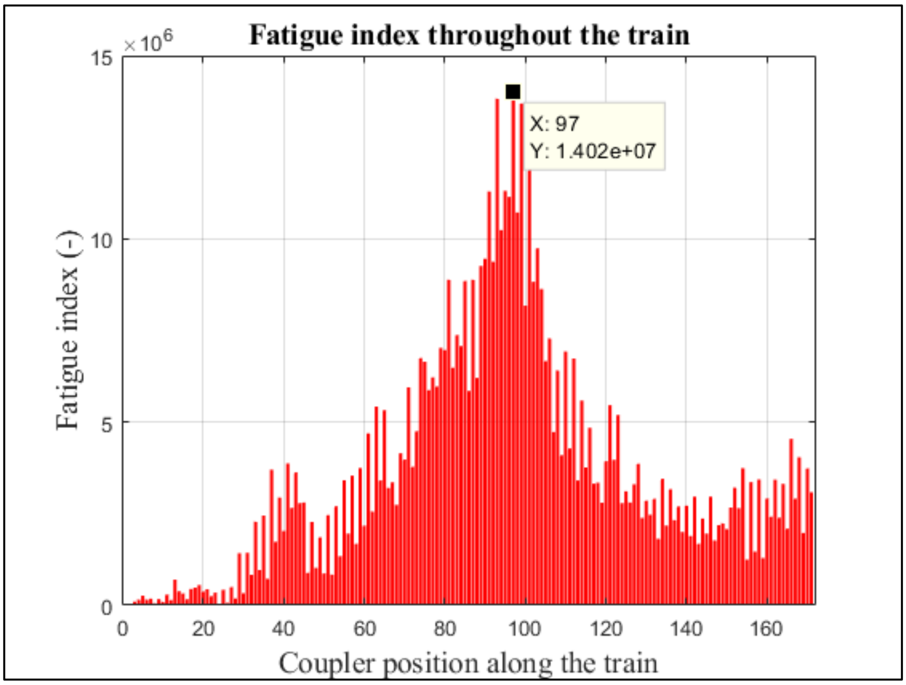

Figure 96 - Case 26: Accumulated fatigue damage of the connection devices in the train.

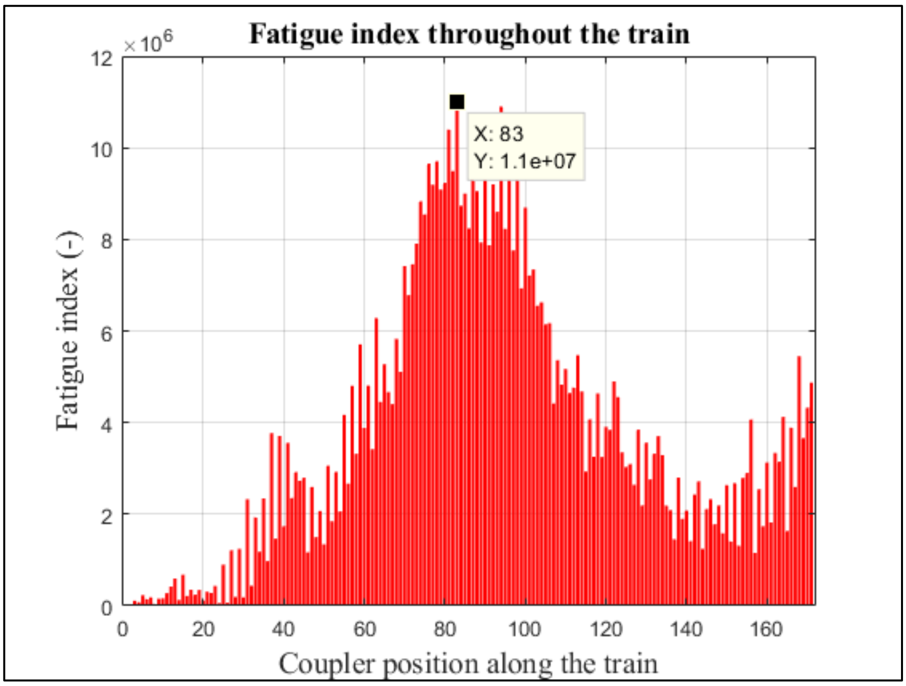

Figure 97 - Case 27: Accumulated fatigue damage of the connection devices in the train.

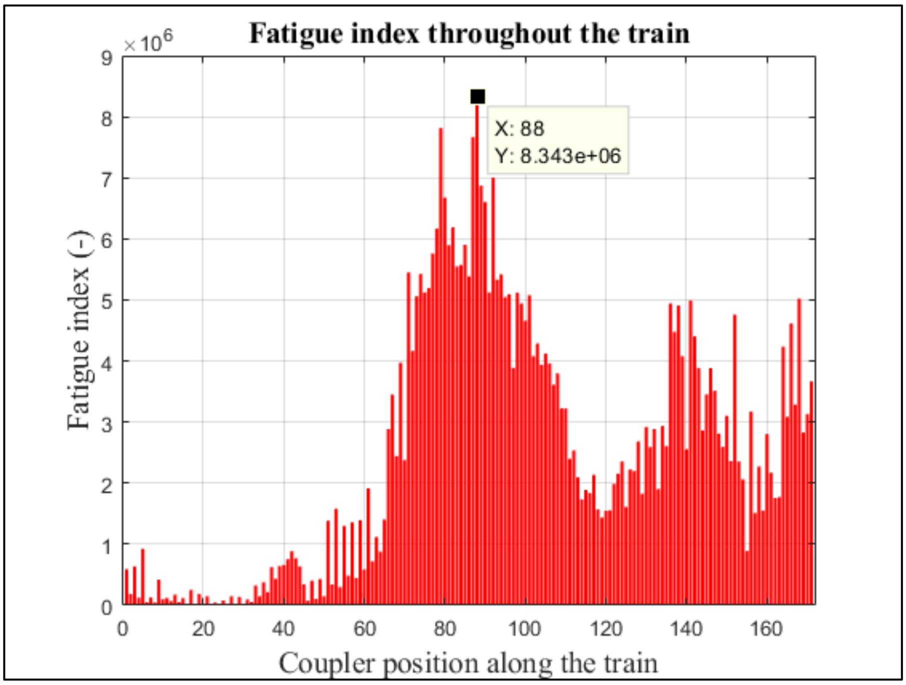

Figure 98 - Case 28: Accumulated fatigue damage of the connection devices in the train.

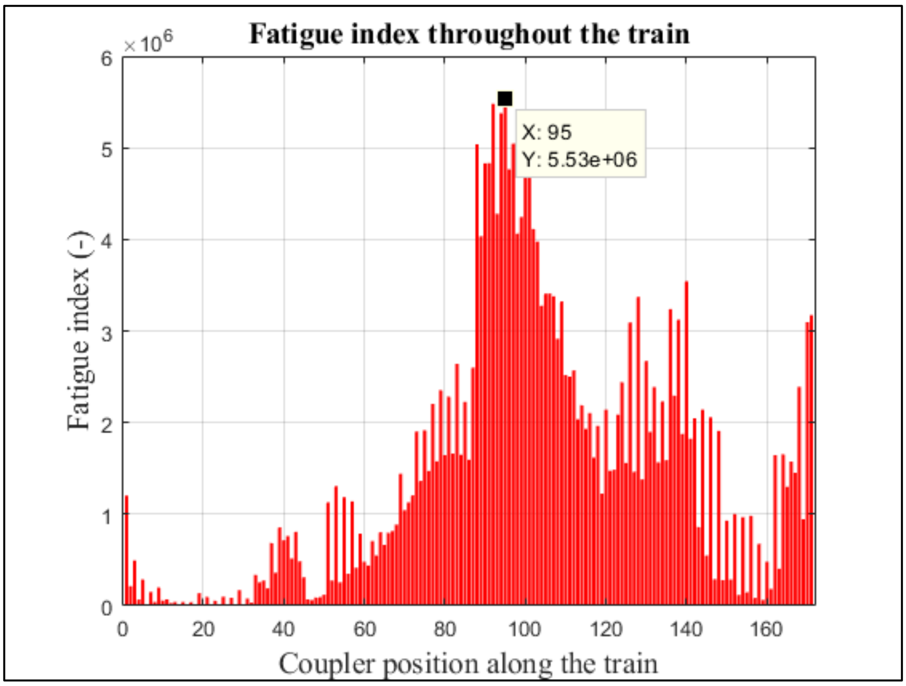

Figure 99 - Case 29: Accumulated fatigue damage of the connection devices in the train.

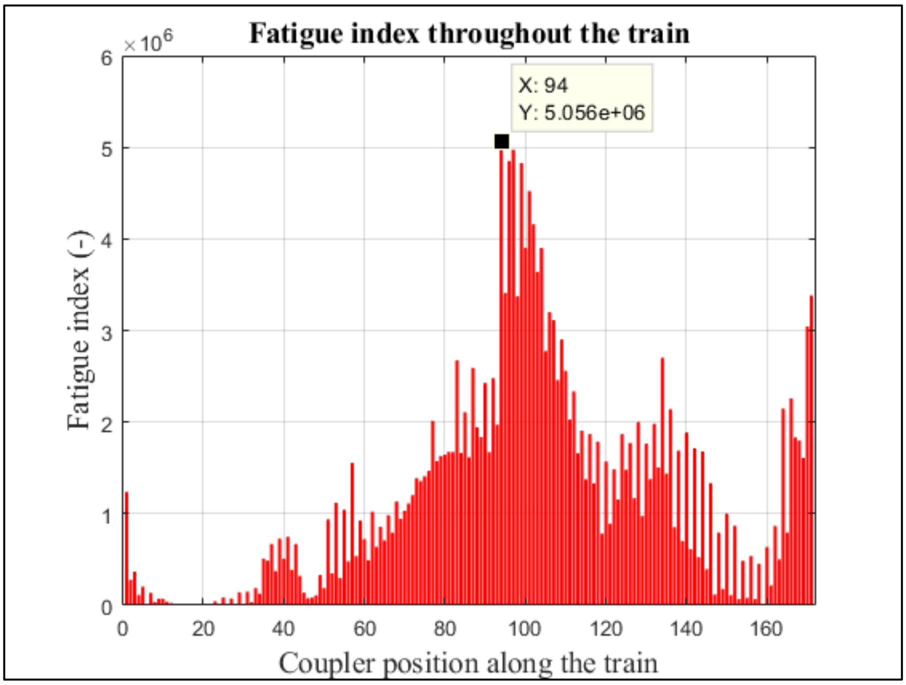

Figure 100 - Case 30: Accumulated fatigue damage of the connection devices in the train.